Alkylation of phenol with methanol over H-ZSM-5, H-Beta, H-Mordenite, H-USY and H-MCM-22

by

Gillian Catherine Moon - MSc (Chem. Eng.)

Thesis Presented for the Degree of
DOCTOR OF PHILOSOPHY
in the Department of Chemical Engineering
UNIVERSITY OF CAPE TOWN
June 2003

Acknowledgements

I would firstly like to acknowledge my supervisors Prof Cyril T. O'Connor and Dr Klaus Möller for all their supervision during my PhD. A special thanks to Mr Walter Böhringer for all his help and assistance especially over the last six months. I would also like to thank the Catalysis Research Unit for the opportunities and support they gave me during my PhD.

I would also like to thank Prof Raul Lobo from the Chemical Engineering department, University of Delaware, USA for his kindness, helpfulness and generosity while I was at the University of Delaware. I also thank his students namely Gopal Juttu, Robyn Accardi and Kaveri Sawant. A special thanks to Kaveri Sawant for the ^{27}Al MAS NMR spectra. Thanks to the NRF student exchange program for the opportunity to go and study at the University of Delaware for three months.

I would also like to thank and acknowledge Helen Divey for all her help and time in doing the elemental analysis, XRDs and BETs. Thanks to the workshop team (Peter, Jochem, David and Martin) for all their assistance over the course of my PhD. Also a special thanks to Thomas Tobler for all his help with the gas phase rig and Peter Dobias for building my liquid phase rig. I also thank Miranda Waldron of the electron microscopy unit for all the SEMs. I would also like to thank Warwick Duncan for all his help with Linux.

A special thanks to my parents as well as Jo-Ann and Andrew for all their patience, encouragement and help they have given to me so that made it possible to do my PhD. Finally, I would like to thank my fiancé, Craig, for all his encouragement, help, support, patience and love.

Synopsis

Alkylphenols are intermediates used in the synthesis of many important substances. The most significant of the commercially important lower alkylphenols are cresols (methyl phenols) and xylenols (dimethyl phenols). The main markets for alkylphenol products are nonionic detergents, phenolic resins, polymer additives and agrochemicals [Weissermel and Arpe, 1997]. Of the western world cresol market, 55% originates from synthetic cresols whereas 45% originates from so-called "natural" cresols obtained from coal tars and refinery caustics [Fiege and Bayer AG, 2001].

The methylation of phenol is the only process specifically developed to produce cresols and xylenols. There are three cresol isomers, namely ortho, para and meta. It is possible to produce a high selectivity to o-cresol by alkylation of phenol with methanol over a basic or a Al_2O_3 catalyst or a Fe/V catalyst. A mixture of the cresol isomers can be obtained over aluminium oxides with strong acid sites, silica alumina, zeolites, aluminium phosphates and phosphoric acid-Kieselguhr catalysts. However, direct synthesis of high purity m-cresol and p-cresol is desirable due to the high costs of separating these two isomers [Parton *et al.*, 1989a]. Thus to synthesize p-cresol, a m-cresol free or very low m-cresol concentration in the product is desirable for purification reasons and a high p/o-cresol ratio is also desirable in the product for yield reasons since separation of the p- and the o-cresols is economically possible.

Various zeolites have been studied for the phenol methylation reaction, viz. H-Y, H-ZSM-5, H-Mordenite, H-Beta, H-X, H-ZSM-11 and various modification of these zeolites. However, most of the zeolites investigated to date have shown poor para-selectivity in the cresol fraction with p/o-cresol ratios between 0.4 to 0.5 which, given the o- and p-directing properties of the phenolic $-OH$ group, is close to the statistically expected ratio of 0.5. These values are also close to the thermodynamic equilibrium p/o-cresol ratio in the temperature range studied, which is 0.43 [Böhringer and Fletcher, 2003]. There are only two reports in literature in which p/o-cresol is observed to be greater than 1 and these are over H-USY [Parton *et al.*, 1989a] and over a sodium or potassium exchanged zeolite Y [Namba *et al.*, 1980]. Unfortunately, the former did not provide any characterization information on the catalyst used and therefore it is difficult to draw any conclusions. The sodium or potassium exchanged zeolite Y samples had a very short lifetime and so are probably not economically viable as a catalyst.

It was found from literature that zeolite Y produced a higher p/o-cresol ratio than zeolite ZSM-5 [Marczewski *et al.*, 1988; Parton *et al.*, 1989a,b]. This is surprising since, as ZSM-5 has narrower channels than Y, it was expected that ZSM-5 would produce more of the shape-selective product p-cresol as found in the case of toluene methylation where p- xylene is favoured. Parton *et al.* [1989a] suggested that o-cresol formed directly from anisole as there is a suppression of bimolecular reactions

involving aromatic rings i.e. a suppression of transalkylation reactions in the pores of ZSM-5, whereas in H-Y, the bimolecular reactions may occur in the supercages. This would result in a higher p/o-cresol ratio in H-Y than in H-ZSM-5.

The primary objective of this thesis was to investigate the activity and selectivities of a range of zeolites under different reaction conditions with a view to determine those catalysts and reaction conditions which optimized the production of p-cresol in the alkylation of phenol with methanol. Zeolites were investigated due to their known shape-selective properties which arise from the channels having similar dimensions to the hydrocarbon molecules. The procedure followed in addressing this objective was as follows:

- Investigation of a zeolite which contained both 10 membered and 12 membered channels, namely zeolite MCM-22. Zeolite MCM-22's pore system consists of two independent channel systems. One comprises of large supercages whose inner free diameter is defined by 12 membered rings but importantly, these supercages can only be accessed through 10 membered ring openings on the side. The second channel is a two-dimensionally interlinked 10-membered ring sinusoidal channel. The pore openings to the supercage are slightly smaller than the pores of ZSM-5 therefore allowing for the bulky bimolecular reactions (which is claimed/proposed to result in a high p/o-cresol ratio over H-Y) to occur in the supercages and shape-selective properties are provided by the supercage openings;
- Comparison of MCM-22 with zeolites with different channel dimensions i.e. H-ZSM-5, H-Beta, H-Mordenite, H-USY and amorphous silica alumina;
- Determination of the effect of different zeolite characteristics on the O/C-alkylation and p/o-cresol ratios, i.e. SiO_2/Al_2O_3 ratio, crystal size, BET surface area, microporous volume and acid site strength;
- Determination of the effect of different reaction conditions on the O/C-alkylation and p/o-cresol ratios, i.e. reaction temperature, methanol : phenol ratio, weight hourly space velocity or reaction time, and partial pressure. The effect of reaction pressure was evaluated by studying the phenol methylation reaction in the gas and liquid phases;
- Derivation of the overall reaction mechanism.

The key findings in the liquid phase alkylation of phenol with methanol are:

- Anisole, o-cresol and p-cresol are the major products. No m-cresol was formed under the liquid phase reaction conditions studied;
- H-ZSM-5 and H-Mordenite produced the highest cresol selectivity;
- Zeolite H-MCM-22 (UCT) produced a high p/o-cresol ratio of greater than 1;
- Internally selective sodium exchanged ZSM-5 and MCM-22, showed a lower activity and a lower p/o-cresol ratio than the unmodified, acid samples;

The key findings in the gas phase alkylation of phenol with methanol are:

- Anisole, o-cresol and p-cresol were also the major products. m-Cresol was formed but at low concentrations (less than 5 % of the cresol fraction);
- H-ZSM-5 and H-MCM-22 (UCT) produced similar p/o-cresol ratios;
- O-alkylation was favoured over C-alkylation, at 300°C, over all the catalysts studied except for H-MCM-22 (DE1);
- p/o-Cresol ratios were between 0.37 (amorphous silica-alumina) and 0.97 over H-MCM-22 (DE2);
- Increasing the crystal size of MCM-22 increased the p/o-cresol ratio;
- Steaming enhanced the activity by approximately 3 times and resulted in a reversal in the O/C-alkylation ratio but hardly effected the cresol isomer distribution;

In conclusion, the alkylation of phenol with methanol was found to be kinetically controlled under the reaction conditions investigated. High para-selectivity from the alkylation of phenol with methanol was obtained over zeolite MCM-22 at high pressure and low temperatures as well as when under low reactants partial pressure where the crystal size of MCM-22 was sufficiently large such that the p/o-cresol ratio increased due to the effective increase in diffusional pathway. The cresols fraction under these conditions also contained little or no m-cresol. The O/C-alkylation ratio was found to be related to the p/o-cresol ratio in that anisole and p-cresol are both the slimmest molecules thereby under shape-selective conditions these two molecules will be preferentially formed.

Table of Contents

List of Figures

List of Tables

Nomenclature

AAS:	Atomic adsorption spectroscopy
^{27}Al MAS NMR:	^{27}Al magic angle spinning nuclear magnetic resonance spectroscopy
BET:	Nitrogen physisorption
GC:	Gas chromotograph
IZA:	International Zeolite Association
NH_3-TPD:	Ammonia temperature-programmed desorption
SEM:	Scanning electron microscopy
WHSV:	Weight hourly space velocity ($g_{methanol+phenol}/g_{catalyst} \cdot h$)
XRD:	X-ray diffraction
A:	Pre-exponential factor or frequency factor in the Arrhenius equation
A_i:	Area on the GC peak of compound i
Al:	Total aluminium content in the catalyst
$A_{mesopores}$:	Mesoporous area of the catalyst
$A_{micropores}$:	Microporous area of the catalyst
b_{AA} and b_A:	Group deactivating contributions
C_A:	Concentration of species A
C_{A0}:	Initial concentration of species A
C_{AS}:	Concentration of species A on the catalyst surface
C_B:	Concentration of species B
C_{B0}:	Initial concentration of species B
C_{BS}:	Concentration of species B on the catalyst surface
C_s:	Concentration of vacant sites
C_{sc}:	Concentration on the surface of the catalyst
C_{SO}:	Initial concentration of vacant sites
D_e:	Effective diffusional constant
E:	Activation energy (J/mol)
F_{A0}:	Entering molar flowrate of species A
k:	Reaction rate constant
k_O:	Kinetic constant for O-alkylation
k_R:	Kinetic constant for C-alkylation
k_1:	Reaction rate constant
K_A:	Equilibrium constant for species A

K_B:	Equilibrium constant for species B
$K_{methanol}$:	Equilibrium constant of methanol adsorption
K_{phenol}:	Equilibrium constants for phenol adsorption
M:	Charge compensating cation (typically H^+, Na^+, K^+, Mg^{2+}, Ca^{2+}, Ba^{2+} or La^{3+})
$n_{feed\ phenol}$:	Number of mole of phenol in the feed
n_i:	Moles of product i
$n_{methanol}$:	Moles of methanol
n_{phenol}:	Moles of phenol
$n_{ring\ components}$:	Number of mole of the ring products
P:	Reaction pressure
$P_{methanol}$:	Partial pressure of methanol
P_{phenol}:	Partial pressure of phenol
r:	Reaction rate of phenol consumption
$(-r_A)$:	Rate of consumption of species A
r_p:	Radius of the catalyst particle
$r_{O-alkylation}$:	Reaction rate of O-alkylation
$r_{R-alkylation}$:	Reaction rate of C-alkylation
R:	Gas constant (8.314 J/mol·K)
R_A:	Rate of the formation of species A
RF_i:	Mass response factor of compound i
T:	Temperature (K)
T_{max}:	Maximum temperature of major desorption peak obtained from $NH_3 - TPD$ (K)
W:	Weight of catalyst
X:	Phenol conversion
X_A:	Conversion of species A
X_B:	Conversion of species B
y_4:	Mole fraction of water
Y_{A_i}:	Mole fraction of the alkylating agent (methanol)
Y_{AA_i}:	Mole fraction of each aromatic component having alkylating properties, that is anisole and methylanisoles
$Y_{o-cresol}$:	Yield of o-cresol
$Y_{p-cresol}$:	Yield of p-cresol
Y_{POH_i}:	Mole fraction of components which can be alkylated at the oxygen, namely phenol and cresols
Y_{R_i}:	Mole fraction of all aromatic compounds
z:	Valence of the charge compensating cation M
ϕ:	Thiele Modulus
η_O:	Catalyst efficiency factors for O-alkylation
η_R:	Catalyst efficiency factors for C-alkylation

Chapter 1

Introduction

Alkylphenols are intermediates used in many important syntheses. The most significant of the commercially important lower alkylphenols are cresols (methyl phenols) and xylenols (dimethyl phenols). They are used in the manufacture of plastics (for example, heat resistant polydimethylphenylene oxide resin) as well as important plant protection agents - hormone-type herbicides and carvacrol that is used as an antiseptic. The main markets for alkylphenol products are nonionic detergents, phenolic resins, polymer additives and agrochemicals [Weissermel and Arpe, 1997]. Table 1.1 shows a more detailed list of the uses of the cresol isomers.

Cresols were originally only obtained from coal tar produced by the gasification of coal and coking of coal. After World War II cresols were also obtained from refinery caustics and from the mid-1960s cresols have be produced synthetically on an increasingly large scale as the cresol recovery from coal tar and refinery caustics had become insufficient to meet the demand [Fiege and Bayer AG, 2001]. The total production of cresols in the United States, Western Europe, Japan and South Africa was estimated at approximately 175 000 tons in 1989, of which 105 000 tons was from synthetic cresols and 70 000 tons was from "natural" cresols [Fiege and Bayer AG, 2001]. An estimated 45% of the total cresols output is used as pure o- or p-cresol, the rest as a mixture of the cresol isomers [Fiege and Bayer AG, 2001].

Synthetic cresols are mainly produced from the following processes: alkali fusion of toluenesulphonates; alkaline chlorotoluene hydrolysis; splitting of cymene hydrolysis and methylation of phenol in the vapour phase. Each of the processes produce a different isomer distribution. Alkali fusion of toluenesulphonates produces mainly p-cresol however the primary drawback of this process is the unavoidable formation of sodium sulphite in aqueous solution. Alkaline chlorotoluene hydrolysis produces a cresol fraction with a high m-cresol content. Cymene hydroperoxide cleavage produces p- and m-cresol but is unsuitable for the formation of o-cresol. This process also has a significantly lower yield that the other processes. The methylation of phenol is the only process specifically developed to produce cresols and xylenols [Fiege and Bayer AG, 2001].

Vapour phase methylation of phenol over a metal catalyst namely, silica-supported Fe-V oxide, magnesium oxide, manganese oxide, chromium oxide, iron oxide or a γ-aluminium oxide catalyst, was mostly used to produce pure o-cresol and 2,6-xylenol [Marczewski *et al.*, 1988; Santacesaria *et al.*, 1990b; Beck and Haag, 1997; Lee *et al.*, 1998; Choi *et al.*, 2000; Fiege and Bayer AG, 2001]. Over aluminium oxides with strong acid sites, silica-alumina, zeolites, aluminium phosphates and phos-

Table 1.1: Uses of the cresol isomers [Fiege and Bayer AG, 2001].

Cresol isomer	Compound made from cresol isomer	Use
o-Cresol	Chlorophenoxyalkanoic acids	Selective herbicides
	4,6-Nitro-o-cresol	Herbicidal and insecticidal properties Polymerization inhibitor for the production of styrene
	Epoxy-o-cresol novolak resins	Sealing material for integrated circuits
	o-Cresotinic acid	Dye intermediate Pharmaceuticals
	2-Methylcyclohexanol 2-Methylcyclohexanone	Solvent
	Carvacrol	Antiseptic and in fragrances
	-	Antioxidants, Pharmaceuticals
p-Cresol	2,6-Di-tert-butyl-p-cresol 2,2-Methylene- / 2,2-thiodiphenols 2,6-Dicyclopentyl-p-cresol	Antioxidants
	Tinuvin 326	Absorber of UV light
	2,6-Nitro-p-cresol	Polymerization inhibitor for the production of styrene
	p-Cresolcarboxylic acid esters	Fragrance industry
	2-Ethylhexyl-p-methoxycinnamate	UV absorber in sunscreens Pharmaceuticals
	2-Nitro-p-cresol	Dyes intermediate
m-Cresol	O,O-dimethyl-O-(3-methyl-4-nitropheynyl)-thionophosphoric acid	Contact insecticides
	m-Phenoxybenzaldehyde	Building block for insecticide of the pyrethroid type
	2,3,6-Trimethylphenol	Starting block for synthesis of vitamin E
	Thymol	Fragrances
	6-Tert-butyl-m-cresol	Fragrances Antioxidant
	4-Chloro-m-cresol	Disinfectant and preservative
	2,4,6-Trinitro-m-cresol	Explosive

phoric acid-Kieselguhr catalysts, due to their enhanced isomerization and transalkylation properties, mixtures of o-, p- and m-cresol were produced [Fiege and Bayer AG, 2001].

Highly selective synthesis of m-cresol and p-cresol respectively is desirable due to the high cost of separating these isomers. m-Cresol and p-cresol have very close boiling points (202.2 and 201.9°C, respectively) which means that the two isomers cannot be separated by distillation economically but need fractionated crystallization, adsorption separation (Cresex process) or derivatisation by butylation with isobutene before being separated by distillation [Fiege and Bayer AG, 2001]. However, a mixture of o- and p-cresol without m-cresol could easily be separated by distillation as their boiling points differ by 10.9°C. Such a process may be of economic interest if the p/o-cresol yields and ratios are sufficiently high.

Zeolites are crystalline aluminosilicate materials with a uniform channel/pore system. Zeolites have pore sizes ranging from 4 to 13 Å, which are similar dimensions to those of hydrocarbons molecules found in petroleum chemistry. Zeolites can therefore influence the product distribution by shape-selective catalysis. For example, in toluene alkylation with methanol, it is known that the product o-xylene diffuses more than three orders of magnitude slower than p-xylene in ZSM-5 [Nagy *et al.*, 1998b]. Therefore, the product spectrum shows a high para-selectivity in the reaction of toluene with methanol over ZSM-5.

Zeolites have been studied in the methylation of phenol. As mentioned above zeolites were found to produce a mixture of cresol isomers. However, it is possible to produce only the o- and p-cresol at low temperatures and conversions (< 14%) over H-ZSM-5 and H-USY [Parton *et al.*, 1989a], as the hydroxyl group on the phenol is ortho- and para-directing. At higher conversions m-cresol was found to formed. Over the different zeolites, p/o-cresol ratios of between 0 and 1.85 are reported in literature. Most of the p/o-cresol ratios obtained over the zeolites fall in the range of 0.4 - 0.5 which corresponds to thermodynamic equilibrium (0.43 as obtained experimentally by Böhringer and Fletcher [2003] at 350°C) and to the statistical ratio (0.5 due to two ortho positions and one para position on the phenol).

Most of the literature has concentrated on obtaining a high o-cresol yield and therefore there are different explanations which relate to the low p/o-cresol ratio in zeolites. For example, Marczewski *et al.* [1988] observed exclusive o-cresol formation over H-Mordenite. This was explained in terms of the orientation of the phenol in the narrow pores of Mordenite which would favour ortho substitution. However, Landau *et al.* [1997] who also studied H-Mordenite and obtained a p/o-cresol ratio of 0.77. The difference between these Mordenite samples was their SiO_2/Al_2O_3 ratios.

Another explanation given for the low p/o-cresol ratio was the intramolecular rearrangement of the product anisole to o-cresol [Venuto *et al.*, 1966; Beltrame *et al.*, 1987; Jacobs *et al.*, 1988; Parton *et al.*, 1989a]. This was used in particular to explain the "low" p/o-cresol ratio obtained over H-ZSM-5 compared to H-Y. As ZSM-5 has narrower pores than Y it was expected that ZSM-5 would produce the shape-selective product p-cresol as it has done in the toluene methylation in the xylene isomers. Parton *et al.* [1989a] suggested that o-cresol forms directly from anisole as there is a suppression of bimolecular reactions involving aromatic rings i.e. a suppression of transalkylation reactions in the pores of ZSM-5. Whereas in H-Y, the bimolecular reactions may occur in the supercages. This would result in a higher p/o-cresol ratio in H-Y than in H-ZSM-5.

High p/o-cresol ratios of above 1 were found by Namba *et al.* [1980] and Parton *et al.* [1989a]

over sodium or potassium exchanged H-Y and H-USY, respectively. Namba *et al.* [1980] concluded that moderate acid sites (-3.0 $\geq$ H_0 $\geq$ -8.2) on zeolite H-Y are advantageous to produce p-cresol (weaker acid sites produce anisole and stronger acid sites allow secondary reactions). Namba *et al.* [1980] did not explain why the moderate acid sites preferentially produced p-cresol and not o-cresol. However, these catalysts are not economically viable due to their very short lifetimes. Over H-USY quite different p/o-cresol ratios were obtained by various researchers [Balsama *et al.*, 1984; Marczewski *et al.*, 1988; Parton *et al.*, 1989a; Landau *et al.*, 1997] ranging from 0.33 to 1.54. Parton *et al.* [1989a] attributed the high p/o-cresol ratio obtained over the H-USY to the effect of acid site strength. However, this does not agree the findings of Marczewski *et al.* [1988] and Parton *et al.* [1989a] did not describe the catalysts that were investigated and therefore it was not possible to extract any meaningful conclusions.

Jacobs *et al.* [1988] concluded that it may be necessary to use a 10 membered ring zeolite with a channel size smaller than ZSM-5 (5.1 x 5.5 Å and 5.3 x 5.6 Å) to achieve a higher p/o-cresol ratio than over H-ZSM-5. Jacobs *et al.* [1988] used H-ZSM-22 (4.6 x 5.7 Å) and H-Ferrierite (4.2 x 5.4 Å) in the self alkylation of anisole and obtained p/o-cresol ratios which were lower over H-ZSM-22 and H-Ferrierite than over H-ZSM-5. It was concluded that the reaction was occurring on the external surface of the catalysts resulting in a higher ortho-selectivity. However, the high ortho-selectivity could be due to the intramolecular rearrangement of anisole to o-cresol as Parton *et al.* [1989a] explained for the low p/o-cresol ratio over H-ZSM-5. A zeolite with a larger internal space than ZSM-5 may be required to allow for bimolecular reactions to occur but with narrow pore opening to promote the formation of the slimmest molecule.

Zeolite MCM-22 has a structure containing both 10 and 12 membered ring pores. Zeolite MCM-22's pore system consists of two independent channel systems. One comprises of large supercages whose inner free diameter is defined by 12 membered rings (7.1 Å) and the inner height is 18.2 Å [Leonowicz *et al.*, 1994]. But importantly, these supercages can only be accessed through 10 membered ring openings on the side. The supercages are separated lengthwise through a "neck", made by a 6 membered ring prism. This second channel is a two-dimensionally interlinked 10-membered ring sinusoidal channel with dimensions of 4.1 x 5.1 Å [Baerlocher *et al.*, 2001; IZA, 2002a]. Both types of channels are interlinked with themselves but not with each other. Therefore, the combined channel/supercage systems in zeolite MCM-22 only allows diffusion in two directions but not perpendicular to them. The pore openings to the supercage are slightly smaller than the pores of ZSM-5 therefore allowing for the bulky bimolecular reactions to occur in the supercages and shape-selective properties are given by the supercage openings. Zeolite MCM-22 has not previously been studied in the methylation of phenol reaction.

This thesis follows the following structure:

- A detailed description of literature on zeolites in terms of their structure, synthesis, acidity and post-synthesis modification of zeolites;
- An analysis of the literature on the alkylation of phenol with methanol;
- The objectives of this research are defined;
- A description of the experimental procedures used in this thesis;

- The characterization of the catalysts used in this thesis;
- The results obtained in the liquid and gas phases studies of the methylation of phenol;
- The discussion of the results obtained in this thesis;
- The conclusions and recommendations for further studies.

Chapter 2

Literature Review

2.1 Zeolites

Zeolites were first recognised by Swedish mineralogist Cronstedt in 1756, who derived the name from the Greek words "zeo" and "lithos" meaning "I am boiling" and "stone" due to the observed intumescence of the mineral when it was heated [Flanigen, 1991]. Zeolites are crystalline aluminosilicate materials which have unique properties, namely [Moscou, 1991; Maxwell and Stork, 2001]:

- microporous character with uniform pore dimensions;
- ion-exchange properties;
- ability to possess acidity;
- high thermal stability;
- high hydrothermal stability.

These properties make zeolites suitable for a wide range of industrial processes. They are widely used in the industrialised countries of North America, Western and Eastern Europe and Japan, which had a combined estimated total usage of approximately 1.4 - 1.6 million tons per annum at the turn of the century [Maesen and Marcus, 2001].

The application of zeolites can be divided into four main areas according to their main application [Moscou, 1991]:

- Adsorbents and separation agents: as drying agents, in gas purification and in separation processes, which utilise zeolite's shape selectivity properties;
- Catalysts: mainly in petroleum refining, synfuels production and petrochemicals production;
- Detergents: as a substitute for phosphates (mainly zeolite A);
- Natural zeolites: waste water treatment, nuclear effluent treatment, animal feed supplements and soil improvement.

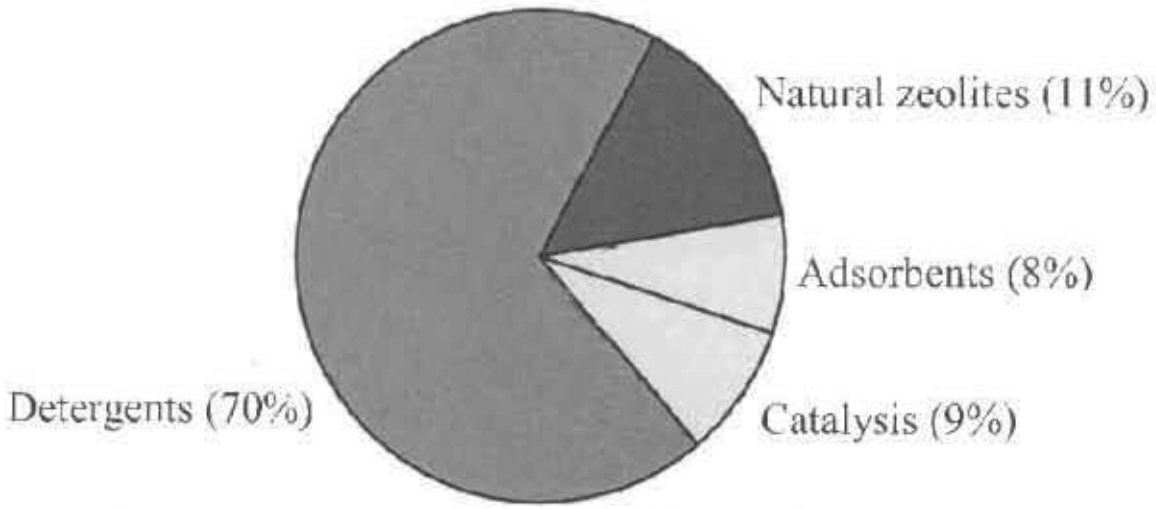

Figure 2.1: Estimated annual zeolite consumption (wt-% of total) by the major individual applications at the turn of the century [Maesen and Marcus, 2001].

In terms of mass, detergents are by far the largest application (cf. Figure 2.1) but in terms of financial market size, catalysts form the largest application of zeolites. For example, the market volume in US$/annum of zeolite catalysts constituted 60% of the total zeolite market (based on 1994 figures) [Blauwhoff *et al.*, 1999]. The total zeolite consumption in catalytic processes at the turn of the century was approximately 120 000 tons per annum [Maxwell and Stork, 2001].

Zeolite Y is the main zeolite used in catalysts application (approximately 90% of the total zeolite consumption for catalytic purposes by mass), mostly consumed in catalytic cracking [Maxwell and Stork, 2001]. ZSM-5, Mordenite and other zeolites also have important commercial applications as catalysts. New applications for zeolites as catalysts are being developed, or existing applications are being fine-tuned, by making use of the many opportunities zeolites offer for tailoring a catalyst [Moscou, 1991].

Zeolites are crystalline aluminosilicate materials with the general unit cell formula [Martens *et al.*, 1997] given by

$$M^{z+}_{x/z}[(AlO_2^-)_x(SiO_2)_y] \cdot nH_2O$$

where z is the valence of the charge compensating cation M (which is typically H^+, Na^+, K^+, Mg^{2+}, Ca^{2+}, Ba^{2+} or La^{3+}). The ratio of x/y is smaller than or equal to 1 as there are no linking Al-O-Al bridges in aluminosilicate frameworks (Löwenstein rule) [Löwenstein, 1954].

Zeolites' framework structures are based on an infinitely extending three-dimensional network of SiO_4 and AlO_4 tetrahedra (primary building units) thereby sharing all the oxygen atoms. Each shared AlO_4 tetrahedron in the framework bears a negative charge, which is balanced by a positive charge from a cation (see unit cell formula). In most zeolite structures the primary structural units are assembled into secondary building units, which are simple polyhedra such as cubes, hexagonal prisms or octahedra. The final zeolite structure consists of an assembly of these secondary building units. The zeolite formed has a well defined, regular void or channel structure of molecular dimensions. The channels and interconnecting voids contain cations and water molecules. The cations are mobile and can undergo ion-exchange. The water can be removed reversibly by heat, which leaves the framework

Table 2.1: Structure of the channel system for selected zeolites [Breck, 1974a; Venuto, 1994; Baerlocher *et al.*, 2001; McCusker and Baerlocher, 2001; IZA, 2002a].

Structure type	Ring size of channels	Channel dimensionality	Intersecting channels	Channel system dimensionality	Supercages present
ZSM-5	10 10	1 1	Yes	3	No
Beta	12 12	2 1	Yes	3	No
Mordenite	12 8 8	1 1 1	Yes*	2*	No*
Faujasite (X/Y)	12	3	Yes	3	Yes
MCM-22	10 10	2 2	No	2	Yes

* The lining of the 12 membered ring channels contains 8 membered rings (which form the crossing channel), but the 8 membered ring openings of adjacent 12 membered ring channels are displaced with respect to one another, so only very limited access from one 12 membered ring channel to the next is possible. Consequently, the channel system is effectively rendered one-dimensional [McCusker and Baelocher, 2001]. These 8 membered ring openings in the lining of the 12 membered ring channels appear as "side pockets" [Breck, 1974a; Venuto, 1994].

structure intact with micropores and voids, which could account for up to 50% of the crystal's volume [Flanigen, 1991]. The silicon and aluminium atoms in the zeolite framework are referred to as T atoms and the framework density of the zeolite, usually expressed as T atoms per 1000 Å^3, is a measure for the void volume. The lower the framework density, the higher the void volume (e.g. zeolite Y - 12.7 T atoms per 1000 Å^3 and zeolite ZSM-5 - 17.9 T atoms per 1000 Å^3 [IZA, 2002a]).

Zeolites are frequently classified according to the number of T atoms in the rings that form the structure of the channels or of the windows between the voids. These may range from very small (8 T atoms, 3 - 4 Å channel diameter viz. Linde A) to very large pore zeolites with up to 20 T atoms in the ring (viz. Cloverite - 13.2 Å channel diameter). The channel system of zeolites may be one-dimensional (non-connecting parallel pores e.g. ZSM-12), two-dimensional (e.g. MCM-22) or three dimensional (e.g. Beta). These channels may interconnect (e.g. Beta) or be independent of each other (e.g. MCM-22). ZSM-5 contains two one-dimensional channel systems which have different orientation. They are interconnected in a way that the total channel system is effectively three dimensional [Baerlocher *et al.*, 2001; IZA, 2002a]. Table 2.1 shows the zeolites used in this study with special regard to the structure of their channel systems.

Zeolites with 10 membered ring or 12 membered ring channel size are the most commonly synthesized for catalytic purposes. Zeolite structures containing 10 or 12 membered ring channels and supercages have also been synthesized. Examples of these are Boggsite, CIT-1, MCM-22 and zeolite Y. These zeolites can thus be used in reactions where the desired reactants and the products can diffuse through the channels but when the transition states required for the formation of these products are relatively bulky, they can only be accommodated in larger void spaces i.e. in the supercages. Zeolites, whose channels are intersecting with a certain offset (e.g. ZSM-5) can accommodate mod-

erately expanded transition states or intermediates at their channel intersections [Gläser *et al.*, 1998; Baerlocher *et al.*, 2001; IZA, 2002a].

In zeolites where supercages are present or where the channels intersect, the primary products can be determined by the void space left in the supercage or the intersection of the channels. The diffusion of these primary products and consecutive reactions then depend on the dimensions of the channels. For example, ZSM-5 has 10 membered ring channels (5.3 x 5.6 Å and 5.1 x 5.5 Å) intersecting with some offset and giving rise to a void space at the intersection with a diameter of 9 Å [Meier *et al.*, 1978; Derouane, 1980]. This void allows the formation of bulkier molecules than what was possible in the 10 membered ring channels. The diffusion of these "bulkier" molecules in the pore system, is then dependent on the size of the channels.

Zeolite Y has supercages (11.4 Å [Venuto, 1994]) as does MCM-22 (7.1 x 7.1 x 18.2 Å [Leonowicz *et al.*, 1994]). The windows to the cages of zeolites Y and MCM-22 are 12 membered rings (7.4 Å) and 10 membered rings (4.0 x 5.5 Å), respectively [IZA, 2002a], and as such influence the product distribution. Bulky molecules, which form inside these supercages are unable to diffuse out. If they aren't transformed into less bulky molecules but accumulate, they will eventually plug the pore system.

In zeolites with different channels but where the channels do not intersect, the final behaviour observed appears to be an average of the primary processes occurring in the different channels [Corma, 1998].

2.1.1 Structures of zeolites studied

The zeolites studied in this research were H-ZSM-5, H-Beta, H-Mordenite, H-MCM-22 and ultrastable zeolite H-Y (H-USY). The pore structures of these zeolites can play large roles in determining the selectivity of the reaction investigated. Silica-alumina was also studied as a comparative amorphous catalyst that does not show any shape-selectivity as expected from zeolites. In the following sections, each zeolite will be described in detail. All zeolite diagrams shown in these sections were obtained from the International Zeolite Association (IZA) website [IZA, 2002a] and [Meier *et al.*, 1978; Augustine, 1995; Lawton *et al.*, 1998; Juttu and Lobo, 2000; Baerlocher *et al.*, 2001]. Dimensions of these zeolite structures are summarised in Table 2.2.

2.1.1.1 Zeolite ZSM-5

Zeolite ZSM-5 has a three-dimensional pore structure as shown in Figure 2.2. The pore system consists of two intersecting, slightly ellipsoidal channels of similar size with 10 membered rings, one sinusoidal and the other straight. The sinusoidal channels intersect with the straight channels. A sinusoidal channel connects the straight channels of two adjacent layers. The next sinusoidal channel links the straight channels in one of these layers to the straight channels in the next layer and so on, effectively building a three dimensionally interconnecting channel system (cf. Figure 2.2 (b)). Therefore, diffusion in the third dimension requires constant manoeuvring between the two types of channels.

ZSM-5 is a medium pore zeolite with free apertures of 5.1 x 5.5 Å for the straight channel and 5.3 x 5.6 Å for the sinusoidal channel [Baerlocher *et al.*, 2001; IZA, 2002a]. The intersection is slightly offset resulting in a comparably spacious cavity with a free diameter of ≈ 9 Å [Meier *et al.*, 1978; Derouane, 1980].

The crystal structure is orthorhombic with a unit cell of dimensions: a = 20.1 Å, b = 19.9 Å and c = 13.4 Å [Szostak, 1992]. The chemical composition of the sodium form is given by $Na_n[Si_{96-n}Al_nO_{192}]$ ($n \leq 8$) i.e. SiO_2/Al_2O_3 molar ratios ≥ 22. ZSM-5 has a framework density of 17.9 T atoms per 1000 Å^3.

2.1.1.2 Zeolite Beta

Zeolite Beta has a three-dimensional pore structure and large pore openings consisting of 12 membered rings (Figure 2.3) [Haggin, 20 June 1988]. The framework of zeolite Beta consist of an intergrown hybrid of three distinct but closely related structures that are arranged in layers [Treacy and Newsam, 1988]. These layers can connect to each other in three different ways resulting in three different structures (Polymorphs A, B and C). Zeolite Beta's framework structure is obtained from a near randomly connected sequence of these layers in the direction of the c-axis [Treacy and Newsam, 1988].

Zeolite Beta's pore system consists of three intersecting 12 membered ring channels. Two of these channels are identical and linear of 6.6 x 6.7 Å dimensions. They are mutually orthogonal and perpendicular to the c axis. These two channels slightly overlap forming a 12 membered ring window between the channels. These windows effectively form the third channel. The third channel is nonlinear and parallel to the c axis with dimensions of 5.6 x 5.6 Å [Higgins *et al.*, 1988]. The tortuosity of the third channel is determined by the stacking sequence of the different kinds of layers forming in the zeolite.

The crystal structure of zeolite Beta is tetragonal with a unit cell of dimensions: a = 12.6 Å, b = 12.6 Å and c = 26.2 Å [Szostak, 1992]. The chemical composition of the sodium form is given by $Na_n[Si_{64-n}Al_nO_{128}]$ ($n \leq 7$), i.e. SiO_2/Al_2O_3 molar ratios ≥ 16. Zeolite Beta has a framework density of 15.1 T atoms per 1000 Å^3.

2.1.1.3 Zeolite Mordenite

The pores of zeolite Mordenite consist of two types of parallel elliptical channels (a "bunch of straws") with free apertures of 6.5 x 7.0 Å (defined by 12 membered rings) and 2.6 x 5.7 Å (defined by 8 membered rings) [Meier and Olson, 1996]. These two channels are interlinked by a small transversal sinusoidal channel of 3.4 x 4.8 Å (defined by 8 membered rings). This crossing channel forms 8 membered ring openings in the lining of the 12 membered ring channels, but the corresponding openings in adjacent 12 membered ring channels are displaced with respect to one another. So only very limited access from one 12 membered ring channel to the next is possible as these openings are too small to allow passage to most molecules. Consequently, the channel system is effectively rendered one-dimensional [McCusker and Baerlocher, 2001]. Effectively, these 8 membered ring openings in the lining of the 12 membered ring channels appear as "side pockets" [Breck, 1974a; Venuto, 1994].

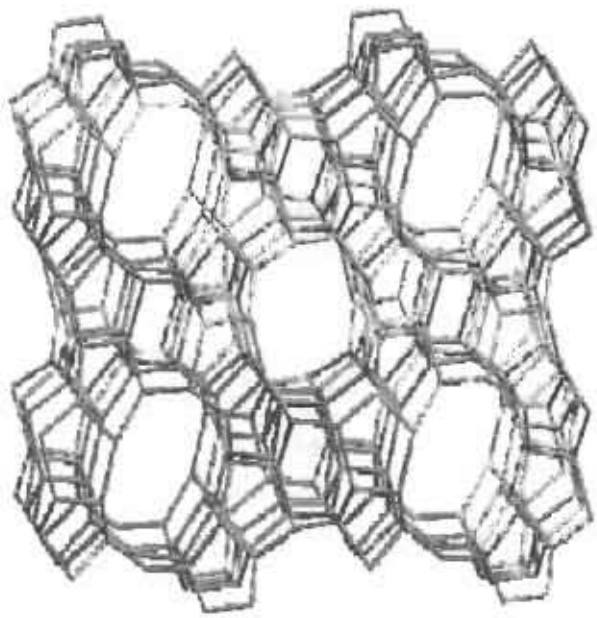

(a) Framework view along (010)

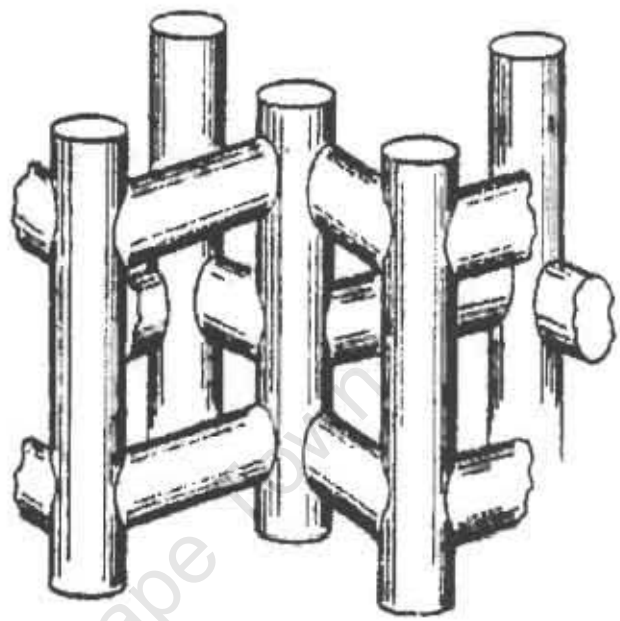

(b) Schematic representation of the pore system

(c) Channel along (010) (5.3 x 5.6 Å)

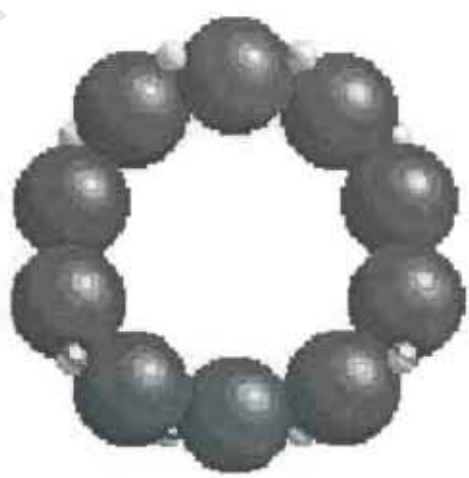

(d) Channel along (100) (5.1 x 5.5 Å)

Figure 2.2: The framework structure and pore openings of zeolite ZSM-5 (MFI) (large black spheres = oxygen, small grey spheres = T atom) [IZA, 2002a] (a), (c) and (d); [Meier *et al.*, 1978] (b).

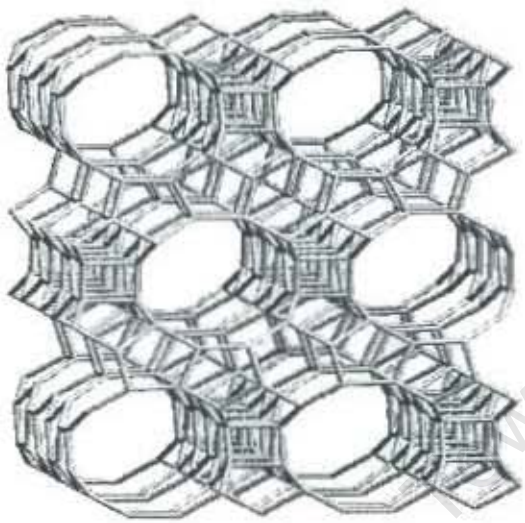

(a) Framework view along (100)

(b) Channels along (100), (010) (6.6 x 6.7 Å)

(c) Channel along (001) (5.6 x 5.6 Å)

Figure 2.3: The framework structure and pore openings of zeolite Beta (BEA) (large black spheres = oxygen, small grey spheres = T atom) [IZA, 2002a].

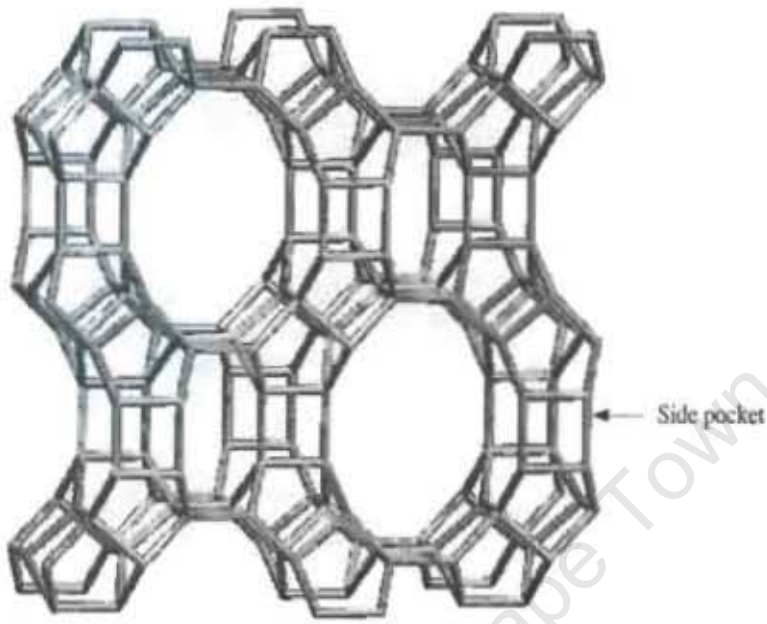

(a) Framework view along (001)

(b) Channel along (001) (6.5 x 7.0 Å)

(c) 8-Ring channel along (010), which forms the "side pockets" (3.4 x 4.8 Å)

Figure 2.4: The framework structure and pore openings of zeolite Mordenite (MOR) (large black spheres = oxygen, small grey spheres = T atom) [IZA, 2002a].

The dimensions of these "side pockets" are 2.9 x 5.7 Å and they are separated by restrictions of 2.8 Å [Breck, 1974a]. Figure 2.4 shows the framework structure of Mordenite.

Mordenite has a crystal structure that is orthorhombic with a unit cell of the dimensions: a = 18.3 Å, b = 20.5 Å, c = 7.5 Å [Szostak, 1992]. The general chemical composition of the sodium form is given by $Na_n[Si_{48-n}Al_nO_{96}]$ ($n \leq 8$), i.e. SiO_2/Al_2O_3 molar ratios ≥ 10. Zeolite Mordenite has a framework density of 17.2 T atoms per 1000 Å^3.

2.1.1.4 Zeolite Y

Zeolite Y has a channel system consisting of a very open, three dimensional network of sodalite cages that are linked together via their hexagonal faces by hexagonal prisms (Figure 2.5). This produces the so-called supercages of roughly spherical dimensions with a diameter of 11.4 Å [Venuto, 1994] with four 12 membered ring openings ("windows") of 7.4 Å [Baerlocher *et al.*, 2001], which are orientated in tetrahedral directions. Thus, the channel system is three dimensional and three dimensionally interconnected. The sodalite cages and the hexagonal prisms make up a small channel system (6 membered ring windows) that gives access to only very small molecules such as water and ammonia and is irrelevant for catalytic conversions of organic molecules.

The crystal structure is cubic with a unit cell of the dimensions: a = 24.3 Å, b = 24.3 Å and c = 24.3 Å [Szostak, 1992]. The chemical composition of the sodium form is given by $Na_n[Si_{192-n}Al_nO_{384}]$ ($n \leq 58$), i.e. SiO_2/Al_2O_3 molar ratios ≥ 4.6. Zeolite Y has a framework density of 12.7 T atoms per 1000 Å^3.

Zeolite Y is often subjected to post-synthesis hydrothermal modification, particularly for industrial applications (catalytic cracking) [Flanigen, 1991]. The modification gives rise to a reduced framework aluminium content, a mesopore system and/or non-framework aluminium species [Naber *et al.*, 1994]. This modified zeolite Y is termed "ultra-stable" (USY). Details of this zeolite Y modification are described in Section 2.1.4.

2.1.1.5 Zeolite MCM-22

Zeolite MCM-22's pore system consists of two independent channel systems (Figure 2.6). One comprises of large supercages whose inner free diameter is defined by 12 membered rings (7.1 Å) and the inner height is 18.2 Å [Leonowicz *et al.*, 1994]. But importantly, these supercages can only be accessed through 10 membered ring openings on the side (Figure 2.6 (b), (d) and (e)). The dimensions of these 10 membered ring openings ("windows") are 4.0 x 5.5 Å [Baerlocher *et al.*, 2001; IZA, 2002a]. The supercages are separated lengthwise through a "neck", made by a 6 membered ring prism.

The smaller, straight channels (4.0 x 5.5 Å) extend in three directions in a plane with 60° angles between each other. These channels cross at the supercages. The wider, sinusoidal channels also extend in three directions in a plane, which is parallel to the former and are interlinked as well.

This second channel is a two-dimensionally interlinked 10-membered ring sinusoidal channel with dimensions of 4.1 x 5.1 Å [Baerlocher *et al.*, 2001; IZA, 2002a]. This channel system extends planar like a honeycomb structure as shown in Figure 2.6 (f) [Lawton *et al.*, 1998]. The "neck" between the

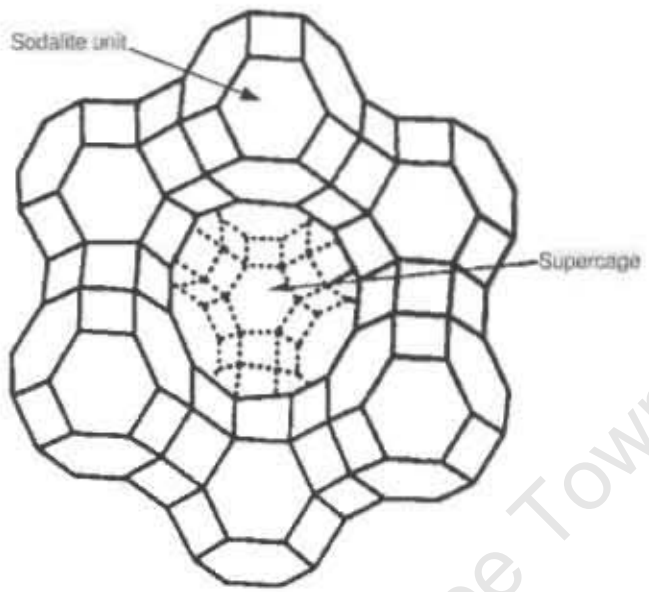

(a) Framework view

(b) Pore openings (7.4 x 7.4 Å)

Figure 2.5: The framework structure and pore openings of zeolite Y (FAU) (large black spheres = oxygen, small grey spheres = T atom) [Augustine, 1995; IZA, 2002a].

supercages extends in the third dimension through the center of these honeycombs without interconnecting with the sinusoidal channels.

Both types of channels are interlinked with themselves but not with each other. Therefore, the combined channel/supercage systems in zeolite MCM-22 only allows diffusion in two directions but not perpendicular to them.

The sequences of lengthwise linked supercages extend perpendicular to the plane in which the channel systems extend. The links, consisting of hexagonal prisms, make up a system of small channels with very narrow 6 membered ring "windows" analogous to the interconnections of the sodalite units in zeolite Y (cf. section 2.1.1.4). These small "windows" only allow the passage of very small molecules such as water and ammonia and are irrelevant for catalytic conversions of organic molecules.

Zeolite MCM-22 crystallizes in very thin platelets. These platelets exhibit hexagonal morphology [Lawton *et al.*, 1998]. Access from the crystal exterior to the internal channels is only possible through the 10 membered ring openings of the two pore systems located at the perimeter of the thin edges of the crystals.

On the face of the thin platelets, there exists a high concentration of zeolitic pockets (often referred to as "cups" [Corma *et al.*, 2000]), with 12 membered ring openings, having a diameter of 7.1 x 7.1 Å and an approximate depth of 7 Å [Lawton *et al.*, 1998]. These "cups" are made up of half a supercage (cf. top edge of Figure 2.6 (b)). There is no access from the bottom of a "cup" to the adjacent supercage and correspondingly there is no access to the pore system through the top and bottom surface of the crystal platelets [Lawton *et al.*, 1998]. However, the "cups" can accommodate quite bulky molecules which are not able to penetrate the pore system.

The crystal structure is hexagonal with unit cell dimensions of: a = 14.4 Å, b = 14.4 Å, c = 25.2 Å [Szostak, 1992]. The chemical composition of the sodium form is given by $Na_n[Si_{72-n}Al_nO_{144}]$ ($n \leq 5.5$), i.e. SiO_2/Al_2O_3 molar ratios ≥ 24. Zeolite MCM-22 has a framework density of 16.5 T atoms per 1000 Å^3. Zeolites SSZ-25, ERB-1, PSH-3 and ITQ-1 are isostructures of zeolite MCM-22 [Baerlocher *et al.*, 2001].

2.1.1.6 Comparison of the zeolite structures studied

The structural parameters of the zeolites studied in this thesis are compared in Table 2.2.

2.1.2 Zeolite synthesis

Natural zeolites are found in cavities in basic volcanic or metamorphic rocks. Although natural zeolites have many applications they are not suited for catalysts as they contain impurities and are too scattered in location for any large scale exploitation [Barrer, 1982a]. Inconsistent quality is another decisive shortcoming of such natural materials [Barrer, 1982b].

Synthetic zeolites are made hydrothermally under autogeneous pressure. The hydrothermal synthesis of aluminosilicate zeolites corresponds to the conversion of a mixture of silicon and aluminium compounds, alkali metal cations, organic molecules and water via an alkaline supersaturated solution into a microporous crystalline aluminosilicate as depicted in Figure 2.7 [Feijen *et al.*, 1997]. Common silica sources are colloidal silica, waterglass, pyrogenic silica or silicon alkoxides (such as tetramethyl

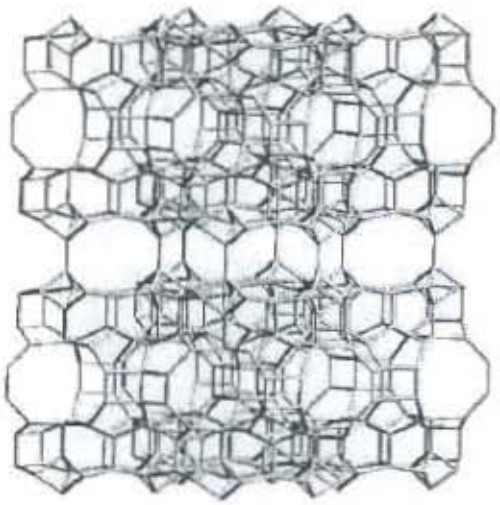

(a) Framework view along (001)

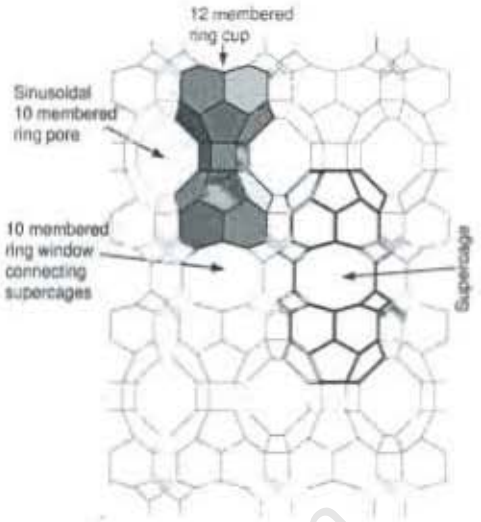

(b) Schematic representation of framework

(c) Sinusoidal channel (4.1 x 5.1 Å)

(d) Supercage opening, straight channel (4.0 x 5.5 Å)

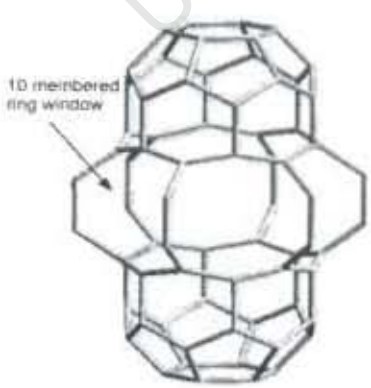

(e) Supercage connecting straight channels (7.1 x 7.1 x 18.2 Å)

(f) Sinusoidal channel system

Figure 2.6: The framework structure, pore openings and pore system of zeolite MCM-22 (MWW) (large black spheres = oxygen, small grey spheres = T atom) [IZA, 2002a] (a), (c) to (e) [Juttu and Lobo, 2000] (b) [Lawton *et al.*, 1998] (f).

Zeolite	ZSM-5	Beta	Mordenite	Y	MCM-22
Channel system	2 intersecting ellipsoidal channels, effectively three-dimensional	3 intersecting almost circular channels, three-dimensional	Parallel elliptical channels with side pockets, formed by intersecting channels, effectively one-dimensional	Network of supercages, interlinked via circular "windows", three-dimensional	Two independent channel systems 1: supercages interlinked by ellipsoidal channels two-dimensional 2: ellipsoidal channels, two-dimensional
Ring size of channels	10-10	12-12-12	12-8-8	12-12-12	10-10
Channel size (Å)	5.3 x 5.6 (sinusoidal) 5.1 x 5.5 (linear)	5.6 x 6.7 (linear) 6.6 x 6.7 (linear) 5.6 x 5.6 (non-linear)	6.5 x 7.0 (12 membered ring, linear) 2.6 x 5.7 (8 membered ring, linear) 3.4 x 4.8 (8 membered ring, highly staggered) (forming the side pockets)	7.4	4.0 x 5.5 (supercage window, linear) 4.1 x 5.1 (sinusoidal)
Intersecting cavity/supercage diameter (Å)	9		side pockets 2.9 x 5.7	11.4	7.1 x 7.1 x 18.2
Unit cell dimensions (Å)	a = 20.1 b = 19.9 c = 13.4	a = 12.6 b = 12.6 c = 26.2	a = 18.3 b = 20.5 c = 7.5	a = 24.3 b = 24.3 c = 24.3	a = 14.4 b = 14.4 c = 25.2
Chemical composition	$Na_n[Si_{96-n}Al_nO_{192}]$ ($n \leq 8$)	$Na_n[Si_{64-n}Al_nO_{128}]$ ($n \leq 7$)	$Na_n[Si_{48-n}Al_nO_{96}]$ ($n \leq 8$)	$Na_n[Si_{192-n}Al_nO_{384}]$ ($n \leq 58$)	$Na_n[Si_{72-n}Al_nO_{144}]$ ($n \leq 5.5$)
Minimum SiO_2/Al_2O_3 molar ratio	22	16	10	4.6	24
Framework density (T atoms per 1000 $Å^3$)	17.9	15.1	17.2	12.7	16.5

Table 2.2: Structure parameters of the zeolites used in this study.

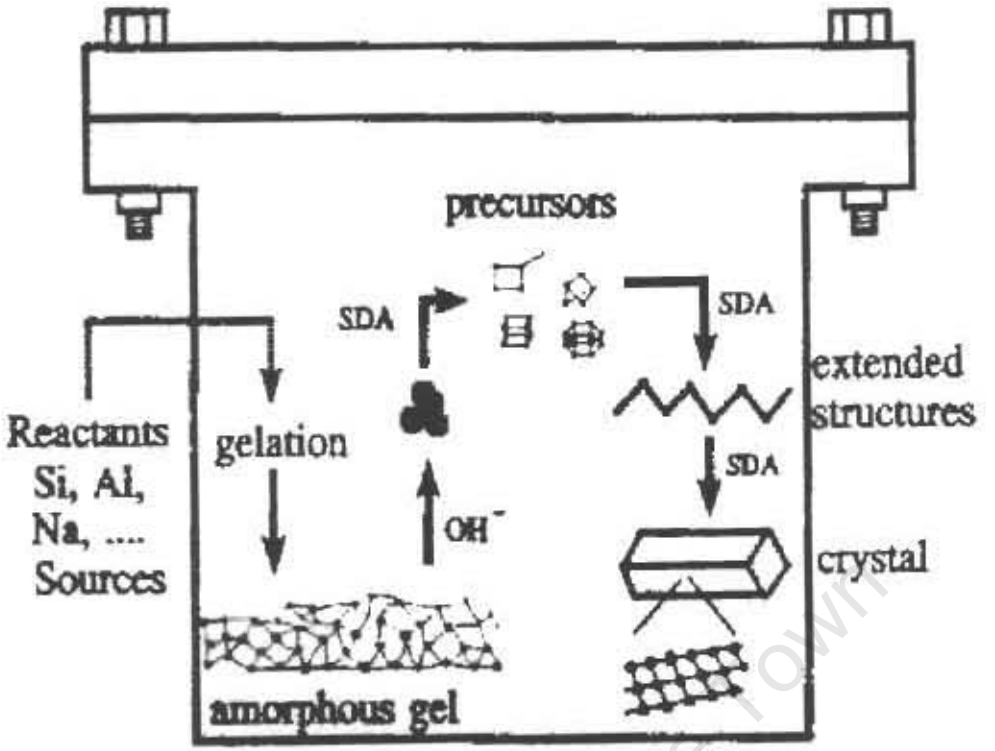

Figure 2.7: Schematic representation of the zeolite formation process (SDA = structure directing agent, otherwise known as the template) [Feijen *et al.*, 1997].

or tetraethyl orthosilicate). These silica sources differ in the degree of polymerization of the silicon dioxide. Aluminium sources are gibbsite, pseudo-boehmite, aluminate salts or the metal powder. Cationic or neutral organic molecules are added to the synthesis gel as solvents or structure directing agents (commonly known as a template). Examples of templates are hexamethyleneimine for zeolite MCM-22, tetraethylammonium hydroxide for zeolite Beta and tetrapropyl ammonium hydroxide for zeolite ZSM-5 synthesis [IZA, 2002b]. The alkalinity of the synthesis gel may be controlled by addition of a mineralizing agent, for example sodium hydroxide.

A mixture of the silica source, aluminium source, template and mineralizing agent rapidly forms a hydrogel or precipitate. Often the hydrogel must be aged, at room temperature or slightly higher temperatures, to increase the concentration of precursor species in the hydrogel. This aging of the gel is often crucial to obtaining the desired crystalline phase and to improve or accelerate crystallization [Jansen and Wilson, 2001].

The crystallization process consists of the dissolution of the hydrogel, mediated by a mineralizing agent, which provides the solution with silicate and aluminate monomers and oligomers. These monomers and oligomers condense into specific precursor structures, which are then organised into more extended structures and finally into the crystalline phase [Feijen *et al.*, 1997]. To start the synthesis, the hydrogel is brought to crystallization temperature, between 60 and 200°C (under autogeneous pressure), and left for a period of time to achieve an acceptable yield of crystals [Jansen and Wilson, 2001].

After a sufficient yield of the crystals is obtained, they are separated from the mother liquor by filtration or centrifugation. The zeolite crystals are then washed to remove excess unreacted reagents

and dried at around 100 - 120°C. This form of the zeolite is know as the "as-synthesized" zeolite. The zeolite contains both cations and the organic template, which are blocking the zeolite pores. The organic template is removed from the zeolite by thermal treatment in air, typically at around 500°C. The cations are then removed by repeated ion-exchange by a mineral acid or an ammonium salt solution (most commonly used is ammonium hydroxide). This salt replaces the cations with ammonium ions. Under thermal treatment, typically around 500°C, ammonia is released from the zeolite leaving a proton. The zeolite is now active for acid catalysed reaction and is commonly written as "H-zeolite".

2.1.2.1 Factors influencing zeolite crystallization

Factors that can influence zeolite crystallization are:

- Composition of the synthesis gel. Namely,
  - the SiO_2 and Al_2O_3 sources, ratios and concentrations;
  - OH^- concentration;
  - cations or anions present in the gel;
  - water concentration;
  - type of organic template.
- Synthesis time.
- Synthesis temperature.
- History of the synthesis gel, for example,
  - order of adding the synthesis reagents to the synthesis mixture;
  - gel aging;
  - stirring.

The influence of the synthesis gel composition varies according to the zeolite structure. For example, zeolite A and high Al faujasite only crystallize in a very narrow range of SiO_2/Al_2O_3 ratio, whereas zeolite ZSM-5 is known to crystallize over a very broad SiO_2/Al_2O_3 range including aluminium free synthesis (silicalite) [Szostak, 1992; Nagy *et al.*, 1998c]. The alkalinity of the synthesis gel is also of key importance in the zeolite synthesis. The role of the OH^- ions is to depolymerize the amorphous aluminosilicate particulates at an appropriate rate. The alkalinity has an impact on the crystallization process, on the SiO_2/Al_2O_3 ratio of the zeolite phase and also on the size of the final zeolite crystals [Feijen *et al.*, 1997].

The roles of the organic templates are [Nagy *et al.*, 1998c]:

- structure-directing - defining the zeolite phase formed;
- gel modifier - could allow the formation of structures with higher SiO_2/Al_2O_3 ratio than could be obtained without such additives;
- interact chemically with the gel - altering the character of the gel (for example alkalinity);
- interact physically with the gel - modifying the solubility of various species, the transport properties etc;
- void filler.

The crystallization of a zeolite usually follows a crystallization curve (crystallinity as defined by powder X-ray diffraction). A desired zeolitic species is often a metastable product, that can undergo re-dissolution, while a more stable species is formed. Therefore, synthesis times are important criteria to obtain a pure crystalline phase [Nagy *et al.*, 1998c].

The synthesis temperature can determine the zeolite phase formed. A higher synthesis temperature may favour a more dense zeolitic phase. Synthesis temperature also affects the crystallization kinetics. Higher temperature may result in shorter induction periods or a metastable species may decompose faster at a higher temperature [Nagy *et al.*, 1998c].

The history of the zeolite synthesis mixture (order of adding of the synthesis reagents, gel aging, stirring, etc.) can result in different crystallization kinetics, modification of crystal compositions or even the formation of a completely different zeolitic phase [Nagy *et al.*, 1998c].

2.1.2.2 Synthesis of zeolites MCM-22, ZSM-5, Beta, Mordenite and USY

Commercial samples of zeolites ZSM-5, Beta, Mordenite and USY were used in this research whereas several samples of zeolite MCM-22 were synthesized by the author. Therefore, the synthesis of zeolite MCM-22 is described in detail in the following section whereas the syntheses of zeolites ZSM-5, Beta, Y and Mordenite are only briefly described.

2.1.2.2.1 Synthesis of zeolite MCM-22 Table 2.3 shows the different reagents used in the synthesis of zeolite MCM-22. Hexamethyleneimine (shown in Figure 2.8 (a)) is used as the template in most synthesis mixtures for the formation of zeolite MCM-22 as it is a readily commercially available organic compound [Ernst, 1998]. N,N,N-trimethyl-1-adamantammomium hydroxide (shown in Figure 2.8 (b)) is used as the template for the SSZ-25, which is an isostructure of MCM-22. Table 2.4 gives the molar regimes from which zeolite MCM-22 has been synthesized as well as the synthesis temperatures and synthesis times.

Typically, MCM-22 crystals are disk shaped with diameters around 1 μm and a thickness which is somewhat less or far less than the diameter (cf. Table 2.5). These disk-like crystals are frequently intergrown with each other [Ernst, 1998]. No comprehensive study of the effect of different synthesis conditions and gel molar regimes has been carried out in terms of crystal size of zeolite MCM-22. However, Güray *et al.* [1999] found that the crystallization rate was higher and the final crystal size

Table 2.3: Typical synthesis reagents used in the synthesis of zeolite MCM-22. The template used throughout was hexamethyleneimine.

	Silica source	Alumina source	Mineralizing agent
Juttu and Lobo [2000]	Ultrasil	Sodium aluminate	Sodium hydroxide
Güray *et al.* [1999]	Silicic acid, silica gel Ultrasil	Sodium aluminate	Sodium hydroxide
Corma *et al.* [1995]	Aerosil 200	Sodium aluminate	Sodium hydroxide
Hunger *et al.* [1995]	Fumed silica	Sodium aluminate	Sodium hydroxide/ Sulphuric acid
Ravishankar *et al.* [1995]	Colloidal silica	Aluminium sulphate	Sulphuric acid
Rubin and Chu [1990]	Ultrasil, precipitated silica	Sodium aluminate	Sodium hydroxide

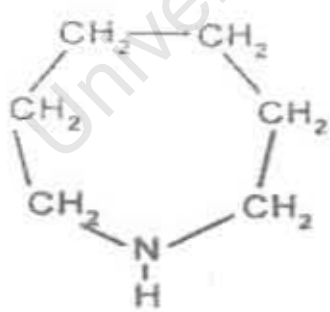

(a) Hexamethyleneimine

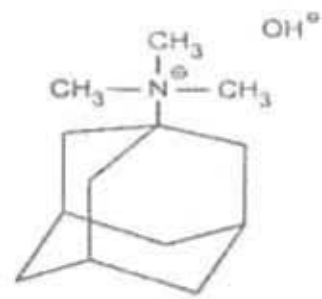

(b) N,N,N-trimethyl-1-adamantammonium hydroxide

Figure 2.8: Organic templates used in the synthesis of zeolite MCM-22 (a) and isostructural zeolite SSZ-25 (b) [Ernst, 1998].

Table 2.4: Molar regimes of the synthesis mixtures and synthesis conditions used for the synthesis of zeolite MCM-22 (silicon and aluminium sources, cf. Table 2.3).

	SiO_2/ Al_2O_3	Na^+/ SiO_2	HMI***/ SiO_2	H_2O/ SiO_2	Synthesis temperature (°C)	Synthesis time (days)
Güray *et al.* [1999]	15 - 80	0.18	0.35	19.5	150	7 - 20
Corma *et al.* [1995]	30 -200	0.14 - 0.3	0.35 - 0.5	35 - 45	135 - 150	7 - 28
Hunger *et al.* [1995]*	32.2	0.41	0.32	10.3	150	12
Ravishankar *et al.* [1995]**	29.8	0.17	0.5	45.9	150	3.3
Rubin and Chu [1990]	30	0.18	0.35	44.9	150	7

* $H_2SO_4/SiO_2 = 0.007$
** $H_2SO_4/SiO_2 = 0.18$
*** Hexamethyleneimine

Table 2.5: Crystal sizes obtained from zeolite MCM-22 syntheses.

	Agitation	Crystal diameter (μm)	Crystal thickness (μm)
Güray *et al.* [1999]	Yes	1 - 2	< 1
	No	3 - 5	1 - 1.5
Hunger *et al.* [1995]	Yes	< 1	ca. 0.1
Ravishankar *et al.* [1995]	Yes	1 - 2	0.1 - 0.2
Lawton *et al.* [1998]*	Yes	1	0.01

* Lawton *et al.* [1998] using Rubin and Chu's [1990] synthesis method.

was smaller in syntheses carried out under stirred synthesis conditions, viz. crystal diameters of 1 - 2 μm and thickness < 1 μm for stirred synthesis and crystal diameters of 3 - 5 μm with thickness of 1 - 1.5 μm for static synthesis (cf. Table 2.5).

The X-ray diffraction patterns of pure, as synthesized and calcined Na-MCM-22 obtained from Ernst [1998] are shown in Figure 2.9. The recorded X-ray diffraction patterns show both sharp and broad peaks, that indicates structural disorder [Ernst, 1998].

2.1.2.2.2 Synthesis of zeolite ZSM-5 A recent review of zeolite ZSM-5 synthesis procedures can be found in Guth and Kessler [1999]. Zeolite ZSM-5 has been synthesized over a wide range of SiO_2/Al_2O_3 ratios starting from 22, which is the minimum molar ratio to that of pure silica "silicalite" [Szostak, 1992]. Zeolite ZSM-5 can be synthesized using a wide range of templates as well as without any template [Narayanan *et al.*, 1998]. Templates used are, for example, tetrapropylammonium hydroxide, tetraproplyammonium bromide [Narayanan *et al.*, 1998], dipropylenetriamine and hexanediol [Barrer, 1985]. Zeolite ZSM-5 can crystallize from batch compositions $(NaAlO_2)_n[Na_mH_{4-m}SiO_4] \cdot pH_2O$ typically in the range n = 20 to 50, m = 0.1 to 0.2 and p = 400 to 500 [IZA, 2002b]. For good yields of ZSM-5 crystal the synthesis temperature should be between 145 and 190°C [IZA, 2002b].

2.1.2.2.3 Synthesis of zeolite Beta The most common template used in the synthesis of zeolite Beta is tetraethylammonium hydroxide (TEAOH) [Zaiku *et al.*, 2001]. Zeolite Beta is claimed

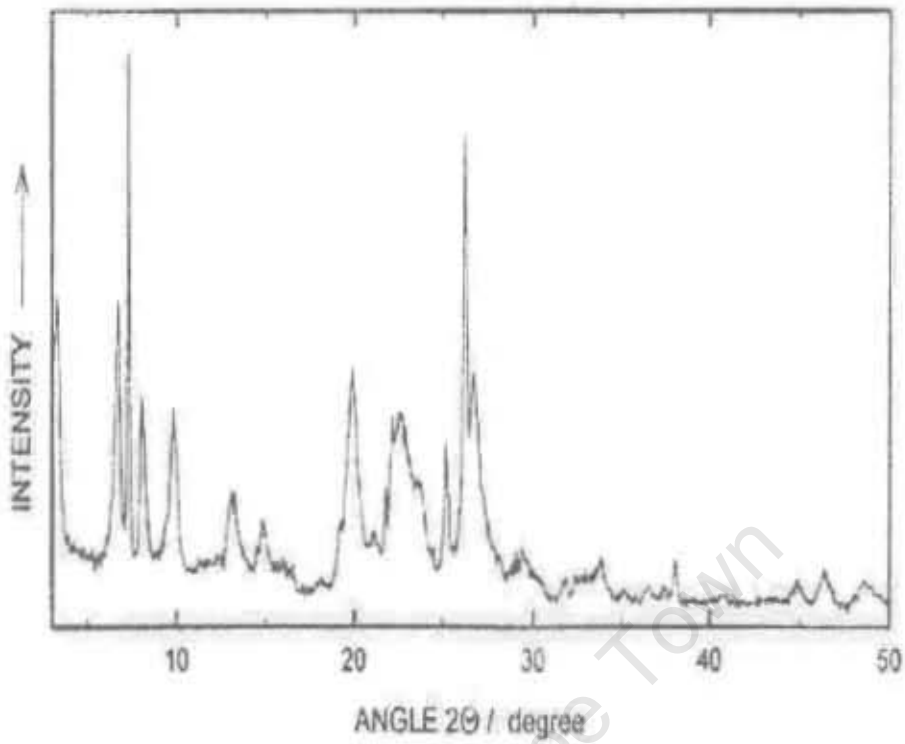

(a) As-synthesized MCM-22

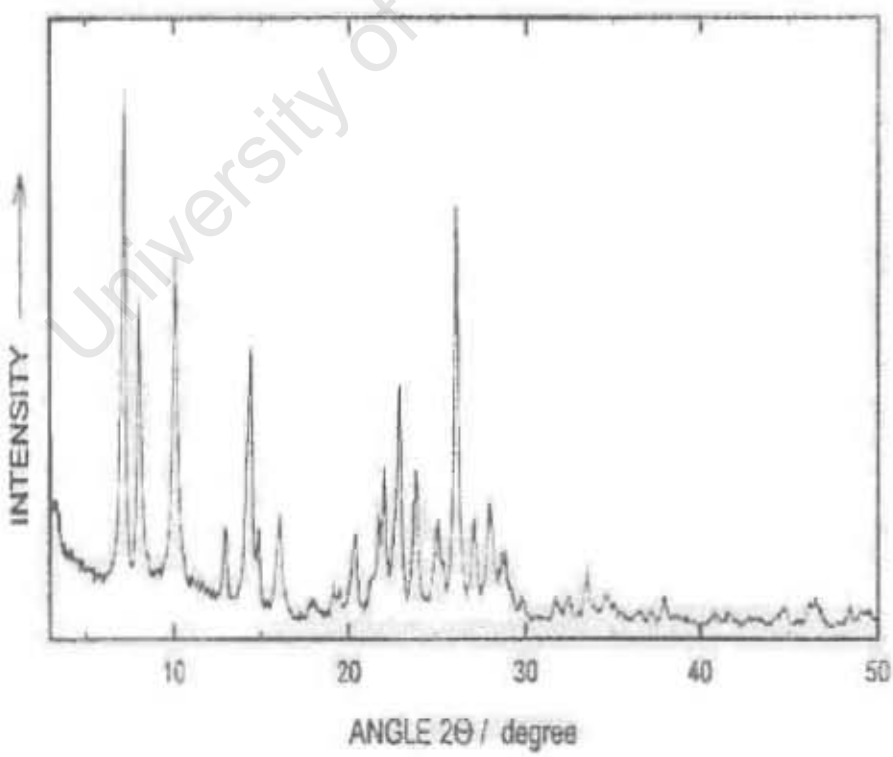

(b) Calcined, template free MCM-22

Figure 2.9: X-ray diffraction pattern of as-synthesized Na/HMI-MCM-22 (contains both cations and template) and calcined Na-MCM-22 [Ernst, 1998].

to crystallize from batch compositions in the range of molar ratios of SiO_2/Al_2O_3 from 10 to 200, Na_2O/TEAOH from 0 to 1.0, TEAOH/SiO_2 from 0.1 to 1.0 and H_2O/TEAOH from 20 to 75. Crystallization occurs between 100 and 150°C [Szostak, 1992]. Zeolite Beta can be synthesized over a wide range of SiO_2/Al_2O_3 ratios starting from the minimum molar ratio of 16.

2.1.2.2.4 Synthesis of zeolite Mordenite A recent review of zeolite Mordenite synthesis procedures can be found in Guth and Kessler [1999]. A range of templates was also used in the synthesis of zeolite Mordenite. For example, benzene-1,2-diol [Shao *et al.*, 2002], 1-butanol [Sano *et al.*, 2001], hexamethyleneimine [Jongkind *et al.*, 1997], tetraethylammonium bromide [Coker *et al.*, 1995], benzyltrimethylammonium salts, alkyl phenols, alkyl sulfonates, N-ethylpyridinium salts and trioctylamine [Szostak, 1992]. Catalytically active zeolite Mordenite is synthesized in the range of batch molar compositions of 10 Na_2O : 0.075 - 0.4 Al_2O_3 : 28 - 40 SiO_2 : 360 H_2O. Mordenite crystallizes between 100 and 260°C [Breck, 1974b; Szostak, 1992]. High SiO_2/Al_2O_3 ratio Mordenite is obtained via post-synthesis dealumination, as described in Section 2.1.4.

2.1.2.2.5 Synthesis of zeolite Y A recent review of zeolite Y synthesis procedures can be found in Guth and Kessler [1999]. Zeolite Y is claimed to crystallize from batch compositions in the ranges of SiO_2/Al_2O_3 from 15 to 25, Na_2O/H_2O from 20 to 50, Na_2O/SiO_2 from 0.4 to 0.6. Tetramethylammonium hydroxide and sodium salts are used as the template for zeolite Y [IZA, 2002b]. Crystallization occurs between 80 and 125°C [Szostak, 1992]. Zeolite Y can only be directly synthesized with a low SiO_2/Al_2O_3 ratio around 5 and is therefore often subjected to post-synthesis dealumination [Flanigen, 1991; Naber *et al.*, 1994]. Procedures for post-synthesis dealumination are described in Section 2.1.4.

2.1.3 Acidity of zeolites

Zeolite framework structures are based on an infinitely extending three-dimensional network of SiO_4 and AlO_4 tetrahedra (primary building units) thereby sharing all the oxygen atoms. The charge imbalance of the tetrahedrally coordinated, trivalent aluminium atoms (Al^{3+}) results in a net negative charge on the zeolite framework. This is compensated by a charge balancing cation or proton. The proton constitutes an acid site in the zeolite framework. The acidity of a zeolite is a function of the nature, strength and density of the acid sites respectively. The nature of the acid sites in zeolites is either Brønsted or Lewis acid sites. Such an acid site is able to either transfer a proton from the solid to the adsorbed molecule (Brønsted acidity) or an electron pair from the adsorbed molecule to the solid surface (Lewis acidity) [Nagy *et al.*, 1998a].

A Brønsted acid site is formed when the charge compensating cation is a proton (cf. Figure 2.10). Brønsted acidity is most often generated from ion-exchanging the as-synthesized zeolite, in the sodium form with ammonium after the removal of the template. The acid site can then be formed by removing ammonia via thermal treatment of the ammonium zeolite (shown in Figure 2.11). Theoretically therefore, each aluminium in the framework can generate a Brønsted acid site. However the strength of the Brønsted acid sites is dependent on a number of factors namely, aluminium concentration (i.e. SiO_2/Al_2O_3 ratio) and location and distribution of the aluminium in the overall

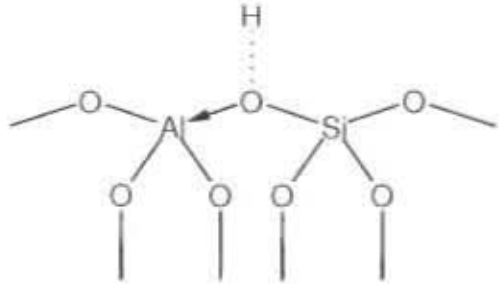

Figure 2.10: The structure of the Brønsted acid site in zeolites [Martens *et al.*, 1997].

Figure 2.11: Formation of Brønsted acid sites from thermal treatment of the ammonium exchanged zeolite [Nagy *et al.*, 1998a].

zeolite framework. In terms of aluminium concentration, as the zeolites framework SiO_2/Al_2O_3 ratio increases, the deprotonation energy decreases, and thus the strength of the Brønsted acid site is seen to increase. High silica zeolites have fewer but stronger acid sites. In terms of aluminium distribution, the strongest acid sites are those associated with the absence of aluminium atoms in the second coordination sphere (next-nearest-neighbour theory) [Mikovsky and Marshall, 1976]. This condition is met for virtually all Brønsted sites in Mordenite with a SiO_2/Al_2O_3 molar ratio larger than 18.4 [Stach and Jänchen, 1992] and zeolite Y with a SiO_2/Al_2O_3 molar ratio larger than 11.2 [Stach *et al.*, 1992].

Lewis acid sites in zeolites can be formed upon dehydroxylation of Brønsted acid sites at elevated temperatures of 500°C and higher, as shown in Figure 2.12 [Nagy *et al.*, 1998a]. In zeolites, Lewis acidity may generally also originate from the presence of extra-framework cations, such as extra-framework aluminium [Karge *et al.*, 1999], charge compensating alkali metal ions, or tricoordinated aluminium and silicon occurring at defect sites in the zeolite [Venuto, 1994; Brunner, 1997]. Strong Lewis acidity appears to be associated with extra-framework alumina, although there is no consensus on the catalytic activity of these acid sites. Weak Lewis acidity appears to originate from charge compensating alkali metal ions (particularly sodium) but does not appear to contribute to the catalytic activity in the catalysis of hydrocarbon reactions [O'Donovan, 1995].

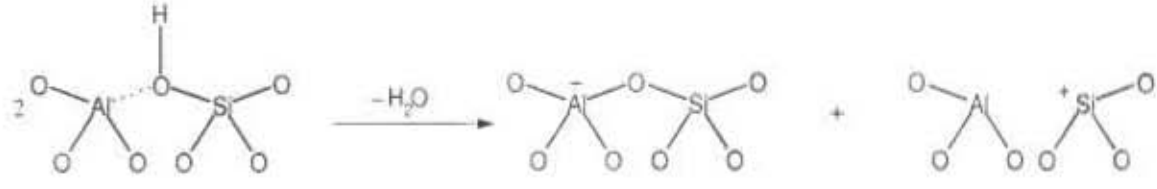

Figure 2.12: Formation of a Lewis acid site from two Brønsted acid sites [Nagy *et al.*, 1998a].

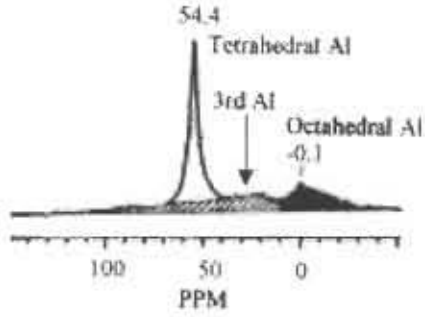

Figure 2.13: ^{27}Al MAS NMR spectrum of steamed H-Beta [Kuehl and Timken, 2000].

2.1.4 Post-synthesis modification of zeolites

Post-synthesis modifications of zeolites are done to improve the activity or stability of a zeolite catalyst or to improve the desired selectivity of a reaction. Special modifications allow one to distinguish between and understand the effects of the internal and external surface on the product selectivity. In the following sections, modifications addressed are steaming and the internally selective ion-exchange of zeolites.

2.1.4.1 Steaming of zeolites

2.1.4.1.1 Procedure for steaming zeolites Dealumination of the zeolite framework usually occurs when the zeolite is subjected to steaming at high temperatures (> 450°C, P_{steam} typically around 0.3 - 0.7 bar for several hours). The degree of dealumination is usually determined by the use of ^{27}Al MAS NMR and ^{1}H MAS NMR (magic angle spinning nuclear magnetic resonance). Framework tetrahedrally coordinated aluminium resonance is in the region of 54 - 68 ppm on a ^{27}Al MAS NMR spectrum [Kennedy *et al.*, 1999]. Steaming the zeolite causes a decrease in the concentration of framework aluminium and an increase in concentration of extra-framework aluminium [Debras *et al.*, 1986]. Different kinds of extra-framework aluminium species were found to correspond to broad peaks around 0 ppm and 30 ppm on a ^{27}Al MAS NMR spectrum namely octahedrally, pentahedrally and tetrahedrally coordinated aluminium, respectively [Gibson *et al.*, 1987; Fernandes *et al.*, 1998; Kuehl and Timken, 2000]. Figure 2.13 shows the ^{27}Al NMR spectrum of steamed H-Beta which illustrates all the aluminium species discussed above. Kuehl and Timken [2000] identified three peaks, namely at 54.4 ppm for tetrahedrally coordinated aluminium, -0.1 ppm for octahedrally coordinated aluminium and a third broad peak with a peak maximum at approximately 30 ppm, which is labelled "3rd Al". These 3rd aluminium species are poorly ordered giving rise to a broad peak and may represent aluminium oxide clusters of variable coordination symmetry [Kuehl and Timken, 2000]. The extra-framework aluminium can be removed from the framework by washing with dilute acids [Szostak, 2001]. Progressive steaming and calcination results in the extra-framework aluminium migrating to the crystal surface as octahedral alumina [Szostak, 2001]. Mesopores are formed during the dealumination process, with diameters ranging from 20 to 250 Å [Nagy *et al.*, 1998d].

2.1.4.1.2 Reactions over steamed zeolites Dealuminated zeolite Y (called ultra-stable zeolite Y, USY) is widely used as a catalytic cracking catalyst [Nagy *et al.*, 1998d]. In fluidized catalytic

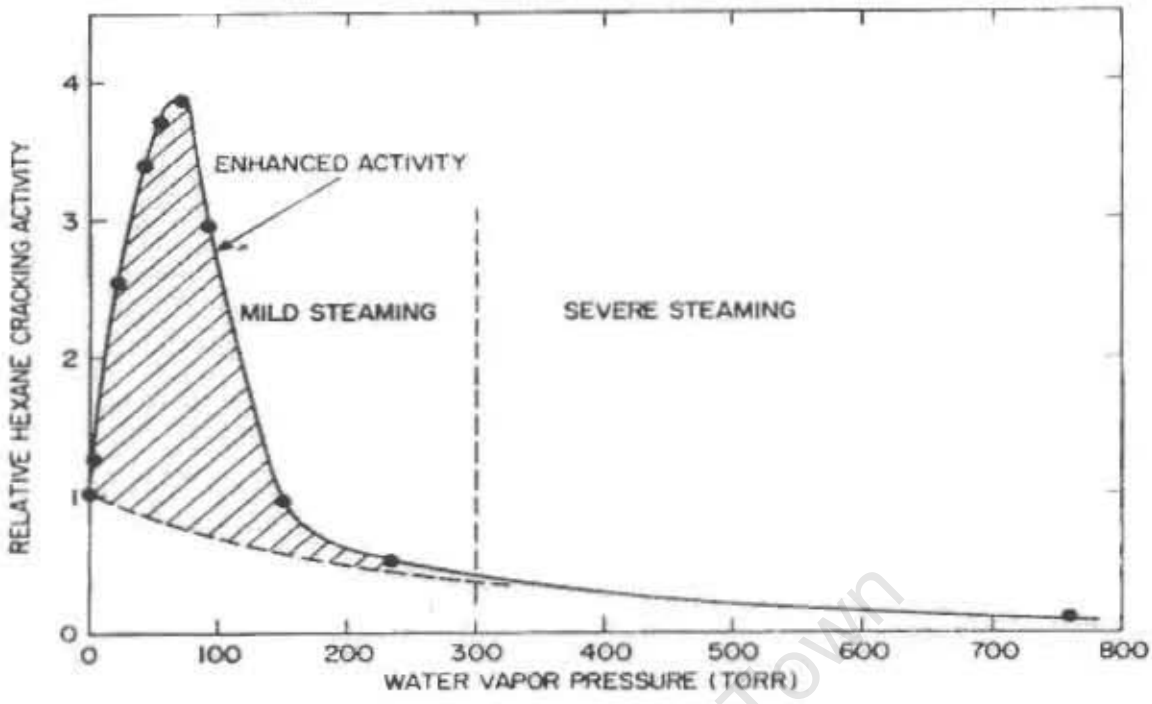

Figure 2.14: Enhanced activity for n-hexane cracking over H-ZSM-5 with steaming (steaming conditions: 2.5 hours at 540°C; n-hexane cracking at 538°C) [Lago *et al.*, 1986].

cracking (FCC), the activity of the catalyst declines during multiple reaction/regeneration cycles. In order to establish unvarying activity, a small percentage of the circulating "equilibrium" catalyst is constantly withdrawn and replaced by fresh catalyst. Therefore, a fluidized catalytic cracker catalyst requires high stability as the long term decline of its activity influences both the activity level of the equilibrium catalyst and the amount of fresh catalyst constantly needed [Halász *et al.*, 1985]. Dealumination leads to zeolite Y being ultra-stable to thermal and hydrothermal strains and also more active towards cracking bulkier molecules, which are larger than Y's channel diameter, in the mesopores formed through steaming.

Mild steaming was often found to increase the catalytic activity of various types of zeolites for hydrocarbon reactions such as isomerization [Haag and Lago, 1983; Nayak and Choudhary, 1984; Hong *et al.*, 1994], alkylation [Corma *et al.*, 1996] and cracking [Haag and Lago, 1983; Lago *et al.*, 1986; Nayak and Choudhary, 1984; Wang *et al.*, 1991; Williams *et al.*, 2000]. However, the activating effect of mild steaming was only observed with carefully made laboratory samples. Commercial samples have undergone such a lot of steaming during manufacturing, that they are already mildly steamed and additional mild steaming has little effect [O'Connor and Haag, 1996].

The enhancement effect of mild steaming of a H-ZSM-5 catalyst on the activity for n-hexane cracking (α-test) is shown in Figure 2.14 [Lago *et al.*, 1986]. Optimum mild steaming resulted in an almost fourfold increase of activity, whereas severe steaming eventually resulted in a decline of activity.

2.1.4.2 Internally selective ion-exchange of zeolites

2.1.4.2.1 Procedure for making internally selective ion-exchanged zeolites

Chester *et al.*

[1998] describe a multi-stage technique of internally selective ion-exchanging the internal acid sites of zeolite MCM-56 crystals with sodium. Firstly, a calcined (i.e. detemplated), as-synthesized Na-zeolite is taken and ion-exchanged with a bulky organic cation (namely, tetrapropylammonium bromide), which is prevented from entering the zeolite pore system due to steric hindrance and therefore only exchanges the Na^+ cations on the external surface sites. The zeolite is then calcined in air, which destroys the organic cation, leaving a proton (analogous to calcining a NH_4-zeolite). Therefore, the crystals have acids sites predominately on the external surface. If Na-zeolite is not available, H-zeolite can be taken, which however, first needs to be ion-exchanged with a sufficiently small cation (namely, a sodium, potassium or cesium cation) which is capable of occupying all the exchangeable sites both internally and externally on the zeolite crystal. Thereafter, the selective ion-exchange is carried out as described above.

2.1.4.2.2 Reactions over selectively ion-exchanged zeolites Juttu and Lobo [2000] applied this internally selective ion-exchange method on zeolites MCM-22 and MCM-56 to determine the reaction pathway of toluene disproportionation over these zeolites. That is, to exclusively study the effect of the zeolite crystal's external acid sites on the reaction pathway and be able to distinguish between internal and external reactions.

2.1.5 Shape-selectivity in zeolites

Controlling the selectivity of a chemical reaction is one of the primary tasks of catalysis. Of increasing importance is shape-selective catalysis. Shape-selectivity effects can occur when the shape and size of the reactants, or products, or transition states or reaction intermediates is similar in dimensions to the pores and cavities of a zeolite [Weitkamp *et al.*, 1999]. Non-shape selective catalysis occurs on the external surface of the zeolite crystallites. There are different classes of shape-selectivity, the most common types are reactant, product and transitions state shape-selectivity. Examples of each of these types of shape selectivity are shown in Figure 2.15.

Reactant shape selectivity is illustrated in Figure 2.15 (a) by the competitive cracking of n-octane and 2,2,4-trimethylpentane (isooctane). 2,2,4-Trimethylpentane is too bulky to enter the pores of the zeolite and is, therefore, hindered from reaching the catalytically active sites inside the pores. However, n-octane can enter the pores and so have access to the acid sites, where it is catalytically converted. Thus the net effect that is measured at the reactor exit is the selective or preferential conversion of the small or slim reactant molecule [Weitkamp and Ernst, 1994].

Product shape selectivity is demonstrated by the ethylation of toluene in Figure 2.15 (b). Here both the reactants are small enough to enter the zeolite pores, but only para-ethyltoluene, out of the potential products (ortho-, meta- and para-ethyltoluene), is small enough to leave the pore system. The bulkier product molecules, although possibly formed in relatively spacious intracrystalline cages or at channel intersections, are either unable to escape from the pores and therefore do not occur in the reactor effluent at all or their diffusion is significantly hindered in the pore system and are therefore present in the reactor effluent with very low selectivity. Ultimately, the bulkier products may be transformed into smaller ones, which are able to escape from the pores, or convert into coke deposits [Weitkamp and Ernst, 1994].

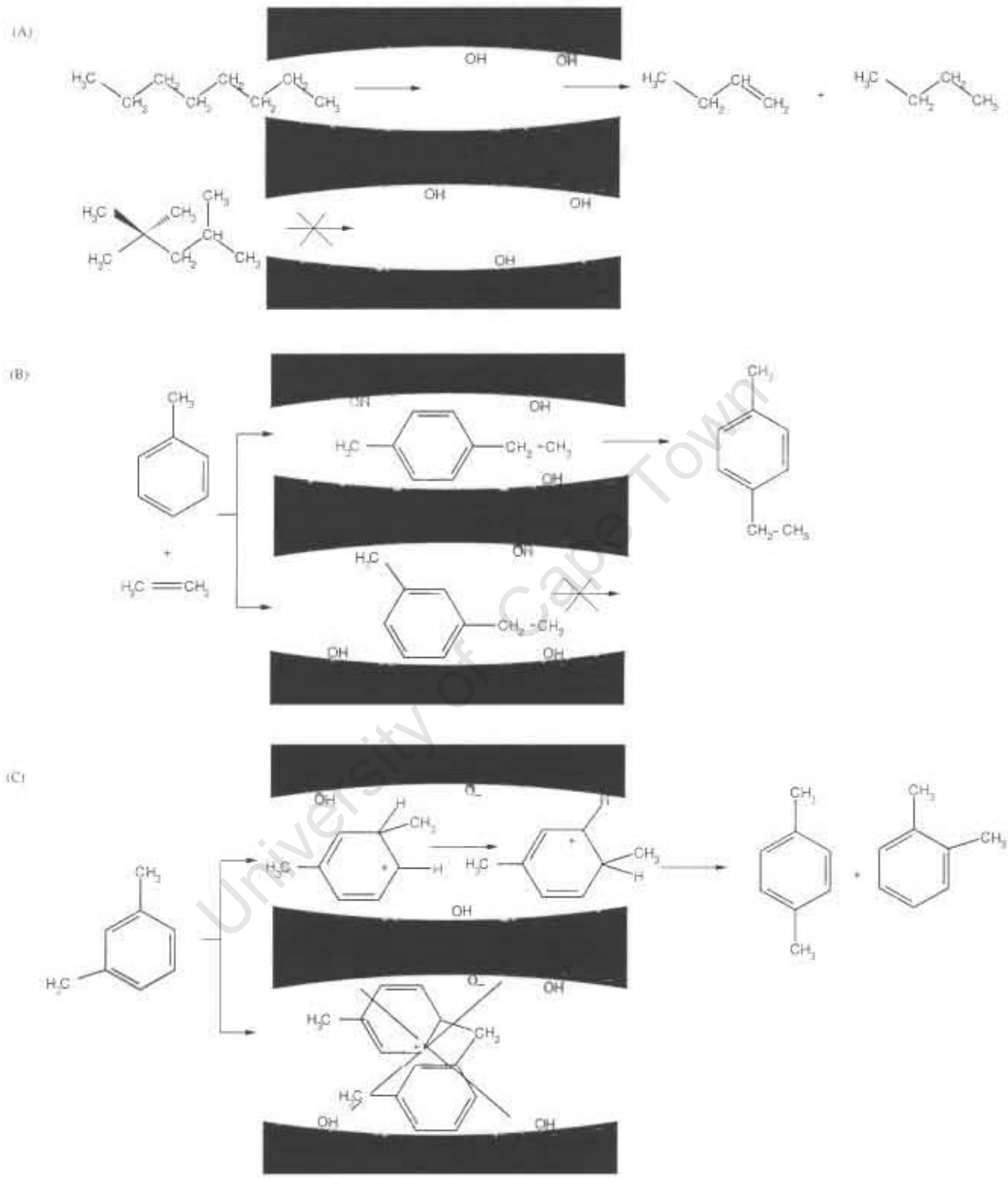

Figure 2.15: Shape selectivity in microporous materials [Weisz, 1980; Csicsery, 1984] (a) Reactant selectivity (e.g. selective cracking of n-paraffins in a n/iso-paraffin mixture) (b) Product selectivity (p-selective toluene ethylation) (c) Restricted transition state selectivity (e.g. selective xylene isomerization with simultaneous transalkylation suppressed).

Restricted transition state shape selectivity is illustrated by meta-xylene isomerization into ortho- and para-xylene and transalkylation into toluene and trimethylbenzenes (Figure 2.15 (c)). Isomerization can occur as a monomolecular reaction via 1,2-shift. Transalkylation of the methyl substituted aromatics is a bimolecular reaction and as such it necessarily proceeds via transition states which are bulkier than with monomolecular isomerization. In a zeolite with the appropriate pore width or void space respectively, there will be just enough space for the accommodation of the transition states for the monomolecular 1,2-shift isomerization reaction, but insufficient space for the formation of the bulky transition states of the bimolecular transalkylation reaction. The net effect is a suppression of the latter reaction [Weitkamp and Ernst, 1994].

Reactant and product shape selectivity is based on the hindered diffusion of bulky reactant or product molecules in the zeolite pores. In many instances, the hindered diffusion just results in a rate of adsorption or desorption and consequently an effective rate of formation of a product which is lower than it would be in the absence of this mass transfer limitation, but which is not zero. In these cases, the observed rates of reaction are limited by diffusional effects, and hence the observed selectivities will depend, under otherwise constant conditions, on the length of the intracrystalline diffusion paths, i.e., the size of the zeolite crystals. By contrast, *restricted transition state shape selectivity* is due to intrinsic effects emerging from the limited space around the intracrystalline active sites and hence the resulting selectivities will not depend on the crystal size [Weitkamp and Ernst, 1994]. The last statement, however, does not consider the possible occurrence of this reaction on active sites on the external surface of the zeolite crystals (cf. Section 2.1.5.1), where space is not limited so that transitional state selectivity won't occur. Since the surface/volume ratio of a crystal depends on its size, size effects on product distributions resulting from restricted transitional state selectivity may still be observed.

In fact, reactant and product shape selectivity are determined by the parameters of the Thiele Modulus. These are the rate constants, the crystal size and the diffusion coefficients of the different molecules. The diffusion coefficients reflect the relationship between the pore size and the critical dimensions of the molecules.

2.1.5.1 Effect of the external surface acid sites

Non-shape selective catalysis occurs on the acid sites situated on the external surface of the zeolite crystals. In all of the above types of shape-selective catalysis, the reactants as well as the products leaving the zeolite pore may react with the acid sites on the external surface therefore reducing the concentration of the shape selective product in the reactor effluent.

2.2 Alkylation of phenol with methanol

The major producers of cresols are the United States, Western Europe, Japan and South Africa. In the United States, Western Europe and Japan, 60% of the cresols produced are synthetic. One of the major routes for the synthetic cresol formation is the alkylation of phenol with methanol [Fiege and Bayer AG, 2001].

Common catalysts used for the alkylation of phenols are H_2SO_4, BF_3, MgO, γ-Al_2O_3 and silica-supported Fe-V [Chakrabarty *et al.*, 1997; Beck and Haag, 1997; Fiege and Bayer AG, 2001]. Zeolites have been investigated for the alkylation of phenols for two reasons. Firstly, they are an environmental friendly alternative to the H_2SO_4 and BF_3 catalysts and secondly, their shape-selective properties can potentially be used to obtain an enhanced selectivity towards a certain product.

The alkylation of phenols is complicated, however, since both C-alkylation (alkylation at the ring carbon atoms) and O-alkylation (alkylation at the oxygen of the hydroxyl group) can occur. A possible reaction scheme of the methylation of phenol is given in Figure 2.16. C-alkylation leads to the formation of cresols (methylphenols) (reaction I) and O-alkylation leads to the formation of anisole (methoxybenzene or methyl phenyl ether) (reaction II). The anisole and cresols formed can also react further. Anisole can be methylated on the ring to from methylanisoles (reaction III), can undergo disproportionation to form methylanisoles and phenol (reaction IV), can be converted to cresols though a reaction with phenol (reaction V) and can undergo internal rearrangement to form o-cresol (reaction VI). Cresols can also undergo C-alkylation to form xylenols (dimethyl phenols) (reaction VII) or undergo O-alkylation to form methylanisoles (reaction VIII). Xylenols and methylanisoles may undergo further alkylation to produce higher alkylated products. Phenol and methanol can also undergo reaction with themselves, forming diphenyl ether (reaction IX) and dimethyl ether (reaction X), respectively. Dimethyl ether, however, is still available as a reactive alkylation agent and thus does not affect product yields (as long as the dimethyl ether does not convert into hydrocarbons).

2.2.1 Chemistry of phenols, alcohols and ethers

An alcohol is an organic compound with a carbon bound to a hydroxyl group for example methanol ($CH_3 - OH$). A phenol is an alcohol consisting of a benzene ring with one of the ring's hydrogens replaced with a hydroxyl group ($C_6H_5 - OH$). The chemistry of alcohols and phenols is determined by the hydroxyl group ($-OH$ group). An ether is a compound in which an oxygen atom is bonded to two alkyl or two aryl groups or one of each (i.e. dimethyl ether, diphenyl ether, anisole, respectively).

Alcohols and phenols are polar molecules as a more electronegative oxygen atom is attached. With alcohols and phenols, intermolecular hydrogen bonding is possible between the positively charged hydrogen on one molecule and the negatively charged oxygen on a neighbouring molecule. This results in higher boiling and melting temperatures for these compounds compared their hydrocarbon equivalents (Table 2.6).

Anisole has a significantly lower melting and boiling point than cresols as no hydrogen bonding is possible between anisole molecules. Minor polarity is introduced due to the non-symmetrical

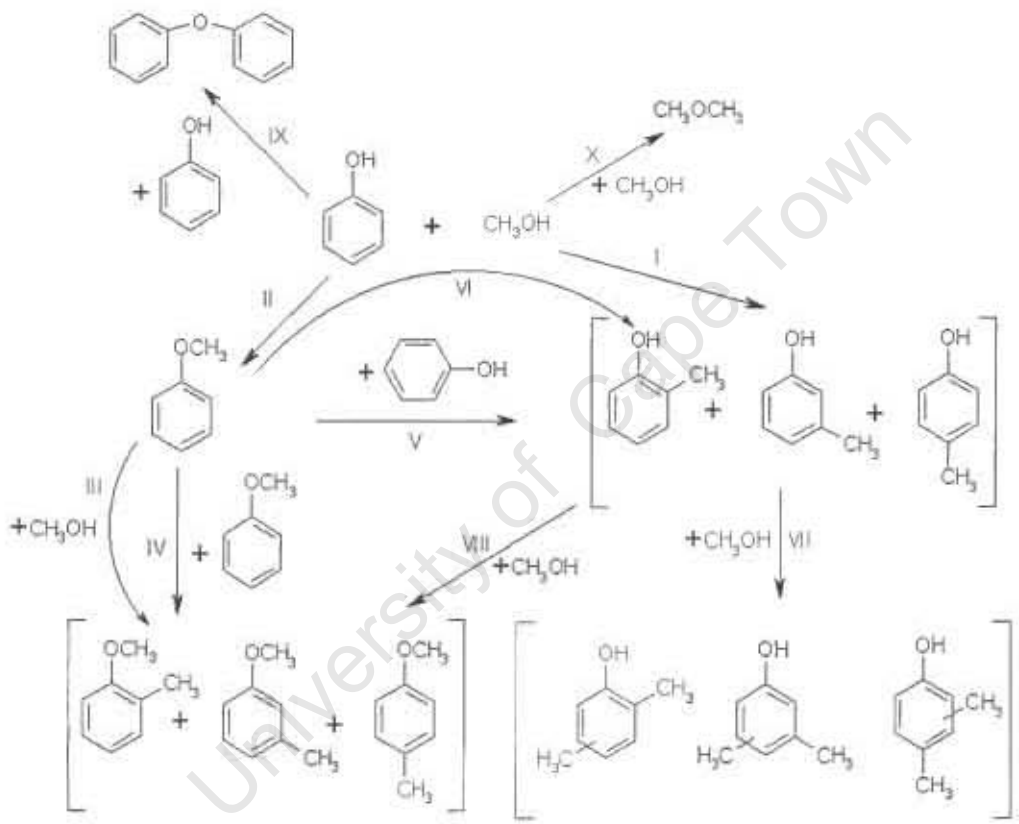

Figure 2.16: Possible reaction scheme for the methylation of phenol. Co-products water (reaction I - III and VII - X) and phenol (reactions IV and V) are not included.

Table 2.6: The physical properties of methanol, phenol, cresols and anisole and their hydrocarbon analogs [Weast, 1991].

	Melting point (°C)	Boiling point (°C)
Methanol	-93.9	65.0
Ethane	-182	-164
Phenol	43.0	181.7
Toluene	-95	110.6
o-Cresol	30.9	191.0
p-Cresol	34.8	201.9
m-Cresol	11.5	202.2
o-xylene	-25.2	144.4
m-xylene	-47.9	139.1
p-xylene	13.3	138.3
Anisole	-37.5	155.0
Ethylbenzene	-95.0	136.2

Table 2.7: The pKa values for methanol, phenol, cresols and anisole compared to benzoic acid and water [Sykes, 1986a].

	pKa
Methanol	16
Phenol	9.95
o-Cresol	10.28
p-Cresol	10.19
m-Cresol	10.08
Anisole	-
Benzoic acid	4.20
Water	14

substituents and the bond angle on the oxygen. This results in melting and boiling points, which are still higher than those of its hydrocarbon equivalent ethylbenzene (Table 2.6).

2.2.1.1 Acidity of alcohols and phenols

Like water, alcohols and phenols are weak acids. The pKa gives an indication of the acidity strength of the molecule (Table 2.7). Aliphatic alcohols are about 100 times weaker acids than water, whereas phenols are 10 000 times more acidic than water. Phenols, however, relative to aromatic carboxylic acids (e.g. benzoic acid), are weak acids.

Dissociation of an alcohol or phenol produces a proton and an alkoxide or phenoxide anion, respectively. The reason for the large difference in acidity between alcohols and phenols can be found in the delocalisation of the negative charge on the anion. The phenoxide anion is stabilised by delocalisation of its negative charge via the delocalised π orbitals of the aromatic nucleus (mesomeric effect) as shown in Figure 2.17. Therefore, the negative charge on a phenoxide ion can be spread over to the ortho and para positions of the benzene ring through resonance. Such delocalisation can also occur in the undissociated phenol molecule involving the lone or free electron pairs on the oxygen but this results in a charge separation so that delocalisation is far less effective (Figure 2.18). The

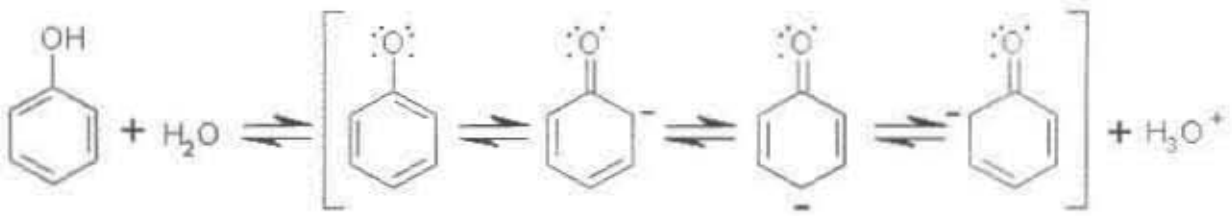

Figure 2.17: The stabilisation of the phenoxide anion [Sykes, 1986a].

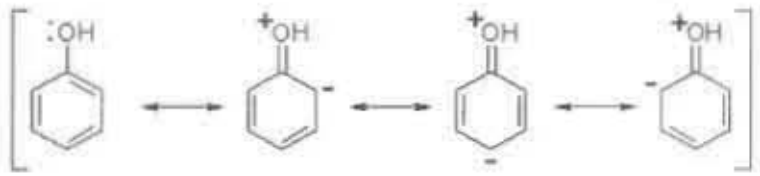

Figure 2.18: The stabilisation of phenol [Sykes, 1986a].

net effect of resonance is therefore to stabilise the phenoxide ion to a much greater extent than the phenol.

In contrast, the dissociation of an alcohol will form an aliphatic alkoxide in which the negative charge is fixed on the oxygen atom and cannot delocalise over the molecule. Therefore, alkoxide ions are not stablized and hence the acidity of alcohols is lower than the acidity of phenols (Table 2.7).

Water is amphoteric, i.e. it has both acid and base properties. Like water (hydroxonium ion, H_3O^+), alcohols and phenols can react with a strong acid to form oxonium ions as illustrated in Figure 2.19.

2.2.1.2 Activating effect of a substituent on the benzene ring

Apart from the acidity, the most striking chemical property of a phenol is the extremely high reactivity of its ring towards electrophilic substitution. A substituent on the benzene ring generally influences its reactivity. $-CH_3$, $-OCH_3$ and $-OH$ substituents are electron-donating and this activates the benzene ring for electrophilic substitution. That is, toluene, anisole and phenol will react faster than benzene in electrophilic substitution reactions. The activating effect increases from $-CH_3$ (weak) < $-OCH_3$ (moderate) < $-OH$ (strong) [Sykes, 1986b; Morrison and Boyd, 1987].

The strong effect of an $-OH$ group on the electrophilic aromatic substitution can be accounted for by assuming that the oxygen can share more than one pair of electrons with the ring (i.e. can form a bond of higher order than a single bond) and can accommodate a positive partial charge which has the effect of producing a partial negative charge on the ring (cf. Figure 2.18).

2.2.1.3 Ortho and para directing

In terms of ring substitution, $-CH_3$, $-OCH_3$ and $-OH$ are ortho and para directing in electrophilic aromatic substitution. This is again due to the effect of the electron donating groups [Morrison and Boyd, 1987]. The ortho and para directing effect increases in the same order as the effect of reactivity namely, $-CH_3 < -OCH_3 < -OH$. The strong effect of an $-OH$ group on the direction of electrophilic aromatic substitution can be accounted for by assuming that the oxygen can share more than one

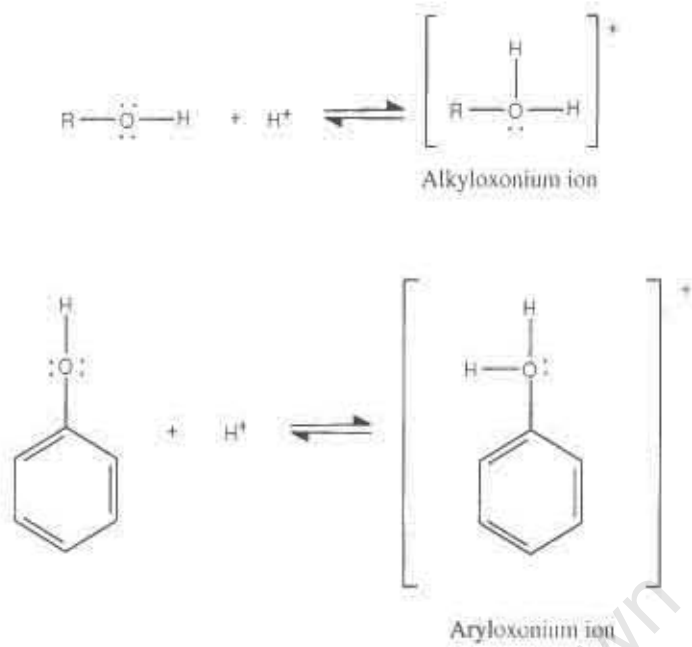

Figure 2.19: Alcohol and phenol reacting as a base [Hart and Schuetz, 1972a].

pair of electrons with the ring (i.e. can form a bond of higher order than a single bond) and can thus accommodate the positive charge introduced through the electrophilic attack by a carbenium ion.

The carbocation formed by electrophilic attack on the ring of a phenol is considered to stabilize this transitional state via delocalisation of the positive charge over the ring, resulting in resonance structures I - III, IV - VI and VII - X, respectively (cf. Figure 2.20), where the positive charge is located on carbon atoms. In case of para- or ortho-attack, the possible resonance structures include an additional one, structures VII and XI, respectively, in which the positive charge is carried by the oxygen. Resonance structures VII and XI are especially favoured, since in these structures every atom (except hydrogen) has a complete octet of electrons [Morrison and Boyd, 1987]. In the carbocation resulting from meta substitution (resonance structures I - III), no resonance structure is found where the positive charge can be carried by the oxygen. Therefore the hydroxyl group on the phenol activates the ring for substitution particularly in the ortho and para positions. Kinetically controlled, ortho- and para-cresol will dominate over m-cresol even though thermodynamically m-cresol is the most stable isomer (Section 2.2.2.6). Similarly $-OCH_3$ and $-CH_3$ substituents on the benzene ring are ortho and para directing but weaker [Sykes, 1986b].

The effect of the hydroxyl group decreases going from the ortho to the para position [Sykes, 1986b]. Also, as there are two ortho positions, the ortho position will be statistically favoured over the para position (in the absence of any steric constraints) [Venuto, 1994]. Therefore the expected kinetically controlled cresol isomer distribution is ortho > para > meta.

Temperature will have an effect on the kinetically controlled cresol isomer distribution. Increasing the temperature has two main effects. Firstly, the less stablized transition state to m-cresol (Figure 2.20 I - III resonance structures) can be assumed to result in a higher activation energy for the formation of m-cresol than the highly stabilized transition states to o- and p-cresol. Secondly, m-cresol concentration will increase due to the conversion of the primary products o- and p-cresol by

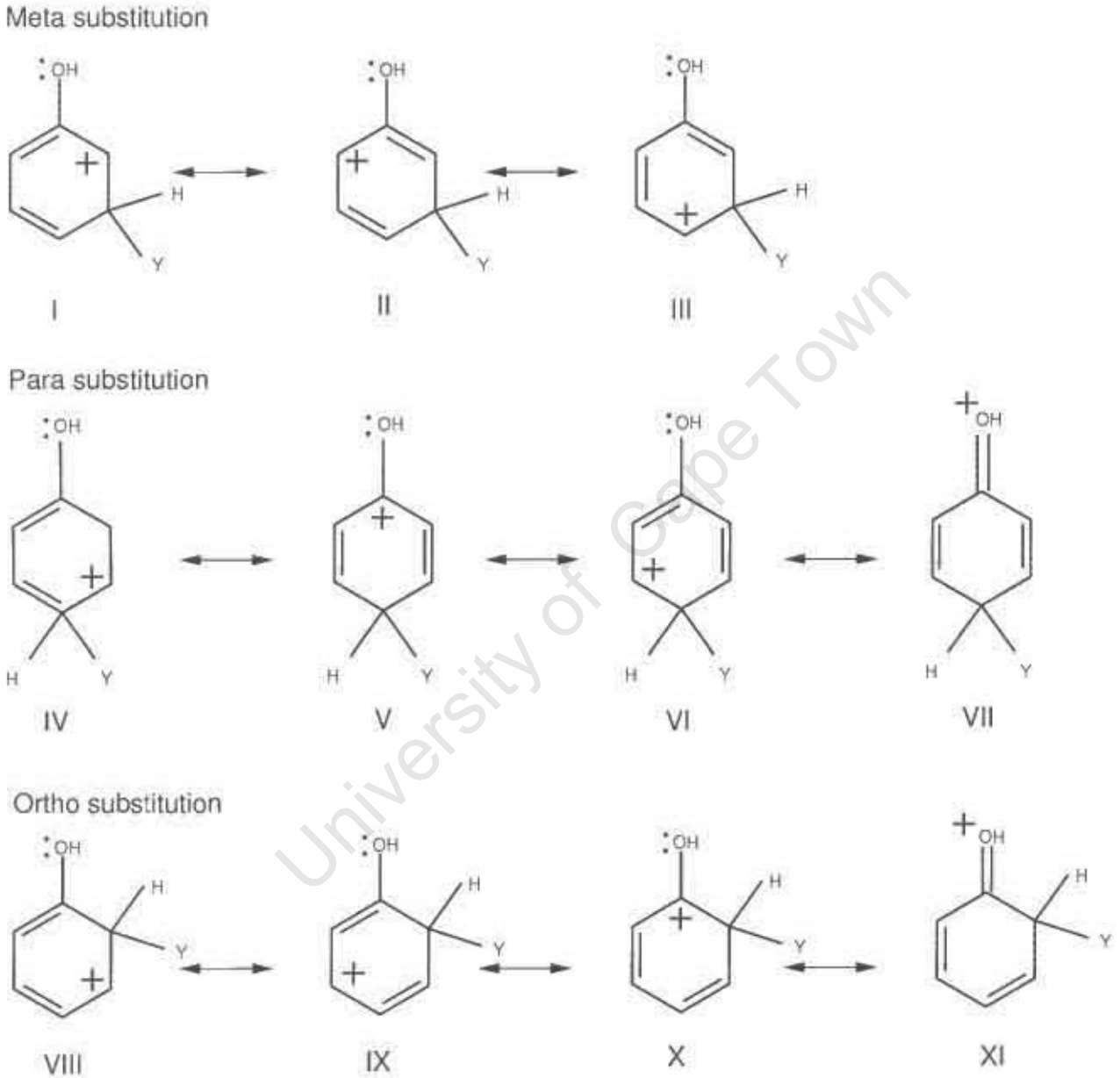

Figure 2.20: Transition state resonance structures from electrophilic aromatic substitution of phenol [Morrison and Boyd, 1987].

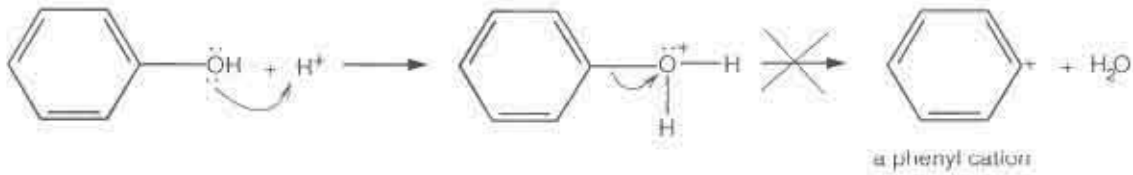

Figure 2.21: Formation of a phenyl cation [Hart and Schuetz, 1972a] (electron shifts indicated additionally).

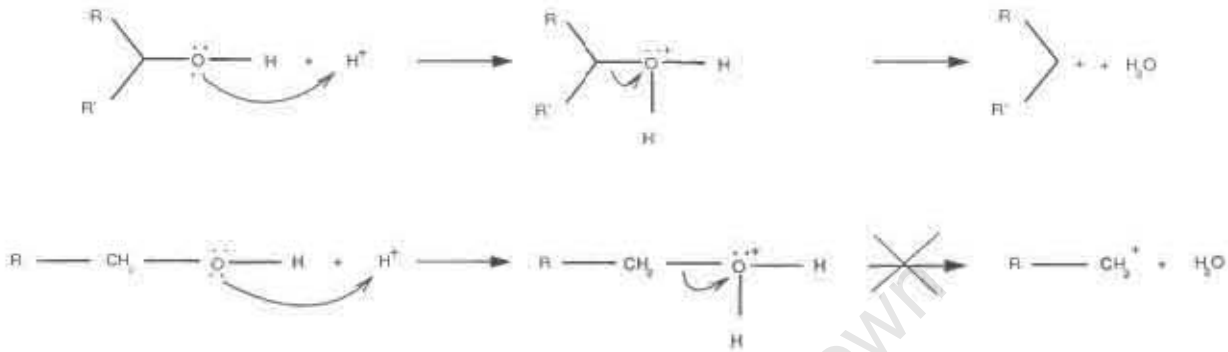

Figure 2.22: Secondary and primary carbenium ions formed from secondary and primary alcohols, respectively [Hart and Schuetz, 1972a] (electron shifts indicated additionally).

isomerization and transalkylation. Therefore, increasing the temperature will allow the m-cresol to increasingly be formed as a primary product as well as a secondary product.

2.2.1.4 Mechanism of reactions of the hydroxyl group on alcohols and phenols

The major difference of alcohols and phenols is in reactions involving the breaking of the C – O bond. It is relative easy with an acid catalyst to break the C – O bond in secondary and tertiary alcohols whereas this bond is very difficult to break in primary alcohols, particular methanol and even more in phenols. Protonation of the hydroxyl group and loss of a water molecule would give a carbocation (Figures 2.21 and 2.22). Secondary and tertiary alcohols form stable secondary or tertiary carbenium ions, respectively (Figure 2.22, top scheme). For substitution reactions on the alcohol, this allows both S_N1 and S_N2 mechanisms to occur. A primary alcohol, methanol in particular, would form an unstable primary carbenium ion (Figure 2.22, bottom scheme). Therefore no S_N1 mechanism is possible with primary alcohols but an S_N2 mechanism (i.e the simultaneous replacement of the protonated $-OH$ group by the incoming group) is still possible (cf. for instance Figures 2.35 and 2.36) [Hart and Schuetz, 1972a].

With only two attached groups, the positively charged carbon in a phenyl cation would want to be *sp*-hybridized and have bonds arranged linearly. But this geometry is prevented by the benzene ring. Therefore phenyl cations are extremely difficult to form (cf. Figure 2.21). This also tells us that phenols cannot undergo replacement of the hydroxyl group neither by an S_N1 mechanism nor by an S_N2 mechanism [Hart and Schuetz, 1972a].

Phenols are also ambident nucleophiles in that they quite readily form phenolic ethers [Venuto, 1994] or mixed phenolic/aliphatic ethers with alcohols.

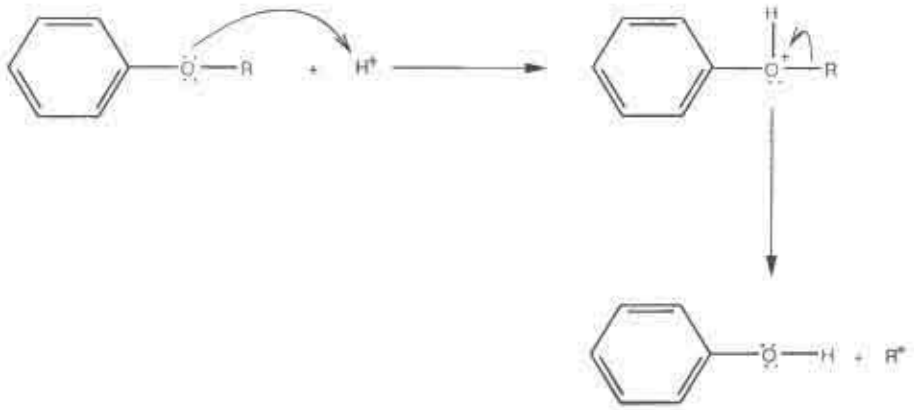

Figure 2.23: Alkyl phenyl ether undergoing acid catalysed cleavage reaction (redrawn from Hart and Schuetz [1972b]) (electron shifts indicated additionally).

2.2.1.5 Anisole chemistry

Anisole is a mixed aromatic and aliphatic ether (Ar – O – R) and is almost non-polar. Minor polarity is introduced due to the non-symmetrical substituents and the bond angle on the oxygen. Ethers are weak bases, by virtue of the unshared electron pairs on the oxygen.

Aromatic ethers, like phenyl ethers, can undergo electrophilic substitution reactions on the ring. While alkoxy groups are activating and ortho, para directing in electrophilic substitution (cf. Section 2.2.1.3), they are considerably less so than a hydroxyl group, as discussed in Section 2.2.1.2.

Ethers can also undergo cleavage reaction by acids if water is present. Because of the low reactivity of the bond between the oxygen and the aromatic ring, an Ar – O – R ether undergoes cleavage of the O – R bond and yields a phenol and an alkyl cation (Figure 2.23). If the alcohol is primary (e.g. anisole), this cleavage reaction occurs by firstly the protonation of the oxygen, necessarily followed by S_N2 displacement with the water [Hart and Schuetz, 1972b].

2.2.1.6 Cresol chemistry

The effect of addition of a $-CH_3$ group to the ring on the chemical properties of phenol is small compared to the effect of the $-OH$ group even though the $-CH_3$ group is electron donating (Table 2.7). As seen from Table 2.7, the electron donating methyl group has a lower effect when located on the meta position than on the ortho and para position of the cresol. This is due to the hydroxyl group being electron donating most dominant to the ortho and para position relative to it, as discussed in Section 2.2.1.3. Therefore, an electron donating methyl group in the ortho or para position will compete with the hydroxyl group and therefore reduce the electron donating effect of this group to the ring i.e. reduce acidity more than a methyl group positioned in the meta position.

2.2.2 Thermodynamic Equilibria

2.2.2.1 Methanol to dimethyl ether

Methanol converts to form dimethyl ether and water as shown in Figure 2.24 [Chang, 1983; Möller *et al.*, 1999]. In the temperature range of 200 - 400°C, which was investigated in this thesis for phenol

$$2\,CH_3OH \rightleftharpoons CH_3OCH_3 + H_2O$$

Figure 2.24: Conversion of methanol to dimethyl ether.

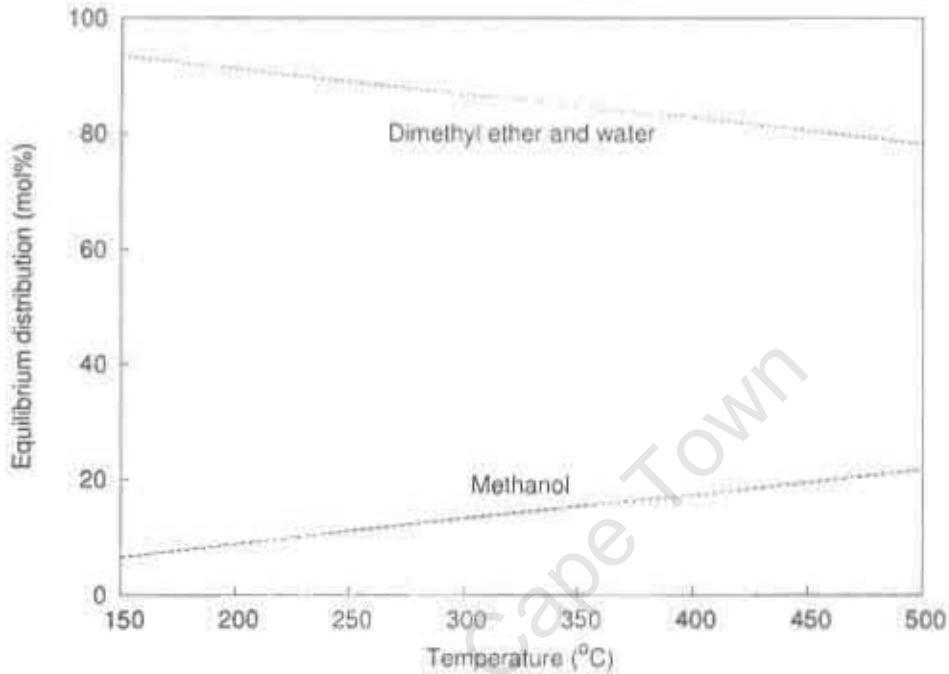

Figure 2.25: Thermodynamic equilibrium distribution of species in the conversion of methanol to dimethyl ether and water [Daubert and Danner, 1989].

methylation, the formation of dimethyl ether is thermodynamically favoured as shown in Figure 2.25, with methanol equilibrium conversion > 80%.

2.2.2.2 Phenol methylation to anisole

For the methylation of phenol to anisole [Parton *et al.*, 1989a] (Figure 2.26) the thermodynamic equilibrium is shown in Figure 2.27 from an equimolar methanol/phenol mixture. Over the temperature range studied in this thesis (200 - 400°C), the equilibrium conversion (ca. 90%) does not change significantly.

Figure 2.26: Formation of anisole from the methylation of phenol with methanol.

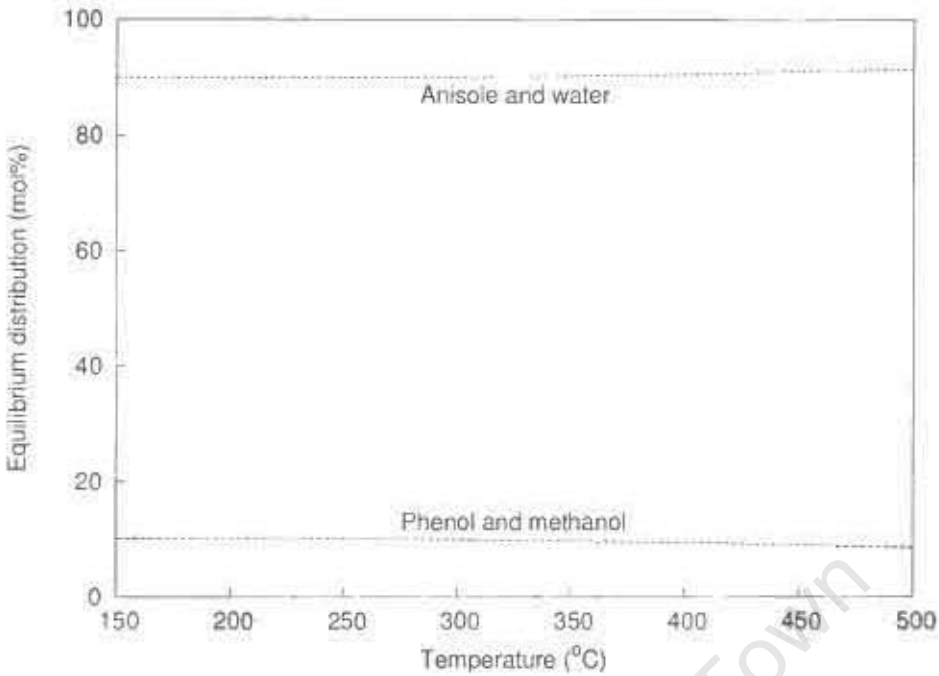

Figure 2.27: Thermodynamic equilibrium of anisole formation from an equimolar phenol and methanol mixture [Daubert and Danner, 1989].

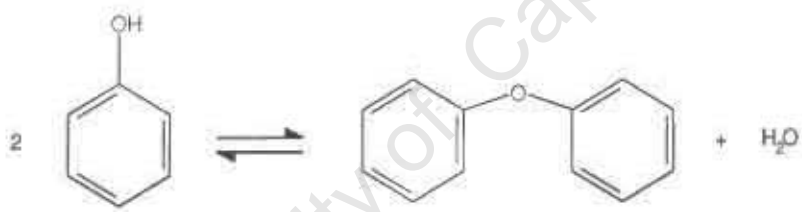

Figure 2.28: Diphenyl ether formation for phenol.

2.2.2.3 Phenol to diphenyl ether

Diphenyl ether can be formed from phenol similar to the formation of dimethyl ether from methanol (Figure 2.28) [Venuto, 1994]. There is no thermodynamic data available for this reaction. Application of several incremental estimation methods based on group combination factors produced quite inconsistent and contradictory results [Ntshabele, in preparation]. Comparison with dimethyl ether and anisole formation equilibria (cf. Sections 2.2.2.1 and 2.2.2.2) suggests equilibrium limitations for diphenyl ether formation with significantly or noticeably less than 100% phenol conversion in the temperature range (200 - 400°C) investigated for phenol conversion in this thesis.

2.2.2.4 Phenol methylation to cresols

The methylation of phenol on the ring forms cresols (Figure 2.29) [Parton *et al.*, 1989a]. In the temperature range studied in this thesis (200 to 400°C), the thermodynamic equilibrium lies far on the side of the product (cresols). That is, the thermodynamic equilibrium is > 99.9% to the cresols.

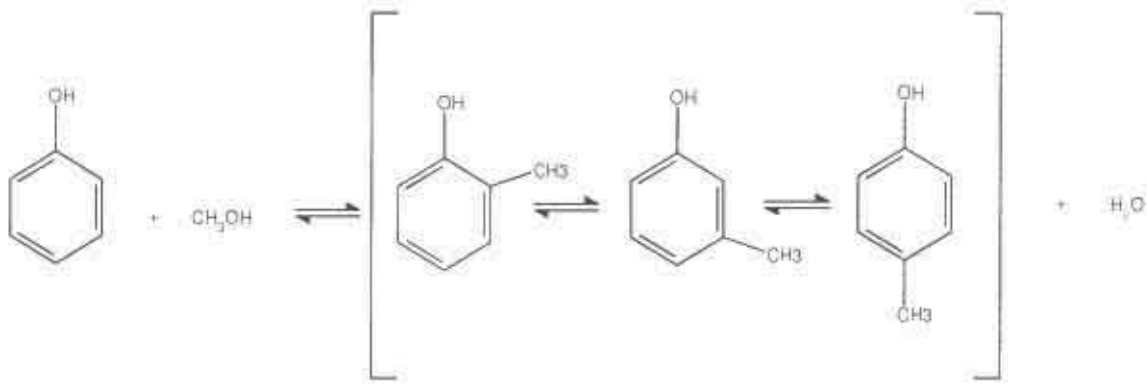

Figure 2.29: Methylation of phenol with methanol to cresols.

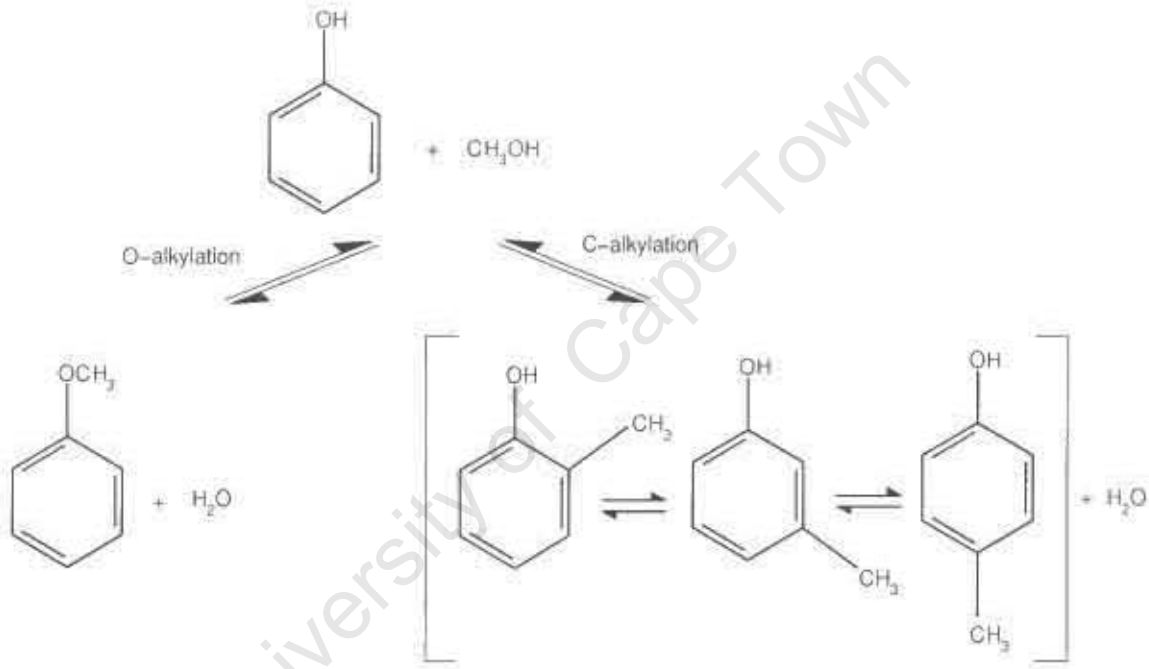

Figure 2.30: O-alkylation vs C-alkylation.

2.2.2.5 O-alkylation versus C-alkylation

The methyl group from the methanol can alkylate the phenol either on the oxygen of the hydroxyl group (O-alkylation) or on the ring (C-alkylation) (Figure 2.30). Thermodynamically, cresols formation (C-alkylation) is largely favoured over anisole formation (O-alkylation) (cf. individual equilibria, Sections 2.2.2.4 and 2.2.2.2, respectively). Pierantozzi and Nordquist [1986] found that at thermodynamic equilibrium, under the reaction conditions used by these authors (300°C), cresols formation is favoured 10^4 times over that of anisole formation. This is because a C – C bond is more stable (has a higher energy of formation) than an O – C bond and the number of molecules is unchanged. Anisole is, however, the kinetically preferred product under mild reaction conditions.

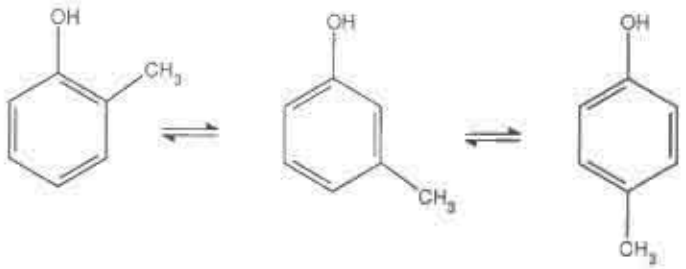

Figure 2.31: The cresol isomers equilibrium.

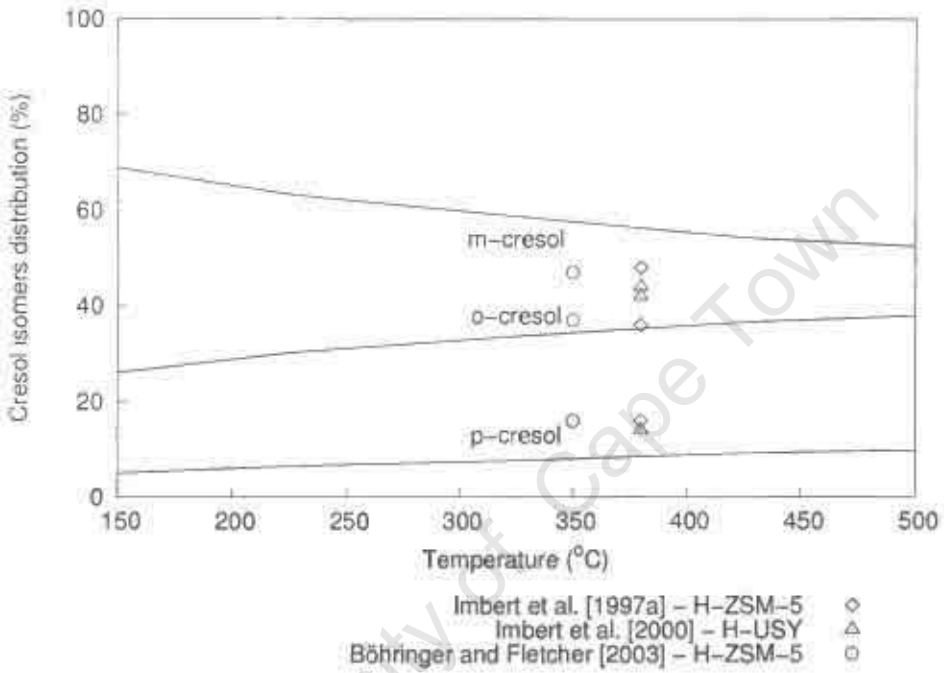

Figure 2.32: Cresol isomer equilibrium in the gas phase (lines calculated from data by Green [1962]; Stull *et al.* [1969]; Chang *et al.* [1989], data points measured by Imbert *et al.* [1997a] and Imbert *et al.* [2000] and Böhringer and Fletcher [2003] (preliminary data)).

2.2.2.6 Cresol isomer distributions

There are three cresol isomers (cf. Figure 2.31), namely o-, m- and p-cresol. Cresols can isomerize as shown in Section 2.2.4.3. The thermodynamic equilibrium distribution of the cresol isomers is shown in Figure 2.32 over the range of temperatures studied in this thesis (from 200 to 400°C). m-Cresol is the thermodynamically favoured isomer whereas the content of p-cresol is low, according to this data.

Lines in Figure 2.32 are based on thermodynamic data obtained from Green [1962], Stull *et al.* [1969] and Chang *et al.* [1989]. Imbert *et al.* [1997a] disagreed with the cresol isomer equilibrium calculated from Stull's data [Stull *et al.*, 1969]. Imbert *et al.* [1997a] obtained experimental isomer equilibrium distributions at 380°C of o : p : m-cresol of 36 : 16 : 48 over H-ZSM-5 but reported 44 : 14 : 42 from more recent work over H-USY (cf. Figure 2.32). Recently Böhringer and Fletcher [2003] has confirmed Imbert's *et al.* [1997a] results and disagreed with the cresol isomer distribution calculated from Stull's *et al.* [1969] data.

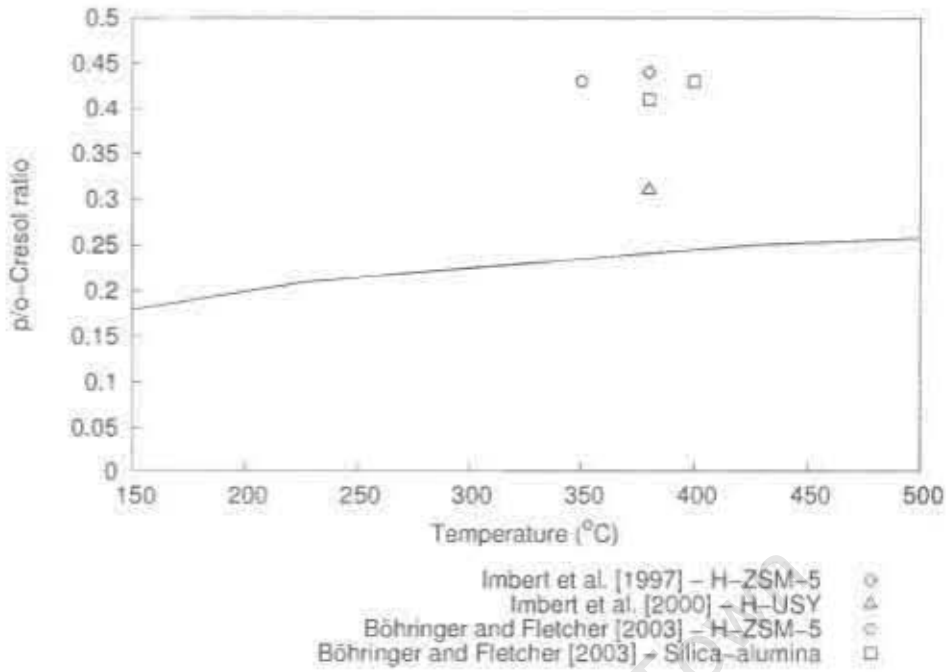

Figure 2.33: Thermodynamic equilibrium p/o-cresol ratio (line calculated from data by Green [1962]; Stull *et al.* [1969]; Chang *et al.* [1989], data points measured by Imbert *et al.* [1997a, 2000] and Böhringer and Fletcher [2003] (preliminary data)).

According to data given by Stull *et al.* [1969] the equilibrium p/o-cresol ratio changes with decreasing temperature in favour of o-cresol (cf. Figure 2.33). This is expected. From Figure 2.33 it is clearly seen that the ratios measured by Imbert *et al.* [1997a, 2000] and Böhringer and Fletcher [2003] are much higher that those calculated from Stull's *et al.* [1969] data.

2.2.3 Methylation of phenol with methanol over acid zeolites, Al_2O_3, amorphous silica-alumina and MgO

Table 2.8 gives a list of authors that have studied the alkylation of phenol with methanol over zeolites. The reaction has been studied to date over zeolites ZSM-5, ZSM-11, X, Y, Beta and Mordenite as well as amorphous catalysts, mineral acids and ion-exchange resins. The zeolites represent a range of channel sizes and dimensionalities.

2.2.3.1 Reaction mechanisms for the alkylation of phenol with methanol

By studying the literature, Parton *et al.* [1989a] proposed an overall reaction network for the alkylation of phenol over acid and basic catalysts, including zeolites and amorphous solids (such as Al_2O_3, MgO, $AlPO_4$ and silica-alumina). The overall reaction network proposed is in agreement with the mechanism Marczewski *et al.* [1988] developed from studies on phenol methylation over various acid zeolites and Al_2O_3. Figure 2.34 gives the overall reaction pathways [Marczewski *et al.*, 1988]. However, the scheme appears quite inconsistent. m-Substitution in the cresol and methylanisole fraction has been ignored by Marczewski *et al.* [1988] but apparently not in the xylenol and dimethylanisole fraction (otherwise there would be two precisely defined isomers in each fraction only, namely 2,4- and 2,6-xylenol and

Table 2.8: Acid zeolites and other acid catalysts applied on the gas phase alkylation of phenol with methanol.

	Catalysts	Temperature (°C)	Reactants partial pressure (bar)
Balasubramanian *et al.* [2000]	Zn-, Ga-, La-, Ce-, H-Beta	250 - 420	0.2
Landau *et al.* [1997]	H-, La-, Ca-Y H-ZSM-5 H-Beta H-Mordenite	300	0.1
Xu *et al.* [1997]	H-Beta	200	0.17
Garcia *et al.* [1996]	H-Y	200	0.2
Marczewski *et al.* [1996]	γ-Al_2O_3	200	0.2
Bautista *et al.* [1993]	$AlPO_4 - Al_2O_3$	250 - 400	Not given
Santacesaria *et al.* [1990b]	Amorphous silica-alumina γ-Al_2O_3 Nafion-H Phosphoric acid	200 - 400	Not given
Santacesaria *et al.* [1990a]	H-ZSM-5	260 - 350	Not given
Chang *et al.* [1989]	Na-, H-ZSM-5 H-Beta γ-Al_2O_3	400	Not given
Parton *et al.* [1989a]	H-, P ZSM 5 H-, H/Na-, H/La-, H/K-Y H-USY	200	0.2 0.17 0.026
Parton *et al.* [1989b]	H-ZSM-5 H-ZSM-11 H-USY	200	0.026
Marczewski *et al.* [1989]	H-USY	200	0.2
Marczewski *et al.* [1988]	H-Y H-USY H-Mordenite H-ZSM-5 Al_2O_3	200	0.2
Pierantozzi and Nordquist [1986]	H-ZSM-5 Al_2O_3	300 - 400	0.86
Renaud *et al.* [1986]	H-, Na-ZSM-5	200 - 250	Not given
Chantal *et al.* [1985]	H-ZSM-5	350 - 400	Not given
Balsama *et al.* [1984]	Na-, La-, H-X Na-, La/Na-, H-Y H-ZSM-5 H-ZSM-11	250	0.2
Namba *et al.* [1980]	H/K-, H/Na-Y	250	0.17
Tanabe and Nishizaki [1977]	MgO Amorphous silica-alumina	250 - 500	Not given

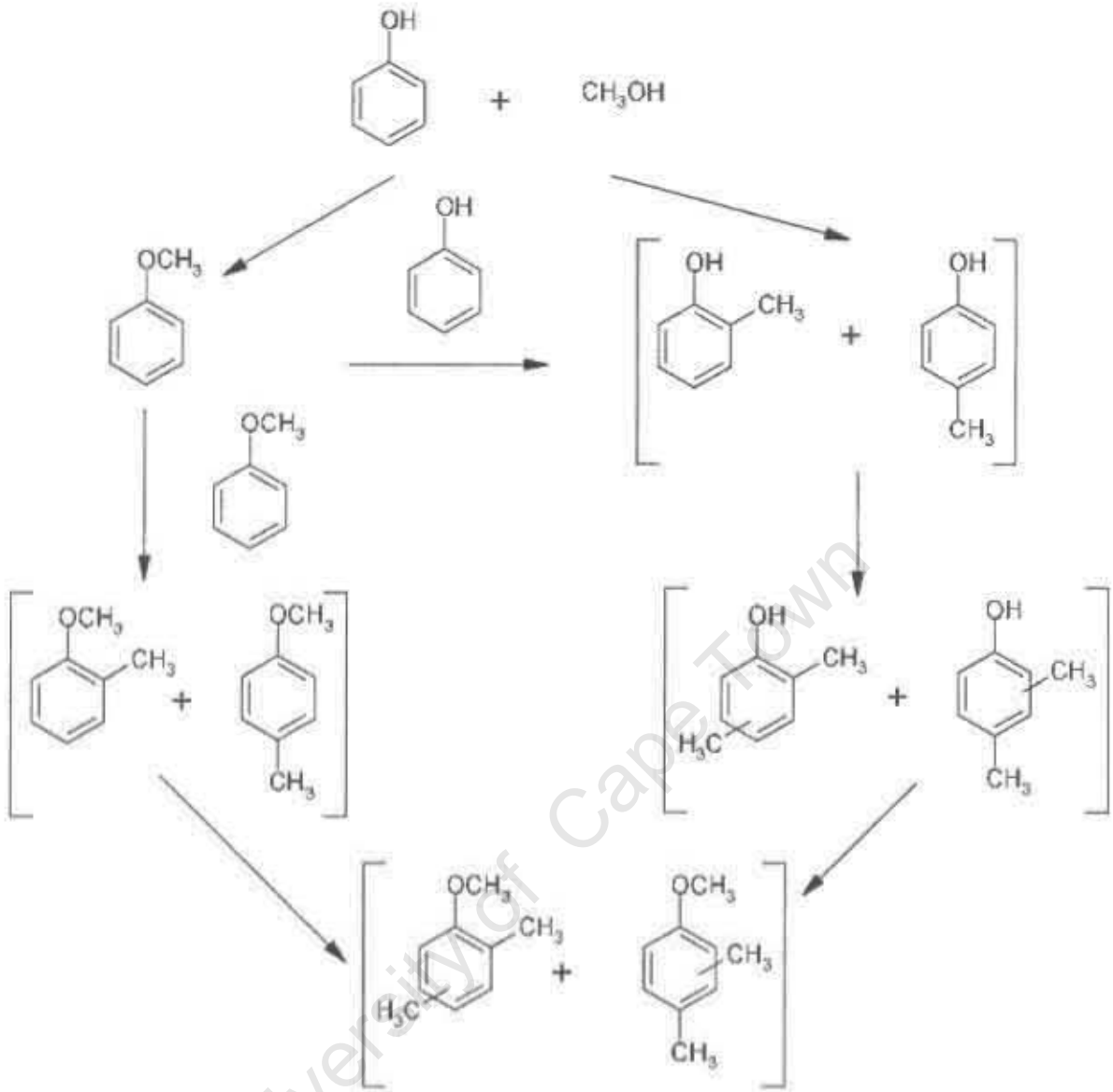

Figure 2.34: Reaction mechanism of the methylation of phenol with methanol [Marczewski *et al.*, 1988]

2,4- and 2,6-dimethylanisole). Phenol involved with transalkylation reactions has been considered as a reactant but ignored as a product. Diphenyl ether formation is not considered either. What is missing in this scheme in particular, is the important secondary reaction of internal rearrangement of anisole to o-cresol (cf. Section 2.2.3.1.2).

2.2.3.1.1 Mechanism for the acid catalysed formation of anisole and cresols The major primary products formed by phenol methylation are anisole and cresols. As discussed in Section 2.2.1.4, cresols and anisole are formed by a S_N2 mechanism from phenol and methanol, as shown in Figures 2.35 and 2.36. Figure 2.35 only shows the formation of o-cresol but an analogous mechanism can be drawn for the formation of m- and p-cresol.

Methanol can react over acid catalysts to form dimethyl ether (Figure 2.24). Dimethyl ether can analogously act as the alkylating agent and as an example the reaction mechanism for o-cresol

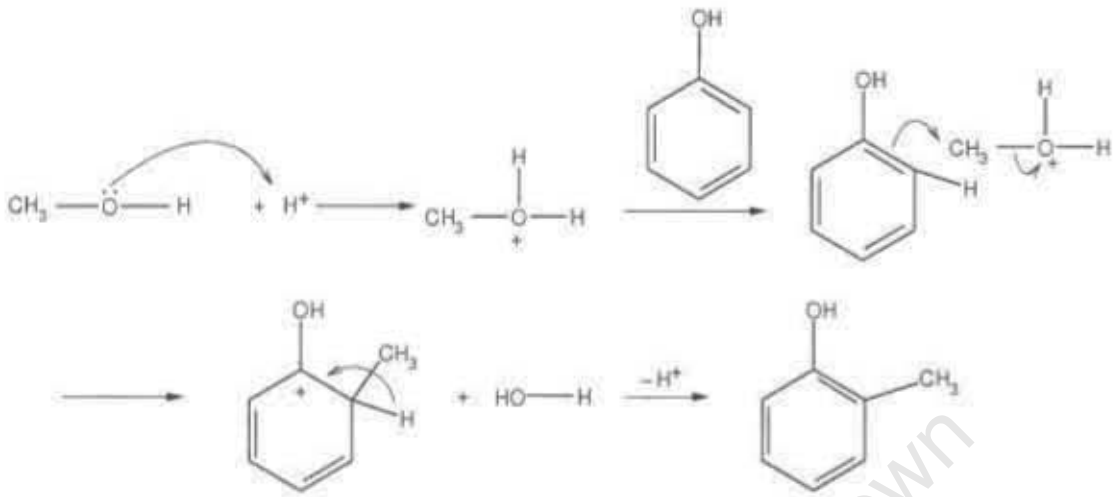

Figure 2.35: Methylation of phenol with methanol in the formation of o-cresol via S_N2 mechanism.

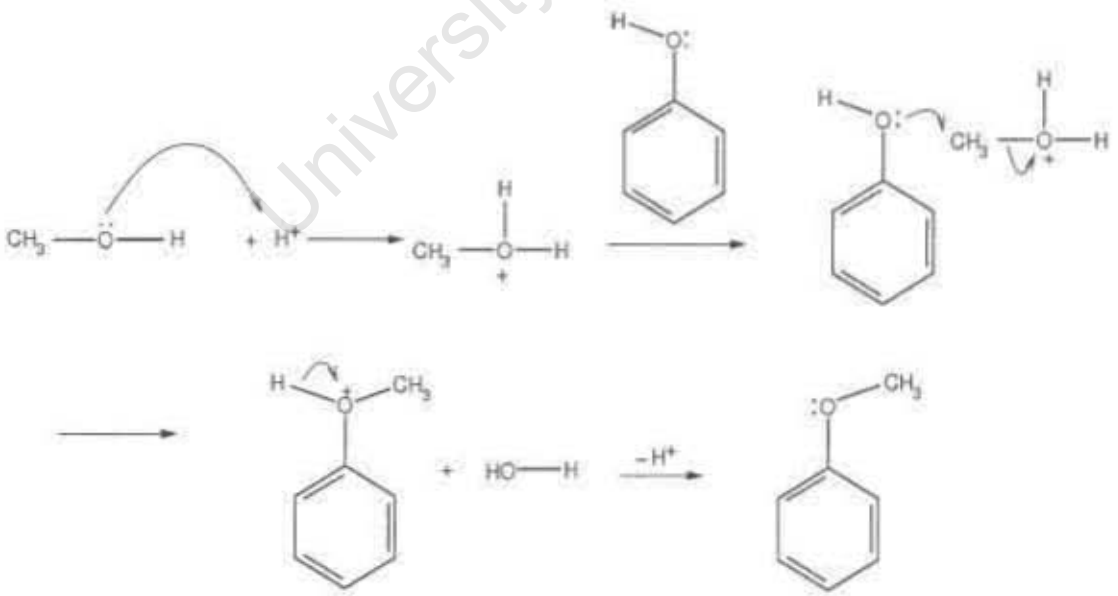

Figure 2.36: Methylation of phenol with methanol in the formation of anisole via S_N2 mechanism.

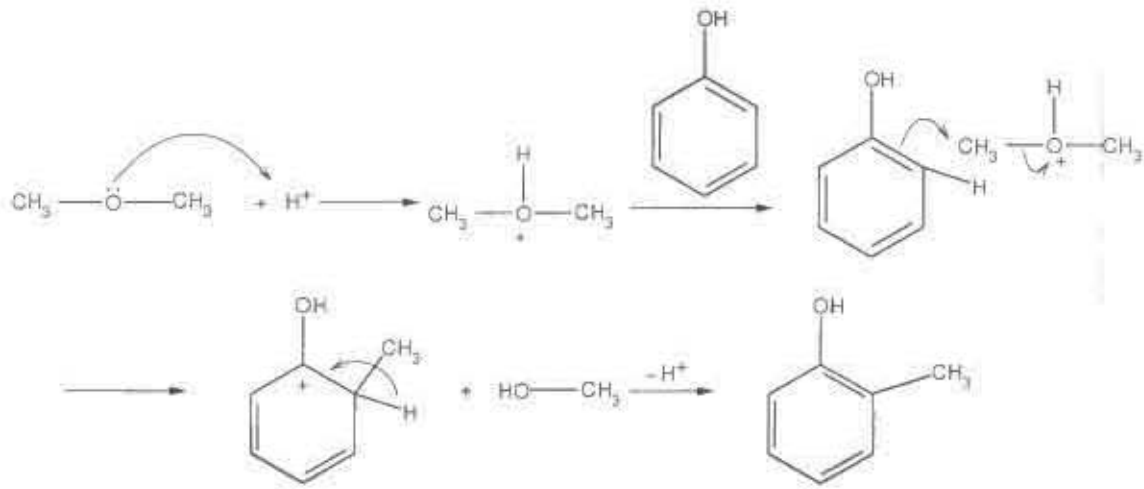

Figure 2.37: Methylation of phenol with dimethyl ether in the formation of o-cresol via S_N2 mechanism.

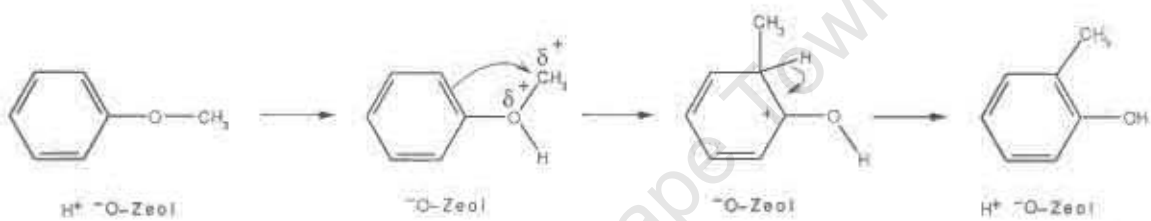

Figure 2.38: Anisole rearrangement to o-cresol on a zeolite Brønsted acid site [Venuto, 1994].

formation with dimethyl ether as the alkylating agent is shown in Figure 2.37.

Over acid catalysts, O-alkylation is kinetically preferred under mild conditions so that a high selectivity to anisole is obtained (cf. Table 2.9), despite its unfavourable thermodynamic stability in comparison with cresols (cf. Section 2.2.2.5).

2.2.3.1.2 Mechanism for the formation of o-cresol from anisole o-Cresol can be formed from the monomolecular rearrangement of anisole [Venuto, 1994]. Figure 2.38 shows the reaction mechanism for the anisole rearrangement to o-cresol.

2.2.3.1.3 Mechanism for the isomerization of m-cresol to o-cresol and p-cresol via 1,2-methyl shift A cresol isomer may isomerize to the other isomers as shown in Figure 2.31. The reaction mechanism for isomerization via a 1,2-methyl shift is shown in Figure 2.39 for the isomerization of m-cresol to o- and p-cresol. Similar mechanisms can be drawn for the isomerization of o-cresol and p-cresol.

2.2.3.1.4 Mechanism for the secondary alkylation of anisole and cresols Anisole and cresols are partially transformed into secondary products via further alkylation, which can be either C-alkylation (anisole to methylanisoles, cresols to xylenols) or O-alkylation (cresols to methylanisoles). Reaction mechanisms are analogous to the primary steps.

Table 2.9: Typical O/C-alkylation ratios obtained in the methylation of phenol over different acid catalysts under mild reaction conditions.

	Catalyst	Temperature (°C)	Reactants partial pressure (bar)	O/C-alkylation ratio
Landau *et al.* [1997]	H-Y	180	0.1	2.3
	H-ZSM-5	180		2.7
	H-Beta	180		2.1
	H-Mordenite	180		1.3
Garcia *et al.* [1996]	H-Y	200	0.17	3
Santacesaria *et al.* [1990b]	Silica-alumina	200	Not	2
	γ-Al_2O_3	200	given	5
	Nafion-H	200		9
	Phosphoric acid	200		9
Marczewski *et al.* [1988]	H-USY	200	0.2	3.2
	H-Mordenite	200		2.3
	H-ZSM-5	200		9
	Al_2O_3	200		1.5

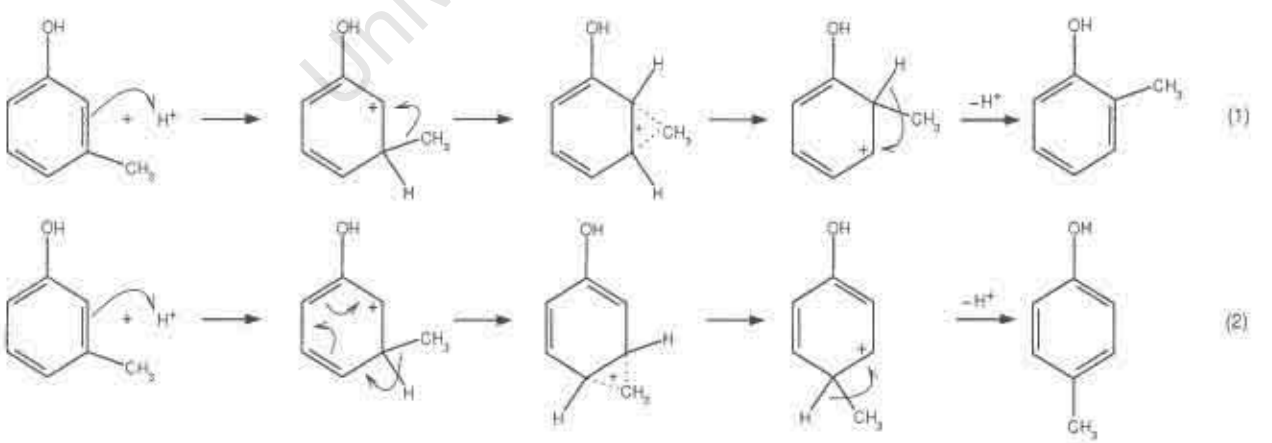

Figure 2.39: Isomerization of m-cresol to o-cresol (1) and p-cresol (2) via 1,2-methyl shift [Imbert *et al.*, 1997a] (electron shifts indicated additionally).

2.2.3.1.5 Side reactions of reactants The alkylating agent can also react with itself over the acid zeolite. For example, methanol is well known to react over acid zeolites [Chang, 1983; Laan and Ward, 1987; Möller *et al.*, 1999]. The presence of methanol side-reactions in phenol alkylation can be seen by the higher conversion of methanol compared to that corresponding to the conversion of phenol [Balsama *et al.*, 1984]. At first, methanol can undergo etherification to form dimethyl ether [Chang, 1983; Laan and Ward, 1987; Möller *et al.*, 1999]. The resulting dimethyl ether, however, is still available for alkylation reactions, cf. Sections 2.2.2.1 and 2.2.3.1 and Figures 2.25 and 2.37. Methanol and dimethyl ether react also to form hydrocarbons [Chang, 1983; Möller *et al.*, 1999]. In addition, phenol can react with another phenol molecule and form diphenyl ether and water (cf. Section 2.2.2.3 and Figure 2.28) [Venuto, 1994].

2.2.3.2 Role of Brønsted acid sites and Lewis acid and basic sites in the methylation of phenol with methanol

For the alkylation of phenol both Brønsted and Lewis acid sites are claimed to participate in the catalytic activation. Santacesaria *et al.* [1990b] studied the different types of acid sites by using γ-Al_2O_3 (strong Lewis acid and basic sites), Nafion-H (strong Brønsted acid sites), silica-alumina (contains strong Brønsted acid sites as well as Lewis acid and basic sites) and Kieselguhr-supported phosphoric acid (medium to weak Brønsted acid sites). Reactions were carried out at comparably low temperatures of 200 and 225°C, respectively. Table 2.10 gives the O/C-alkylation and p/o-cresol ratios found on the different catalysts.

Over all the catalysts studied by Santacesaria *et al.* [1990b], at low reaction temperatures, anisole was the major reaction product but the selectivity to anisole decreases with increasing reaction temperature. Balasubramanian *et al.* [2000] concluded that the decrease in anisole selectivity with increasing temperature was due to the conversion of anisole to o-cresol whereas Santacesaria *et al.* [1990b] assigned this to the fact that C-alkylation has a higher activation energy (134 kJ/mol over γ-Al_2O_3) than O-alkylation (67 kJ/mol over γ-Al_2O_3) and so, higher temperatures will promote C-alkylation. In terms of cresol isomers, all catalysts studied showed preference for o-cresol.

Over γ-Al_2O_3, an O/C-alkylation ratio of 2 was obtained and in terms of cresol isomers, γ-Al_2O_3 is highly ortho selective (cf. Table 2.10). Santacesaria *et al.* [1990b] concluded that this high ortho-selectivity is due to the amphoteric character of γ-Al_2O_3. That is, a Lewis acid site exists adjacent to a Lewis basic site (Figure 2.40). Phenol molecules will interact with both by giving a phenolate ion absorbed on the acid site and a hydrogen ion bound to the basic one, as shown in Figure 2.41. The hydrogen ions formed should have sufficient mobility to activate the methyl group of methanol. Alkylation at the oxygen or at the ring, very selectively in the ortho position, will occur. However, the authors did not detail the actual substitution steps.

Tanabe [1985] hypothesised that on a basic surface the phenol is adsorbed perpendicularly to the catalyst surface. So the ortho-position is closest to the surface and hence alkylation will occur in this position. Santacesaria's *et al.* [1990a] conclusions compare to Tanabe's [1985] regarding the perpendicular orientation of adsorption on a basic site.

Over Nafion-H, which has only Brønsted super-acid sites, anisole was the main product again, with even higher selectivity, and a p/o-cresol ratio of 0.5 was obtained [Santacesaria *et al.*, 1990b].

Table 2.10: O/C-alkylation ratio obtained from phenol alkylation with methanol over different acid site types at 200°C and 225°C (phosphoric acid), respectively, and "zero" contact time (reactants partial pressure not stated) [Santacesaria *et al.*, 1990b].

Catalyst	Acid site type	Basic site type	O/C-alkylation ratio	p/o-cresol ratio*
γ-Al_2O_3	Strong Lewis	Strong Lewis	2	0
Nafion-H	Strong Brønsted	-	5	0.5
Silica-alumina	Strong Lewis and Brønsted	Strong Lewis	9	0.5
Phosphoric acid	Medium to weak Brønsted	-	9	0.6

* No m-cresol formed at the low reaction temperatures.

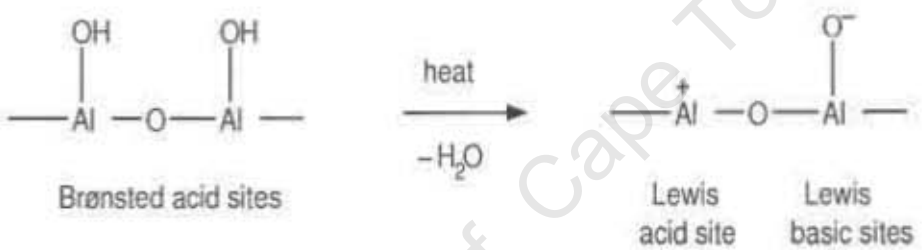

Figure 2.40: Amphoteric character of γ-Al_2O_3 [Santacesaria *et al.*, 1990b].

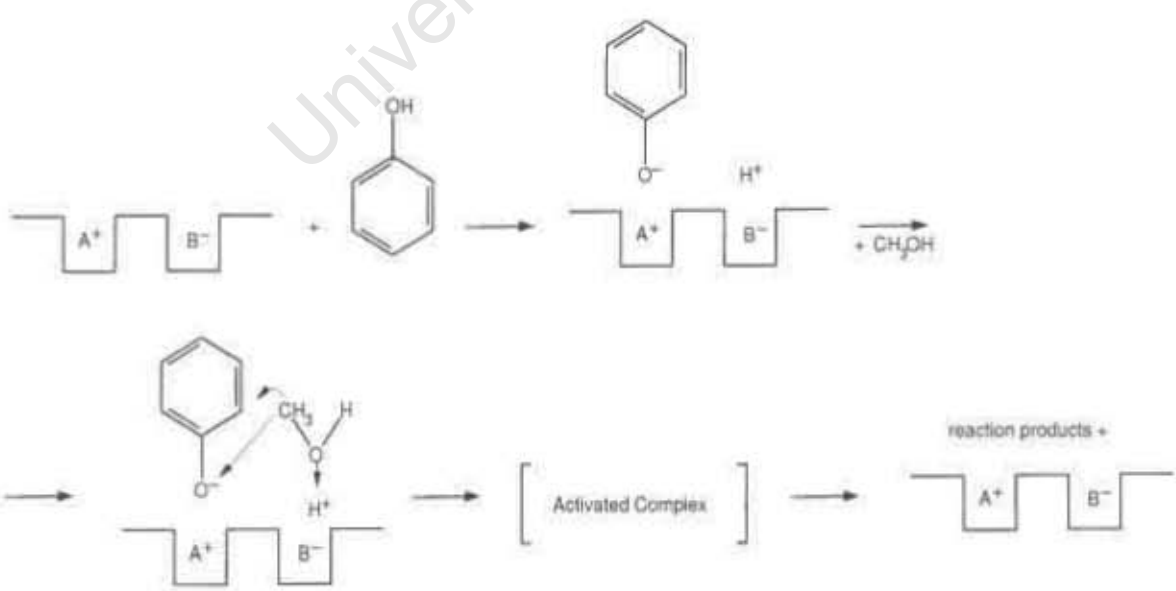

Figure 2.41: Formation of anisole or o-cresol over adjacent Lewis acid (A^+) and Lewis basic (B^-) sites on γ-Al_2O_3 [Santacesaria *et al.*, 1990b].

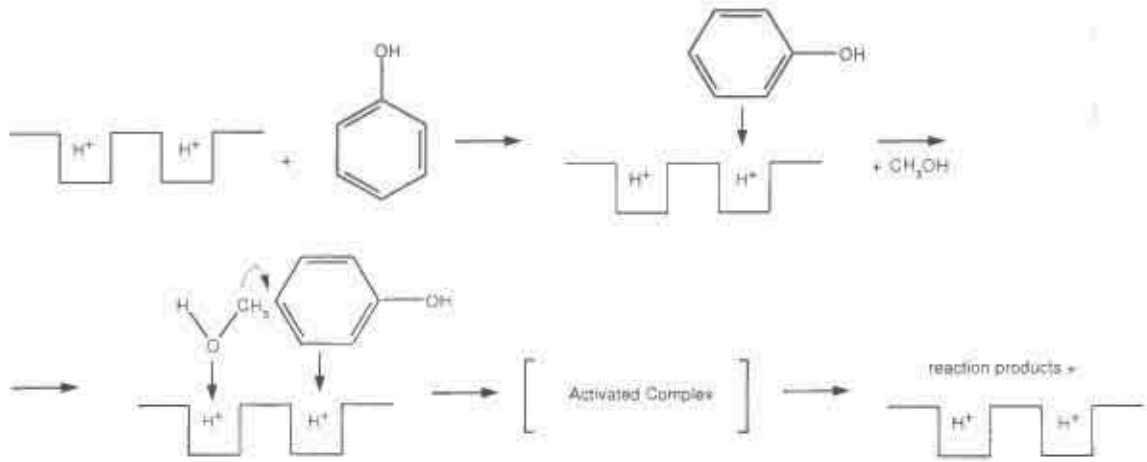

Figure 2.42: Possible reaction mechanism between two Brønsted adjacent acid sites Santacesaria *et al.* [1990b].

Santacesaria *et al.* [1990b] explained the product formation by two possible mechanisms. First, a dual site mechanism (cf. Figure 2.42), in which the first acid site directly interacts with the aromatic ring while the other acid site strongly binds the oxygen of the methanol. Note that Figure 2.42 only shows the mechanism for the formation of p-cresol and that similar reaction mechanisms can be drawn for the formation of anisole and o-cresol. Secondly, a Rideal mechanism, in which the reaction occurs between the molecules of alkylating agent adsorbed on the acid site and the aromatic molecule from the vapour phase.

Over silica-alumina both Brønsted and Lewis acid sites are present. Anisole was the predominant product formed (O/C-alkylation ratio of 9). There was strong deactivation with time-on-stream due to coke formation over silica-alumina. The p/o-cresol ratio decreases with increasing deactivation starting at about a ratio of 0.5 at 200°C. Santacesaria *et al.* [1990b] explain this decreasing p/o-cresol ratio by selective deactivation, as the Brønsted acid sites are regarded as being responsible for the deactivation and the Lewis acid and basic sites become more predominant as a consequence of this poisoning/coking of the Brønsted acid sites. Brønsted acid sites interact strongly with the aromatic ring (Figure 2.42). Therefore, phenol adsorption is never vertical as is in the case of phenolate ion adsorption (Figure 2.41). For this reason, ortho selectivity is not promoted over Brønsted acid sites and coke is easily formed. If the Brønsted acid sites are widely separated from each other (due to the coking), the reaction could only occur through the Rideal mechanism as described above [Santacesaria *et al.*, 1990b]. Since there are less Brønsted acid sites due to the coking, the formation of p-cresol decreases further.

Phosphoric acid has medium and weak Brønsted acid sites. Over phosphoric acid, anisole was again the predominant product and a p/o-cresol ratio of 0.58 was obtained at 225°C. Santacesaria *et al.* [1990b] attributed this higher p-selectivity to "geometric factors" in adsorption. It was speculated that phenol adsorption was strongly effected by the presence of many adjacent hydroxyls on the catalyst surface.

In summary, over Brønsted acid sites, the reaction mechanism involves that the alkylating species adsorbs on the acid site, which protonates the $-OH$ group. The adsorbed alkylating species can either react with the oxygen or with a carbon on the aromatic ring. On adjacent Brønsted acid

sites, the second acid site may interact with the aromatic ring. However, an aromatic compound adsorbed on a Brønsted site will be positively charged and have reduced susceptibility to electrophilic attack. Therefore, according to Parton *et al.* [1989a], the electrophilic aromatic substitution on the phenol must be seen as a reaction between the adsorbed alkylating agent and the free aromatic (i.e. corresponding to the Rideal mechanism). Both mechanisms give rise to anisole, o- and p-cresol.

Lewis acid sites can activate the alkylating agent and the phenol by deprotonation of the phenol or just by co-ordination [Feast and Lercher, 1996]. Over Lewis acid and basic site pairs, the phenol adsorbs dissociatively on the acid site and the alkylating species adsorbs on the then protonated basic site to produce the protonated alcohol. Lewis acid and basic site pairs give high selectivity to o-cresol due to the orientation of the adsorbed phenol perpendicular to the catalyst surface.

2.2.3.3 O/C-alkylation ratio and strength of acid sites

Pierantozzi and Nordquist [1986] explored the formation of anisole via O-alkylation over the following acid catalysts: Al_2O_3, H-ZSM-5, $La_2(HPO_4)_3$ and $BaSO_4$ at 300°C. They found that $La_2(HPO_4)_3$ and $BaSO_4$ were selective catalysts for O-alkylation (O/C-alkylation ratios of 17.1 and 9.9, respectively). Al_2O_3 was found to give O/C-alkylation ratios of 4.3 and zeolite H-ZSM-5 was found to give a lower O/C-alkylation ratio of only 1.6. Pierantozzi and Nordquist [1986] concluded that weak acidity is required to prevent ring alkylation from occurring. In other words, ring alkylation requires strong acid sites.

Work done by Garcia *et al.* [1996] apparently agrees with Pierantozzi's [1986]. Garcia *et al.* [1996] poisoned dealuminated zeolite H-Y (molar SiO_2/Al_2O_3 = 40) by partial ion-exchanging of the acid sites with sodium. Varying degrees of ion-exchange were used in an attempt to obtain different acid strengths since the sodium was assumed to preferentially poison the strongest sites. Catalysts were compared at short time-on-stream at the same conversion (10% at 200°C after 15 min on stream), and it was found that the O/C-alkylation ratio increased with increasing sodium content (cf. Table 2.11). Garcia *et al.* [1996] concluded from these initial results that in phenol alkylation, O-alkylation occurs over weaker acidic sites (high sodium content sample) while C-alkylation requires the presence of stronger acid sites (low sodium content sample). However, these different O/C-alkylation ratios were only obtained over the very fresh catalysts i.e. only after 15 minutes of reaction. Drawing conclusions from initial product samples obtained from reactions over heterogeous catalysts (in particular zeolites), can be deceptive. In fact, over the entire duration of the experiment after the initial period (experiments lasted up to 6 hours) and over a wide range of conversion (obtained during catalyst deactivation), there was no difference at all in the product selectivities as the authors emphasize. So, as soon as the samples are slightly deactivated by coking, the O/C-alkylation ratios were the same for all the catalysts (ca. 4.5, cf. Table 2.11) and even lower than the initial ratio obtained over the high sodium content sample (ca. 13). This contradicts, in particular, since the latter meant, in the context of the author's argument, that coking increased the strength of sites and left the strong sites selectively unaffected. However, Garcia *et al.* [1996] claimed that coking poisons the "stronger" acid sites preferentially. Therefore an even higher O/C-alkylation ratio should be found over the deactivated catalysts than over the fresh ones but this is not what was observed over the partially sodium-exchanged samples (cf. Table 2.11).

Table 2.11: The effect of partial sodium exchange of zeolite H-Y (molar SiO_2/Al_2O_3 = 40) on the O/C-alkylation ratio from phenol methylation with methanol at constant phenol conversion of 10% (via different space velocities) after 15 minutes on stream and over the partially coked catalysts (reactants partial pressure = 0.2 bar) [Garcia *et al.*, 1996].

Catalysts	Na/Al*	Time-on-stream	O/C-alkylation ratio
0.03 Na/H-Y	0.014	15 min	3
0.44 Na/H-Y	0.2	15 min	7
0.77 Na/H-Y	0.36	15 min	13
All catalysts, coked**	-	from initial samples to 6 hours	ca. 4.5

* Presumably atomic ratio, authors don't specify.
** Derived from a graph in Garcia *et al.* [1996].

Table 2.12: The O/C-alkylation ratio from phenol alkylation with methanol over partially dealuminated zeolite NH_4-Y (reaction temperature = 200°C, reactant partial pressure = 0.2 bar) [Garcia *et al.*, 1996].

NH_3-desorption temperature (°C) (hold for 1 hour)	Yield of anisole and cresols (%)*	O/C-alkylation ratio	Ratio of conversion over the ammonia poisoned/unpoisoned zeolite*
200	0.3	∞	0.01
250	1.3	10	0.04
300	13	6.7	0.38
350	22	5.9	0.68
450	30	4.8	0.9
500	33	3	1.0

* Derived from graphs in Garcia *et al.* [1996].

Garcia *et al.* [1996] obtained further observations by selectively poisoning dealuminated zeolite H-Y with ammonia and partially desorbing the ammonia at different temperatures, prior to phenol alkylation with methanol at 200°C (Table 2.12). The results were interpreted in a way, which supports their hypothesis that O-alkylation occurs on weaker acid sites namely, that a high degree of poisoning (the result of low ammonia desorption temperature) preferentially affects the stronger acid sites. Hence, only the weaker acid sites are left and hence O/C-alkylation ratio is increased.

Marczewski *et al.* [1988] dealuminated zeolite H-Y by steaming and acid washing (molar SiO_2/Al_2O_3 ratio between 4 and 29). Product yields were recorded, at a reaction temperature of 200°C, as a function of phenol conversion (below 15%) either obtained during catalyst deactivation or obtained by changing the feed rate, at a time-on-stream sufficiently long for the rate of catalyst decay to be very low. It was found with all the catalysts that these two sets of data points were on the same curves. Marczewski *et al.* [1988] conclude that "since one can expect the acid centers to be elimated by coke coverage in decreasing order of acid strength, the results indicate that the selectivity of the reaction does not depend on the strength of the sites". This is a clear contradiction to the above, already questionable statements by Garcia *et al.* [1996]. Another conclusion from these results might be that in H-zeolites, particularly in high silica H-zeolites such as dealuminated H-Y, there are no sites of

different acid strength or that the differences are marginal and irrelevant.

As mentioned above, Pierantozzi and Nordquist [1986] found different O/C-alkylation ratios, indeed, over different acid catalysts, but of very different type and very different strength of the acid sites (ranging from $BaSO_4$ to H-ZSM-5). In contrast, the difference in the acid strength of different and differently pretreated H-zeolites appears noticeably insufficient to influence the O/C-alkylation selectivity.

2.2.3.4 Competitive adsorption of phenol and the alkylating agent?

There is also the possible complication that phenol and the alkylating agent may competitively adsorb on the acid sites. Over Brønsted sites, methanol adsorbs with its oxygen atom, phenol adsorbs with the ring (cf. Figure 2.42). This possible competitive adsorption is increased by molecular weight, the presence of polarizable electron-rich π-charge clouds (the aromatic nucleus) or by polar functional groups (i.e. the $-OH$ group) [Venuto, 1994].

Parton *et al.* [1989a] compared data obtained by Namba *et al.* [1980] and Haung *et al.* [1986] and stated that the increase of phenol conversion with increasing methanol to phenol ratio, as illustrated by Figure 2.43, would be evidence of competitive adsorption of the phenol and methanol on the catalyst. However, at constant pressure, a maximum reaction rate is always achieved with an equimolar mixture of two reactants which react with the same reaction order. The reaction rate gradually declines with increasing as well as decreasing reactants ratio. In this case, at a methanol to phenol ratio of 4, the reaction rate is still two-thirds the equimolar rate (assuming for instance first order in each of the reactants) but the phenol feed concentration is 40% only of the equimolar concentration. This inevitably results in a higher phenol consumption than for the equimolar mixture. Therefore, the observed increase in phenol conversion does not indicate an increase in reaction rate so that the observed increase in the phenol conversion with increasing methanol to phenol ratio does not give any proof for competitive adsorption between methanol and phenol, as was concluded by Parton *et al.* [1989a].

Pierantozzi and Nordquist [1986] studied the effect of the methanol to phenol ratio (molar ratios between 1 and 5) on anisole formation rates. They found that over Al_2O_3, increasing the methanol to phenol ratio had no effect on the anisole formation rate but anisole selectivity increased, whereas over H-ZSM-5 the anisole selectivity was not effected by the methanol to phenol ratio but the anisole formation rate decreased significantly with increasing methanol to phenol ratio (from 1.8 mmol anisole g/cat · h to 0.77 mmol anisole g/cat · h). The latter, observed over an acid zeolite, confirms the critical address of Parton's *et al.* [1989a] conclusions outlined above.

2.2.3.5 Coke formation

In the alkylation of phenol, the catalysts containing Brønsted acid sites always deactivate by coke deposition. Santacesaria *et al.* [1990b] determined that coke formation occurs on Brønsted acid sites but not on Lewis acid sites. Marczewski *et al.* [1988] showed that at a given conversion the selectivity observed over acid zeolites remained unchanged irrespective of how the conversion was

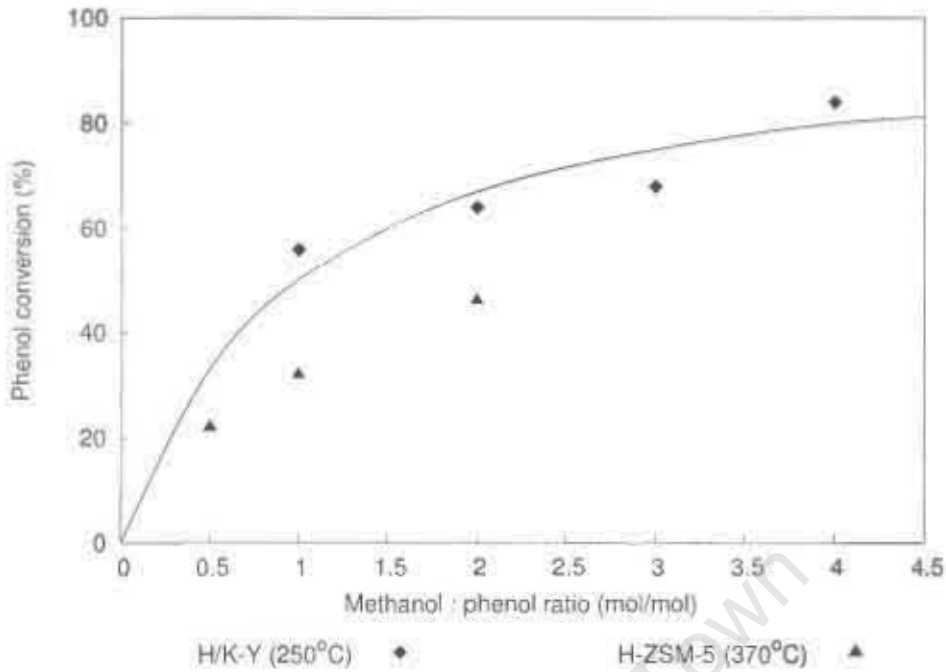

Figure 2.43: Phenol conversion versus the methanol/phenol molar ratio in the reaction of phenol with methanol on H/K-Y at 250°C in the vapour phase after 60 min data from Namba *et al.* [1980] and on H-ZSM-5 at 370°C in the liquid phase after 70 min data from Haung *et al.* [1986]. Solid line represents the modelling of phenol conversion with methanol : phenol ratio using an overall second order rate expression.

reached (changed by contact time or by catalyst decay), but this did not hold for amorphous silica-alumina, where coking was found to change selectivity through changing the ratio of Brønsted to Lewis acid sites by selectively poisoning the former (cf. Section 2.2.3.2) [Santacesaria *et al.*, 1990b].

It was found that air regeneration (coke burn-off) restores the acid zeolite catalysts to their initial activity [Renaud *et al.*, 1986; Chantal *et al.*, 1985; Beltrame *et al.*, 1987].

2.2.4 Cresol isomers formation

It is possible to produce a very high percentage of o-cresol in the cresol fraction over basic catalysts (such as MgO) or amphoteric catalysts (such as Al_2O_3) [Marczewski *et al.*, 1988; Santacesaria *et al.*, 1990b; Beck and Haag, 1997; Lee *et al.*, 1998; Choi *et al.*, 2000; Fiege and Bayer AG, 2001]. Fe/V based catalysts exclusively form o-substituted phenols (o-cresol and 2,6-xylenol) and no anisole [Fiege and Bayer AG, 2001], but this is a different reaction mechanism. However, the major disadvantage of this process is substantial decomposition of methanol (to H_2 and CO). Acid catalysts usually produce both o-cresol and p-cresol as well as m-cresol (under severe reaction conditions in particular).

Highly selective synthesis of m-cresol and p-cresol respectively is desirable due to the high cost of separating these isomers. m-Cresol and p-cresol have very close boiling points (202.2 and 201.9°C, respectively) which means that the two isomers cannot be separated by distillation economically but need fractionated crystallization, adsorption separation (Cresex process) or derivatisation by butylation with isobutene before being separated by distillation [Fiege and Bayer AG, 2001]. However, a mixture of o- and p-cresol without m-cresol could easily be separated by distillation as their boiling

Table 2.13: Comparison of the distribution of cresol isomers from phenol alkylation with methanol [Parton *et al.*, 1989a].

Catalyst	Reaction temperature (°C)*	Phenol conversion (%)	Cresols selectivity (%)	Cresols distribution o- (%)	m- (%)	p- (%)	p/o-ratio	p/(m+p) primary p-cresol purity (%)
H-Y	250	46.9	64.2	60	22	18	0.30	45
H-Y	200	6.0	29.0	58.6	0	41.4	0.71	100
H-USY	200	20.2	63.9	38.9	1.3	59.8	1.54	98
H/La-Y	250	49.7	46.3	52	8.9	39.1	0.75	81
H/K-Y	250	32.0	57.5	33	6.0	61	1.85	91
H/Na-Y	250	66.0	70.2	33.3	9.1	57.6	1.73	86
P-ZSM-5	200	6.0	10.0	65	0	35	0.54	100
P-ZSM-5	450	26.6	43.2	60.9	7.0	32.1	0.53	82
H-ZSM-5	300	13.5	31.3	68.6	0	31.4	0.46	100
H-ZSM-5	200	10.2	73.3	65.3	0	34.7	0.53	100

* Reactant partial pressure are given in Table 2.8.

points differ by 10.9°C. Such a process may be of economic interest if p/o-cresol yields and ratios are sufficiently high.

Exclusively or nearly exclusively ortho-substituted phenols are obtained in a "classical" organic reaction system (Venuto [1994], without specifying what "classical" refers to but probably meaning Friedel-Crafts catalysts systems), where the attacking electrophile is complexed or otherwise associated with the substituent already on the aromatic ring. The electrophile can then easily be guided into the adjacent ortho position (cf. below).

Zeolites tend to give a mixture of mainly ortho and para-substituted phenols. Over acid catalysts (silica-alumina, H-ZSM-5 and H-USY for instance), at low temperatures and conversions (< 13.5%), the meta-isomer of cresol (the thermodynamically favoured isomer) was found to be absent (Table 2.13) [Parton *et al.*, 1989a], meaning that p-cresol is formed directly under electrophilic substitution in the para positions, rather than by subsequent isomerization of an initially formed ortho-alkylated product via 1,2-methyl group shift [Beck and Haag, 1997]. This is as expected as the hydroxyl group of phenol is both o- and p- directing (cf. Section 2.2.1.3). The resulting p-cresol fraction is of high primary purity (cf. Table 2.13). At higher conversions, m-cresol was obtained (cf. Table 2.13).

Statistically, a p/o-cresol ratio of 0.5 is expected from phenol alkylation, since there is one para position on the phenol ring but two ortho positions. Slightly lower ratios, around 0.4 or lower, are obtained at equilibrium between these two isomers in the given temperature range (cf. Figure 2.33). p/o-Cresol ratios in this range (0.4 - 0.5) are often observed over all kinds of acid catalysts (cf. Table 2.14). Over zeolites, p/o-cresol ratios can occasionally be found lower but more often somewhat significantly higher. There are various hypotheses for the lower and higher p/o-cresol ratios.

2.2.4.1 Low p/o-cresol ratios from phenol methylation

Marczewski *et al.* [1988] studied the methylation of phenol over dealuminated H-Y, dealuminated H-

Table 2.14: p/o-Cresol ratios obtained from phenol methylation over different catalysts.

	Catalyst*	Temperature (°C)***	p/o-Cresol ratio
Landau *et al.* [1997]	H-Y (7)	180	0.60
	H-Y (12)	180	0.32
	H-Y (60)	180	0.51
	La-Y (5)	180	0.88
	Ca-Y (6)	180	0.83
	H-Y (60)	300	0.65
	H-ZSM-5 (30)	180	0.56
	H-ZSM-5 (50)	180	0.61
	H-ZSM-5 (90)	180	0.61
	H-ZSM-5 (30)	300	0.39
	H-Beta (25)	180	0.64
	H-Beta (25)	300	0.45
	H-Beta (25)	500	0.61
	H-Mordenite (17)	180	0.85
	H-Mordenite (17)	300	0.77
Santacesaria *et al.* [1990b]	Silica-alumina	200	0.51
	γ-Al_2O_3	200	0
	Nafion-H	200	0.49
	Phosphoric acid	225	0.58
Santacesaria *et al.* [1990a]	H-ZSM-5 (58)	300	0.50
Chang *et al.* [1989]	Na-ZSM-5 (35)	400	0.43
	H-ZSM-5 (60)	400	0.43
	H-Beta (30)	400	0.33
	γ-Al_2O_3	400	0.04
Parton *et al.* [1989a]	H-ZSM-5	200	0.53
	P-ZSM-5	200	0.54
	H-Y	200	0.71
	H/Na-Y	250	1.73**
	H/K-Y	250	1.85**
	H-USY (40)	200	1.54
Parton *et al.* [1989b]	H-ZSM-5 (200)	200	0.59
	H-ZSM-11 (200)	200	0.53
	H-USY (9)	200	0.62
Marczewski *et al.* [1988]	H-Y (8)	200	0.71
	H-Y (9)	200	0.67
	H-Y (27)	200	0.67
	H-Y (59)	200	0.33
	H-Mordenite (136)	200	0
	H-ZSM-5 (98)	200	0.54
	Al_2O_3	200	0
Balsama *et al.* [1984]	Na/La-X (1.6)	250	0.50
	La-X (1.6)	250	0.75
	H-Y (2)	250	0.33
	Ca/Na-Y (3.2)	250	0.46
	H/Na-Y (3.2)	250	0.80
	H/RE/Na-Y (2.9)	250	0.67
	H-ZSM-11	250	0.50
Namba *et al.* [1980]	H/K-Y	250	1.3 - 1.85**
	H/Na-Y	250	1.0 - 1.73**

* Brackets indicate SiO_2/Al_2O_3 molar ratio of zeolite catalysts;

** These catalysts have very limited lifetimes;

*** Reactant partial pressure are given in Table 2.8.

Table 2.15: Phenol alkylation with methanol at 200°C (phenol conversion < 20 %, reactants partial pressure = 0.2 bar) [Marczewski *et al.*, 1988].

Catalyst (SiO_2/Al_2O_3 molar ratio)	Selectivity to* anisole (%)	o-cresol (%)	p-cresol (%)	O/C-alkylation ratio	p/o-Cresol ratio
H-Y (8)	71	17	12	2.4	0.71
H-Y (9)	76	14.5	9.5	3.2	0.67
H-Y (27)	79	12	8	3.9	0.67
H-Y (59)	84	12	4	5.3	0.33
H-Mordenite (136)	70	60	0	1.2	0.00
H-ZSM-5 (98)	90	6.5	3.5	9.0	0.56
Al_2O_3	60	40	0	1.5	0.00

* No m-cresol was formed under these conditions.

Mordenite, H-ZSM-5 and Al_2O_3 at 200°C (cf. Table 2.15). Within the series of H-Y samples studied, the p/o-cresol ratio decreased over the most dealuminated sample. This decrease was linked to the number of acid sites in the supercage of H-Y. Marczewski *et al.* [1988] postulated that para-selectivity required more than one acid site in the supercage, whereas H-Y (59), which has only one or less acid sites per supercage on average, would therefore have a decreased p/o-cresol ratio. However, this contradicts to the data given by Parton *et al.* [1989a] and Namba *et al.* [1980] for ultra-stable and partially alkali exchanged samples of zeolite Y (cf. Table 2.14) where the low acid site density zeolites (H-USY, H/Na-Y and H/K-Y) had the highest p/o-cresol ratios, all greater than 1.

Marczewski *et al.* [1988] observed that both H-Mordenite and Al_2O_3 formed exclusively o-cresol (cf. Table 2.14). The latter is commonly observed over Al_2O_3 (cf. Table 2.14 and Section 2.2.3.2) but the exclusive formation of o-cresol over H-Mordenite is quite unusual (cf. Table 2.14). Over Al_2O_3, the selectivity to ortho-alkylation could be facilitated (at relatively low temperature) if phenol was weakly adsorbed perpendicularly to the catalyst surface by H-bonding via its OH-group on a site adjacent to the adsorbed alkylation agent (cf. Section 2.2.3.2 and Figure 2.41). The exclusive ortho selectivity in H-Mordenite was explained in terms of its "narrow pores" [Marczewski *et al.*, 1988], which may cause the diffusion of phenol with the long axis parallel to the channel (Figure 2.44). This configuration may favour ortho-substitution. Note that approaching with the "rear" end exposes the m-position to the adsorbed alkylating agent (which is far less reactive), not the p-position. Other papers, however, describe quite high p/o-cresol ratios over H-Mordenite (for example 0.77 [Landau *et al.*, 1997], cf. Table 2.14), which questions this effect of special orientation in the pore system. Marczewski *et al.* [1988] also speculated that the high SiO_2/Al_2O_3 ratio of the H-Mordenite used (136) could also effect the p/o-cresol ratio similar to the highly dealuminated H-Y. Landau's *et al.* [1997] H-Mordenite, indeed had a SiO_2/Al_2O_3 molar ratio = 17.

Venuto *et al.* [1966] found low p/o-ratios (below 0.33) for the ethylation of phenol over rare-earth-exchanged zeolite X at very low temperatures (< 150°C). It was postulated that this may be due to an initial O-alkylation to form phenylethyl ether, which subsequently rearranges to form o-ethylphenol. The mechanism suggested for this rearrangement is analogous to the mechanism suggested for the

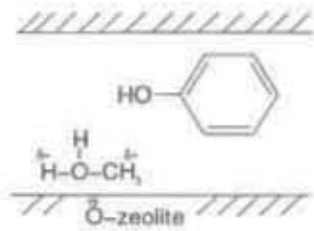

Figure 2.44: Hypothesized orientation of a phenol molecule in the H-Mordenite channel system leading to high o-selectivity [Venuto, 1994; Marczewski *et al.*, 1988].

anisole rearrangement to o-cresol (cf. Figure 2.38).

After investigating the alkylation of phenol with anisole, Beltrame *et al.* [1987] produced an explanation for the "low" p/o-cresol ratio of 0.33 over H-Y previously obtained by members of the same research group [Balsama *et al.*, 1984]. Beltrame *et al.* [1987] obtained a much lower p/o-cresol ratio (0.11) from phenol alkylation with anisole than from phenol alkylation with methanol (0.33). Beltrame *et al.* [1987] hypothesised that for acid catalysts strongly adsorbed anisole, which is formed in the phenol methylation, reacts with phenol from the gas phase by a Rideal mechanism. This would enable the hydroxyl group of the phenol to interact with the activated oxygen of the absorbed anisole that would bring the ortho position of the phenol closer to the methyl group. Thus the ortho position on the phenol would be more accessible to an attack by the methyl group from the anisole than the para position.

Venuto *et al.* [1966], Beltrame *et al.* [1987] and Jacobs *et al.* [1988] hypothesised that anisole is an intermediate in the formation of o-cresol. In ZSM-5, o-cresol is suggested to form directly from anisole since in pentasils there is a suppression of bimolecular reactions involving aromatic rings i.e. a suppression of transalkylation reactions [Parton *et al.*, 1989a]. Therefore, the transformation of anisole into o-cresol would occur intramolecularly. This hypothesis was stressed to explain the lower p/o-cresol ratio in H-ZSM-5 over zeolite H-Y (p/o-cresol ratios of 0.53 for H-ZSM-5 versus 0.71 for H-Y at 200°C and low conversions (Table 2.13)). However, as discussed above, a p/o-cresol ratio of 0.5 just reflects the statistical probabilities of o- and p-alkylation and is close to the slightly lower thermodynamic equilibrium ratio too.

Apparently most authors regarded p/o-cresol ratios around 0.5 or somewhat lower as something unexpectedly special that required special explanation and this gave rise to a multiplicity of hypotheses explaining why the selectivity to o-cresol is "so" high, or conversely, why p/o-cresol ratios were often far below 1. These authors, apparently, have overseen that p/o-cresol ratios around 0.5 correspond to nothing else but the trivial, statistically expected distribution of these two isomers in a kinetically controlled phenol methylation reaction, when the reactivity of both the o- and the p-positions is equal. Somewhat lower values meet the thermodynamic equilibrium ratio of the p- and the o-isomer in the temperature ranges investigated (cf. Section 2.2.2.6). This individual equilibrium could establish via transalkylation with reactant component phenol, except, possibly, in pentasils and Mordenite.

2.2.4.2 High p/o-cresol ratios from phenol methylation

In comparing phenol methylation over the high SiO_2/Al_2O_3 ratio zeolites H-Y (59) and H-ZSM-5 (98) (cf. Table 2.15), Marczewski *et al.* [1988] concluded that H-ZSM-5 showed enhanced para-selectivity

(p/o-cresol ratio of 0.56 versus 0.33 for the H-Y (59) sample) due to product shape selectivity which would favour the desorption of the linear molecule. However, the ratio observed over the H-ZSM-5 corresponds almost to the statistical ratio of 0.5 and the low SiO_2/Al_2O_3 ratio samples of wide pore zeolite H-Y produced an even higher p/o-ratio (cf. Table 2.15).

As can be seen from Table 2.14, there are various catalysts that have a p/o-cresol ratio above 0.7 and even some above 1.0. This high p/o-cresol ratio has not been discussed in the respective publications as the main focus in literature has been on the explanation of "high" o-cresol selectivity, i.e. p/o-cresol ratios < 1 as discussed in the previous section.

Studying Table 2.14 shows that the highest p/o-cresol ratios (greater than 1.0) were obtained with the addition of sodium or potassium cations in the zeolite framework [Namba *et al.*, 1980; Parton *et al.*, 1989a]. Namba *et al.* [1980] concluded that moderate acid sites ($-3.0 \geq H_0 \geq -8.2$) on zeolite H-Y are advantageous to produce p-cresol (weaker acid sites produce anisole and stronger acid sites allow secondary reactions). However, Namba *et al.* [1980] did not explain why the moderate acid sites preferentially produced just p-cresol and not o-cresol. Also, these catalyst have a very limited lifetime as the phenol conversion was found to initially increase reaching a maximum (approximately 22% over H/Na/K-Y) after 60 minutes thereafter decreasing sharply (to approximately 3% after 120 minutes over H/Na/K-Y). Correspondingly the yield of p-cresol also reached a maximum and thereafter decreased as the conversion decreased. Namba *et al.* [1980] compared the different degrees of exchanged at the maximum yield of p-cresol and not at quasi-steady state. These catalysts are not commercially viable due to their strong deactivation. Similar conversion curves were found for disproportionation of ethylbenzene which was attributed the formation of higher alkylated aromatics such as polyalkylated diphenylethanes in the pore system [Mabaso, 2000; De Vos *et al.*, 2002]. However, Namba *et al.* [1980] gave no reference to the material balances they obtained in the phenol methylation reaction, therefore it can just be speculated that the conversion curves could be due to the formation of higher alkylated products.

The p/o-ratios obtained over dealuminated H-Y zeolite and H-USY, respectively, are strikingly inconsistent. Table 2.14, for instance gives 1.54 over H-USY (40) [Parton *et al.*, 1989a], 0.62 over H-USY (9) [Parton *et al.*, 1989b] and 0.33 over H-Y (59) [Marczewski *et al.*, 1988], all obtained at 200°C reaction temperature. Parton *et al.* [1989a] state that H-USY (40) was a commercially obtained sample from Toyo Soda and H-USY (9) was steamed but no steaming conditions are given or was any characterization details on these two zeolites given. Parton *et al.* [1989a] attributed the high p/o-cresol ratio on the H-USY (40) due to its higher acid strength, which promotes carbon alkylation over oxygen alkylation giving a higher p/o-cresol ratio. However, Marczewski *et al.* [1988] used a H-Y with a even higher SiO_2/Al_2O_3 ratio than Parton *et al.* [1989a] and obtained a low p/o-cresol ratio. It was not possible to compare these catalysts as already mentioned Parton *et al.* [1989b] did not give any details on the zeolites.

Over the H-zeolites listed in Table 2.14 the ranges of p/o-cresol ratios obtained in the temperature range of 180 - 250°C were as follows:

- H-Y: $0.32 \leq$ p/o-cresol ratio ≤ 0.71;
- H-USY and H/alkali-Y: $0.62 \leq$ p/o-cresol ratio ≤ 1.85;

- H-ZSM-5: $0.53 \leq$ p/o-cresol ratio ≤ 0.61;
- H-ZSM-11: p/o-cresol ratio = 0.50;
- H-Beta: p/o-cresol ratio = 0.64;
- H-Mordenite: $0 \leq$ p/o-cresol ratio ≤ 0.85.

As mentioned above there is a large range in p/o-cresol ratio obtained over H-Y zeolites. Shape selectivity can be excluded as a possible reason with these spacious materials. It was suggested that the different p/o-ratios obtained could be due to the range of SiO_2/Al_2O_3 ratios applied but available data appears inconsistent. The most remarkable p/o-cresol ratios, with values around 1 and up to almost 2 were reported, consistently by different research groups, over partially alkali exchanged zeolite H-Y and some samples of H-USY (Table 2.14, Figures 2.47 and 2.48). All these samples might contain Lewis acid sites, be they introduced by the alkali or by the extra-framework aluminium in the steamed samples (H-USY) (cf. Section 2.1.3).

The differences over the H-Mordenites may be due to the large difference in SiO_2/Al_2O_3 ratios as discussed above in Section 2.2.4.1. p/o-Cresol ratios which are insignificantly higher only than 0.5 were reported from phenol methylation over medium pore size zeolites H-ZSM-5 and H-ZSM-11. Shape selective effects, apparently, were weak, if present at all, over the samples used and at the conditions applied.

2.2.4.3 Cresol isomerizersion and transalkylation

The thermodynamic equilibrium distribution of the cresol isomers is given in Section 2.2.2.6 and Figures 2.32 and 2.33. The thermodynamically favoured isomer is m-cresol whereas p-cresol is the least stable one. It was found that cresols isomerize by two major routes. Firstly, directly by a unimolecular isomerization via a 1,2-methyl shift (Figures 2.31 and 2.39) as suggested by Parton *et al.* [1989a]; Chen *et al.* [1996]; Imbert *et al.* [1997b] and Imbert *et al.* [2000]. A second route is also possible, that is isomerization can occur via a transalkylation reaction (Figure 2.45) [Imbert *et al.*, 2000]. This bimolecular reaction may occur with phenol in a single step as shown in Figure 2.45 (1), (note that much phenol is present in phenol methylation reaction mixtures as part of the reactants) or with another cresol molecule in a two step reaction (Figures 2.45 (2) and 2.45 (3)). Over H-ZSM-5, Imbert *et al.* [2000] and Böhringer and Fletcher [2003] found that isomerization by 1,2-methyl shift is dominant as transalkylation (a bimolecular reaction) is limited by the space available near the acid sites and by the acid site density. Over H-USY and other large pore zeolites with a higher acid site density, the transalkylation reaction was found to be more significant.

2.2.5 Effect of reaction parameters

2.2.5.1 Reaction temperature

The reaction temperature has been shown to have an effect on the O-alkylation : C-alkylation ratio and on the cresol isomer distribution. Figure 2.46 shows the effect of increasing reaction temperature

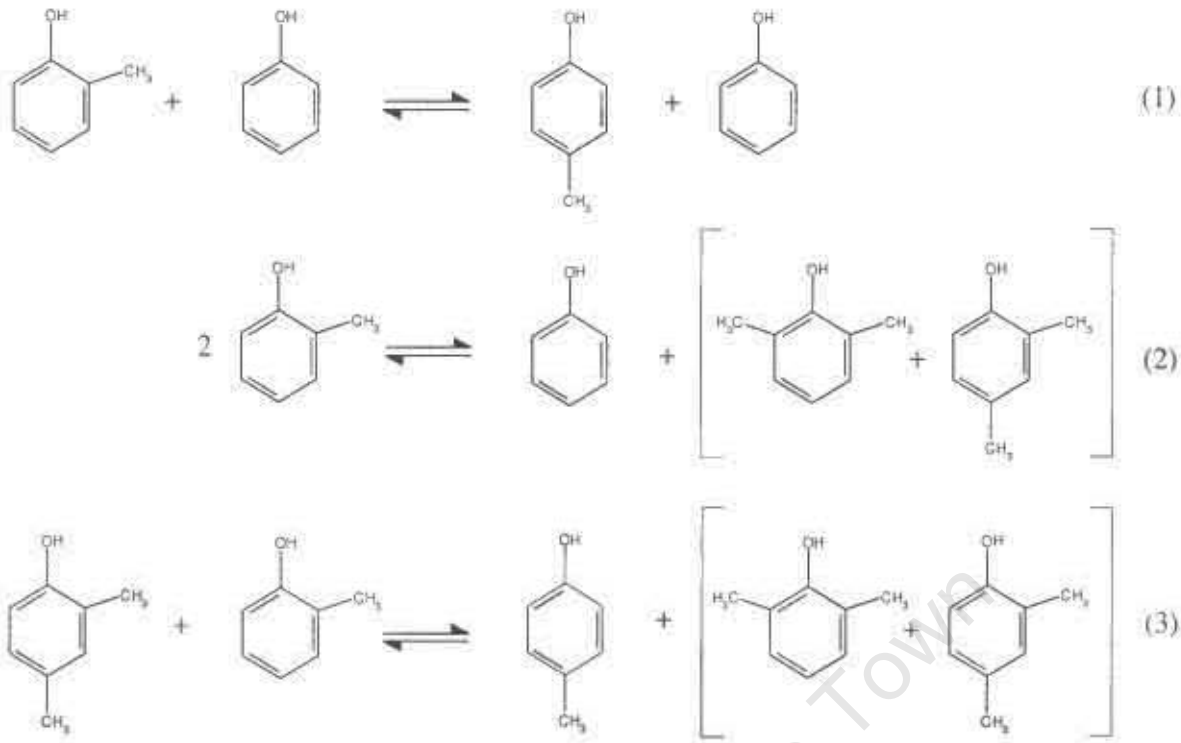

Figure 2.45: Cresol isomerization via transalkylation with phenol (1) or with another cresol molecule (2) - (3).

from 200 to 400°C over H/K-Y and H-ZSM-5 [Parton *et al.*, 1989a]. Firstly, it is worth noting that phenol conversion increases with increasing reaction temperature although only slightly over H/K-Y. Secondly, increasing the reaction temperature decreases the O/C-alkylation ratio. At higher reaction temperatures, the C-alkylation products are favoured over the O-alkylation reaction product. This is in agreement with Landau *et al.* [1997] (cf. Table 2.16) who compared O/C-alkylation selectivities at different temperatures but similar conversions. Pierantozzi and Nordquist [1986]; Santacesaria *et al.* [1990b]; Bautista *et al.* [1993] also obtained a decrease of the O/C-alkylation ratio with increasing reaction temperature but compared experimental results at different conversions (cf. Table 2.17). Balasubramanian *et al.* [2000] concluded that the decrease in anisole selectivity with increasing reaction temperature was due to the conversion of anisole to o-cresol whereas Santacesaria *et al.* [1990b] attributed the increase in the C-alkylation selectivity to the higher activation energy required for C-alkylation (134 kJ/mol vs 67 kJ/mol for O-alkylation). The latter may hold at least for low reaction temperatures (around 200°C) since selectivity was found independent from conversion under such mild conditions [Marczewski *et al.*, 1988; Garcia *et al.*, 1996] (cf. Section 2.2.3.3).

The effect of the reaction temperature on the cresol isomer distribution is that the selectivity of m- and p-cresol isomers increases with increasing reaction temperature at the same conversion, as shown in Table 2.16 [Landau *et al.*, 1997].

In some papers, the influence of reaction temperature on the product selectivity is interconnected with the influence of phenol conversion. Parton *et al.* [1989a] studied the "effect of temperature" on the p/o-cresol ratio over different catalysts as shown in Table 2.13. A critical analysis of these p/o-cresol ratios as a function of phenol conversion and reaction temperature is shown in Figures 2.47

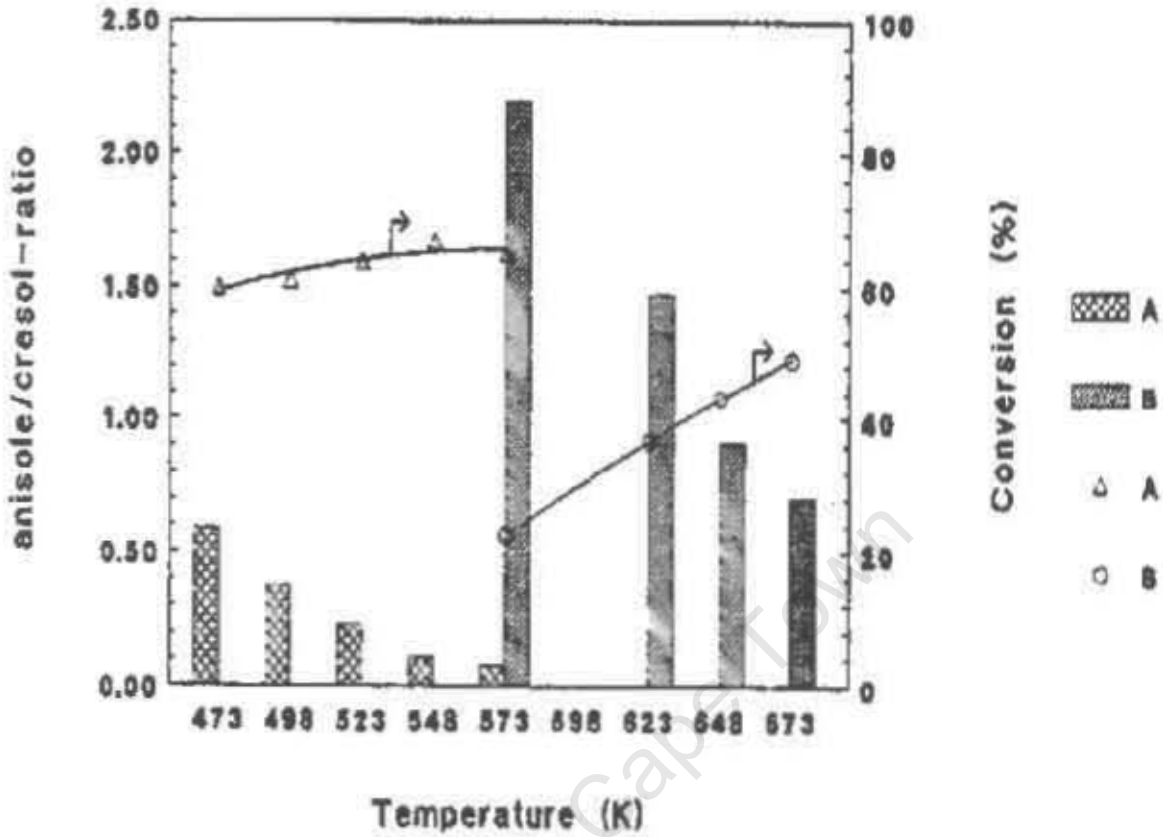

Figure 2.46: Conversion and anisole/cresol ratio versus reaction temperature for the methylation of phenol with methanol. (A) H/K-Y in the vapour phase and (B) H-ZSM-5 in the liquid phase (comparative drawing by Parton *et al.* [1989a] from data reported by Haung *et al.* [1986] (A) and Namba *et al.* [1980] (B)).

Table 2.16: Temperature effect on product selectivity for the methylation of phenol with methanol over zeolite H-Beta (reactants partial pressure = 0.1 bar) [Landau *et al.*, 1997].

Temperature (°C)	300	500
Phenol conversion (%)*	27	31
Anisole	43	32
o-Cresol	32	31
p-Cresol	13	19
m-Cresol	8	14
Other	4	4
O/C-Alkylation ratio	0.8	0.5
p/o-Cresol ratio	0.45	0.61

* Phenol conversions at 300 and 500°C are similar due to extensive catalyst deactivation at 500°C.

Table 2.17: The effect of reaction temperature and phenol conversion on the O/C-alkylation ratio for the methylation of phenol.

	Catalyst	Temperature (°C)**	Phenol conversion (%)	O/C-alkylation ratio	p/o-cresol ratio
Bautista *et al.* [1993]	$AlPO_4$-Al_2O_3	250	-*	5.0	-
		300	-	4.8	-
		350	-	2.6	-
		400	-	1.4	-
Santancesaria *et al.* [1990a]	γ-Al_2O_3	200	12.4	1.5	0
		300	35.5	0	0.03
		400	44.6	0	0.09
	Silica-alumina	200	2.5	4.9	0.51
		250	4.9	3.1	0.47
		300	8.7	2.5	0.44
	Phosphoric acid	225	7.5	9.5	0.58
		300	27.6	1.8	1.08
Pierantozzi and Nordquist [1986]	$La_2(HPO_4)_3$	300	12.6	17.1	-
		350	42.3	7.0	-
		400	73.0	2.9	-

* Phenol conversions not given;

** Reactant partial pressure given in Table 2.8.

and 2.48. As can be seen from the figures, there is no trend of the p/o-cresol ratio with either the phenol conversion nor with reaction temperature. The only apparent difference is that the low site density Y-zeolites (H-USY, H/K-Y and H/Na-Y) exhibited a much higher p/o-cresol ratio than the other zeolites studied, as discussed in Section 2.2.4.2.

2.2.5.2 Methanol : phenol ratio

Pierantozzi and Nordquist [1986] studied the effect of the reactants methanol to phenol ratio on phenol conversion, reaction rates and selectivity to anisole over Al_2O_3 and H-ZSM-5. Phenol conversion generally increased with increasing methanol to phenol ratio but was essentially constant at methanol to phenol ratios above 4. However, over Al_2O_3 the methanol to phenol ratio did not influence the reaction rates significantly but the anisole selectivity increased moderately (from 65.9 to 76.5 %) when the molar ratio was increased from 1 to 5. The exact opposite was found over H-ZSM-5, i.e. anisole selectivities were not affected by the methanol to phenol ratio but the anisole formation rates were significantly lower for the ratio of 5 than for the ratio 1 (1.8 mmol anisole /g cat · h compared to 0.77 mmol anisole /g cat · h).

Bautista *et al.* [1993] found that over an $AlPO_4$-Al_2O_3 catalysts, between a methanol to phenol ratio of 4 and 8, the O/C-alkylation ratio remained unchanged. It was also found that decreasing the ratio below 4 caused the selectivities to anisole, methylanisoles and dimethylanisoles to decrease and the selectivity to cresols increase.

Landau *et al.* [1997] studied the effect of reactants methanol to phenol ratio over zeolites H-Y and H-Beta with methanol to phenol molar ratios ranging from 0.03 to 1.4. Over H-Y, the phenol

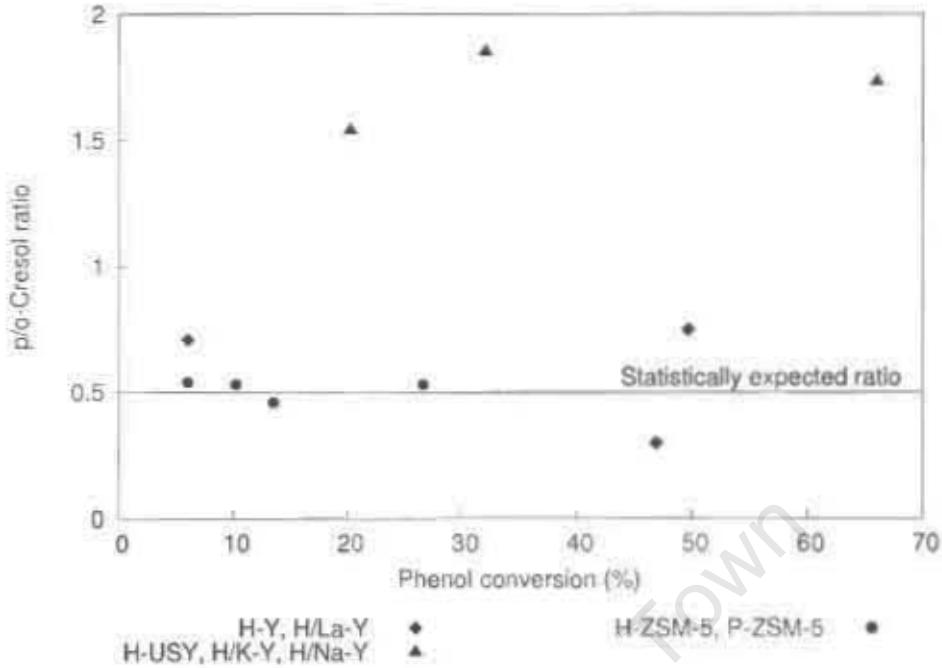

Figure 2.47: The relationship between p/o-cresol ratio and phenol conversion in the methylation of phenol with methanol (data from Parton *et al.* [1989a], statistical ratio due to two ortho position on the phenol and only one para position).

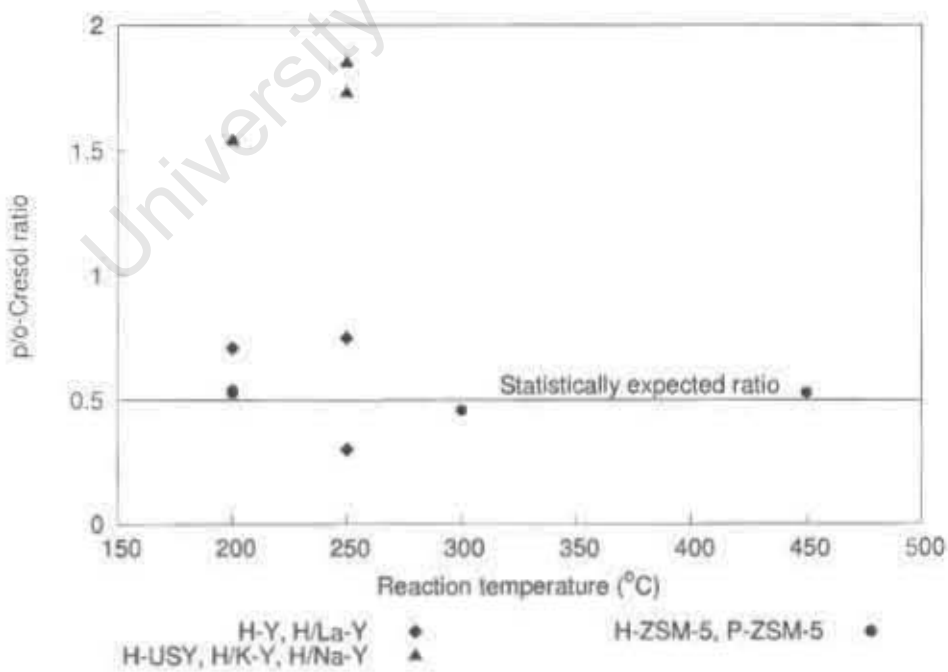

Figure 2.48: The relationship between p/o-cresol ratio and reaction temperature in the methylation of phenol with methanol (data from Parton *et al.* [1989a], statistical ratio due to two ortho position on the phenol and only one para position).

Table 2.18: The effect of methanol to phenol ratio on the phenol conversion and product selectivity in phenol methylation with methanol (reactant partial pressures are given in Table 2.8).

	Methanol to phenol molar ratio	Catalyst	Phenol conversion (%)	O/C-alkylation ratio	p/o-cresol ratio
Landau *et al.* [1997]	0.03 to 1.4 0.03 to 1.4	H-Y H-Beta	19 to 26 22 to 37	1.1 to 0.7 0.7	1.3 to 0.5 2
Bautista *et al.* [1993]	less than 4 4 to 8	$AlPO_4 - Al_2O_3$	increased constant at 2.3	4.9 3.6 to 4.9	- -
Pierantozzi and Nordquist [1986]	1 to 5 1 to 5	Al_2O_3 H-ZSM-5	10.7 to 23.9 19.8 to 22.0	2.04 to 4.32 1.5	- -

conversion increased only slightly with increasing methanol to phenol ratio but the p/o-cresol ratio decreased from 1.3 to 0.5 with increasing methanol to phenol ratio. Over H-Beta, the phenol conversion was dependent on the methanol to phenol ratio, increasing sharply between molar ratios of 0.03 and 0.1. The p/o-cresol ratio was found to remain constant at approximately 2. Landau *et al.* [1997] did not give an explanation for the differences between the zeolites.

Table 2.18 summaries all the results discussed above. Over all the catalyst, phenol conversion increases with increasing methanol to phenol ratio except at high ratios. However, since the molar concentration of phenol in the reactants mixture declined with increasing methanol to phenol ratio, this does not equal an increase in rates as clearly shown by Pierantozzi and Nordquist [1986] and also discussed in Section 2.2.3.4. Table 2.18 clearly indicates that there is no consistent trend with the methanol to phenol ratio neither for the O/C-alkylation ratio nor for the p/o-cresol ratio. The limited amount of data, however, does not allow to distinguish or group and classify the different types of catalysts.

2.2.5.3 Reaction pressure

The effect of pressure on the product selectivity and cresol isomer distribution has not yet been systematically investigated over zeolites. Most research groups have studied the phenol methylation reaction over zeolites in the gas phase with reactants partial pressures below 1 bar except for Haung *et al.* [1986] who studied the zeolites in the liquid phase.

Pierantozzi and Nordquist [1986] investigated the liquid phase methylation (autogeneous pressure = 82.7 bar) versus the gas phase methylation (reactants partial pressure = 0.2 bar) over $La_2(HPO_4)_3$ and $BaSO_4$ (Table 2.19). Increasing the pressure increased the O/C-alkylation ratio quite significantly. At 80 bar in the liquid phase, cresol formation was largely suppressed. Unfortunately, an explanation for the pressure effect on the O/C-alkylation ratio was not given nor was any data on the influence of pressure on the cresol isomer distribution presented.

Table 2.19: The effect of high pressure on the O/C-alkylation ratio (300°C, methanol : phenol molar ratio = 5, reactants partial pressure = 0.86 bar) [Pierantozzi and Nordquist, 1986].

Catalyst	Pressure (bar)	Phenol conversion (%)	Selectivity (mol%)				O/C-alkylation ratio
			Anisole	Cresols	Methylanisoles	Other	
$La_2(HPO_4)_3$	0.2*	12.6	94.3	5.5	0	0	17.1
	82.7**	50.2	96.6	2.7	0.6	0	35.8
$BaSO_4$	0.2*	7.2	90.9	9.1	0	0	9.9
	82.7**	30.3	98.9	1.11	0	0	89.1

* Gas phase - carrier gas = helium, GHSV = 450 - 650 h^{-1}

** Liquid phase - after 4 hours, reactants : catalyst mass ratio = 10.

2.2.6 Phenol methylation products conversion

The conversion of primary phenol methylation products, namely anisole and cresols, has been studied over different catalysts to help elucidate the reaction mechanism.

2.2.6.1 Anisole conversion

Anisole is one of the primary products and it can rearrange monomolecularly to form o-cresol or it can react with another anisole molecule, with a phenol molecule or with a methanol molecule. The mechanism of anisole rearrangement is discussed in Section 2.2.3.1.2 and illustrated in Figure 2.38.

2.2.6.1.1 Self alkylation of anisole The self alkylation of anisole over medium pore zeolites (H-ZSM-5, H-Ferrierite, H-ZSM-22) was investigated by Jacobs *et al.* [1988]. Reaction conditions of 180, 350 and 400°C, an anisole vapour pressure of 0.013 bar and W/F of 864 and 1728 kg·s/mol were studied. The products obtained were cresols, xylenols, methylanisoles and phenol (Table 2.20). Phenol was found to be in large excess of the sum of the molar selectivities of the xylenols and methylanisoles and this was attributed to dealkylation of the anisole with the formation of hydrocarbons. Namba *et al.* [1980] found that when reacting pure anisole, phenol can account for approximately 60 mol% of the product formed over a H/Na-Y catalyst and this was also attributed to dealkylation. Namba *et al.* [1980] found that the phenol formed by transalkylation to xylenols and methylanisoles accounts to 19 mol% of the product so it follows that 41 mol% of the phenol was formed through dealkylation. It was not mentioned what species other than phenol were formed by the dealkylation of anisole.

Jacobs *et al.* [1988] determined an overall reaction scheme of the conversion of anisole over zeolite H-ZSM-5, which is shown in Figure 2.49. It was found that methylanisoles and co-product phenol are primary products (reaction 1) whereas cresols were formed both as primary and secondary products (namely from the intramolecular rearrangement of anisole to o-cresol (reaction 2) or from the dealkylation of methylanisoles (reaction 5 in Figure 2.49)). Phenol as a primary product also forms by dealkylation of anisole (reaction 3). Xylenols were found to be secondary products formed by the intramolecular rearrangement of methylanisoles (reaction 4). Chantal *et al.* [1985] and Renaud *et al.*

Table 2.20: Product selectivity in anisole conversion over H-ZSM-5 at 400°C after 20 hours on stream (partial pressure of anisole = 0.013 bar) [Jacobs *et al.*, 1988].

W/F (kg · s/mol)	864	1728
Anisole conversion (%)	30.4	59.0
Product distribution of oxygenates (mol%)		
Phenol	48.1	47.6
Cresols	28.9	34.6
Xylenols	0.0	6.9
Methylanisoles	23.0	10.9

Table 2.21: Distribution of cresols from anisole conversion on H-ZSM-5 as a function of temperature (partial pressure of anisole = 0.013 bar, W/F = 1728 kg·s/mol) [Jacobs *et al.*, 1988].

Temperature (°C)	Anisole conversion (%)	Cresol distribution (%)		
		o-	p-	m-
180	25.3	83.1	16.9	0.0
350	41.2	72.6	23.9	3.5
400	57.4	54.4	19.2	26.4

[1986] found trace amounts of diphenyl ether formed over H-ZSM-5 presumably by transetherification of anisole as shown in Figure 2.50. Co-product dimethyl ether could be a major source of hydrocarbon formation [Chang, 1983; Laan and Ward, 1987; Möller *et al.*, 1999].

In terms of the cresol isomer distribution, Jacobs *et al.* [1988] found that at the lowest investigated temperature of 180°C, o-cresol was found, in the cresol fraction, in large excess (83.1 mol% o-cresol, 16.9 mol% p-cresol, no m-cresol), indicating that o-cresol is the only primary cresol formed from reaction 2 (Figure 2.49). m-Cresol was not present in the cresol fraction at low conversions but p-cresol is formed. This indicates that p-cresol is not formed from o-cresol by 1,2-methyl shift (cf. Figure 2.31) but is formed from the methylanisoles (reaction 5). At higher reaction temperatures, Jacobs *et al.* [1988] found that the o-cresol content in the cresols fraction decreased in favour of m-cresol (Table 2.21).

If high para-selectivity is desired, Jacobs *et al.* [1988] concluded that it maybe necessary to use a 10 membered ring zeolite with a channel size smaller than ZSM-5 (5.1 x 5.5 Å and 5.3 x 5.6 Å). Jacobs *et al.* [1988] used H-ZSM-22 (4.6 x 5.7 Å) and H-Ferrierite (4.2 x 5.4 Å) in the self alkylation of anisole. However, a p/o-cresol ratio was found which was lower over H-ZSM-22 and H-Ferrierite than over H-ZSM-5 (cf. Table 2.22). It was concluded that the reaction occurred on the external surface of H-ZSM-22 and H-Ferrierite, resulting in a higher o-cresol selectivity.

Marczewski *et al.* [1989] studied the self-alkylation of anisole at 200°C over zeolite H-USY. At low conversion, the molar ratio of phenol to methylanisoles was close to unity, indicating that methylanisoles and phenol are formed from anisole disproportionation (cf. Figure 2.51). From curves of product selectivity versus anisole conversion (cf. Figure 2.52), Marczewski *et al.* [1989] concluded

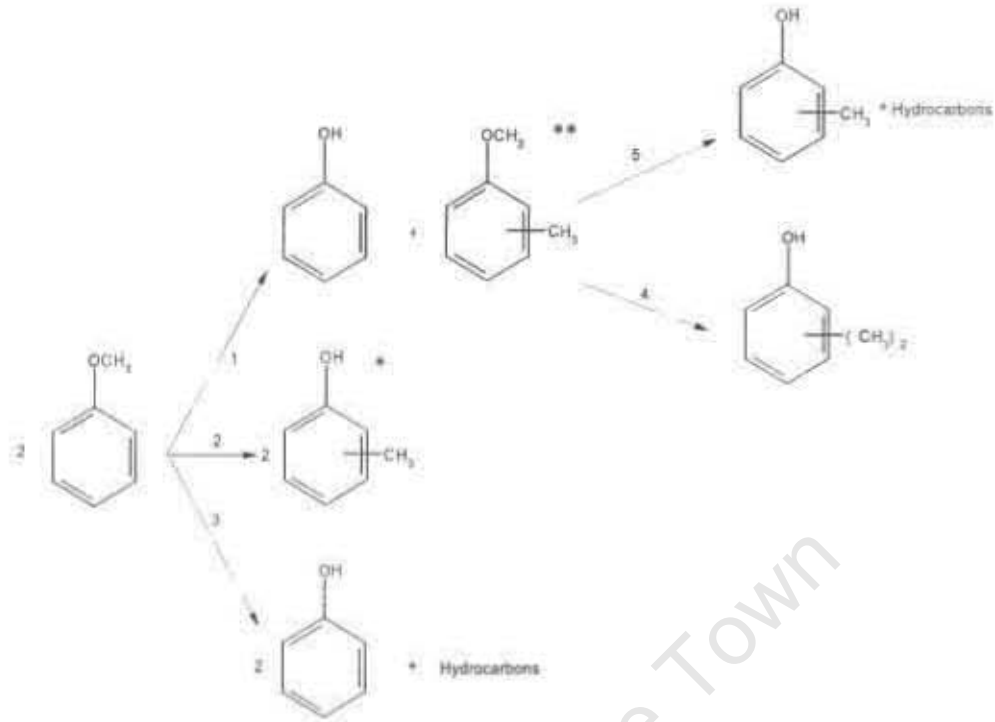

Figure 2.49: Overall reaction mechanism of the self-alkylation of anisole over H-ZSM-5 [Jacobs *et al.*, 1988].
* At low temperatures (180°C) only o-cresol is formed;
** At low temperatures (180°C), this is only o- and p-methylanisole.

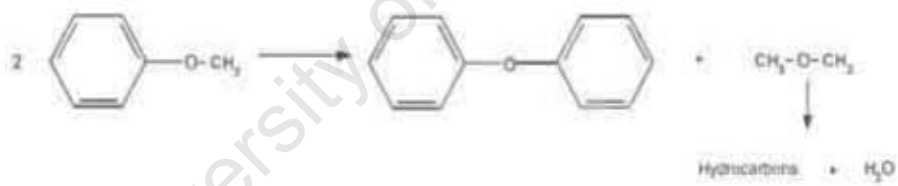

Figure 2.50: Diphenyl ether and hydrocarbon formation from anisole.

Table 2.22: Product distribution from anisole conversion over H-ZSM-5, H-ZSM-22 and H-Ferrierite (400°C and reactants partial pressure of 0.013 bar) [Jacobs *et al.*, 1988].

	H-ZSM-5	H-ZSM-22	H-Ferrierite
Phenol conversion (%)	52.0	43.9	59.5
Product selectivities (mol%)			
Phenol	54.6	62.1	60.0
Cresols	26.7	27.6	30.8
Xylenols	7.2	6.1	5.5
Methylanisoles	11.5	4.2	3.7
Cresol isomer distribution			
o-cresol	60.4	82.5	83.5
p-cresol	28.1	8.8	10.8
m-cresol	11.5	8.7	5.7
p/o-cresol ratio	0.47	0.11	0.13

Figure 2.51: Anisole disproportionation to methylanisole and phenol [Marczewski *et al.*, 1989].

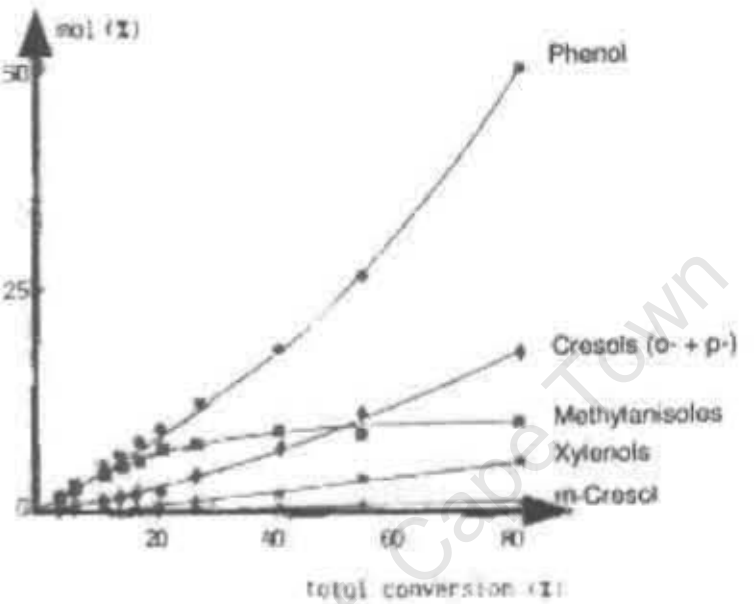

Figure 2.52: Transformation of anisole over H-USY at 200°C (reactants partial pressure = 0.2 bar, reactants rate 0.5 - 2 ml/h) [Marczewski *et al.*, 1989].

that the primary products are only phenol and methylanisoles and that cresols, xylenols and dimethylanisoles were formed in secondary reactions.

In summary, over zeolites H-ZSM-5 and H-Y the primary products are methylanisole and phenol. Over H-ZSM-5, o-cresol was found to be a primary product as well, formed via anisole rearrangement, whereas over H-Y, cresols were found to form only as secondary products. A possible explanation for the difference may be the high anisole rearrangement over H-ZSM-5 could be due to the low reactants partial pressure (0.013 bar) which will not favour bimolecular reactions whereas over H-USY the reactants partial pressure (0.2 bar) was sufficiently high to favour bimolecular reactions.

2.2.6.1.2 Anisole transalkylation with phenol Beltrame *et al.* [1987] studied the alkylation of phenol with anisole over zeolites H-X, La/Na-X, La-X, H-Y, La/H/Na-Y, La/Na-Y, H/RE/Na-Y, Ca/Na-Y, H-ZSM-5, H-ZSM-11 and γ-Al_2O_3 at 250°C. Figure 2.53 shows all the reactions that were postulated to occur to explain their observed product mixture of xylenols, cresols, methylanisoles and phenol. Anisole disproportionation forms methylanisoles and phenol (reaction 1). Transalkylation between anisole and phenol forms cresols and restores the phenol (reaction 2). In secondary reactions, the cresols can react further with another anisole to form xylenols and phenol (reaction 3). Cresols, as well as dimethylanisoles could also be formed from disproportionation reactions between methylanisole

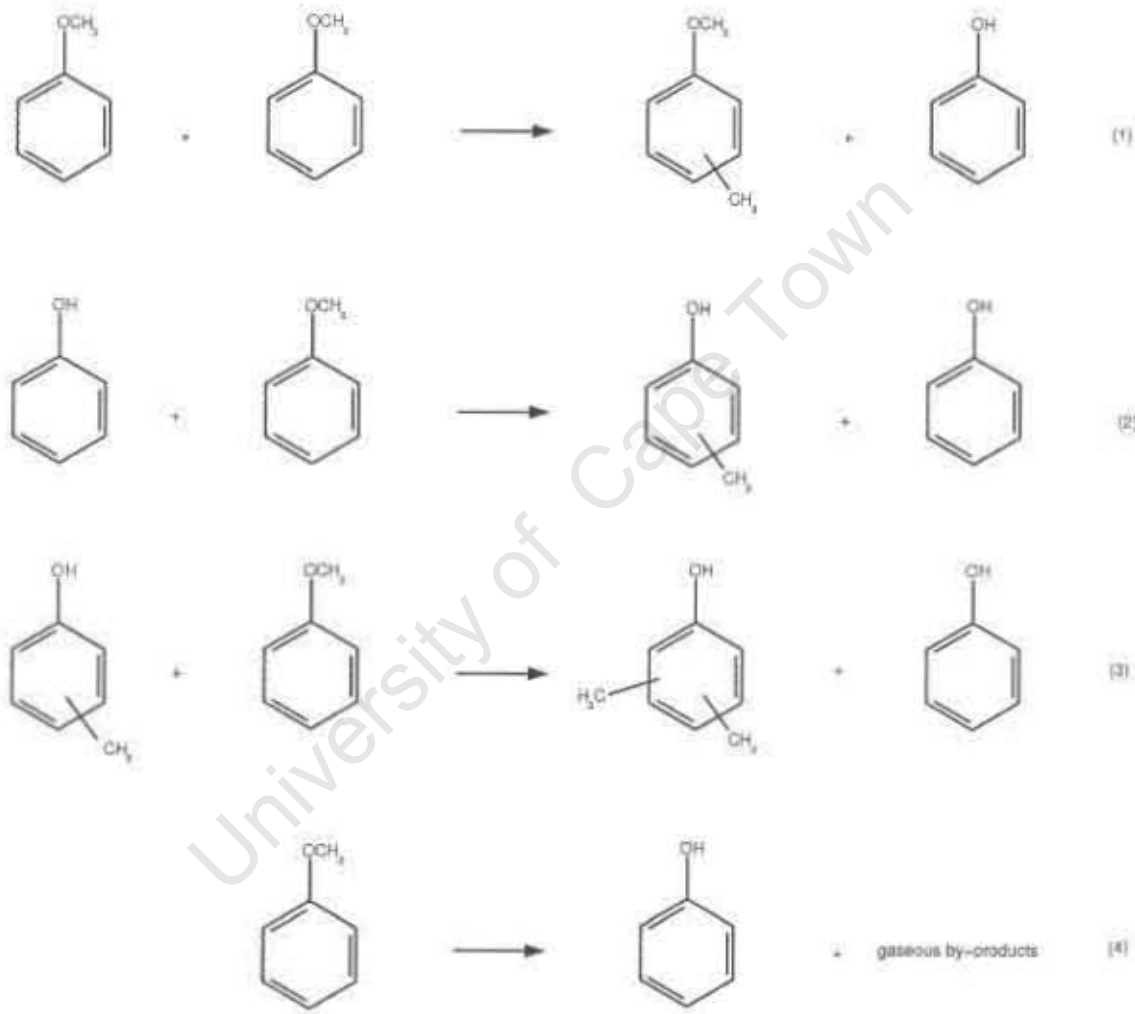

Figure 2.53: Anisole and phenol reactions [Beltrame *et al.*, 1987].

Table 2.23: p/o-Cresol ratios obtained from alkylation of phenol with anisole over different catalysts (250°C, phenol : anisole molar ratio = 1, reactants partial pressure = 0.2 bar, after 2 hours on stream) [Beltrame *et al.*, 1987].

Catalyst	p/o-Cresol ratio*
H-X	0.13
La-X	0.50
H-Y	0.10
La/Na-Y	0.17
H/RE/Na-Y	0.50
H-ZSM-11	0.43
γ-Al_2O_3	0.01

* Derived from graphs from Beltrame *et al.* [1987].

molecules, which are formed in reaction 1, and reactants compounds phenol and anisole, respectively, but this has not been addressed by Beltrame *et al.* [1987] and not included in Figure 2.53. Beltrame *et al.* [1987] could not distinguish between the xylenols formed from transalkylation with anisole (reaction 3) and from phenol alkylation with anisole (reaction 2). The dealkylation of anisole (reaction 4) was also observed in the alkylation of phenol with anisole since a higher phenol selectivity was obtained than what was formed in reactions 1 to 3. Anisole dealkylation was regarded as the source of the gaseous by-products obtained.

Marczewski *et al.* [1989] found that in converting an equimolar mixture of phenol and anisole over zeolite H-USY at 200°C, the amount of cresols formed was approximately twice the amount of methylanisoles formed (for conversions of less than 15%). It was concluded that the alkylation of phenol by anisole is twice as fast as the disproportionation of anisole i.e. the alkylation of anisole by anisole. This is not unexpected, since a hydroxyl group (phenol) is a much more effective activator of the benzene ring for electrophilic substitution than a methoxy group (anisole) [Sykes, 1986b; Morrison and Boyd, 1987].

H-Y showed the highest selectivity to cresols and xylenols of all the zeolites studied by Beltrame *et al.* [1987]. In terms of the cresol isomer distribution, Beltrame *et al.* [1987] found that the ortho-selectivity observed in the alkylation of phenol with anisole was higher than that obtained in the alkylation of phenol with methanol over all the catalyst studied in earlier work by this group (Balsama *et al.* [1984]).

Table 2.23 gives the different p/o-cresol ratios obtained by Beltrame *et al.* [1987] over different catalysts. The p/o-cresol ratios were quite low over all the catalysts. La-X, H/RE/Na-Y and ZSM-11 had the highest p/o-cresol ratios of around 0.5. Phenol alkylation with anisole over γ-Al_2O_3 gave a cresol fraction consisting of over 99% ortho-cresol. Beltrame *et al.* [1987] don't explain the different p/o-cresol ratios obtained over the different catalysts. The high o-cresol content in the cresol fraction over γ-Al_2O_3 may be due to the internal rearrangement of anisole to o-cresol as described by some authors such as Jacobs *et al.* [1988] (Section 2.2.6.1.1) and Section 2.2.3.1.2 and Figure 2.38.

Table 2.24: Product selectivity in the alkylation of anisole with methanol at 200°C, anisole to methanol ratio of 1, reactants partial pressure = 0.013 bar, W/F = 1736 kg·s/mol and after 3 hours on stream [Parton *et al.*, 1989b]. (Methyl balance calculated from the data reported by Parton *et al.* [1989b]).

Catalyst	H-USY	H-ZSM-5
Anisole conversion (%)	58.4	60.9
Product selectivity of oxygenates (mol%)		
Phenol	32.5	79.3
Cresols	23.8	15.3
Xylenols	6.8	0.0
Methylanisoles	36.9	5.4
From these data the following methyl group balance results		
Xylenols + methylanisoles - phenol (mol%)	+11.2	-73.9

2.2.6.1.3 Anisole alkylation with methanol The addition of methanol to anisole did not significantly change the reaction selectivity compared to the conversion of pure anisole. Disproportionation and the internal rearrangement to o-cresol remained the main anisole reactions [Marczewski *et al.*, 1989].

Over H-ZSM-5 and H-USY, at 200°C and an anisole to methanol molar ratio of 1, the major products in the anisole and methanol reaction were still cresols, methylanisoles and phenol (Table 2.24) [Parton *et al.*, 1989b]. Therefore, it was concluded that anisole alkylation by methanol was very slow in comparison to anisole disproportionation or dealkylation. Indeed, a methyl group balance over the products of anisole methylation with methanol (Table 2.24) indicates an only marginal gain of additional methyl groups over H-USY. Over H-ZSM-5, the major reaction is still dealkylation, as generally obtained in the conversion of pure anisole over medium pore zeolites (Table 2.20 and 2.22).

Figure 2.54 shows the o-cresol content in the cresol fraction against anisole conversion in the anisole methylation reaction studied by Parton *et al.* [1989b]. m-Cresol was not formed at the reaction conditions applied (200°C). The content of o-cresol at low conversions is 100%, i.e. o-cresol is obviously a primary product and so it is necessarily formed via the monomolecular internal reaction of anisole. p-Cresol is clearly of secondary nature and is necessarily obtained by a sequence of bimolecular (transalkylation) reactions since m-cresol, which is the intermediate of a possible monomolecular 1,2-shift reaction sequence starting from o-cresol, was not obtained at all. The bimolecular formation of p-cresol starting with an anisole disproportionation or o-cresol transalkylation step, is largely suppressed in a pentasils compared to a Y zeolite [Parton *et al.*, 1989b]. Therefore, at a given medium conversion of anisole (say 40%) over H-ZSM-5, the o-cresol content in the cresol fraction (o/(o+p)-cresol = 98%) is still higher in anisole methylation than in phenol methylation with methanol (o/(o+p)-cresol = 67%). This confirms that the intramolecular rearrangement of anisole to o-cresol is the major primary reaction pathway for this reaction [Parton *et al.*, 1989b].

Bautista *et al.* [1995] also investigated anisole conversion in the presence of methanol over an $AlPO_4$-Al_2O_3 catalyst at 250 - 300°C. It was found that the major primary reactions were the

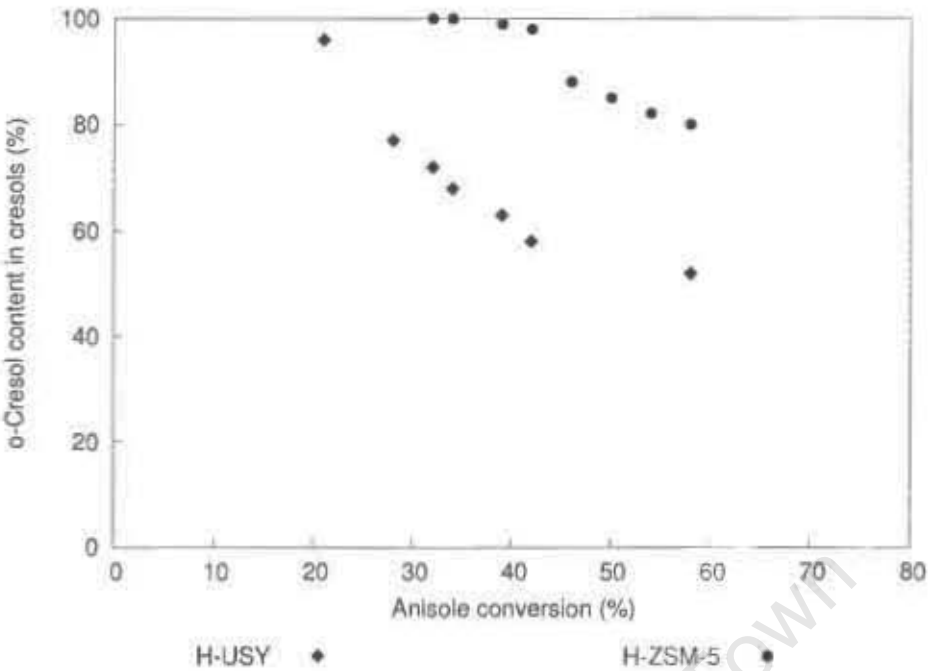

Figure 2.54: o-Cresol content in the cresol fraction from the methylation of anisole (200°C, reactants partial pressure = 0.013 bar and W/F = 1736kg·s/mol) (redrawn graph from [Parton *et al.*, 1989b]).

Table 2.25: Selectivities (mol%) at different reaction temperatures of conversion of anisole with methanol over $AlPO_4$-Al_2O_3 (5 wt% Al_2O_3) catalyst (reactants partial pressure not stated) [Bautista *et al.*, 1995].

Temperature (°C)	Phenol	Cresols	Methylanisoles	Dimethylanisoles	Cresol distribution (%)		Other
					o-	p- + m-	
250	60.9	15.1	12.9	2.0	80.8	19.2	9.1
300	45.7	17.1	12.7	5.5	73.1	26.9	19.1

* Other = pentamethylbenzene and xylenols and trimethylphenols

dealkylation to phenol, the intramolecular rearrangement to o-cresol and alkylation preferentially to 2-methylanisole as shown in Table 2.25.

2.2.6.1.4 Summary of anisole conversion studies In the conversion of anisole either with itself, with phenol or with methanol, the major products are cresols, methylanisoles, xylenols and phenol. With the two former reactions, phenol molar selectivities were found to be higher or even much higher than the sum of molar selectivities of methylanisole and xylenols except at low conversions. This was attributed to the dealkylation of anisole to phenol but what the other dealkylation products are, was not given in detail ("gaseous" products and "hydrocarbons" were mentioned).

Marczewski *et al.* [1989] summarized the rates of formation of the major products from the gas phase alkylation of phenol with methanol, anisole with methanol and phenol with anisole as shown in Table 2.26. The rate of cresols formation from phenol methylation does not depend on the methylating agent (methanol or anisole) but is at least 4 times the rate of cresol formation via internal rearrangement of anisole (in the anisole/methanol mixture). The rate of methylanisoles formation

Table 2.26: Alkylation reactions over H-USY at 200°C in the gas phase and in equimolar amounts (reactants partial pressure = 0.2 bar) [Marczewski *et al.*, 1989].

Reaction mixture	Total conversion (%)	Reactivities (mmol/h·g) reactant transformed into			
		phenol	anisole	cresols	methylanisoles
Phenol/methanol	14.3	-	15.4	5.3	1.4
Anisole/methanol	8.6	4.3	-	1.2	4.8
Phenol/anisole	4.2	-	-	5.0	2.9

from disproportionation of anisole is about two times lower with the anisole/phenol mixture than with the anisole/methanol mixture (note that anisole alkylation by methanol was found to be very slow in comparison to anisole disproportionation (cf. Section 2.2.6.1.3) [Marczewski *et al.*, 1989]). The lower rate in the presence of phenol indicates that phenol inhibits this reaction [Marczewski *et al.*, 1989].

2.2.6.2 Cresol conversions

A cresol can isomerize to the other isomers either by a 1,2-methyl shift isomerization, as discussed in Section 2.2.4.3 or can undergo subsequent disproportionation reactions to first yield xylenols and phenol, then the different cresol isomers.

Figure 2.55 shows the possible m-cresol reactions over H-USY zeolites [Imbert *et al.*, 2001]. The major reactions at 380°C are the cresols isomerization via 1,2-methyl shift (reaction 1) and cresol disproportionation to form phenol and xylenols (reaction 2). Minor reactions are the transalkylation between a reactant cresol and a product xylenol (reaction 3 and 3'). Reaction 3' produces cresol isomers as well. Another relevant side-reaction is the dealkylation (reaction 4). The suggestion of methane as the immediate co-product from dealkylation phenol (reaction 4), cannot easily be understood.

Imbert *et al.* [2000] studied the cresol transformations over medium pore zeolite H-ZSM-5 (SiO_2/Al_2O_3 molar ratio = 54) and large pore zeolite, "H-USY" (SiO_2/Al_2O_3 molar ratio = 5, which corresponds to an undealuminated H-Y). Over H-ZSM-5, Imbert *et al.* [2000] observed that the 1,2-methyl shift isomerization reaction was dominant (isomerization to disproportionation ratios between 10 and 140) as the disproportionation reaction is limited by the space available near the acid sites and by the acid site density. Over the spacious H-Y with its higher acid site density, the disproportionation reaction was more dominant (isomerization to disproportionation ratios between 0.5 and 3).

Engel *et al.* [1985] found that H-ZSM-5 exhibited shape-selective effects in the isomerization of m-cresol and o-cresol over the temperature range of 250 to 450°C. In the isomerization of m-cresol, the formation of p-cresol was favoured over the formation of o-cresol. As Parton *et al.* [1989a] derived from Engel *et al.* [1985], p/(p+o)-cresol ratios between 0.7 and 0.8 were obtained at m-cresol conversions between 10 and 20%. This corresponds to a ca. four-fold preference of the slim p-isomer over the more bulky o-isomer.

In the isomerization of o-cresol to m-cresol and p-cresol over H-ZSM-5, Parton *et al.* [1989a] claim that a definite shape selectivity to p-cresol was found, since p/(p+m)-ratios, which are higher than

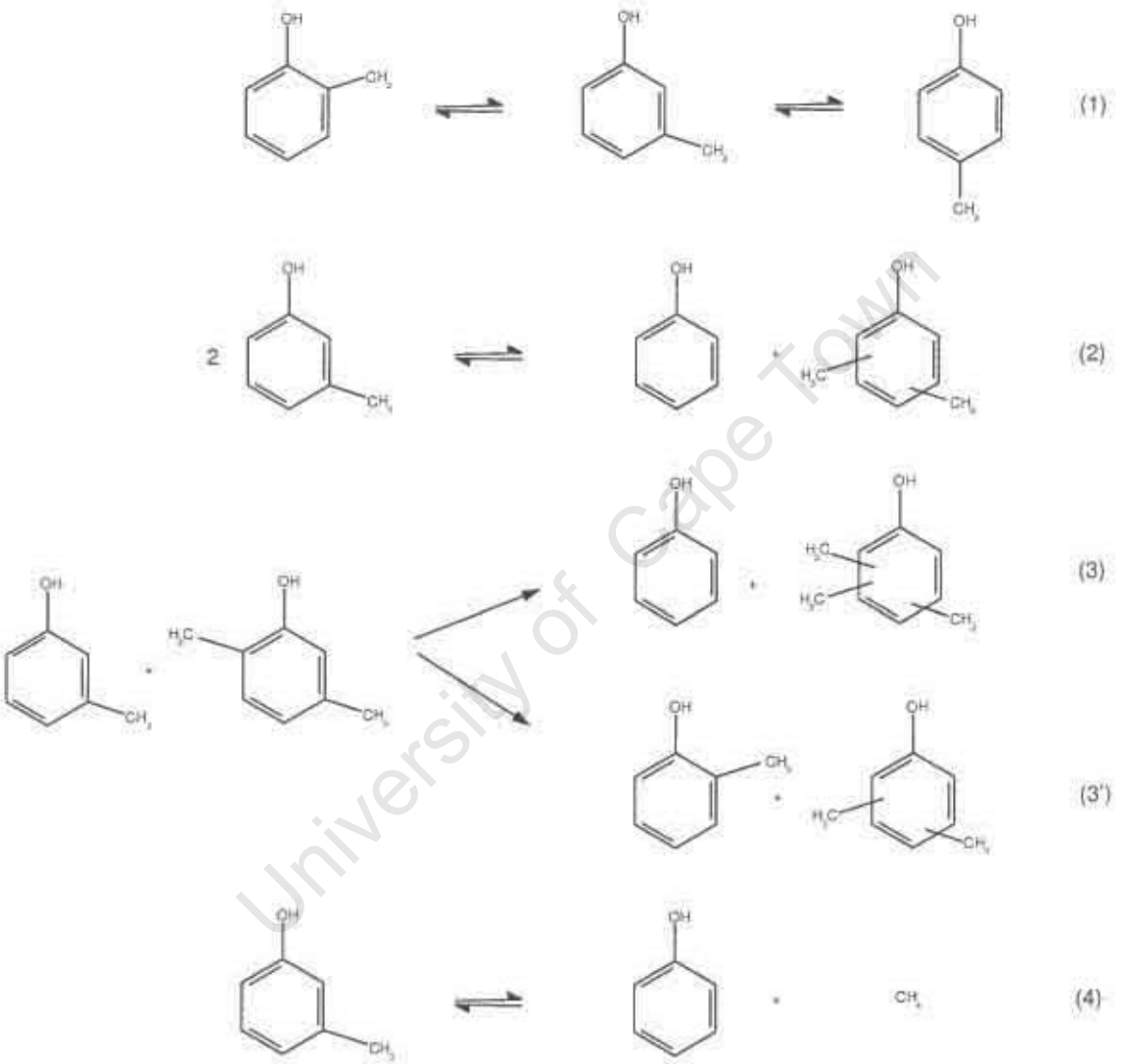

Figure 2.55: Reaction scheme for (1) 1,2-shift isomerization (2) disproportionation (3) transalkylation with primary product xylenols and (4) dealkylation of m-cresol over H-FAU zeolites [Imbert *et al.*, 2001].

the thermodynamic equilibrium ratio, were observed. For high o-cresol conversions between 30 and 55%, a constant p/(p+m)-cresol ratio of 0.24 was obtained at 380°C. Indeed, the thermodynamic equilibrium calculated for the p/(p+m)-cresol ratio is 0.08, using only Stull's [1969] data, but using Imbert's [1997a] and Böhringer and Fletcher's [2003] data results in a p/(p+m)-cresol equilibrium ratio around 0.25 (cf. the critical discussion of Stull's *et al.* [1969] data in Section 2.2.2.6). Therefore, it must be assumed that for o-cresol conversion an equilibrium was reached between p- and m-cresol under the given reaction conditions, i.e. that no shape selective effect occurred, whereas for m-cresol conversion, p-cresol formation indeed is favoured over o-cresol formation.

Steck *et al.* [1990] studied o-cresol isomerization over H-ZSM-5 with different crystal sizes. It was claimed that the zeolite crystal size has a large effect on the p- to m-cresol ratio in the product, in particular for crystals larger than 3 μm. Steck *et al.* [1990] obtained a 1.54 p/m-cresol ratio at 500°C over H-ZSM-5 with a crystal size of 9 μm.

2.2.7 Kinetics of the alkylation of phenol with methanol

The kinetics of the alkylation of phenol with methanol were studied by Santacesaria *et al.* [1990a] and Marczewski *et al.* [1996]. Santacesaria *et al.* [1990a] studied the reaction over H-ZSM-5 whereas Marczewski *et al.* [1996] carried out a kinetic study over γ-Al_2O_3.

2.2.7.1 Kinetic studies over H-ZSM-5

Santacesaria *et al.* [1990a] assumed a Rideal mechanism as the Brønsted acid sites in H-ZSM-5 are widely separated from one another. This Rideal mechanism occurs between an adsorbed methanol species and a phenol from the "gas phase". Santacesaria *et al.* [1990a] considered the following reaction scheme:

		Alkylation to
(1)	phenol + methanol → anisole + water	Oxygen
(2)	phenol + methanol → cresols + water	Ring
(3)	anisole + anisole → phenol + methylanisoles	Ring
(4)	anisole + phenol → phenol + cresols	Ring
(5)	anisole + methanol → methylanisoles + water	Ring
(6)	cresols + methanol → methylanisoles + water	Oxygen
(7)	cresols + methanol → xylenols + water	Ring
(8)	cresols + anisole → methylanisoles + phenol	Oxygen
(9)	cresols + anisole → xylenols + phenol	Ring
(10)	methylanisoles + Ar − OH → 2 cresols	Ring
(11)	2 methylanisoles → cresols + xylenols	Ring
(12)	methylanisoles + cresols → cresols + xylenols	Ring

Due to the large number of reactions, the reactions were divided into two classes, namely oxygen (O-) and ring (C-) alkylation. The assumption was made that the same type of kinetic law applies for the two alkylation reaction classes. Santacesaria *et al.* [1990a] thereby obtained the following kinetic expressions for the O-alkylation reaction and for the C-alkylation reaction:

$$r_{O-alkylation} = \frac{\eta_O k_O Y_{A_i} Y_{POH_i} P^2}{1 + b_{AA} P \sum_i Y_{AA_i} + b_A P y_4} \tag{2.1}$$

$$r_{R-alkylation} = \frac{\eta_R k_R Y_{A_i} Y_{R_i} P^2}{1 + b_{AA} P \sum_i Y_{AA_i} + b_A P y_4} \tag{2.2}$$

where:

- $r_{O-alkylation}$ and $r_{R-alkylation}$ are the reaction rates of the O-alkylation and C-alkylation respectively;
- η_O and η_R are the catalyst efficiency factors;
- k_O and k_R are the kinetic constants for O-alkylation and C-alkylation, respectively;
- Y_{A_i} refers to the mole fraction of the alkylating agent (methanol);
- Y_{POH_i} refers to the mole fraction of components which can be alkylated at the oxygen, namely phenol and cresols;
- Y_{R_i} refers to the mole fraction of all aromatic compounds;
- P refers to the reaction pressure;
- b_{AA} and b_A are "group deactivating contributions";
- Y_{AA_i} refers to the mole fraction of each aromatic component having alkylating properties, that is anisole and methylanisoles;
- y_4 is the mole fraction of water.

At low conversion the methylation of phenol with methanol over H-ZSM-5 at 300°C, is first order with respect to each of the reactants components, methanol and phenol.

At 300°C over H-ZSM-5 (no reactants partial pressure was given), the following kinetic parameters were obtained:

$$\eta_O k_O = 4629\ mol \cdot h^{-1} \cdot bar^{-2}$$
$$\eta_R k_R = 2478\ mol \cdot h^{-1} \cdot bar^{-2}$$
$$b_A = 207\ bar^{-1}$$
$$b_{AA} = 1184\ bar^{-1}$$

At low conversions, Y_{POH_i} and Y_{R_i} refer only to phenol, therefore the difference between $r_{O-alkylation}$ and $r_{R-alkylation}$ is only in the combined catalyst efficiency factor and rate constant ($\eta_O k_O$ and $\eta_R k_R$ terms, respectively). The kinetic parameters suggest that O-alkylation is twice as fast as C-alkylation at 300°C.

Marczewski *et al.* [1989] found that O-alkylation was three times as fast as C-alkylation at 200°C over H-USY. This difference between Santacesaria *et al.* [1990a] and Marczewski *et al.* [1989] could be due to the temperature difference. As already mentioned, C-alkylation has a higher activation energy [Santacesaria *et al.*, 1990b] and so it was expected and was found that the preference for O-alkylation will increase with decreasing temperature (cf. Section 2.2.3.2).

From equations 2.1 and 2.2, the inhibitory factors for the methylation of phenol with methanol are the adsorption of anisole, methylanisoles and water on the active sites. This infers that phenol and cresols are not inhibitory as they are either not adsorbed or very weakly absorbed on the catalyst.

2.2.7.2 Kinetics over other H-zeolites at low reaction temperatures

Marczewski *et al.* [1996] found that all zeolites investigated in their work showed first order for methanol but a zero reaction order for phenol when studied at 200°C. This was accounted to the "capillary condensation" of phenol in the zeolite pores, that is, the pores are completely filled with (mainly) phenol, resulting in a constant concentration and high surplus of phenol in the vicinity of the acid sites irrespective of the gas phase phenol concentration.

2.2.7.3 Kinetics over γ-Al_2O_3

To avoid "capillary condensation" in micropores as occurs in zeolites, Marczewski *et al.* [1996] studied the kinetics of the phenol methylation reaction using γ-Al_2O_3 at 200°C and a reactant partial pressure of 0.2 bar. Phenol conversion was less than 5% and anisole, o-cresol and p-cresol were the only products. Assuming a simple power rate law:

$$r = kP^{a}_{phenol}P^{b}_{methanol} \tag{2.3}$$

Apparent reaction orders for phenol of -0.2 and for methanol of 0.1 were obtained. The opposite signs for the reaction order of phenol and methanol over γ-Al_2O_3, indicate that both reactants adsorb strongly and competitively on the same kind of active site. These findings suggest a Langmuir type rate law.

The active sites on γ-Al_2O_3 are assumed to be Lewis acid-base pairs [Marczewski *et al.*, 1996], whereby the phenol interacts with the basic center and the methanol interacts with the acidic center. If a rate equation is developed where the surface reaction between strongly chemisorbed molecules of phenol and methanol was the rate-determining step, the following rate expression was obtained:

$$r = \frac{kP_{phenol}P_{methanol}}{(K_{phenol}P_{phenol} + K_{methanol}P_{methanol})^2} \tag{2.4}$$

where:

- r is the reaction rate of phenol consumption;
- k is the rate constant;
- P_{phenol} is the partial pressure of phenol;

- $P_{methanol}$ is the partial pressure of methanol;
- K_{phenol} is the equilibrium constants for phenol adsorption;
- $K_{methanol}$ is the equilibrium constant of methanol adsorption.

Marczewski *et al.* [1996] found by doing a least-square fit to the rate equation (Equation 2.4) gave a 0.94 correlation coefficient for the mechanism involving the strongly adsorbed phenol and methanol.

It follows that studying phenol methylation over γ-Al_2O_3 does not provide additional information for the understanding of phenol methylation kinetics over H-zeolites at low reaction temperatures.

2.2.7.4 Comparison of the two mechanisms and rate laws under discussion

Firstly, Santacesaria *et al.* [1990a] tried to consider all the possible reactions of reactants (methanol and phenol) and major primary products (anisole, cresols and methylanisole) but lumped them into oxygen (O-) and ring (C-) alkylation. Phenol conversions up to 25% were considered, whereas Marczewski *et al.* [1996] only modelled the primary reaction of phenol and methanol forming anisole and cresols (at phenol conversions less than 5%).

Secondly, at low conversion, Santacesaria *et al.* [1990a] and Marczewski *et al.* [1996] obtain the same reaction orders over H-ZSM-5 (300°C) and γ-Al_2O_3 (200°C), respectively. That is, first order with respect to each of the reactants components (phenol and methanol). However, Marczewski *et al.* [1996] stated that over H-zeolites at 200°C, zero reaction order was obtained with respect to phenol.

Thirdly, Santacesaria *et al.* [1990a] and Marczewski *et al.* [1996] disagree on the species that inhibit the alkylation reaction. Santacesaria *et al.* [1990a] found that anisole and methylanisole were inhibitory, whereas Marczewski *et al.* [1996] found that the inhibitory species were the reactants components. So one of the major differences between Santacesaria *et al.* [1990a] and Marczewski *et al.* [1996] is that the latter found phenol to inhibit the phenol methylation reaction whereas the former found this not to be the case. A possible reason for this discrepancy is that Santacesaria *et al.* [1990a] studied the reaction at much higher phenol conversion than Marczewski *et al.* [1996], thereby found the products to inhibit the reaction. Santacesaria *et al.* [1990a] considered the reaction at 300°C, to be between adsorbed methanol and a free phenol whereas Marczewski *et al.* [1996] considered the reaction at 200°C, to be between adsorbed methanol and adsorbed phenol molecules.

Chapter 3

Objectives of research

Phenol alkylation with methanol mainly yields anisole, cresols, methylanisoles and xylenols. Cresols are important raw materials in many industrial applications. Of the western world cresol market, 55% originates from synthetic cresols whereas 45% originates from so-called "natural" cresols obtained from coal tars [Fiege and Bayer AG, 2001]. It is possible to produce a high selectivity to o-cresol by methylation of phenol with methanol over a basic or Al_2O_3 catalyst or Fe/V catalyst. Direct synthesis of high purity m-cresol and p-cresol is desired due to the high separation costs of these two isomers [Parton *et al.*, 1989a]. A m-cresol free or very low m-cresol concentration in the product is desired for purification reasons and a high p/o-cresol is also desired in the product for yield reasons since separation of p- and o-cresol is economically possible. Zeolites often lead to a relatively high m/p-cresol ratio in the gas phase (200 - 450°C) whereas in the liquid phase the p-cresol formed was mostly free of m-cresol (200 - 240°C) [Fiege and Bayer AG, 2001]. As outlined in the previous chapter, various zeolites have been studied for this reaction, namely H-Y, H-ZSM-5, H-Mordenite, H-Beta, H-X, H-ZSM-11 and various modification of these zeolites. However, most of the zeolites investigated to date have showed poor para-selectivity in the cresol fraction.

The objectives of the research are:

1. To determine the effect of a zeolite containing both 10 and 12 membered ring channels (i.e. MCM-22) on the product spectrum in the methylation of phenol compared to 10 membered ring zeolites as typified by zeolite ZSM-5 and 12 membered ring zeolites as typified by zeolites Beta, Mordenite and USY.

2. To determine the effect of zeolite characteristics on the p/o-cresol ratio in the methylation of phenol, namely zeolite Si/Al and crystal size;

3. To determine the extent of reaction on the external and internal acid sites of the zeolite crystals. That is, to what extent non-shape selective reactions occur on the external acid sites versus the shape-selective reactions occurring on the internal acid sites of the zeolite;

4. To establish the effect of reaction parameters on the product selectivity of the phenol methylation reaction. These are: reaction temperature, reactants methanol : phenol ratio, weight hourly space velocity or reaction time and the influence of water;

5. To determine the effect of reaction phases (liquid or gas) on the product selectivity of the phenol methylation reaction;

6. To determine a reaction mechanism for the alkylation of phenol with methanol over zeolites.

An outline of research is given below:

1. Investigation of H-ZSM-5, H-Beta, H-Mordenite, H-USY, H-MCM-22 in the phenol alkylation with methanol in the liquid phase and gas phase in terms of product selectivity and cresol isomer distribution. The zeolites were also compared with silica-alumina (a non-shape selective catalyst) to determine the extent of shape selectivity occurring in the zeolites;

2. Different MCM-22 samples were synthesised with different Si/Al ratios and crystal sizes. The effect of steaming of MCM-22 on the product selectivities and cresol isomer distribution was also investigated in determining the effect of the extra-framework aluminium.

3. Selective sodium-exchanging of the internal acid sites of ZSM-5 and MCM-22 was done to determine the extent of reaction on the external and internal acid sites;

4. Investigation of the effect of reaction parameters on the product selectivity and cresol isomer distribution, namely reaction temperature, reactants methanol : phenol ratio, weight hourly space velocity or reaction time and partial pressure. The effect of reaction pressure was evaluated by studying the phenol methylation reaction in the gas and liquid phases;

5. Conversion of the major products in the phenol methylation reaction, namely anisole, o-cresol and p-cresol, was done to help determine the reaction mechanism.

Chapter 4

Experimental

In this chapter the catalysts used in the alkylation of phenol with methanol will be described in terms of their origin and in the case of H-MCM-22, the synthesis procedures used. The post-synthesis modifications of H-MCM-22 by internally selective sodium-exchange and steaming is also described. An overview of the characterization techniques used in the analysis of the catalysts is then given. This is followed by the description of the liquid phase and gas phase experimental apparatus used in the alkylation of phenol with methanol. Finally, kinetic test reactions to characterize the internally selective sodium-exchanged samples are described in terms of reaction conditions and experimental apparatus.

4.1 Catalysts studied

The catalysts used in this study were zeolites H-ZSM-5, H-Beta, H-Mordenite, H-USY and H-MCM-22. Amorphous silica-alumina was used as a comparison of a non-shape selective catalyst. Zeolites H-ZSM-5, H-Beta and H-Mordenite were commercial catalysts obtained from Süd-Chemie. The H-USY sample was obtained from Akzo Nobel and silica-alumina was obtained from Kali-Chemie. Different H-MCM-22 samples were synthesised by the author locally and in the group of Prof R. Lobo at the University of Delaware, USA.

4.1.1 Synthesis of zeolite MCM-22

4.1.1.1 Synthesis at the University of Cape Town

The synthesis of the first sample of zeolite MCM-22 was carried out by the author at the University of Cape Town and followed the synthesis procedure described by Ravishankar *et al.* [1995]. The synthesis gel molar composition was 9.83 Na_2O : 29.78 SiO_2 : Al_2O_3 : 13.70 R : 1367.9 H_2O (R = hexamethyleneimine). The synthesis procedure was as follows: 87.17 g sodium silicate (Fluka, NaOH≈14 wt%, SiO_2≈27 wt% in water) was mixed with 44.46 g distilled water. 17.62 g Hexamethyleneimine (Sigma, 99% purity) was added to this solution drop-wise over a period of 30 minutes under vigorous mixing. A second solution of 8.66 g aluminium sulfate-18-hydrate (Riedel-de-Haën, 99.9%) and 7.04 g concentrated sulfuric acid (Continental Laboratory, 98 wt%) in 220.5 g de-ionised water was then

slowly added to the silicate solution over a period of 15 minutes under vigorous stirring. The synthesis gel was then stirred for 1 hour.

The synthesis gel was then placed in a 250 ml autoclave and heated at 150°C for 80 hours with agitation. After the synthesis was completed the autoclave was rapidly cooled by quenching with water. The synthesis mixture was then filtered and washed. The filter cake was dried overnight in an oven at 100°C. Approximately 30.2 g of dried as-synthesised zeolite was obtained from this synthesis mixture. The dried zeolite still contained the organic template (hexamethyleneimine) which was burned off in air in a furnace using the following temperature programme:

- heated to 120°C over 1 hour;
- held for 2 hours;
- heated to 550°C over 3 hours;
- held for 6 hours;
- cooled to 120°C.

After this procedure the zeolite was transferred immediately to a dessicator where it cooled to room temperature.

This procedure yielded Na-MCM-22. To obtain the acid form of the zeolite, Na-MCM-22 was ion-exchanged twice with aqueous 1 M ammonium acetate solution with stirring for 6 hours at 80°C. The resulting zeolite was washed with de-ionised water, dried at 120°C and then calcined again as mentioned above but at a maximum temperature of 500°C. The zeolite produced using this synthesis method will be referred to as H-MCM-22 (UCT) throughout this thesis.

4.1.1.2 Synthesis at the University of Delaware

The synthesis of the three other samples of zeolite MCM-22 was carried out by the author at the University of Delaware and followed the synthesis procedure described by Corma *et al.* [1995]. The synthesis gel molar composition was 4.5 Na_2O : 30 SiO_2 : Al_2O_3 : 15 R : 1200 H_2O (R = hexamethyleneimine). 0.77 g Sodium hydroxide (Fisher Scientific, 98.1%) was dissolved in 30 ml de-ionised water. While stirring, 5 g silicic acid (Aldrich, 100 mesh) was added. 4.12 g of hexamethyleneimine (Aldrich, 99%) was then added to the solution drop-wise and under vigorous stirring. A second solution of 0.48 g sodium aluminate (EM Science, 35.9% Na_2O, 59.1% Al_2O_3) and 30 g de-ionised water was prepared and then added to this solution. The synthesis mixture was then stirred for 3 hours.

The synthesis gel was divided into four 75 ml teflon lined Parr autoclaves (Parr Instruments Co.) and placed in a oven with a rotiserie. The oven was heated to 150°C and autoclaves were left in the oven for 3 days. After the required synthesis time the autoclaves were removed and cold quenched. The zeolite samples were washed, filtered and placed in an oven at 80°C to dry overnight. Approximately 3.4 g of dried as-synthesised zeolite was obtained from this synthesis mixture. The zeolite samples were then calcined using the following temperature program:

- heated to 120°C over 1 hour;
- held for 2 hours;
- heated to 550°C over 10 hours;
- held for 6 hours;
- cooled to room temperature.

The acid form of the zeolite was obtained by ion-exchanging the zeolite twice with 1 M ammonium acetate. 2 g zeolites was ion-exchanged in 200 ml ammonium acetate solution for 2 hours with stirring at room temperature. The zeolite was then calcined again to obtain the acid form of the zeolite. The zeolite prepared using this procedure will be referred to as H-MCM-22 (DE1) throughout this thesis.

A second batch of MCM-22 was prepared similarly to the procedure mentioned above but with a synthesis gel molar composition of 3.5 Na_2O : 50 SiO_2 : Al_2O_3 : 17.5 R : 2250 H_2O (R = hexamethyleneimine). The silica source was also changed to fumed silica (Carbosil M5). This synthesis mixture was placed in the oven for 7 days at 150°C. This zeolite sample under went the same calcination and ion-exchange procedure as H-MCM-22 (DE1). Approximately 4.9 g of dried as-synthesised zeolite was obtained from this synthesis mixture. The zeolite prepared using this procedure will be referred to as H-MCM-22 (DE2) throughout this thesis.

A third batch of MCM-22 was prepared similarly to the procedure as H-MCM-22 (DE1) but with a synthesis gel composition of 9 Na_2O : 100 SiO_2 : Al_2O_3 : 50 R : 4500 H_2O (R = hexamethyleneimine) and fumed silica (Carbosil M5) as the silica source. This synthesis mixture was placed in the oven for 8 days at 135°C. This zeolite sample under went the same calcination and ion-exchange procedure as H-MCM-22 (DE1). Approximately 3.7 g of dried as-synthesised zeolite was obtained from this synthesis mixture. The zeolite prepared using this procedure will be referred to as H-MCM-22 (DE3) throughout this thesis.

4.1.2 Internally selective sodium-exchange of ZSM-5 and MCM-22

Internally selective sodium-exchange of ZSM-5 and MCM-22 (UCT) is a process whereby protons internal to the zeolitic structure were selectively exchanged with sodium ions (cf. Section 2.1.4.2). This was done to determine the effect of the external surface acid sites of the zeolite crystals in certain catalytic reactions. The method followed was that of Chester *et al.* [1998]. Since both the ZSM-5 and MCM-22 (UCT) samples were obtained or prepared in their H-form, respectively, a sodium ion-exchange was first performed to eliminate all the acid sites. Subsequent ion-exchange with tetrapropylammonium bromide (TPABr) followed the sodium exchange. In this way only sodium on the external surface is exchanged with TPA^+ ions as TPABr is too bulky a molecule to enter the 10 membered ring pore openings. The procedure is described below:

Table 4.1: Steaming conditions of H-MCM-22 (DE1).

Steaming temperature	500°C
Steaming time	8 hours
Steam pressure	0.31 bar
Saturator temperature	70°C
Carrier gas	nitrogen
Total Pressure	1 bar
Catalyst mass	0.8 g
Sand to catalyst mass ratio	9
Nitrogen flowrate	60.1 ml/min

- 12 g of the zeolite sample was slurried in 200 ml of 1 M NaCl solution for 2 hours with stirring. The sample was then filtered and washed with de-ionised water. This was repeated. The filter cake was then dried at 80°C overnight.

- The tetrapropylammonium bromide (TPABr) exchange was carried out as follows: The sodium exchanged sample was slurried in 250ml of 1 M TPABr solution for 2 hours with stirring. The sample was then filtered and washed with de-ionised water. This was repeated twice. The filter cake was then dried overnight at 80 °C.

- The TPA/Na-sample was then calcined at 500°C for ZSM-5 and 550°C for MCM-22 following the procedure given in Section 4.1.1.1, to burn off the organic material so that the sample remained with the external crystal surface activated.

4.1.3 Steaming of H-MCM-22

For certain reaction studies it was decided to steam H-MCM-22 for reasons which will be explained later. A sample of H-MCM-22 (DE1) was loaded with diluent into the test reactor (cf. Section 4.3.1) and steamed in-situ (conditions given in Table 4.1). Nitrogen was saturated with water by passing through a saturator. This saturated nitrogen stream was then heated in the pre-heater section (cf. Section 4.3.1) to the steaming temperature before being passed over the catalyst bed (cf. Figure 4.3). After steaming, the reactor was flushed with nitrogen for 3 hours before the phenol alkylation reaction was performed over the steamed zeolite.

4.1.4 Physical and physico-chemical zeolite characterization

The zeolites were characterized using the following techniques:

- Powder X-ray diffraction (XRD);

- Scanning electron microscopy (SEM);

- Nitrogen physisorption (BET);

Table 4.2: XRD operating parameters.

Radiation source	Cu-Kα
Radiation wavelength (λ)	1.542 Å
Range	10^4
Time constant	1 s
Preset	1000 counts/s
Voltage	40 kV
Current	25 mA
2θ range	$4° < 2\theta < 60°$
2θ/step	0.1°
Anti-scatter slit	1°

- Atomic adsorption spectroscopy (AAS);
- Ammonia temperature-programmed desorption (NH_3-TPD);
- ^{27}Al magic angle spinning nuclear magnetic resonance spectroscopy (^{27}Al MAS NMR).

4.1.4.1 Powder X-ray diffraction (XRD)

X-ray diffraction patterns of zeolites help determine the type of zeolite sample. X-ray diffraction patterns of all catalysts were obtained using a Phillips X-ray diffractometer with Cu-Kα radiation. The XRD operating parameters are given in Table 4.2.

4.1.4.2 Scanning electron microscopy (SEM)

Scanning electron microscopy was used to identify the crystal morphology and size. A Leica S440 digital scanning electron microscope was used to take electron micrographs of the zeolite samples. The samples were mounted on aluminium stubs, which were covered on top with a mixture of water-based glue and colloidal carbon. The zeolite samples were placed on the glue/carbon mixture and covered with a thin layer of Au/Pd.

4.1.4.3 Nitrogen physisorption (BET)

Nitrogen physisorption (BET) was performed on the catalysts using a Micromeritics ASAP 2000, which allowed a stepwise scan over the entire P/P_0 range. Nitrogen adsorption was done to determine the "BET" surface area and used to calculate the mesoporous and microporous surface areas and pore volumes of the catalysts. Before the nitrogen physisorption analysis is performed the samples were dried overnight under vacuum at 250°C.

4.1.4.4 Elemental analysis using atomic absorption spectroscopy (AAS)

Atomic absorption spectroscopy (AAS) was used to determine the silicon/aluminium ratio and the sodium content of the zeolites. Analyses were carried out on a Varian Spectra AA 110. The sample was digested in a teflon lined steel vessel ("Parr bombs", Parr Instruments Co.) by additions of 40%

Table 4.3: Experimental conditions for elemental analysis using atomic absorption spectroscopy.

Sample mass	0.2 g
HF concentration	40%
Volume of HF added to the sample	5 ml
Oven temperature	100°C
Heating time	35 min
Volume of boric acid added	50 ml
Final volume of solution	500 ml

Table 4.4: Conditions of ammonia temperature-desorption (NH_3-TPD.

Mass of sample	0.25 g
Calcination temperature before ammonia adsorption	500°C
Precentage ammonia in Helium	4%
Ammonia adsorption time	1 hour
Flowrate of ammonia/helium gas	60 ml/min
Adsorption temperature	150°C
Physi-desorption time	8 hours
Heating rate	10°/min
Final desorption temperature	600°C
Sulphuric acid concentration	0.1 N
Sodium hydroxide concentration	0.1 N
Titration indicator	Bromo-thymol blue

HF and heated in an oven. After the dissolution of the zeolite boric acid and de-ionised water was added.

4.1.4.5 Ammonia temperature-programmed desorption (NH_3-TPD)

Ammonia temperature-programmed desorption (NH_3-TPD) was used to determine the acidity and the strength of the acid sites in the zeolites. NH_3-TPD experiments were carried out in a quartz reactor and the experimental conditions are given in Table 4.4. The samples were calcined in air before the ammonia was adsorbed. Ammonia was adsorbed onto the zeolite for 1 hour followed by desorption of the physically adsorbed ammonia at 150°C for 8 hours under the flow of helium. The sample was then heated to the final desorption temperature and the quantity of chemisorbed ammonia was recorded by a thermal conductivity detector (TCD). The total quantity of chemisorbed ammonia is also determined by back titration. After passing through the sample the ammonia/helium gas was bubbled through 20 ml 0.1 N sulphuric acid in 100 ml water. Back titration, using 0.1 N sodium hydroxide, was able to determine the amount of sulphuric acid remaining after the desorption of the ammonia. The amount of ammonia desorbed from the sample determined by back titration or by curve integration must agree within 5% otherwise the experiment was rejected.

Table 4.5: Operating conditions used in the liquid phase alkylation of phenol with methanol.

Operating conditions	Standard conditions	Range studied
Reaction temperature (°C)	200	180 - 250
Reaction pressure (bar)	autogeneous	5 - 54
Reaction time (hours)	5	1 - 72
Mass of phenol (g)	147.3	73 - 200
Mass of methanol (g)	50.1	5 - 124
Methanol : phenol molar ratio	1	0.07 - 5
Mass of catalyst (g)	5	1 - 10
Reactants : catalysts mass ratio	39.4	20 - 250
Phenol : catalyst mass ratio	29.4	14 - 40
Heating up time (min)	15	-

4.1.4.6 ^{27}Al Magic angle spinning nuclear magnetic resonance (^{27}Al MAS NMR)

^{27}Al Magic angle spinning nuclear magnetic resonance (^{27}Al MAS NMR) was used to determine the extent of extra-framework aluminium formed during the synthesis and calcination procedures. ^{27}Al MAS NMR analyses were done at the Department of Chemistry, University of Delaware, USA. The ^{27}Al MAS NMR spectra were recorded using a Bruker MSL 300 spectrometer (B_0 = 7.4 T) operating at a resonance frequency of 78.205 MHz. The samples were spun in zirconia rotors. The ^{27}Al MAS NMR spectra were obtained using a $\pi/12$ pulse of 1 μs and a recycle delay of 2 s using a 4 mm outside diameter rotor spinning at a rate of 9 kHz. The chemical shifts were referenced to a 1 M $Al(NO_3)_3$ solution.

4.2 Liquid-phase alkylation of phenol with methanol

4.2.1 Experimental apparatus

A 600 ml batch autoclave was used. The reactor consisted of a gas inlet line, cooling water loops, pressure gauge, safety pressure release valve, a gas outlet, a thermowell and a magnetically driven stirrer as seen in Figure 4.1. The maximum operating temperature of the reactor was 250°C (limited by the teflon gasket sealing the lid of the autoclave) and the reactor could be pressurised up to 100 bar. Figure 4.2 shows the complete set-up of the liquid phase rig.

4.2.2 Experimental procedure

The batch reactor was typically loaded as given in Table 4.5. The reactor was flushed with nitrogen to a pressure of 10 bar and then depressurised, repeatedly, to remove all traces of oxygen. The reactor was then heated to reaction temperature. After the reaction time had elapsed the reactor was cooled quickly by passing water through the cooling loops inside the autoclave (Figure 4.1). Once cooled the reactor had a pressure of approximately 2 bar. A sample of the gas phase was collected in a gas trap via the gas outlet and this was then analysed by gas chromatography. The reactor was then depressurised and the content of the reactor vessel was removed.

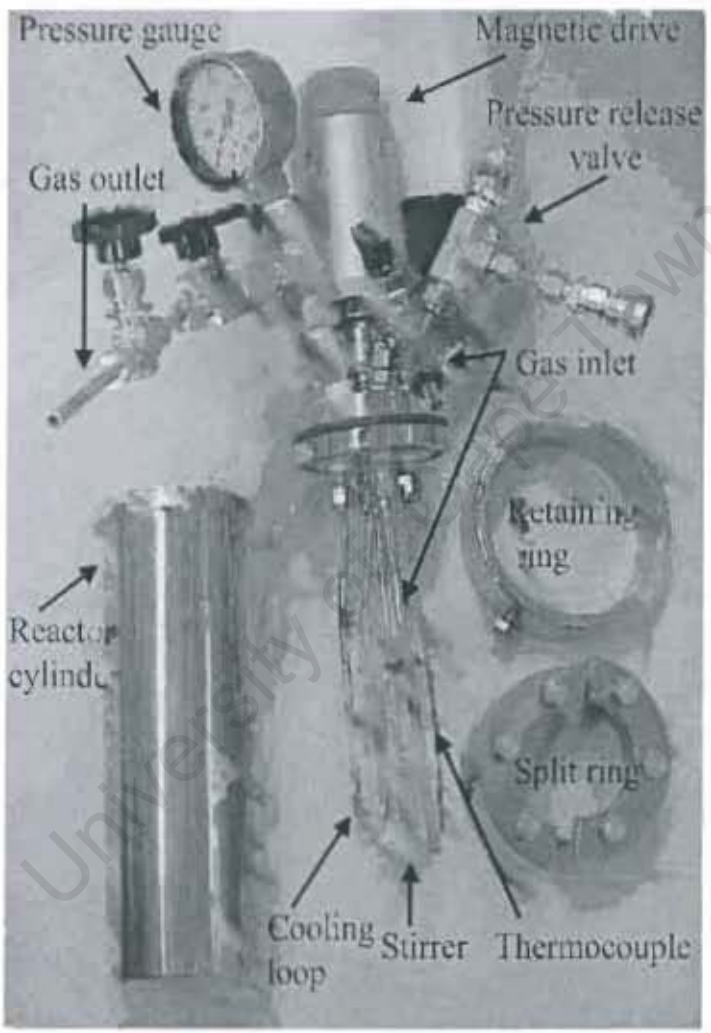

Figure 4.1: The interior of the batch autoclave used for liquid phase phenol methylation with methanol.

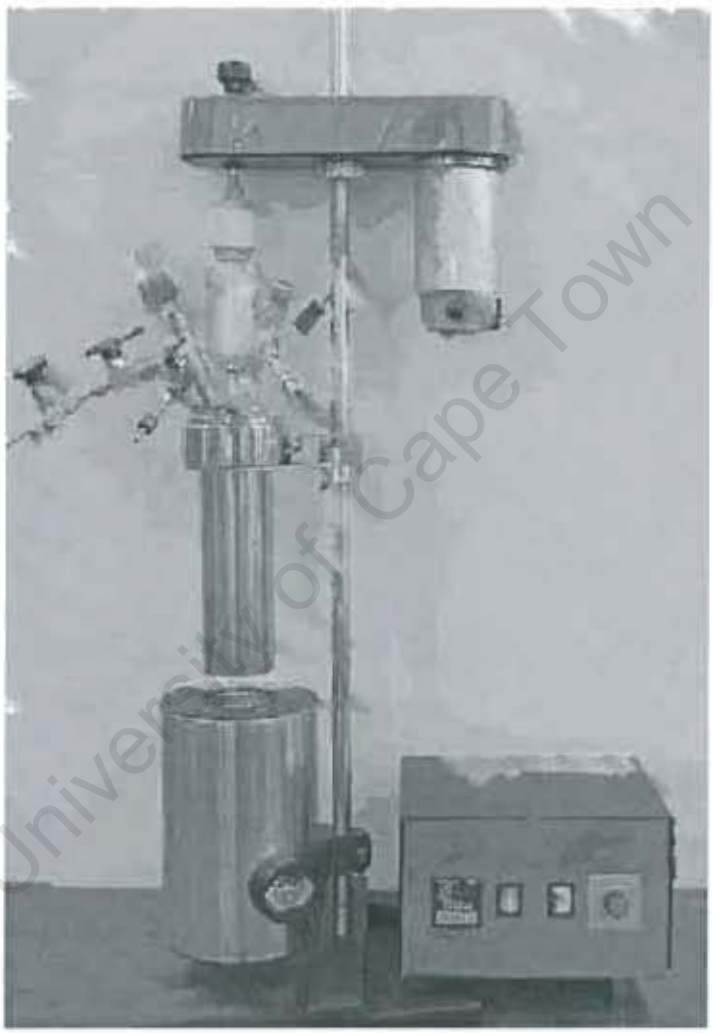

Figure 4.2: Set-up of the batch autoclave used for liquid-phase alkylation of phenol with methanol.

Table 4.6: The GC set-up and conditions for the analysis of the liquid phase products.

Gas chromotography	HP 5890A
Colomn	RH-1
Length and inner diameter	60 m, 0.25 mm
Stationery phase	100% Dimethylpolysiloxane
Film thickness	0.25μm
Carrier gas	Hydrogen
Colomn head pressure	1.1 bar
Injector	Split injector
Injector temperature	250°C
Split	1 : 100
Detector	Flame ionisation detector
Detector temperature	325°C
Temperature program	5 min isothermal at 50°C, heat at 10°C/min to 250°C, hold for 5 min at 250°C.

4.2.3 Product analysis

Four 1.5 ml aliquots were placed in microcentrifuge tubes and centrifuged at 15000 rmp to remove the catalyst. After centrifugation the liquid product was weighed (ca. 1.5 g) and then a precise weight of toluene (ca. 0.15 g) was added to the liquid product as the internal standard. The product was then analysed by gas chromatography. The GC set-up and conditions are given in Table A.1. Appendix A shows a typical GC spectrum obtained from a liquid phase phenol alkylation with methanol and Appendix B shows a typical example of a complete material balance calculation for the liquid phase alkylation of phenol with methanol. The reproducibility of the liquid phase system is shown in Section 6.1.1.

4.3 Gas-phase alkylation of phenol with methanol

4.3.1 Experimental apparatus

Gas phase alkylation was done in a flow reactor as illustrated by the flowsheet is shown in Figure 4.3. A feed mixture of phenol and methanol was metered via a HP 1100 series HPLC pump to an evaporator (Figure 4.4). A carrier gas (nitrogen) was introduced via a thermal mass flow controller at the top of the evaporator. There is a reactor bypass line to allow the analysis of the feed before and after an experiment. The needle valve in this bypass line ensures the same conditions in the reactor bypass line as in the reactor line. The pre-heat coil and reactor (Figure 4.5) were placed inside the chamber of a furnace to maintain an isothermal bed temperature. Toluene was used as an internal standard. The internal standard was evaporated into a flow controlled nitrogen stream, via a saturator between the reactor and the GC. After the GC sampling valve the condensable products were knocked out from the gas stream with an ice-trap. Table 4.7 shows the operating conditions of

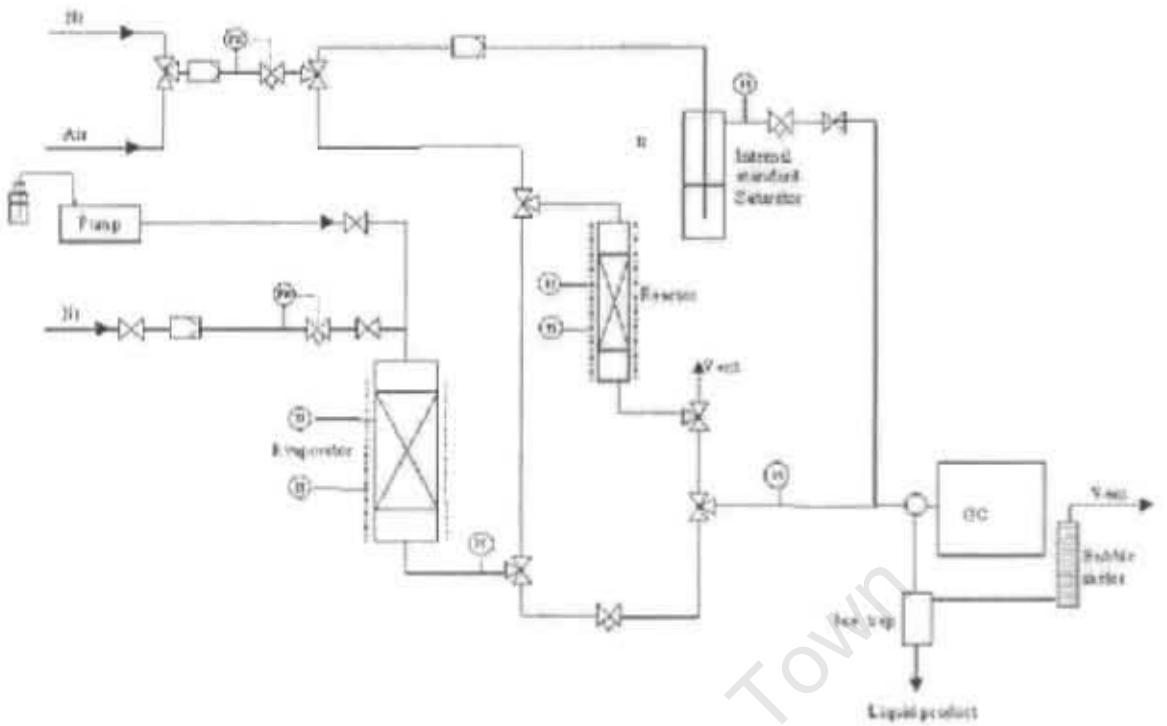

Figure 4.3: Gas-phase apparatus used for the alkylation of phenol with methanol.

the evaporator, the internal standard saturator and the HPLC pump.

4.3.2 Experimental procedure

Table 4.8 shows the operating conditions used in the gas phase alkylation of phenol with methanol. The catalyst in the reactor was diluted with acid washed sand (100 - 500μm) in the ratio of 9 : 1 to maintain isothermal conditions (Figure 4.5). The catalyst was calcined before each experiment in air at 500°C for approximately 6 hours then cooled to reaction temperature and flushed with nitrogen for 2 hours to remove all traces of oxygen.

At the start of the experiment, the evaporator was allowed to stabilise via the reactor bypass line

Table 4.7: Operating conditions for the evaporator, internal standard saturator and HPLC pump.

Operating conditions	Standard conditions	Range studied
Evaporator		
Temperature at inlet (°C)	32	-
Temperature at outlet (°C)	180	-
Nitogen flowrate to evaporator (ml/min)	284	35 - 284
Internal standard saturator		
Temperature of water bath (°C)	28	-
Flowrate of nitrogen (ml/min)	60	-
HPLC Pump		
Reactants rate (ml/min)	0.2	0.1 - 0.2

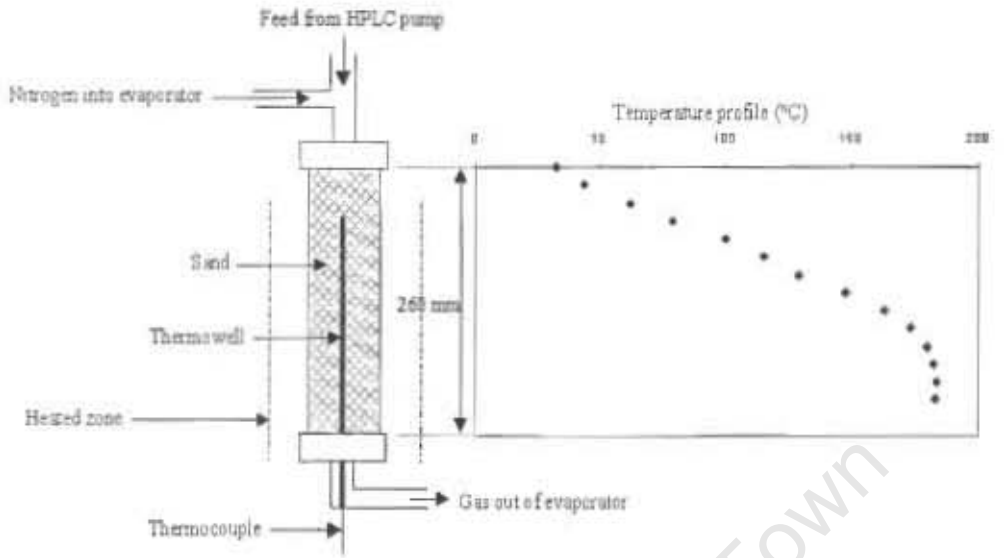

Figure 4.4: A sketch of the evaporator and temperature profile inside the evaporator.

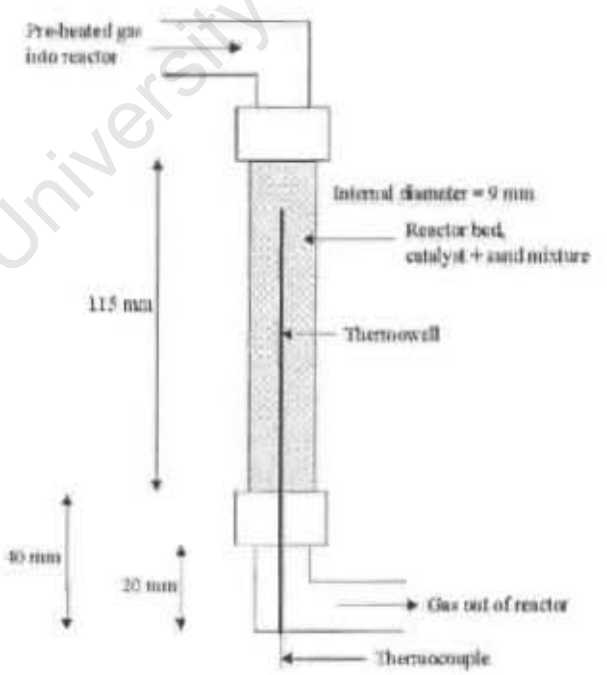

Figure 4.5: A sketch of the reactor.

Table 4.8: Operating conditions for gas phase alkylation of phenol with methanol.

Operating conditions	Standard conditions	Range studied
Reaction temperature (°C)	300	200 - 400
Total reaction pressure (bar)	1	1
Reactants partial pressure (bar)	0.2	0.2 - 0.8
Methanol : phenol molar ratio	1	0.3 - 6
$WHSV_{reactants}$ (h^{-1})	14	3 - 23
Catalyst mass (g)	0.8	0.8 - 1.9
Sand : catalyst mass ratio	9	9
Carrier gas	Nitrogen	-
Carrier gas : reactants molar ratio	4	4

Table 4.9: The GC set-up and conditions for the analysis of the gas phase products.

Gas chromotography	Varian 3100
Column	CP cresol fused silica WCOT
Length and inner diameter	50 m, 0.25 mm
Film thickness	0.2μm
Make-up gas	Nitrogen
Carrier gas	Hydrogen
Column head pressure	4 bar
Injector	Split injector
Injector temperature	200°C
Split	1 : 80
Detector	Flame ionisation detector
Detector temperature	200°C
Temperature program	50°C for 3 min, heat to 120°C at 15°C/min, hold at 120°C for 40 min.

for 4 hours with simultaneous stabilization of the internal standard saturator. Reactor bypass samples were taken in this period to monitor the evaporator and saturator operation. After stabilization of the evaporator and saturator, the three-way valve was switched from bypass to the reactor. Samples were taken every 40 minutes until quasi-steady state was reached. Finally, bypass samples were taken again for a final control sample at the end of the experiment.

4.3.3 Product analysis

The gaseous product analysis was done using an on-line gas chromatograph. The GC set-up and conditions are given in Table A.2. Appendix A shows a typical GC spectrum obtained from a gas phase phenol methylation with methanol and Appendix D shows a typical example of a complete material balance calculation for the gas phase alkylation of phenol with methanol. The reproducibility of the liquid phase system is shown in Section 7.1.1.

Table 4.10: Reaction conditions for 1,3,5-TIPB and n-hexane cracking [Röger *et al.*, 1998].

	n-Hexane	1,3,5-TIPB
$T_{reactor}$ (°C)	500	270
$P_{reactant}$ (kPa)	4.0	0.16
WHSV (h^{-1})	1.6	0.6
Carrier gas	Nitrogen	Nitrogen

Table 4.11: GC temperature program for 1,3,5-TIPB and n-hexane cracking.

1,3,5-TIPB cracking	Isothermal at 120°C
n-Hexane cracking	Isothermal at 50°C

4.4 Determination of the external and internal surface activity of the zeolite crystals

The external surface activity of zeolite crystals was determined by using the test reaction of cracking 1,3,5-triisopropyl benzene (1,3,5-TIPB). 1,3,5-TIPB is too large to fit through a 10-membered ring pore and hence can only be cracked on the external surface sites. The total activity of the crystals was tested using n-hexane cracking (α-test). These two test reactions were carried out on fresh and internally selectively sodium-exchanged catalysts ZSM-5 and MCM-22 (UCT).

The gas phase experimental rig set-up (cf. Section 4.3.1) was used for these reactions except that the evaporator was replaced by saturators containing either 1,3,5-TIPB or n-hexane. The reaction conditions for the 1,3,5-TIPB cracking test reaction and the n-hexane cracking test reaction are given in Table 4.10. The experimental procedure was similar to the gas phase phenol alkylation reactions as described in Section 4.3.2. The reaction was traced by time-on-stream sampling on-line using the same GC conditions as shown in Table A.2, except for the temperature program which is described in Table 4.11.

Chapter 5

Catalyst characterization

This chapter presents the results of the physico-chemical characterization of all the catalysts used in this research, viz. zeolites H-ZSM-5, H-Beta, H-Mordenite, H-USY, different samples of H-MCM-22 and amorphous silica-alumina. All the catalysts were characterized by the following methods: X-ray diffraction (XRD), scanning electron microscopy (SEM), nitrogen physisorption (BET), atomic adsorption spectroscopy (AAS), ammonia temperature-programmed desorption (NH_3-TPD) and ^{27}Al magic angle spinning nuclear magnetic resonance (^{27}Al MAS NMR).

5.1 X-ray diffraction (XRD)

X-ray diffraction spectra of the zeolites were obtained to determine (and confirm) the zeolite phase present in the samples. Figure 5.1 shows the powder X-ray diffraction spectra of H-ZSM-5, H-Beta, H-Mordenite and H-USY, these catalysts were commercial samples obtained from Süd-Chemie and Akzo Nobel (H-USY), respectively. Comparison of these X-ray diffraction spectra with simulated spectra given by von Ballmoss and Higgins [1990] confirmed their identification, as shown in Figure 5.2. H-ZSM-5, H-Mordenite and H-USY all have sharp peaks in their X-ray pattern compared to H-Beta which has broad peaks. H-Beta has broad peaks due to the high degree of stacking disorder in the framework structure [Newsam *et al.*, 1988]. Figure 5.3 shows the X-ray diffraction spectra obtained for the H-MCM-22 samples made at the University of Cape Town and those made at the University of Delaware. Comparing these X-ray diffraction spectra with X-ray diffraction pattern obtained by Ernst [1998] (shown in Figure 2.9) indicated that all the samples were indeed MCM-22.

5.2 Scanning electron microscopy (SEM)

Figures 5.4 to 5.11 show the scanning electron micrographs of the different zeolites used. Table 5.1 summarises the analyses of the micrographs with respect to the morphology and average crystal size of the different zeolites. All the zeolite crystals except H-MCM-22 have spherical or cubic morphologies. H-MCM-22 crystals have a platelet morphology and these crystals are intergrown. The MCM-22 crystal's morphology and size is analogous to that found by Ernst [1998]. No amorphous material was detected in any of the scanning electron micrographs of the zeolite samples.

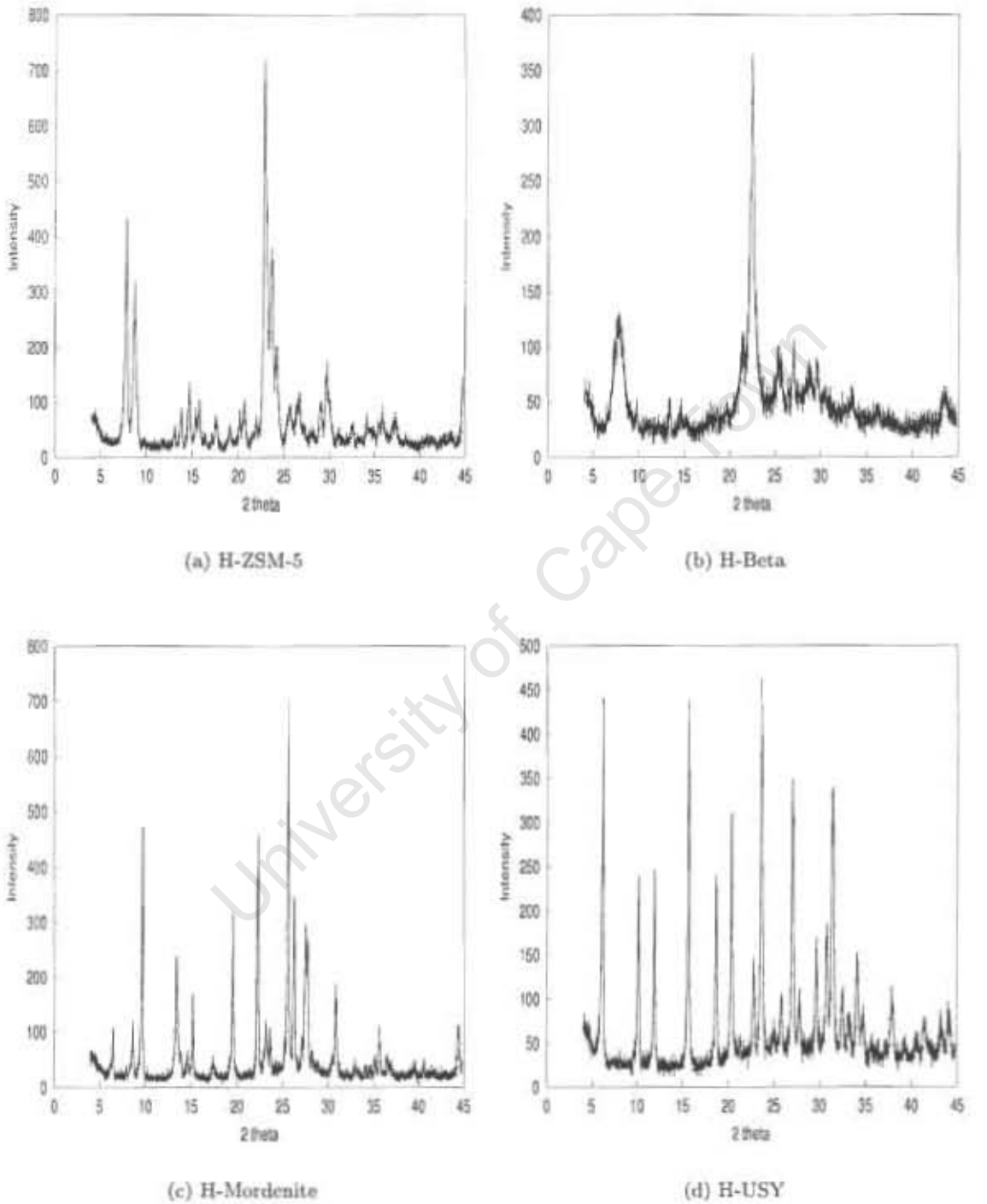

(a) H-ZSM-5

(b) H-Beta

(c) H-Mordenite

(d) H-USY

Figure 5.1: X-ray diffraction spectra of H-ZSM-5, H-Beta, Na-Mordenite, H-USY.

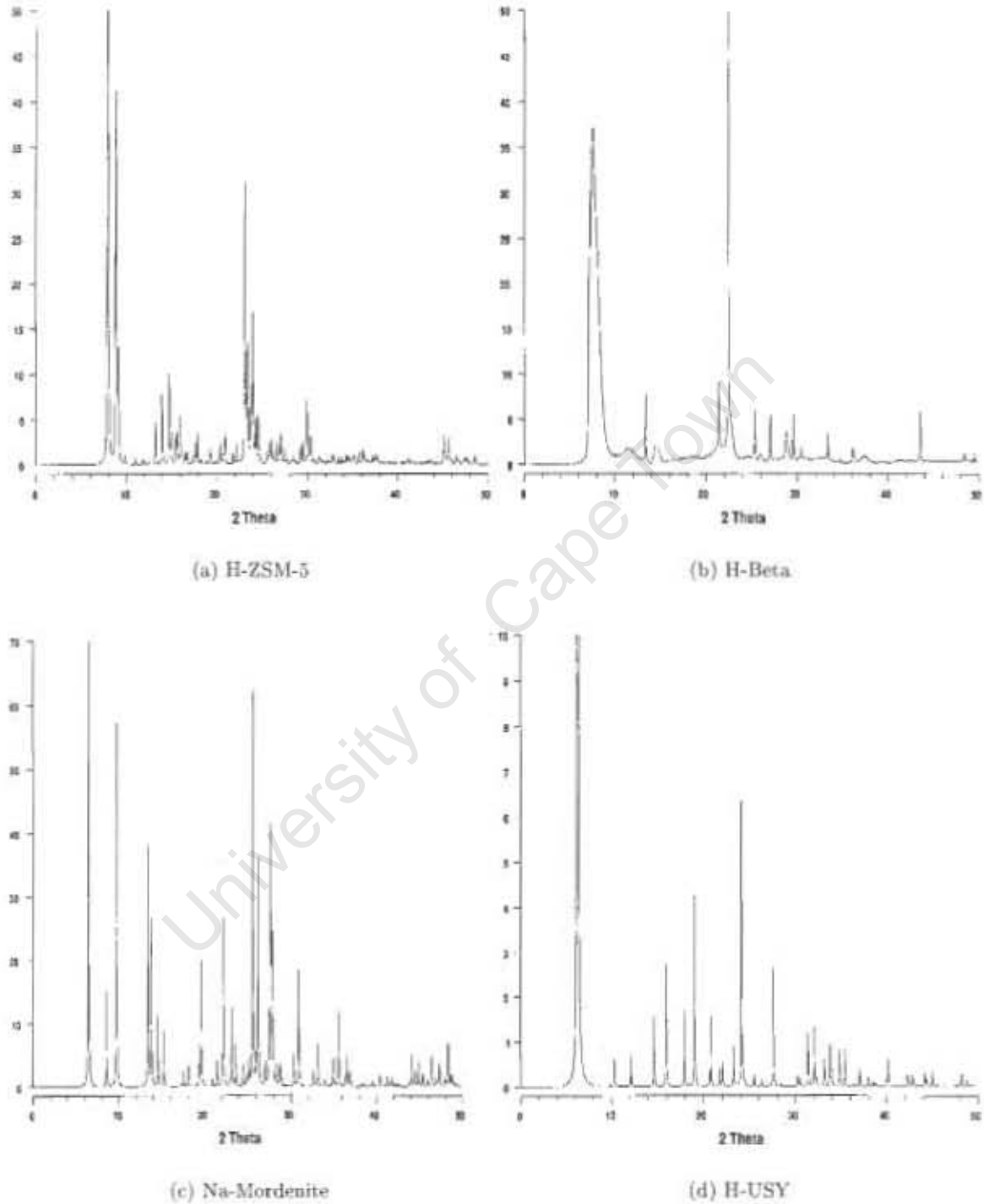

(a) H-ZSM-5 (b) H-Beta

(c) Na-Mordenite (d) H-USY

Figure 5.2: Simulated X-ray diffraction spectra of H-ZSM-5, H-Beta, H-Mordenite, H-USY [von Ballmoss and Higgins, 1990].

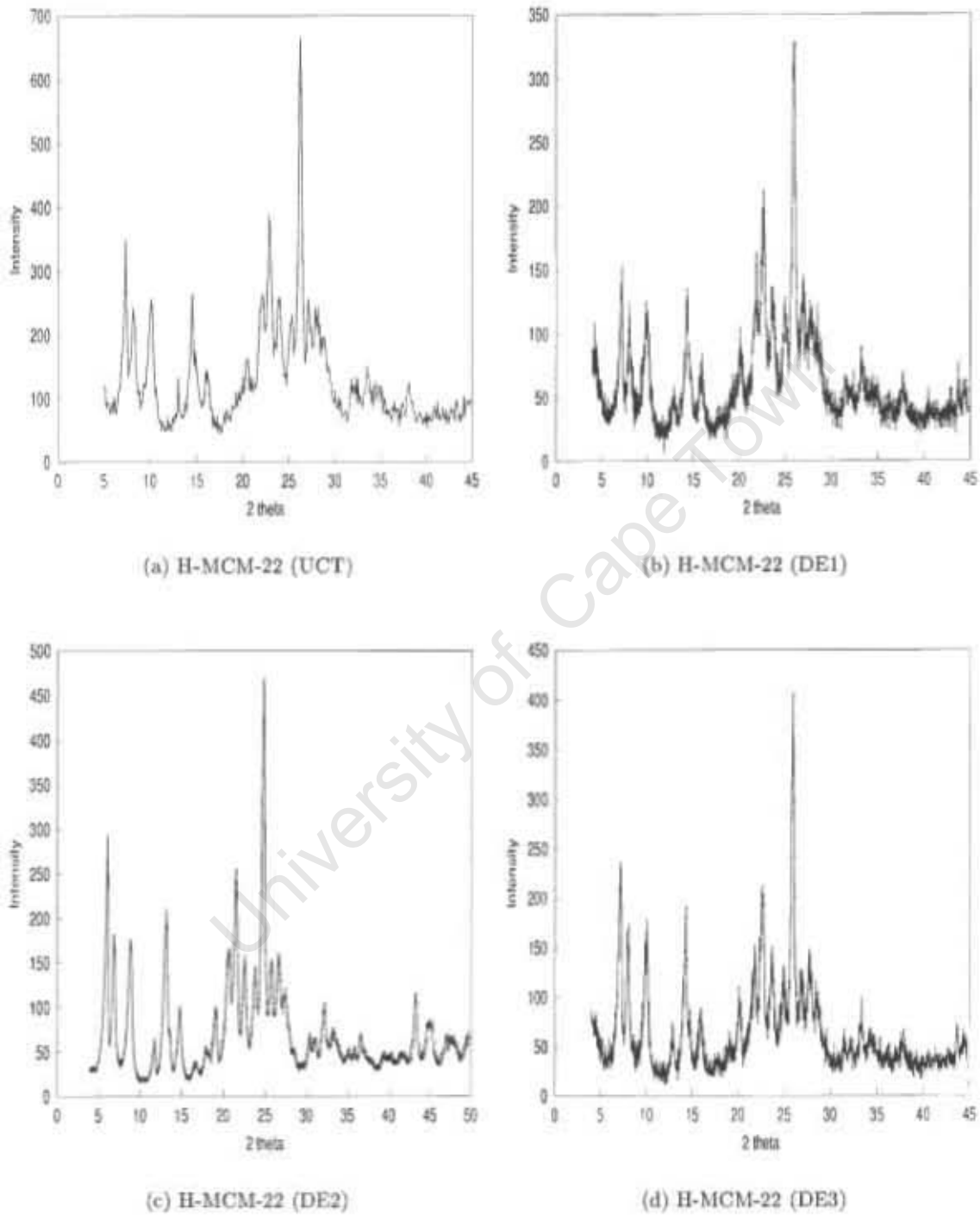

(a) H-MCM-22 (UCT)

(b) H-MCM-22 (DE1)

(c) H-MCM-22 (DE2)

(d) H-MCM-22 (DE3)

Figure 5.3: X-ray diffraction spectra of the H-MCM-22 samples made at the University of Cape Town (UCT) and the University of Delaware (DE).

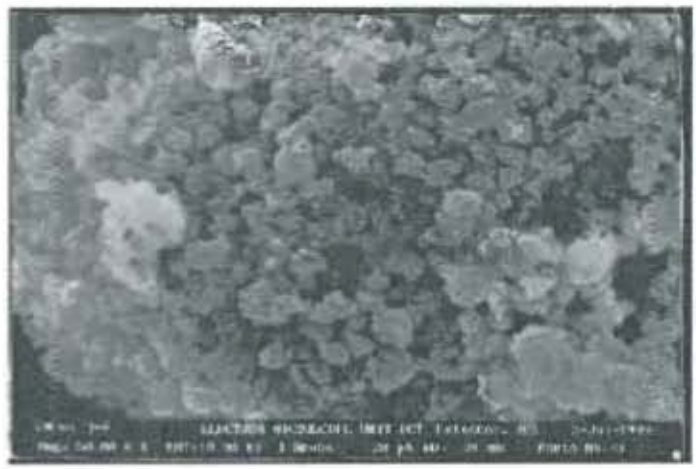

Figure 5.4: Scanning electron micrograph of zeolite H-ZSM-5.

Figure 5.5: Scanning electron micrograph of zeolite H-Beta.

Figure 5.6: Scanning electron micrograph of zeolite H-Mordenite.

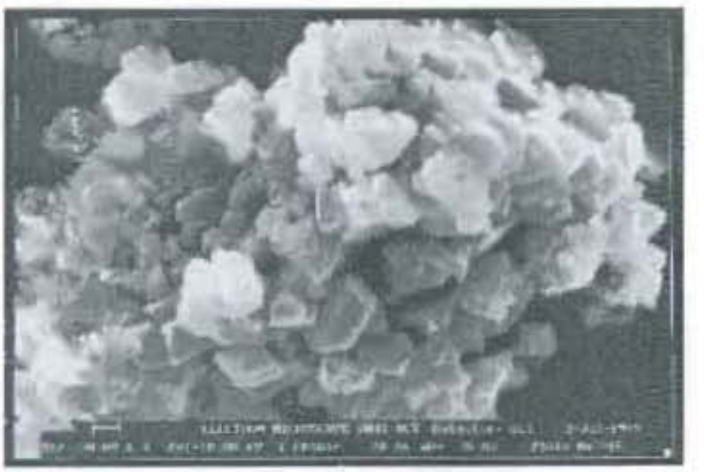

Figure 5.7: Scanning electron micrograph of zeolite H-USY.

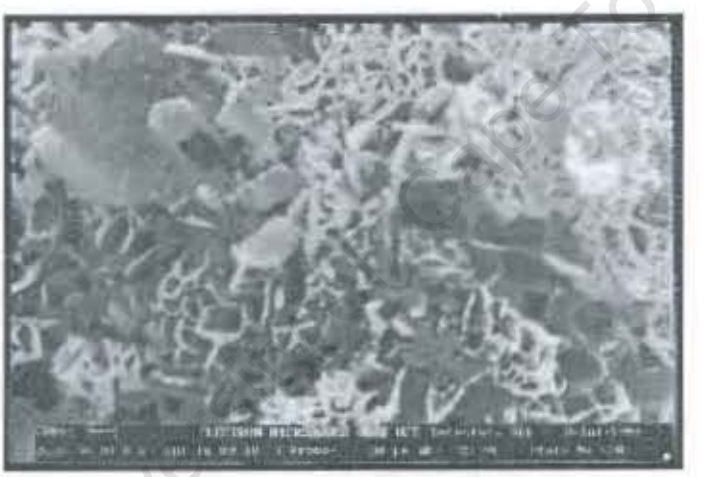

Figure 5.8: Scanning electron micrograph of zeolite H-MCM-22 (UCT).

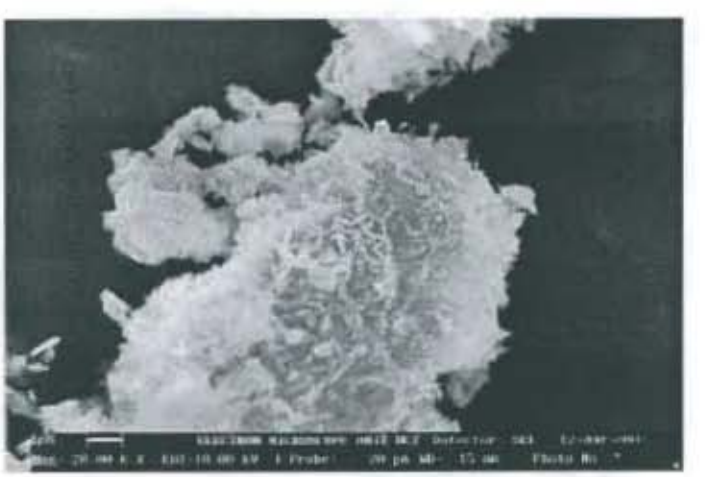

Figure 5.9: Scanning electron micrograph of zeolite H-MCM-22 (DE1).

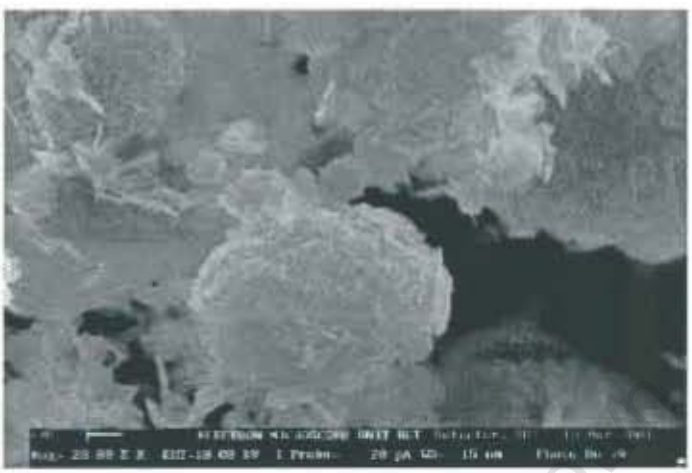

Figure 5.10: Scanning electron micrograph of zeolite H-MCM-22 (DE2).

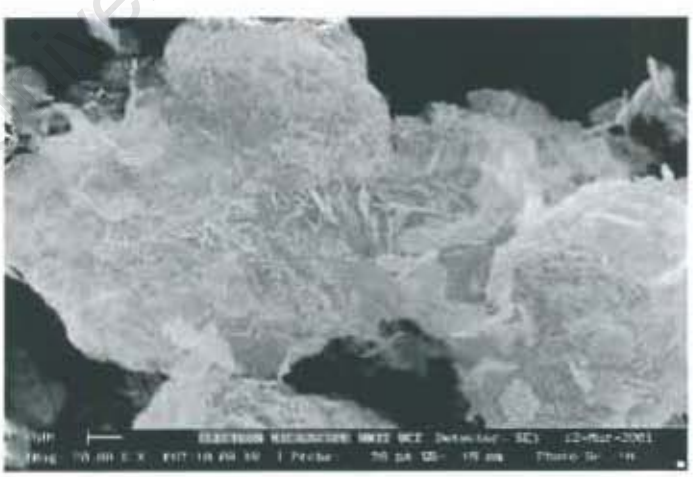

Figure 5.11: Scanning electron micrograph of zeolite H-MCM-22 (DE3).

Table 5.1: The morphology and average crystal size of the different catalysts.

Catalyst	Morphology	Average crystal size (μm)
H-ZSM5	Spherical	0.2 - 0.4
H-Beta	Spherical	0.3 - 0.6
H-Mordenite	Spherical	0.3 - 0.5
H-USY	Cubic	0.6 - 0.7
H-MCM-22 (UCT)	Platelets	thickness = 0.1, diameter = 0.2
H-MCM-22 (DE1)	Platelets	thickness = 0.1, diameter = 0.8
H-MCM-22 (DE2)	Platelets	thickness = 0.1, diameter = 1
H-MCM-22 (DE3)	Platelets	thickness = 0.1, diameter = 1
Silica-alumina	-	particles > 106

Table 5.2: Nitrogen BET areas and pore volumes of catalysts used.

Catalyst	Total BET surface area (m^2/g)	Microporous area (m^2/g)	Mesoporous area (m^2/g)	Micropore volume (cm^3/g)	Mesopore volume (cm^3/g)
H-ZSM-5	425	298	127	0.10	0.44
H-Beta	559	349	210	0.17	0.47
H-Mordenite	404	384	20	0.17	0.02
H-USY	607	556	51	0.25	0.09
H-MCM-22 (UCT)	412	278	134	0.12	0.50
H-MCM-22 (DE1)	436	311	125	0.14	0.34
H-MCM-22 (DE2)	526	407	119	0.18	0.28
H-MCM-22 (DE3)	490	382	108	0.17	0.25
Silica-alumina	508	0	508	-	0.78

5.3 Nitrogen physisorption (BET)

Table 5.2 gives the BET surface areas, microporous and mesoporous areas, micropore volume and mesopore volumes of the catalysts used in this study. All the zeolites had BET surface areas between 404 and 607 m^2/g and micropore volumes between 0.1 and 0.25 cm^3/g. Note no data available for the steamed H-MCM-22 (DE1) sample, since steaming was carried out in situ.

5.4 Atomic absorption Spectroscopy (AAS)

The bulk Si/Al atomic ratios of the catalysts were determined by atomic absorption spectroscopy. Table 5.3 gives the aluminium content and the bulk Si/Al ratios for the different catalysts. H-ZSM-5 has the highest Si/Al ratio of 45 whereas H-USY has the lowest ratio of 4. The different H-MCM-22 samples have Si/Al ratios ranging from 11 to 29.

5.5 Ammonia temperature-programmed desorption (NH_3-TPD)

Appendix F gives the ammonia temperature-programmed desorption curves obtained over all the catalysts. The amount of ammonia desorbed and the temperatures of the maximum of the major

Table 5.3: The aluminium content and bulk Si/Al atomic ratios of the catalysts.

Catalysts	Al content (mmol Al/g catalyst)	Bulk Si/Al atomic ratio
H-ZSM-5	0.41	45
H-Beta	1.08	15
H-Mordenite	1.40	11
H-USY	2.50	4
H-MCM-22 (UCT)	1.06	11
H-MCM-22 (DE1)	1.08	11
H-MCM-22 (DE2)	0.86	19
H-MCM-22 (DE3)	0.75	29
Silica-alumina	2.11	6

desorption peak in the NH_3-TPD spectra are given in Table 5.4. The amount of desorbed ammonia (mmol NH_3/g catalyst) is an indication of the number of acid sites available for reaction of molecules with a size comparable to that of NH_3. The catalysts thus arranged in order of decreasing number of available acid sites are: silica-alumina > H-USY > H-Mordenite ≈ H-Beta > H-MCM-22 (DE1) ≈ H-MCM-22 (UCT) > H-MCM-22 (DE2) > H-MCM-22 (DE3) > H-ZSM-5.

Figure 5.12 shows the relationship between the number of acid sites per gram catalyst determined by NH_3-TPD (Al_{NH_3-TPD}) and aluminium atoms per gram catalyst determined by atomic absorption (Al_{AAS}). Generally there is good agreement between the two methods for all zeolite except H-USY. For the cases where $Al_{AAS} > Al_{NH_3-TPD}$, this may be caused by the following:

- Some of the acid sites are not accessible which could be due to structural defects. This may hold for the Mordenite in particular due to its non-interconnecting pore system;

- Some extra-framework aluminium form weaker sites. The ammonia desorption from these sites occurs at a lower temperature and thus doesn't contribute to the major desorption peak. This may hold in particular for H-USY, since leaching the extra-framework alumina, which was produced in the steaming step, may be incomplete. This is also confirmed by ^{27}Al MAS NMR analysis of the H-MCM-22 samples, where H-MCM-22 (DE2) was found to have the lowest content of extra-framework aluminium (cf. Figures 5.14 to 5.17 and Section 5.6) and the best correlation;

- Silica-alumina is not expected to match the theoretical line since only part of the aluminium is exposed to the surface.

The temperature of maximum of major desorption peak gives an indication of the strength of the acid sites. Thus, in decreasing order of acid strength: H-Mordenite > H-ZSM-5 > MCM-22 (DE2) > H-MCM-22 (DE3) > H-MCM-22 (DE1) > H-USY > H-Beta > H-MCM-22 (UCT) > silica-alumina.

Figure 5.13 shows the correlation between temperature of maximum of major ammonia desorption peak and bulk Si/Al atomic ratio. There is a clear and consistent trend showing that the higher Si/Al ratio catalyst is producing the stronger acid sites. The exception is H-Mordenite which has very strong sites for its relatively low Si/Al ratio.

Table 5.4: Results from NH_3-TPD for the different catalysts.

Catalyst	mmol NH_3/ g catalyst	Temperature of the maximum of major desorption peak (°C)
H-ZSM-5	0.38	372
H-Beta	1.06	299
H-Mordenite	1.10	443
H-USY	1.36	303
H-MCM-22 (UCT)	0.90	282
H-MCM-22 (DE1)	0.92	306
H-MCM-22 (DE2)	0.83	360
H-MCM-22 (DE3)	0.60	342
Silica-alumina	1.62	274

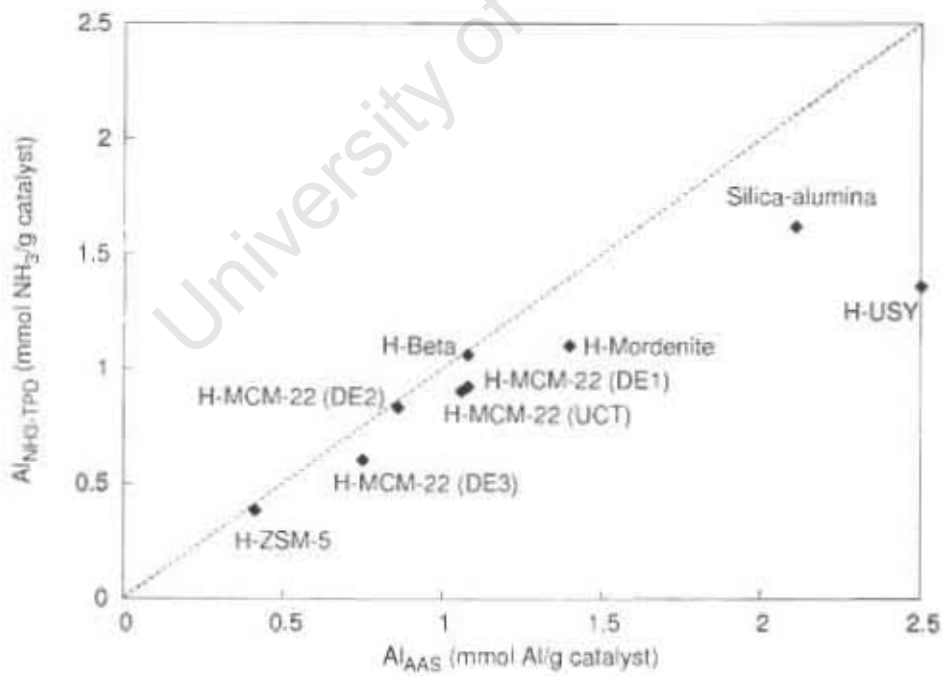

Figure 5.12: The relationship between aluminium content in the different catalysts as determined by atomic adsorption spectroscopy (Al_{AAS}) and by ammonia temperature-programmed desorption (Al_{NH_3-TPD}) (Data taken from Tables 5.3 and 5.4).

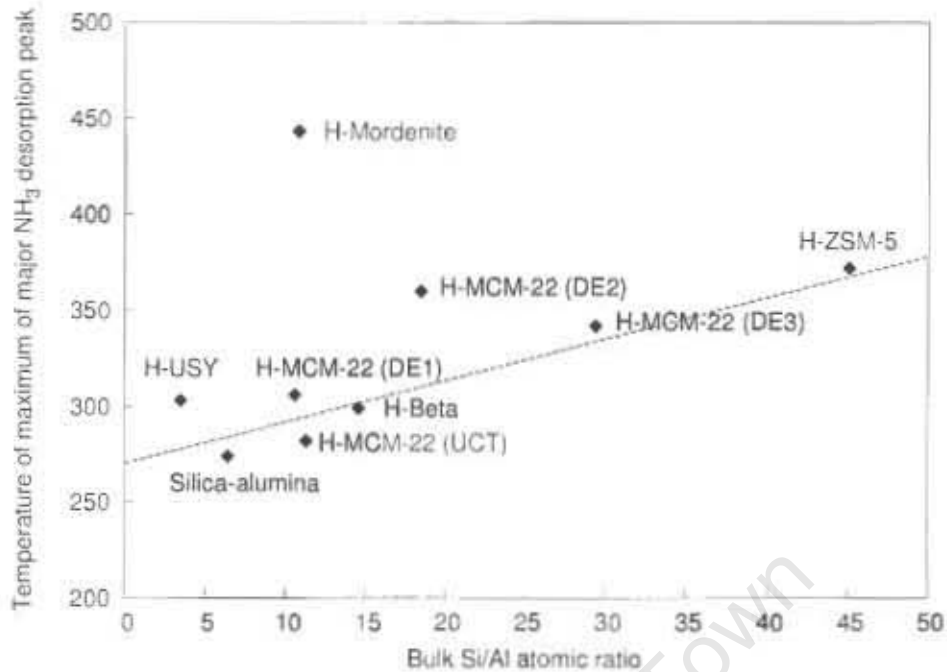

Figure 5.13: The correlation between temperature of maximum of major ammonia desorption peak and bulk Si/Al atomic ratio.

5.6 ^{27}Al Magic angle spinning nuclear magnetic resonance (^{27}Al MAS NMR)

The ^{27}Al MAS NMR spectra for the H-MCM-22 samples are given in Figures 5.14 to 5.17. All these zeolites contained some non-tetrahedrally coordinated extra-framework aluminium (0 - 40 ppm).

Figure 5.18 shows the ^{27}Al MAS NMR spectrum of the as-synthesized template containing Na-MCM-22 (DE1) indicating that only tetrahedral aluminium is present in the sample. Figure 5.15 shows the spectrum of the sample after removing the template, ion-exchanging and calcination. It is clear that the extra-framework aluminium species are formed during calcination of the zeolite. H-MCM-22 (DE2) clearly showed the lowest amount of extra-framework aluminium in all the H-MCM-22 samples. H-MCM-22 (DE2) was also found to have almost every aluminium atom converted to a strong acid site (cf. Figure 5.12).

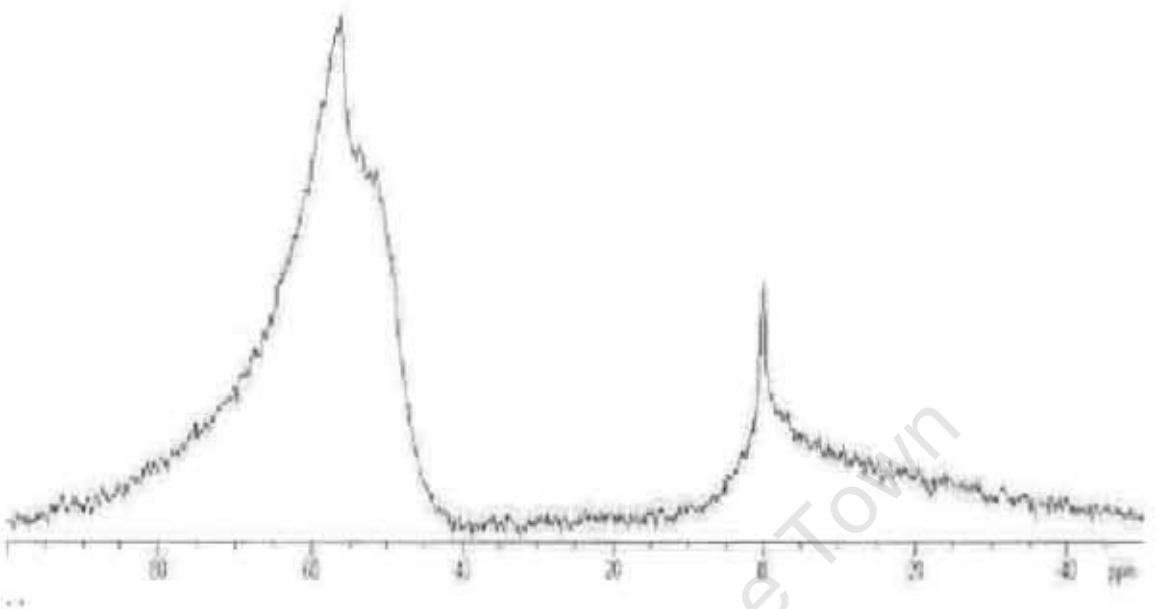

Figure 5.14: ^{27}Al MAS NMR spectrum of H-MCM-22 (UCT).

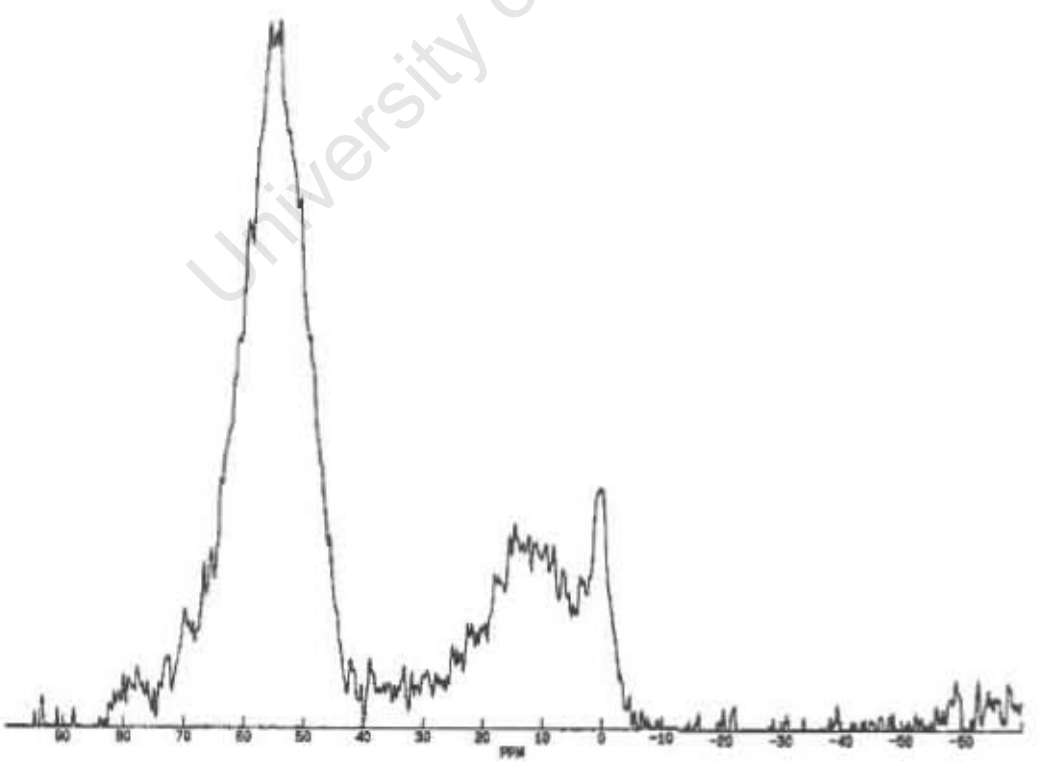

Figure 5.15: ^{27}Al MAS NMR spectrum of H-MCM-22 (DE1).

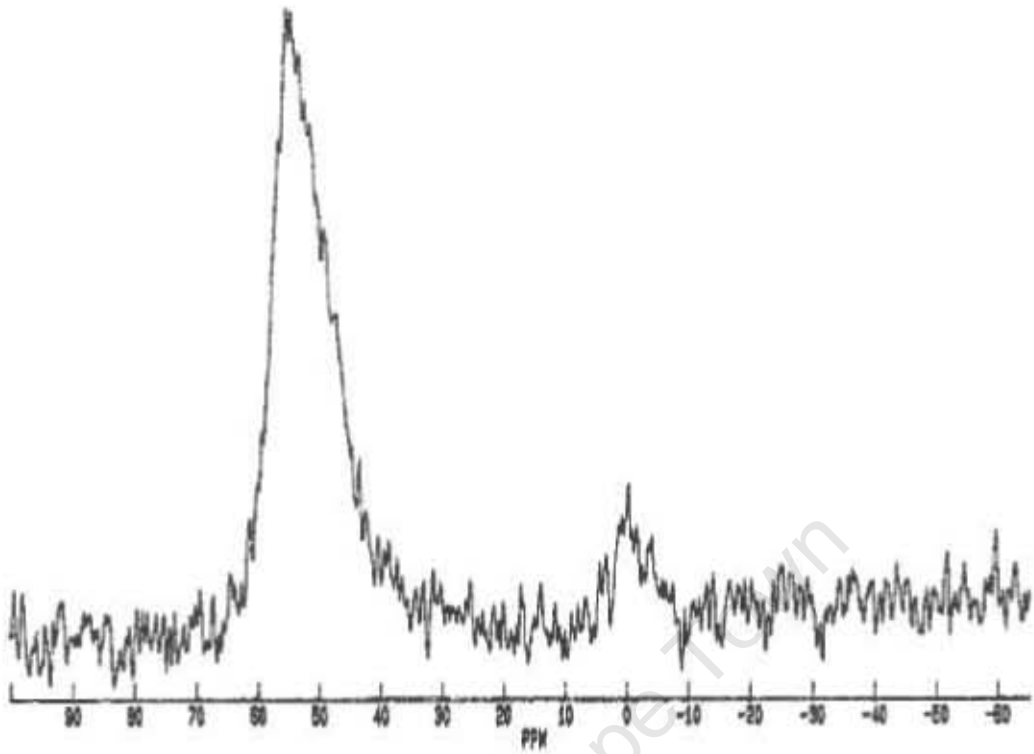

Figure 5.16: ^{27}Al MAS NMR spectrum of H-MCM-22 (DE2).

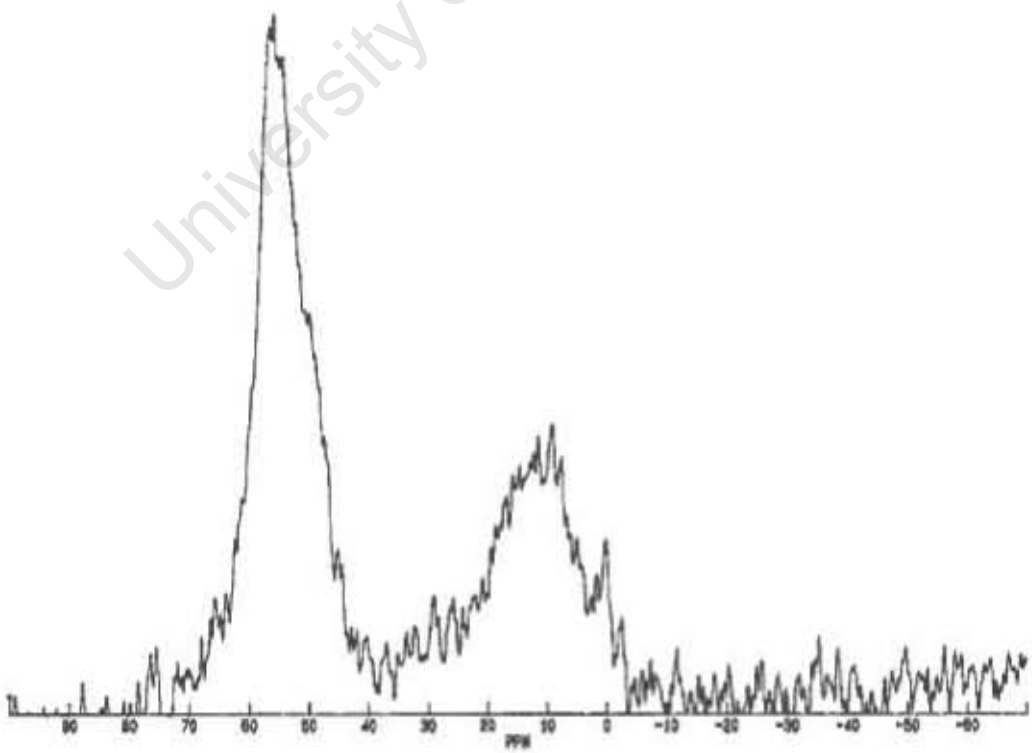

Figure 5.17: ^{27}Al MAS NMR spectrum of H-MCM-22 (DE3).

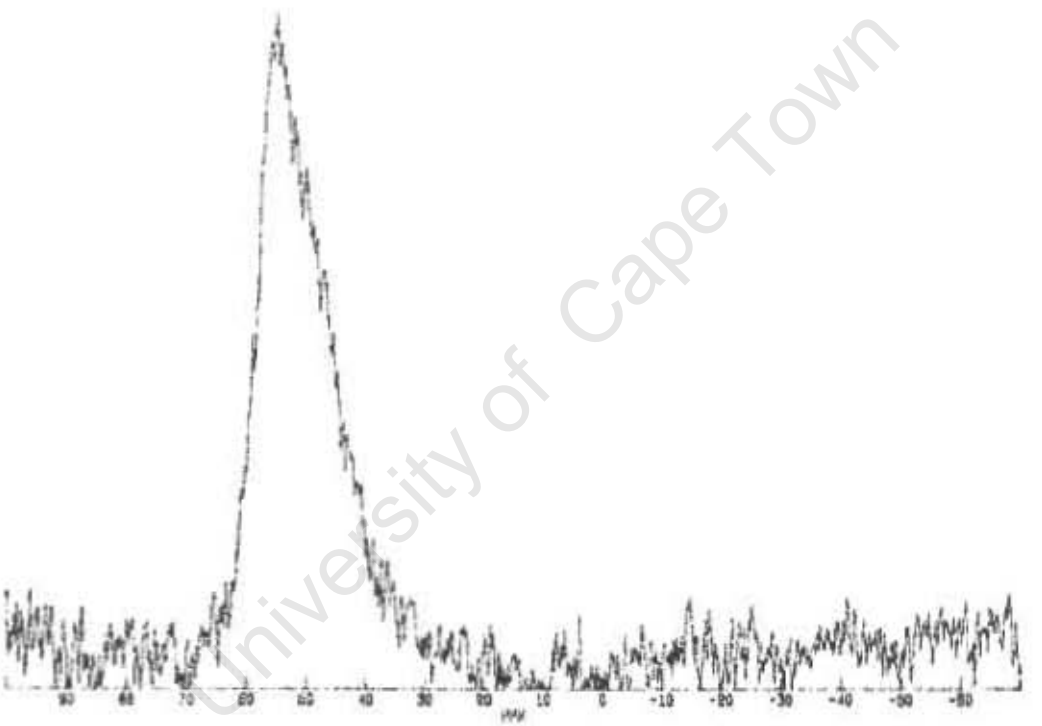

Figure 5.18: ^{27}Al MAS NMR spectrum of as-synthesised template containing Na-MCM-22 (DE1).

Chapter 6

Liquid phase alkylation of phenol with methanol

This chapter presents the results obtained in the liquid phase alkylation of phenol with methanol over zeolites H-ZSM-5, H-Beta, H-Mordenite, H-USY, H-MCM-22 (UCT), H-MCM-22 (DE2) and amorphous silica-alumina. It begins with the examination of the reproducibility of experiments in the system used. This is followed by an investigation into the relationship between product selectivity and phenol conversion over all the catalysts. All the catalysts are then compared at the same reaction condition and at phenol conversions below 10%. This section includes phenol conversion over internally selective sodium-exchanged ZSM-5 and MCM-22 as well as additional kinetic studies to characterize the catalytic properties of these materials. The effects of reaction time, reaction temperature, methanol : phenol ratio and addition of water were also examined. The conversion of the major primary products, namely anisole, o-cresol and p-cresol, are also examined including an anisole/phenol mixture. In all cases the catalysts are compared according to the conversion of the aromatic reactant component, product selectivity, O-alkylation versus C-alkylation and cresol isomer distribution with special regard to the p/o-cresol ratio. Finally, the isomer distribution obtained in the methylation of toluene with methanol over H-ZSM-5 and H-MCM-22 (UCT) are compared with that obtained from phenol methylation. The chapter closes with a summary of all the key results. Reaction conditions and reaction data for the liquid phase phenol methylation with methanol is given in Appendix C.

6.1 Liquid phase standard reaction conditions

A standard reaction condition was defined and applied to most of the experiments in the liquid phase and also taken as the base case for parameter variation studies. These liquid phase standard reaction conditions are given in Table 6.1.

Table 6.1: Liquid phase standard reaction conditions applied.

Reaction temperature	200°C
Starting reaction pressure	16 bar
Final reaction pressure	autogenous (between 18 and 25 bar)*
Reaction time	5 hours
Methanol : phenol molar ratio	1
Reactants : catalyst mass ratio	39.4

* Final reaction pressure is dependent on the conversion and selectivity, cf. Section 6.4.

6.2 Experimental reproducibility and material balance

6.2.1 Experimental reproducibility

The reproducibility of experiments in the liquid phase reaction system was carried out under the liquid phase standard reaction conditions (Table 6.1) over four different catalysts. The results are given in Table 6.2. The criteria used to evaluate reproducibility are:

- phenol conversion;
- selectivity to anisole;
- selectivity to cresol;
- distribution of the cresol isomers;
- selectivity to other products, which are typically xylenols and methylanisoles.

The system showed equivalent reproducibility characteristics for all the catalysts used in this study on reproducibility.

6.2.2 Material balance

Appendix A shows a typical GC trace obtained in the liquid phase phenol methylation with methanol. For material balances, an exact amount of internal standard was added to a known sample mass. Balances were calculated as molar balances on a ring basis. Ring mole balances between 96 and 100 mol% were found for all the cases studied. A model calculation of a material balance, is shown in Appendix B.

6.3 Relationship between phenol conversion and product selectivity

As a number of different catalysts of different activity were studied (cf. Section 6.4), the effect that phenol conversion has on product selectivity first needed to be evaluated in order to allow a valid comparison of the different catalysts. Reactions were carried out under the liquid phase standard

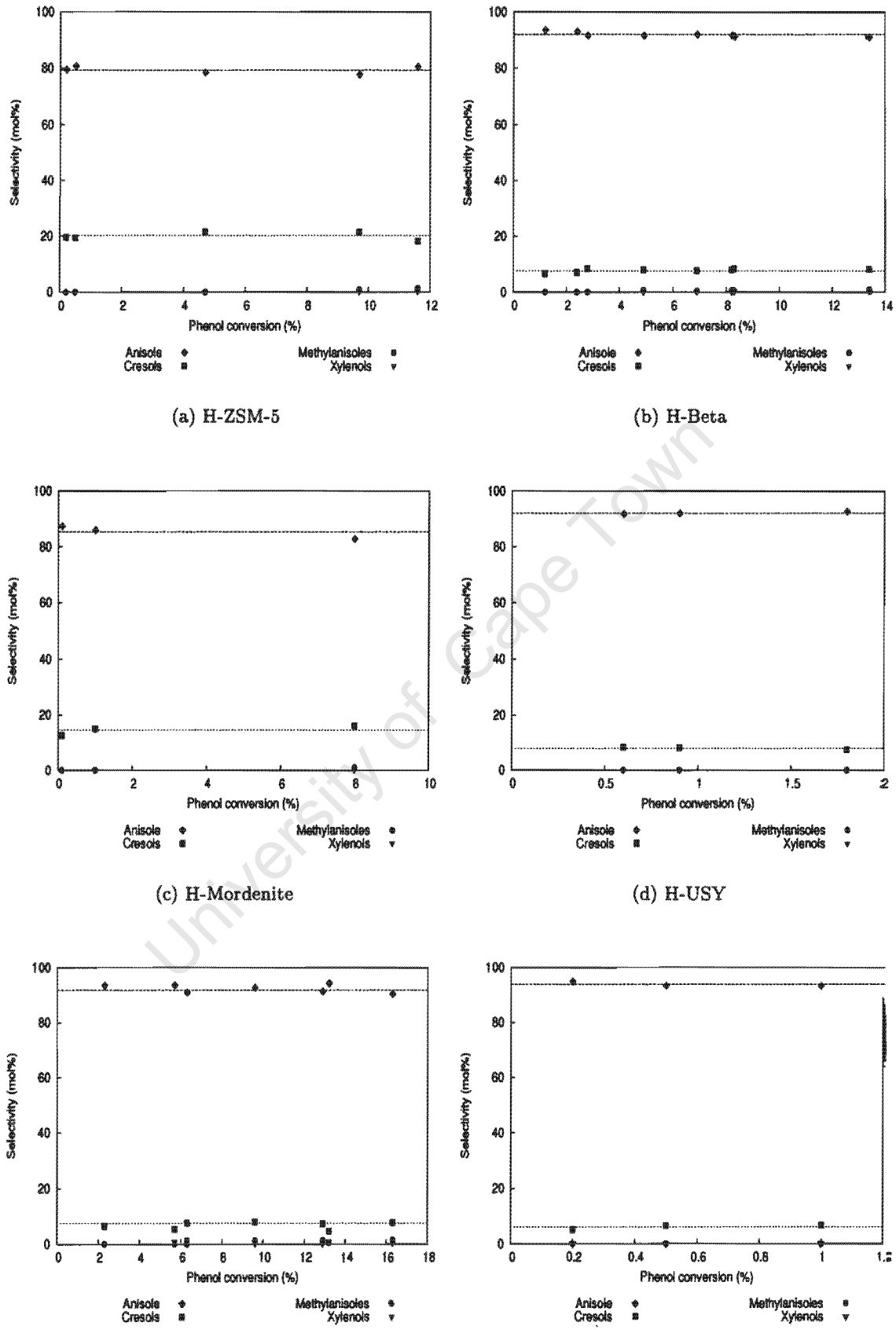

(a) H-ZSM-5

(b) H-Beta

(c) H-Mordenite

(d) H-USY

(e) H-MCM-22 (UCT)

(f) Amorphous silica-alumina

Figure 6.1: Product selectivity versus phenol conversion at liquid phase standard reaction conditions (200°C, starting pressure = 16 bar, methanol to phenol molar ratio = 1) with varying reaction time and reactants : catalyst mass ratio.

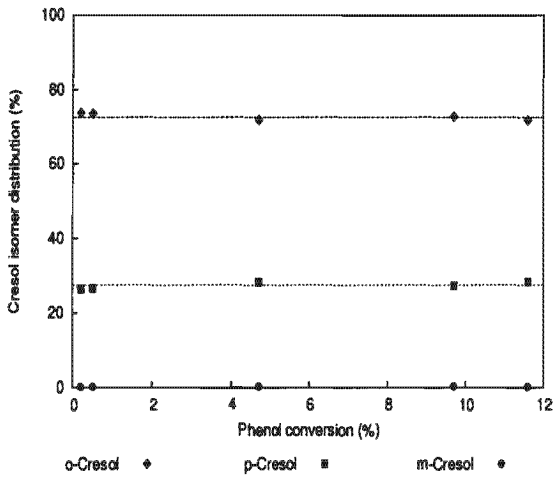

(a) H-ZSM-5

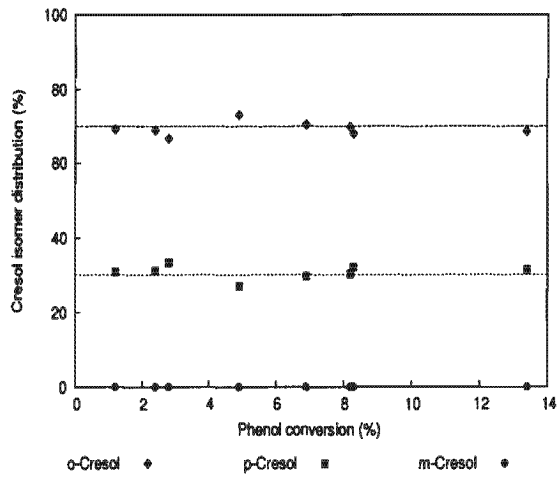

(b) H-Beta

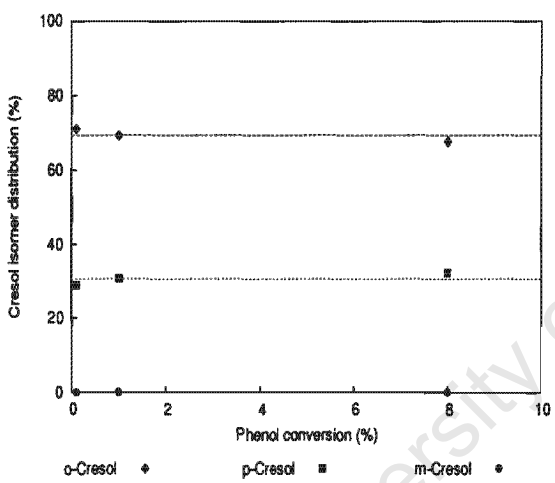

(c) H-Mordenite

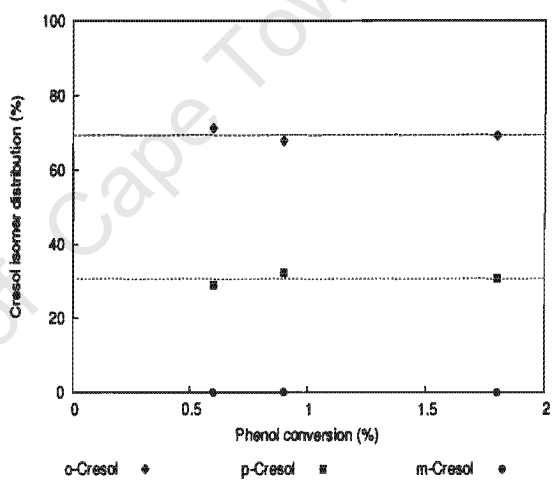

(d) H-USY

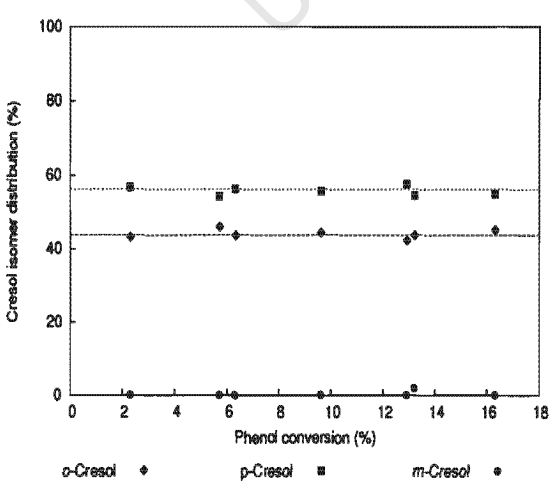

(e) H-MCM-22 (UCT)

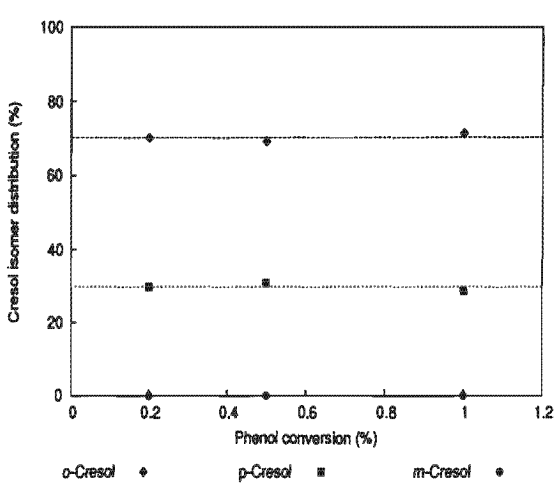

(f) Amorphous silica-alumina

Figure 6.2: Cresol isomer distribution versus phenol conversion at liquid phase standard reaction conditions (200°C, starting pressure = 16 bar, methanol to phenol molar ratio = 1) with varying reaction time and reactants : catalyst mass ratio.

Table 6.2: Reproducibility of liquid phase alkylation of phenol with methanol over different catalysts.

Catalyst	Phenol conversion (%)	Selectivity (mol%)			Cresol distribution (%)		
		Anisole	Cresols	Other*	o-	p-	m-
H-ZSM-5**	9.7	77.7	21.4	0.9	72.6	27.4	0.0
	9.6	79.7	19.7	0.6	73.3	26.7	0.0
H-ZSM-5***	0.5	80.7	19.3	0.0	73.5	26.5	0.0
	0.6	80.2	19.8	0.0	71.3	28.7	0.0
H-Beta**	9.1	92.3	7.7	0.0	69.7	30.3	0.0
	9.3	92.0	8.0	0.0	67.9	32.1	0.0
Silica-alumina**	0.5	93.4	6.6	0.0	69.2	30.8	0.0
	1.0	93.3	6.7	0.0	71.3	28.7	0.0

* Other = higher alkylated products, namely methylanisoles and xylenols;
** Liquid phase standard reaction conditions; 200°C, starting pressure = 16 bar, 5 hours, methanol : phenol molar ratio = 1, reactants : catalyst mass ratio = 39.4;
*** Liquid phase standard reaction conditions except catalyst mass ratio = 250, methanol : phenol molar ratio = 5.

reaction conditions (cf. Table 6.1) except for reactant to catalyst ratio and reaction time (this was achieved through individual experiments of different durations), which were varied to achieve different phenol conversions. Figures 6.1 and 6.2 show the relationship between product selectivity and cresol isomer distributions and phenol conversion for all types of catalysts applied. Within the conversion range of up to 16%, product selectivity and cresol isomer distribution were found to be independent of phenol conversion. This validates the comparison of the product selectivities of the different catalysts at the different phenol conversions, which were achieved when applied under the liquid phase standard reaction conditions.

6.4 Comparison of different zeolite catalysts and amorphous silica-alumina

The zeolites H-ZSM-5, H-Beta, H-Mordenite, H-USY, H-MCM-22 (UCT) and H-MCM-22 (DE2), amorphous silica-alumina as well as internally selective sodium-exchanged ZSM-5 and MCM-22 (UCT) were compared in terms of phenol conversion, product selectivity and cresol isomer distribution under the liquid phase standard reaction conditions (cf. Table 6.1).

6.4.1 Final reaction pressure

The different autogeneous reaction pressures obtained for the different catalysts at these reaction conditions at the end of the reaction are given in Table 6.3. The differences in the autogeneous pressures at the end of the reaction may be due to a shift in the average volatility of the molecules in the reactant/product mixture as the major reactions in phenol methylation result in no change in the number of molecules:

Table 6.3: The autogeneous reaction pressure at the end of the reaction obtained for the different catalysts under liquid phase standard reaction conditions at the end of the experiment.

Catalyst	Reaction pressure (bar)*
H-ZSM-5	23
H-Beta	22
H-Mordenite	22
H-USY	20
H-MCM-22 (UCT)	23
H-MCM-22 (DE2)	25
Silica-alumina	18
H/Na-ZSM-5	22
H/Na-MCM-22	21

*Starting reaction pressure = 16 bar.

$$2\,\text{Methanol} \rightleftharpoons \text{dimethyl ether} + \text{water}$$

$$\text{Phenol} + \text{methanol} \rightarrow \text{anisole or cresol} + \text{water}$$

$$\text{Phenol} + \text{dimethyl ether} \rightarrow \text{anisole or cresol} + \text{water}$$

Methanol, dimethyl ether and water are mostly in the gas phase. Phenol and the aromatic products are mostly in the liquid phase but are also present in the vapour phase thereby contributing to the autogeneous pressure. Anisole is the most volatile of the aromatic compounds, significantly more than phenol and the cresols (boiling points are given in Table 2.6).

Figure 6.3 shows the relationships between the autogeneous pressure at the end of the reaction and the phenol conversion, anisole yield and cresol yield. The autogeneous pressure at the end of the reaction is dependent on the phenol conversion (Figure 6.3 (a)) but this is due to the formation of the more volatile anisole and not due to the less volatile cresols as the correlation between the autogeneous pressures at the end of the reaction with anisole yield (Figure 6.3 (b)) is much steeper than with cresol yield (Figure 6.3 (c)).

6.4.2 Reactions over H-zeolites and amorphous silica-alumina

Table 6.4 gives the phenol conversions and the product distributions found for all the catalysts studied. H-ZSM-5, H-Beta, H-Mordenite, H-MCM-22 (UCT) and H-MCM-22 (DE2) were considerably more active than H-USY and amorphous silica-alumina in terms of phenol conversion. In all the catalysts studied, anisole was by far the major product formed. Cresols selectivity was much lower. Apparently, O-alkylation was also the preferred reaction compared to C-alkylation with O/C-alkylation ratios between 3.6 and 25.1. H-ZSM-5 and H-Mordenite produced the highest selectivity to cresols. The other catalysts showed similar, low cresols selectivities. Only trace amounts of higher alkylated

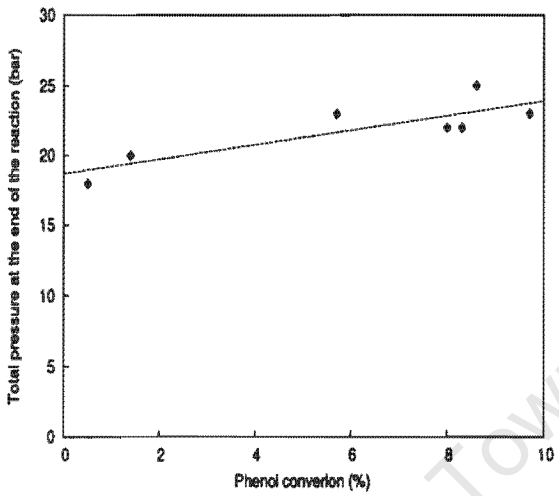

(a) Phenol conversion

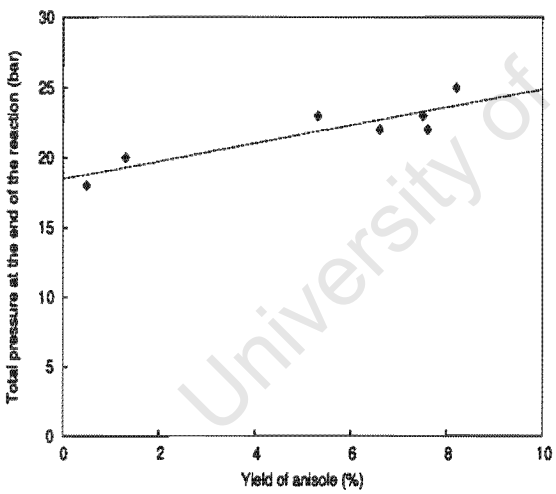

(b) Anisole yield

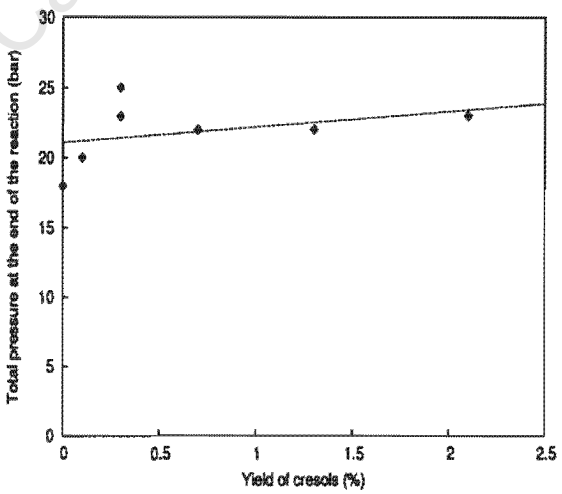

(c) Cresol yield

Figure 6.3: The dependency of the autogeneous pressure at the end of the reaction on the phenol conversion, anisole yield and cresol yield. Data points represent the results obtained over the different catalysts, cf. Table 6.3 and 6.4 (liquid phase standard reaction conditions: 200°C, starting pressure = 16 bar, reaction time = 5 hours, methanol : phenol molar ratio = 1, reactants : catalyst mass ratio = 39.4).

Table 6.4: Conversion and product selectivities for phenol methylation over the different catalysts studied under liquid phase standard reaction conditions (200°C, starting pressure = 16 bar, reaction time = 5 hours, methanol : phenol molar ratio = 1, reactants : catalyst mass ratio = 39.4).

Catalyst	Phenol Conversion (%)	Selectivity (mol%)				O/C-alkylation ratio
		Anisole	Cresols	Methylanisoles	Xylenols	
H-ZSM-5	9.7	77.7	21.4	0.9	0.0	3.6
H-Beta	8.3	91.2	8.3	0.5	0.0	11.0
H-Mordenite	8.0	82.8	16.2	1.0	0.0	5.1
H-USY	1.4	91.9	8.1	0.0	0.0	11.3
H-MCM-22 (UCT)	5.7	93.6	5.4	1.0	0.0	17.3
H-MCM-22 (DE2)	8.6	95.2	3.8	1.0	0.0	25.1
Silica-alumina	0.5	93.4	6.6	0.0	0.0	14.2

Table 6.5: Distribution of cresol isomers formed in phenol methylation under the liquid phase standard reaction conditions (200°C, starting pressure = 16 bar, reaction time = 5 hours, methanol : phenol molar ratio = 1, reactants : catalyst mass ratio = 39.4).

Catalyst	o-Cresol (%)	p-Cresol (%)	m-Cresol (%)	p/o-Cresol ratio	Anisole/ o-cresol ratio
H-ZSM-5	72.6	27.4	0.0	0.38	5.0
H-Beta	67.9	32.1	0.0	0.47	16.2
H-Mordenite	67.6	32.4	0.0	0.48	7.5
H-USY	62.6	37.4	0.0	0.60	18.1
H-MCM-22 (UCT)	45.5	54.5	0.0	1.20	38.1
H-MCM-22 (DE2)	49.4	50.6	0.0	1.02	50.7
Silica-alumina	69.2	30.8	0.0	0.45	20.5
Thermodynamic equilibrium*	37	16	47	ca. 0.43	

* Preliminary data of Böhringer and Fletcher [2003] at 350°C. Note that the effect of reaction temperature on cresol isomer distribution is minor, cf. Section 2.2.2.6.

products (methylanisoles) were produced.

Table 6.5 shows the distributions of cresol isomers obtained from the different catalysts. H-MCM-22 (UCT) and H-MCM-22 (DE2) stand out due to their high p/o-cresol ratio. All the other catalysts favoured the formation of the ortho-isomer producing p/o-cresol ratios close to thermodynamic equilibrium (0.43) and the statistical ratio (0.50), respectively. In all the catalysts, at 200°C, no m-cresol was formed.

6.4.3 Reactions over internally selectively sodium-exchanged ZSM-5 and MCM-22 (UCT)

ZSM-5 and MCM-22 (UCT) were internally selectively sodium-exchanged such that the internal acid sites within the pores of the zeolite crystals (not the external sites) were removed by sodium-H^+-

exchange as described in Section 2.1.4.2.1. Hence it can be assumed that only external acid sites are available for reactions.

6.4.3.1 Test reactions to kinetically characterize the internally selectively sodium-exchanged zeolites ZSM-5 and MCM-22 (UCT)

The external surface activity of the zeolite crystals was determined by using the test reaction of 1,3,5-triisopropyl benzene (1,3,5-TIPB) cracking and the total activity was tested using n-hexane cracking (cf. Section 4.4 for the procedures and reaction conditions). The results for the 1,3,5-TIPB cracking reaction and the n-hexane cracking reaction are given in Table 6.6.

For the 1,3,5-TIPB cracking activity there is a moderate decrease for the internally selective sodium-exchanged H-ZSM-5 whereas for MCM-22 (UCT) the high conversions did not allow the determination of a slight or moderate change but clearly there is no significant decrease in activity. For ZSM-5, the decrease in activity indicates that a small fraction of the external surface sites may have been removed as well.

The large difference in the 1,3,5-TIPB cracking activity (i.e. the activity of the external surface of the crystals) between ZSM-5 and MCM-22 (UCT) is noteworthy. Since mesoporous surface areas are very similar with both the samples (127 and 134 m^2/g, respectively), and volume to surface ratios calculated from the crystal dimensions do not differ much (0.047 and 0.033, respectively, as can be derived from data given in Table 5.1), the reason for the huge MCM-22 (UCT) activity may be due to the contribution of the "cups" on the external surface of the MCM-22 crystal platelets (cf. Section 2.1.1.5).

The n-hexane cracking activity decreased, much more than the 1,3,5-TIPB cracking activity, for both zeolites upon internally selectively sodium-exchanging as expected due to the sodium blocking the internal acid sites. However, the decrease in the n-hexane cracking activity is much greater for H-ZSM-5 than for H-MCM-22 (UCT) despite the fact that the ratios of internal to total surface area in both samples are equal (0.70 and 0.68, respectively, as can be derived from Table 5.2). The activity changes in n-hexane cracking reflect to some extent the changes observed in TIPB cracking and may also be explained in terms of the contribution of the "cups" on the external surface of the MCM-22 crystal platelets.

In summary, the decline of the internal activity is significantly higher than the decline of the external activity (if there is a decline at all), indicating that the internal sites were selectively removed to a significant extent.

6.4.3.2 Phenol methylation with methanol over internally selectively sodium-exchanged ZSM-5 and MCM-22 (UCT)

From Table 6.7 it can be seen that the conversion of phenol in the methylation reaction over the internally selectively sodium-exchanged zeolites decreased by 88% for ZSM-5 and 60% for MCM-22 (UCT). The declines are correspond to the results from n-hexane cracking, cf. Table 6.6. The influence on O/C-alkylation ratio is marginal and in the range of scatter. There was also a decrease of methylanisole formation in both zeolites.

Table 6.6: Conversions (%) obtained from the 1,3,5-TIPB cracking and the n-hexane cracking test reactions over the H-zeolite and internally selectively sodium-exchanged H/Na-zeolites.

Zeolite	1,3,5-TIPB* cracking conversion (%)	Relative decline (%)	n-Hexane** cracking conversion (%)	Relative decline (%)
H-ZSM-5	37	35	79	81
H/Na-ZSM-5	24		15	
H-MCM-22 (UCT)	99	-	50	42
H/Na-MCM-22 (UCT)	99		29	

* 1,3,5-TIPB cracking reaction conditions: reaction temperature = 270°C, 1,3,5-TIPB partial pressure = 0.0016 bar, WHSV = 0.6 h^{-1}, nitrogen carrier gas, cf. Section 4.4;

** n-Hexane cracking reaction conditions: reaction temperature = 500°C, n-hexane partial pressure = 0.04 bar, WHSV = 1.6 h^{-1}, nitrogen carrier gas; cf. Section 4.4.

Table 6.7: Conversion and product selectivities from phenol alkylation with methanol over acid and internally selectively sodium-exchanged zeolites ZSM-5 and MCM-22 (UCT) under the liquid phase standard reaction conditions (200°C, starting pressure = 16 bar, reaction time = 5 hours, methanol : phenol molar ratio = 1, reactants : catalyst mass ratio = 39.4).

Zeolite	Phenol conversion (%)	Relative decline (%)	Selectivity (mol%)				O/C-alkylation ratio
			Anisole	Cresols	Methyl-anisoles	Xylenols	
H-ZSM-5	9.7	88	77.7	21.4	0.9	0.0	3.6
H/Na-ZSM-5	1.2		81.0	19.0	0.0	0.0	4.3
H-MCM-22 (UCT)	5.7	60	93.6	5.4	1.0	0.0	17.3
H/Na-MCM-22 (UCT)	2.3		93.8	5.7	0.5	0.0	16.5

Table 6.8: Cresol isomer distribution obtained from phenol methylation with methanol over acid and internally selectively sodium-exchanged zeolite catalysts under the liquid phase standard reaction conditions (200°C, starting pressure = 16 bar, reaction time = 5 hours, methanol : phenol molar ratio = 1, reactants : catalyst mass ratio = 39.4).

Zeolite	o-Cresol (%)	p-Cresol (%)	m-Cresol (%)	p/o-Cresol ratio	Anisole/ o-cresol ratio
H-ZSM-5	72.6	27.4	0.0	0.38	5.0
H/Na-ZSM-5	77.5	22.5	0.0	0.29	5.5
H-MCM-22 (UCT)	45.5	54.5	0.0	1.20	38.1
H/Na-MCM-22 (UCT)	59.8	40.2	0.0	0.67	27.5
Thermodynamic equilibrium*	37	16	47	ca. 0.43	

* Preliminary data of Böhringer and Fletcher [2003] at 350°C. Note that the effect of reaction temperature on cresol isomer distribution is minor, cf. Section 2.2.2.6.

The effect of internally selectively sodium-exchanged zeolites on the cresol isomer distribution is shown in Table 6.8. In both zeolites there was an increase in the o-cresol content in the cresol fraction and a decrease in the p-cresol content in the cresol fraction resulting in a significant decline of the p/o-cresol ratio. This effect is much more noticeable in MCM-22 (UCT) than ZSM-5. In all cases no m-cresol was formed.

6.5 Effect of reaction parameters

6.5.1 Effect of reaction time

Figure 6.4 shows the relationship between phenol conversion and reaction time (this was achieved through individual experiments of different durations) under liquid phase standard reaction conditions (cf. Table 6.1). Over all the catalysts as reaction time increased so phenol conversion increased, as expected. The activity of amorphous silica-alumina was comparably low.

Figure 6.5 shows the product selectivity and cresol isomer distribution over time for H-Beta and H-MCM-22 (UCT). With reaction time selectivities hardly changed. Apparent trends are in the range of scatter, indicated clearly by Figure 6.5 (c) and (d). Selectivity to methylanisoles was minor and the selectivity to xylenols remained insignificant.

6.5.2 Reaction temperature

The effect of reaction temperature on phenol conversion was studied over zeolites H-ZSM-5, H-Beta and H-MCM-22 (UCT). As the temperature increased so did the phenol conversion, as expected (Figure 6.6).

Over H-ZSM-5 and H-Beta as the temperature increased, so the selectivity to anisole decreased, the selectivity to cresols increased and relatively, the selectivity to the higher alkylated products (methylanisoles and xylenols) increased even more (Figure 6.7 (a) and (b)). Over H-MCM-22 (UCT) selectivities hardly changed over the temperature range applied (Figure 6.7 (c)).

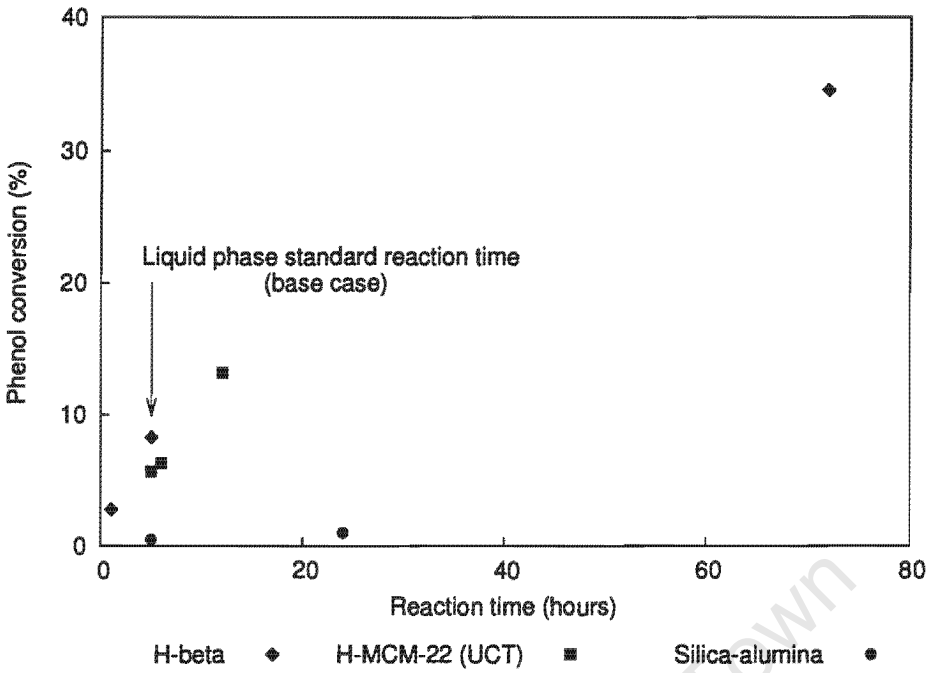

Figure 6.4: The effect of reaction time on the phenol conversion (200°C, methanol : phenol molar ratio = 1, reactants to catalyst mass ratio = 39.4).

In terms of the cresol isomer distribution, the distribution of o- and p-cresol hardly changed with temperature for the three zeolites (Figure 6.8), apparently not exceeding the range of scatter. Figure 6.9 also shows that the reaction temperature has only a minor effect on the p/o-cresol ratio. At 250°C very small quantities of m-cresol were formed.

6.5.3 Reaction pressure

The effect of reaction pressure on the phenol alkylation with methanol was not studied in the liquid phase as the reactions were done at autogeneous pressure. Low pressure experiments were done in the gas phase to compare with the high pressure liquid phase results. The results of the gas phase experiments are presented in Chapter 7.

6.5.4 Effect of methanol to phenol ratio

The effect of reactants methanol : phenol ratio was studied on zeolites H-ZSM-5, H-Beta, H-MCM-22 (UCT) and silica-alumina under liquid phase standard reaction conditions (cf. Table 6.1). The reactants methanol : phenol molar ratio was varied in four steps between 0.07 : 1 and 5 : 1. Figure 6.10 shows the effect of methanol : phenol ratio on phenol conversion.

The relationship between phenol conversion and increasing methanol : phenol ratio over these zeolites is quite inconsistent, ranging from a steady increase of conversion (H-MCM-22) passing through a maximum (H-ZSM-5 and H-Beta) to a steady decline (silica-alumina).

In terms of product selectivities (Figure 6.11), all the catalysts showed similar trends with increasing methanol : phenol ratio. As methanol concentration increased relative to phenol in the reactants,

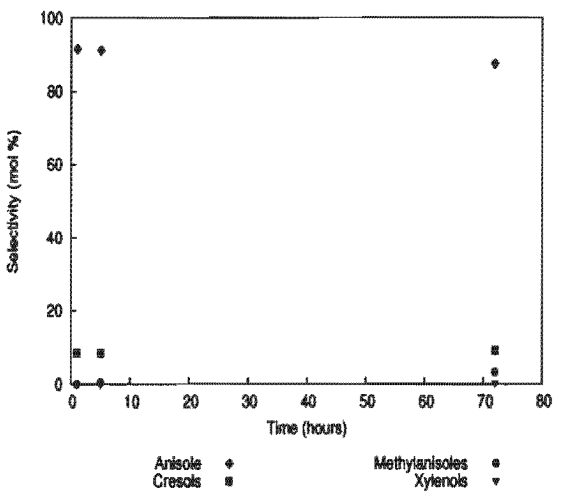

(a) H-Beta

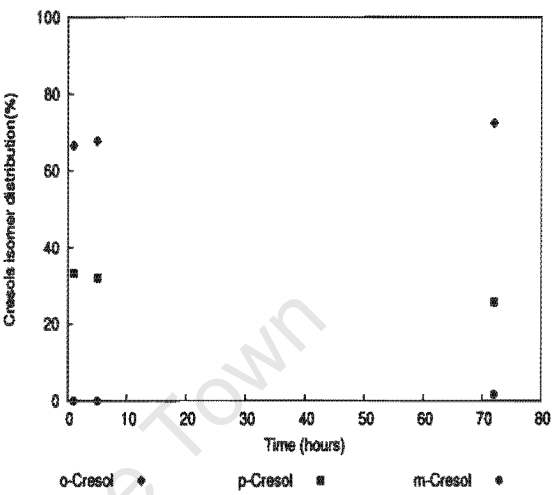

(b) H-Beta

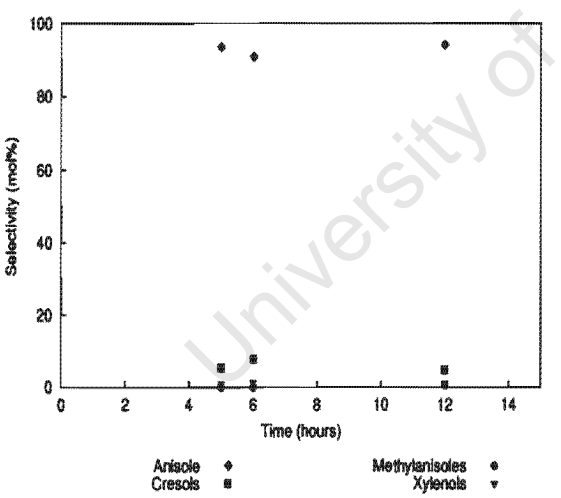

(c) H-MCM-22 (UCT)

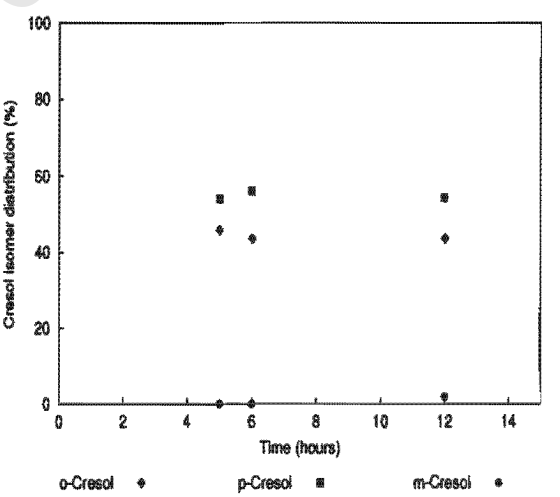

(d) H-MCM-22 (UCT)

Figure 6.5: Effect of reaction time on product selectivities for H-Beta and H-MCM-22 (UCT) (200°C, methanol : phenol molar ratio = 1, reactants to catalyst mass ratio 39.4).

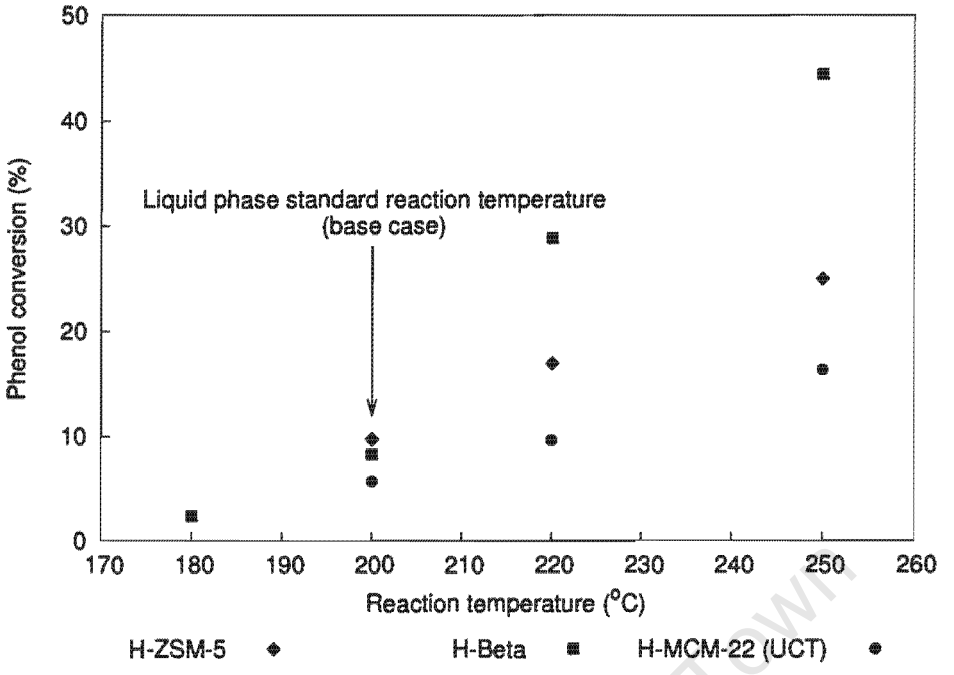

Figure 6.6: Effect of reaction temperature on phenol conversion (standard liquid phase reaction conditions : methanol : phenol molar ratio = 1, reaction time = 5 hours, reactants to catalyst mass ratio = 39.4, except reaction temperature).

anisole was preferentially formed in all cases whereas cresol selectivity declined. Minor inconsistency was observed over H-ZSM-5, where this common trend appears reversed at ratios < 1. The selectivity to xylenols and methylanisoles remains insignificant and unchanged with changing methanol : phenol ratio.

For H-ZSM-5, H-Beta and silica-alumina the content of o-cresol in the cresol fraction was always around 70%. This is equivalent to a p/o-cresol ratio of 0.42, which corresponds to the thermodynamic equilibrium (0.43) between the o- and p-cresol isomers as determined by Böhringer and Fletcher [2003] at 350°C (cf. Figure 2.33). The content of o-cresol in the cresol fraction increased slightly with increasing methanol : phenol ratio. At the highest methanol concentration applied, o-cresol was the only cresol isomer detected (Figure 6.12 (a), (b) and (d)). However, at the highest methanol concentration, the phenol conversion and the cresol selectivity were very low resulting in a very low cresol yield. These cresol yields were too low for detection of the p-isomer at the given gas chromatography conditions.

H-MCM-22 (UCT) showed a very different profile for the cresol distribution as a function of methanol : phenol reactants ratio (Figure 6.12 (c)), namely a significantly higher content of p-cresol (43 to 57%), resulting in a p/o-cresol molar ratio between 0.75 and 1.3 (Figure 6.13), almost twice the thermodynamic equilibrium ratio between the o- and p-cresol isomers as determined by Böhringer and Fletcher [2003] at 350°C. The percentage of p-cresol slightly declined at methanol : phenol ratios less than 1. No m-cresol was found in any of these product mixtures.

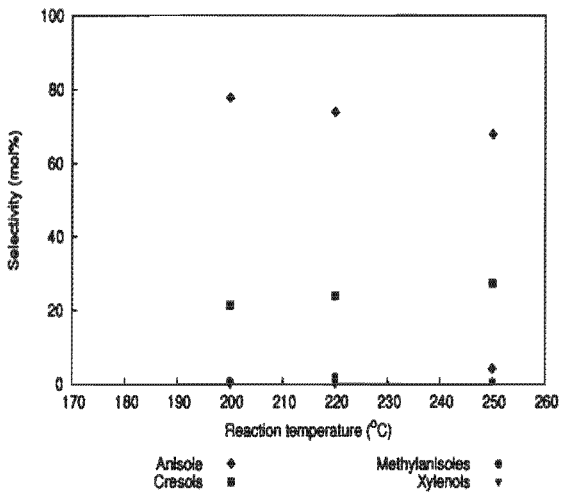

(a) H-ZSM-5

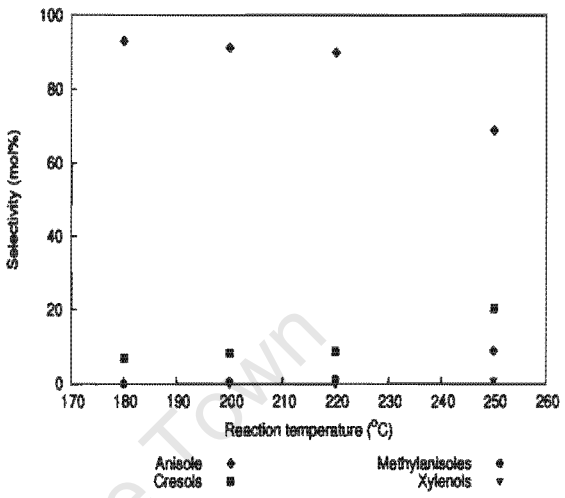

(b) H-Beta

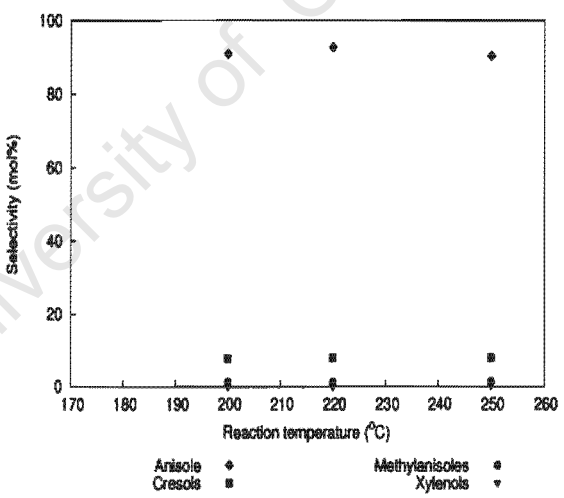

(c) H-MCM-22 (UCT)

Figure 6.7: Effect of reaction temperature on product selectivity (liquid phase standard reaction conditions: methanol : phenol molar ratio = 1, reaction time = 5 hours, reactants to catalyst mass ratio = 39.4, except for reaction temperature).

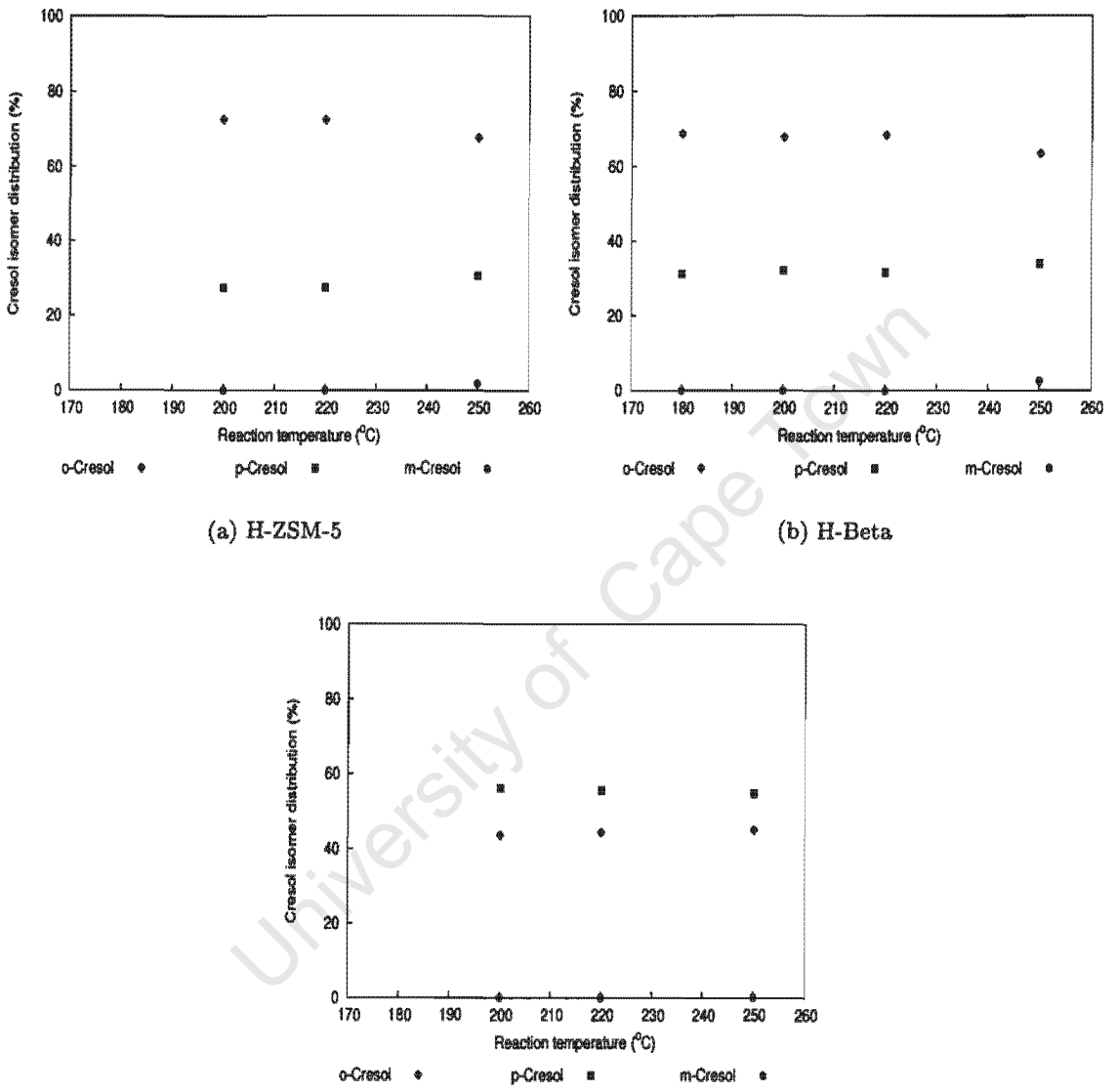

(a) H-ZSM-5

(b) H-Beta

(c) H-MCM-22 (UCT)

Figure 6.8: Effect of reaction temperature on cresol isomer distribution (liquid phase standard reaction conditions: methanol : phenol molar ratio = 1, reaction time = 5 hours, reactants to catalyst mass ratio = 39.4, except for reaction temperature).

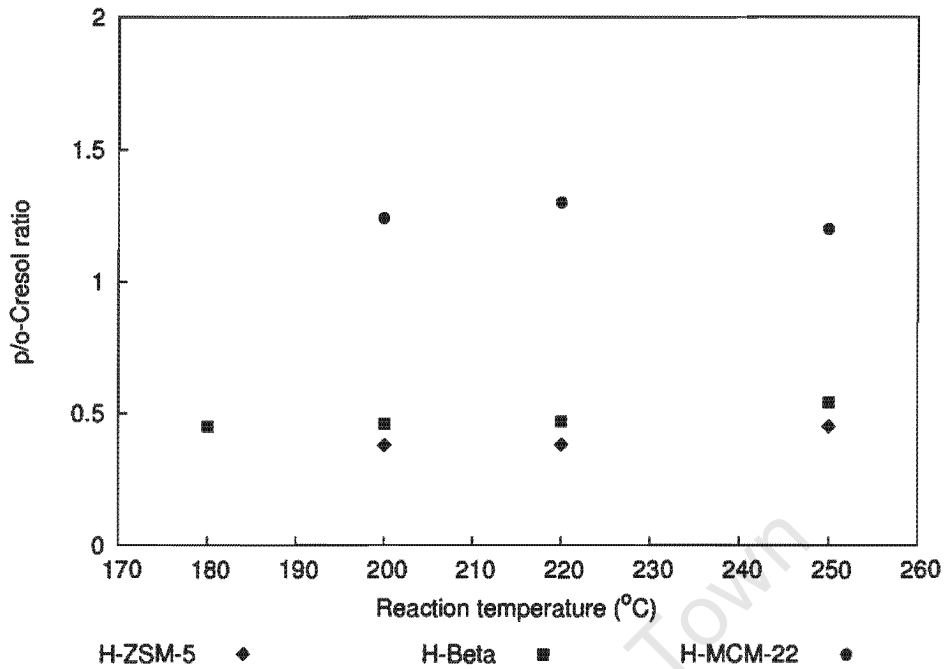

Figure 6.9: Effect of reaction temperature on the p/o-cresol ratio under liquid phase standard reaction conditions (methanol : phenol molar ratio = 1, reaction time = 5 hours, reactants to catalyst mass ratio = 39.4, except for reaction temperature).

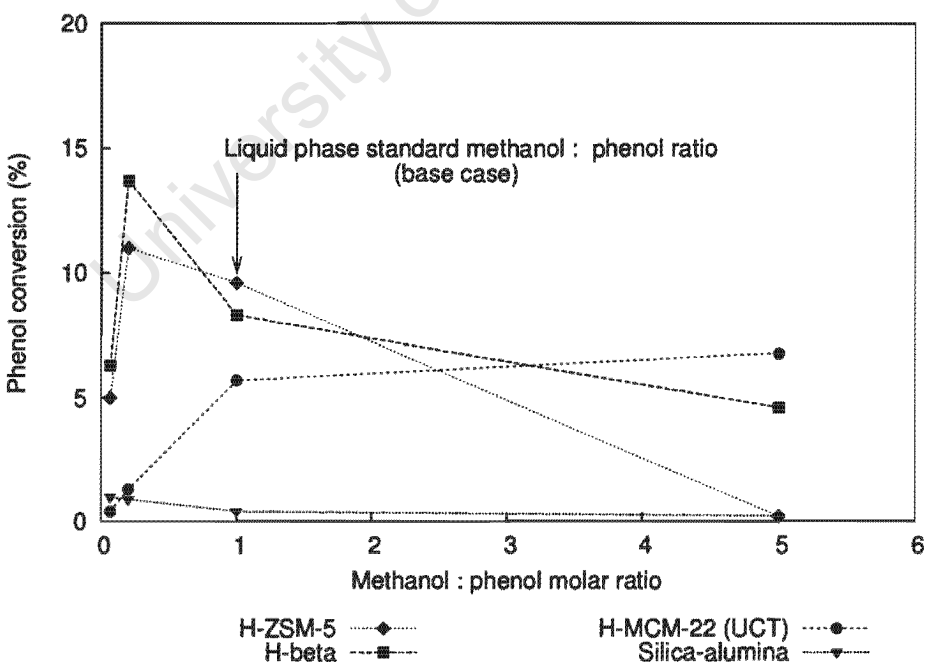

Figure 6.10: Effect of methanol : phenol ratio on the phenol conversion (liquid phase standard reaction conditions: 200°C, reaction time = 5 hours, reactants to catalyst mass ratio = 39.4, except for methanol : phenol ratio. Total reactants to catalyst mass ratio kept constant).

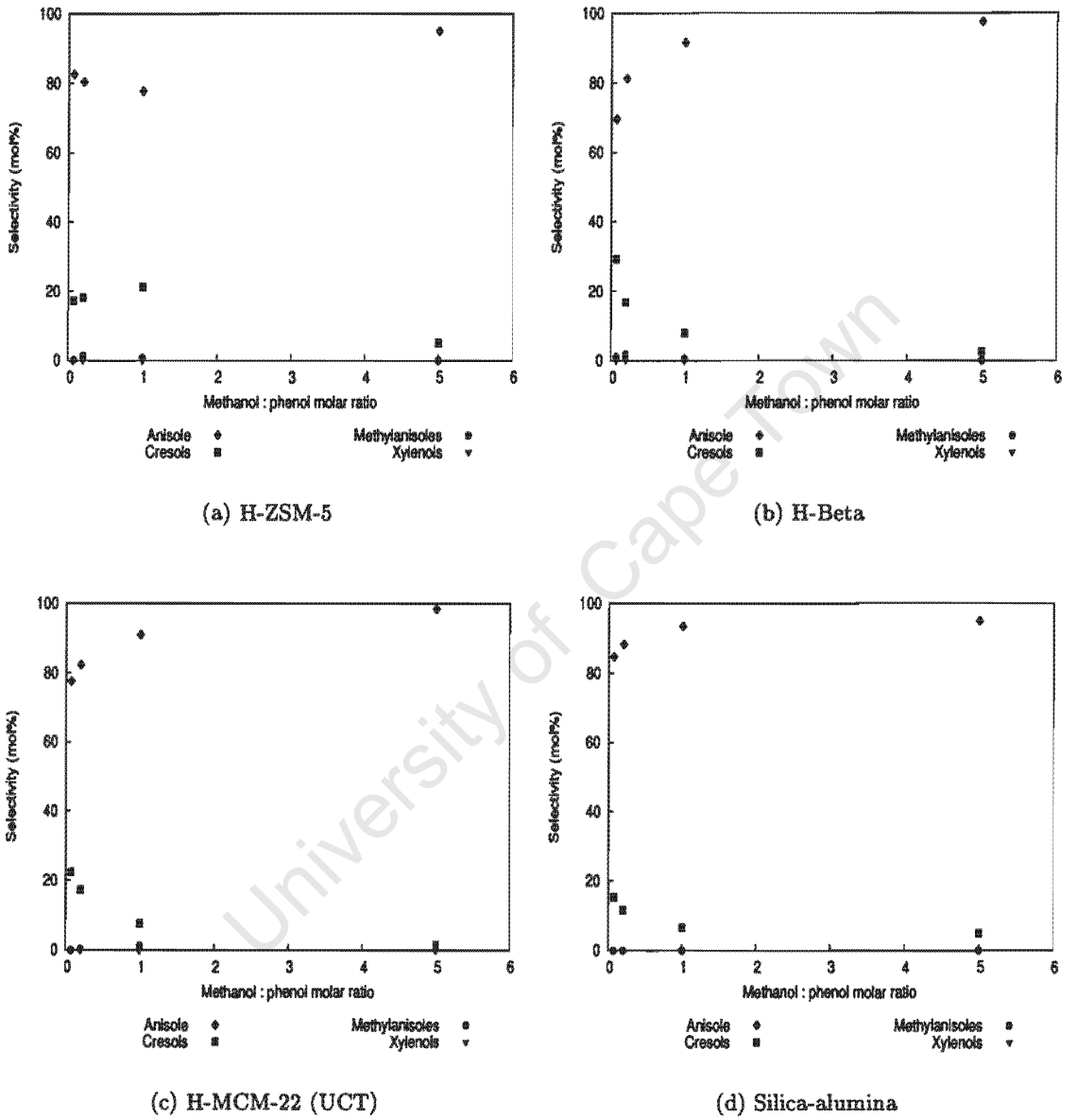

(a) H-ZSM-5

(b) H-Beta

(c) H-MCM-22 (UCT)

(d) Silica-alumina

Figure 6.11: Effect of methanol : phenol ratio on product selectivity under liquid phase standard reaction conditions (200°C, reaction time = 5 hours, reactants to catalyst mass ratio = 39.4, except for methanol : phenol ratio).

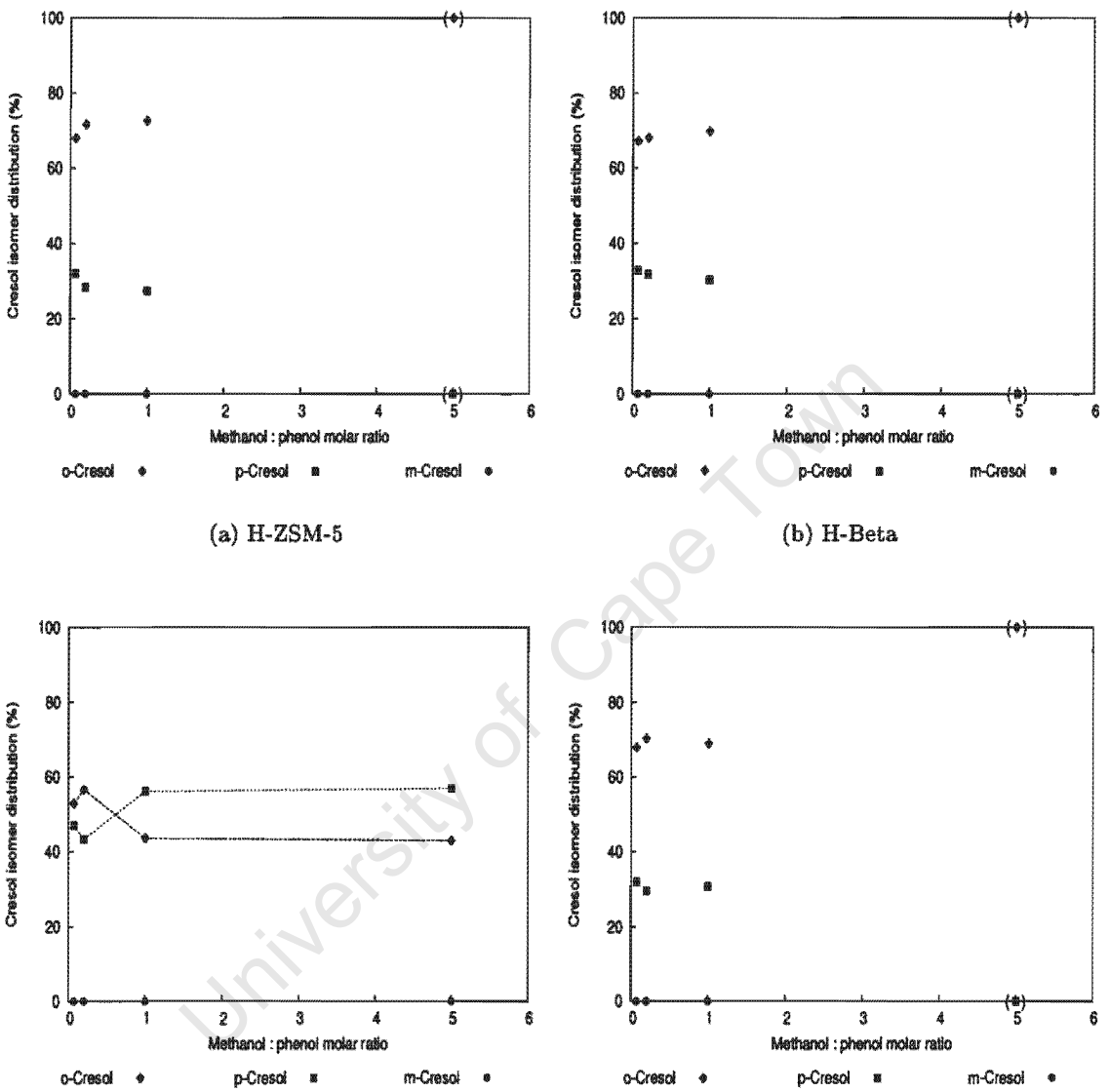

(a) H-ZSM-5

(b) H-Beta

(c) H-MCM-22 (UCT)

(d) Silica-alumina

Figure 6.12: Effect of methanol : phenol ratio on cresol isomer distribution under liquid phase standard reaction conditions (200°C, reaction time = 5 hours, reactants to catalyst mass ratio = 39.4, except for methanol : phenol ratio)
(Values in brackets indicate that cresol selectivity, cf. Figure 6.11, and cresol yields were too low to detect any p-isomer at the given gas chromatography conditions. Dotted lines in figure (c) are intended to guide the eye).

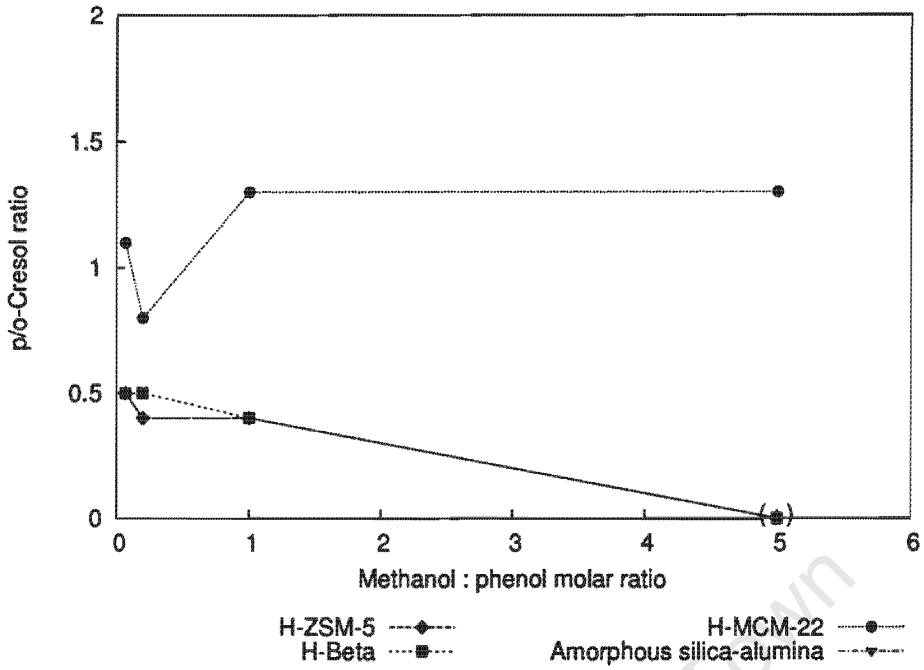

Figure 6.13: Effect of methanol : phenol ratio on the p/o-cresol ratio under liquid phase standard reaction conditions (200°C, reaction time = 5 hours, reactants to catalyst mass ratio = 39.4, except for methanol : phenol ratio).

6.5.5 Effect of water

Water is formed during phenol methylation reactions and in the conversion of methanol to dimethyl ether. Hence it was considered important to investigate the effect of water on conversion and product selectivities. The molar reactants composition for these experiments was 1 : 1 : 0.8 of methanol : phenol : water, other conditions were identical with the liquid phase standard reaction conditions (cf. Table 6.1). Tables 6.9 and 6.10 show the effect of the addition of water.

The presence of water largely affected phenol conversion i.e. the activity of the catalysts, in particular H-MCM-22 (UCT). The effect of water on selectivity differs. For H-ZSM-5 and H-MCM-22 (UCT) there was an increase in total cresols selectivity as well as p-selectivity with the addition of water, whereas H-Beta showed a decrease in both the selectivities. However, there is a consistent trend, namely that the effect of water on anisole selectivity and on p/o-cresol ratio is opposite. The increase of the selectivity to methylanisoles to 4.4% and increase in the p/o-cresol molar ratio to 1.66 through the addition of water in the case of H-MCM-22 (UCT) is noteworthy.

6.6 Conversion of the major phenol methylation products

The conversion of anisole, o-cresol and p-cresol was studied over the different catalysts studied (H-ZSM-5, H-Beta, H-Mordenite, H-USY, H-MCM-22 (UCT) and amorphous silica-alumina) to determine the extent to which secondary reactions occurred at the reaction conditions used. Over H-MCM-22 (UCT) the effect of the presence of phenol on anisole conversion was also studied. All theses reactions were carried out under the liquid phase standard reaction conditions (cf. Table 6.1) Auto-

Table 6.9: Effect of water with the reactants on conversion and product distribution under liquid phase standard reaction conditions (200°C, starting pressure = 16 bar, reaction time = 5 hours, methanol : phenol : water molar ratio = 1 : 1 : 0.8, reactants : catalyst mass ratio = 39.4).

Zeolites	Water in the feed	Phenol conversion (%)	Selectivity (mol%)			
			Anisole	Cresols	Methylanisoles	Xylenols
H-ZSM-5	No	9.7	77.7	21.4	0.9	0.0
	Yes	3.0	75.9	23.6	0.5	0.0
H-Beta	No	8.3	91.2	8.3	0.5	0.0
	Yes	2.9	94.9	5.1	0.0	0.0
H-MCM-22 (UCT)	No	5.7	93.6	5.4	1.0	0.0
	Yes	1.1	90.0	5.6	4.4	0.0

Table 6.10: Effect of water with the reactants on cresol isomers distribution under liquid phase standard reaction conditions (200°C, starting pressure = 16 bar, reaction time = 5 hours, methanol : phenol : water molar ratio = 1 : 1 : 0.8 , reactants : catalyst mass ratio = 39.4).

Zeolite	Water in the feed	o-Cresol (%)	p-Cresol (%)	m-Cresol (%)	p/o-Cresol ratio
H-ZSM-5	No	72.6	27.4	0.0	0.38
	Yes	63.5	36.5	0.0	0.57
H-Beta	No	67.9	32.1	0.0	0.47
	Yes	74.7	25.3	0.0	0.34
H-MCM-22 (UCT)	No	45.5	54.5	0.0	1.20
	Yes	37.6	62.4	0.0	1.66

Table 6.11: Conversion and product selectivities to oxygenates in the anisole conversion over different catalysts under liquid phase standard reaction conditions (200°C, reaction time = 5 hours, reactant : catalyst mass ratio = 30).

Catalyst	Conversion (%)	Final* pressure (bar)	Selectivity (mol %)				
			Cresols	Methyl-anisoles	Xylenols	Phenol	Other **
H-ZSM-5	3.2	3	5.2	46.5	0.9	47.4	0.0
H-Beta	17.3	2	12.6	42.8	0.9	43.7	0.0
H-Mordenite	54.7	2	20.8	27.5	2.8	42.7	6.2
H-USY	12.2	1.5	6.2	44.9	2.0	46.9	0.0
H-MCM-22 (UCT)	21.0	2	13.0	38.5	1.1	44.8	2.6
Silica-alumina	3.4	1.5	16.3	39.4	2.5	41.8	0.0

* Autogeneous reaction pressure at the end of the reaction;
** Other are higher products assumed to be dimethylanisoles.

Table 6.12: Distribution of cresol isomers obtained from anisole conversion under liquid phase standard reaction conditions (200°C, reaction time = 5 hours, reactant to catalyst mass ratio = 30).

	o-Cresol (%)	p-Cresol (%)	m-Cresol (%)	p/o-Cresol ratio
H-ZSM-5	80.2	19.8	0.0	0.25
H-Beta	53.4	46.6	0.0	0.87
H-Mordenite	70.3	29.7	0.0	0.42
H-USY	75.3	24.7	0.0	0.33
H-MCM-22 (UCT)	47.3	52.7	0.0	1.11
Silica-alumina	7.9	92.1	0.0	11.7

geneous pressure build-up, however, was low, since there was no highly volatile reactants component as in the phenol methylation experiments.

6.6.1 Conversion of anisole

The results of anisole conversion over the different catalysts are given in Tables 6.11 and 6.12. H-Mordenite showed the highest conversion of anisole whereas H-ZSM-5 and silica-alumina showed a relatively low conversion. Over all the catalysts, the dominant products were the disproportionation products of anisole, namely methylanisoles and phenol.

In terms of the cresol isomer distribution H-ZSM-5, H-Mordenite and H-USY all produced high o-cresol selectivity and low para-selectivity. H-Beta, H-MCM-22 (UCT) and silica-alumina on the other hand, the latter in particular, produced high para-selectivity. No m-cresol was formed.

6.6.1.1 Conversion of an anisole/phenol mixture

Reacting an anisole/phenol mixture in a 1 : 1 molar ratio over H-MCM-22 (UCT) showed a remarkable difference in conversion and product selectivity compared to the case of pure anisole. Table 6.13 shows that in the presence of phenol the conversion of anisole decreased substantially. The product spectrum

Table 6.13: Conversion and product selectivities to oxygenates in the conversion of anisole and an anisole/phenol mixture over H-MCM-22 (UCT) (200°C, reaction time = 5 hours).

Feed	Anisole conversion (%)	Selectivity (mol%)				Other ****
		Cresols	Methylanisoles	Xylenols	Phenol	
Anisole*	21.0	13.0	38.5	1.1	44.8	2.6
Anisole/phenol**	1.0	39.5	30.3	0.0	30.5***	-

* Reactants to catalyst mass ratio = 30;
** Anisole : phenol molar ratio = 1, reactant to catalyst mass ratio = 40;
*** Calculated as 1 : 1 molar co-product of methylanisoles;
**** Other are higher products assumed to be dimethylanisoles.

Table 6.14: Cresol distribution for the conversion of anisole and anisole/phenol mixture over H-MCM-22 (UCT) (200°C, reaction time = 5 hours).

Feed	o-Cresol (%)	p-Cresol (%)	m-Cresol (%)	p/o-Cresol ratio
Anisole*	47.3	52.7	0.0	1.11
Anisole/phenol**	61.6	38.4	0.0	0.62

* Reactants to catalyst mass ratio = 30;
** Anisole : phenol molar ratio = 1, reactant to catalyst mass ratio = 40.

changed in favour of the formation of cresols. In terms of the cresol isomer distribution, Table 6.14 shows that in the presence of phenol, p-cresol was less favoured as a product but the p/o-cresol ratio was still significantly higher than the equilibrium ratio of 0.43 as obtained by Böhringer and Fletcher [2003].

6.6.2 Conversion of cresols

Tables 6.15 and 6.16 show the conversion of pure o-cresol and pure p-cresol respectively over the different catalysts. It is important to consider that in all cases the conversions were very low (< 1%).

In the conversion of o-cresol, all catalysts produced xylenols and phenol as the major products. Only in the case of H-MCM-22 (UCT) and H-Mordenite is the formation of p-cresol significant. No m-cresol was formed.

In the conversion of p-cresol, over all the catalysts except for H-USY, xylenols and phenol are the major products with anisole and methylanisoles also formed. Anisole is dominant over H-USY. All the catalysts showed a higher tendency to form o-cresol than that found in the case of p-cresol formation from o-cresol. No m-cresol was formed.

6.7 Alkylation of toluene with methanol

Over H-ZSM-5 and H-MCM-22 (UCT), the methylation of toluene was compared to the methylation of phenol in order to investigate the role of the hydroxyl group compared to a methyl group on

Table 6.15: Conversion and product selectivities to oxygenates in the o-cresol conversion over different catalysts under liquid phase standard reaction conditions (200°C, reaction time = 5 hours, reactant to catalyst mass ratio = 30).

Catalyst	Conversion (%)	Selectivity (mol %)					
		Anisole	p-Cresol *	Methyl-anisoles	Xylenols	Phenol	Other **
H-ZSM-5	0.4	4.6	0.0	0.0	47.7	47.7	0.0
H-Beta	0.5	0.0	0.7	0.0	36.2	54.1	9.0
H-Mordenite	0.6	0.0	10.2	0.0	44.9	44.9	0.0
H-USY	0.3	0.0	0.6	0.0	49.7	49.7	0.0
H-MCM-22 (UCT)	0.9	0.0	22.6	0.0	33.1	40.6	3.7
Silica-alumina	0.4	0.0	0.0	0.0	43.5	52.6	3.9

* No m-cresol was formed;

** Other are higher products assumed to be dimethylanisoles.

Table 6.16: Conversion and product selectivities to oxygenates in the p-cresol conversion over different catalysts under liquid phase standard reaction conditions (200°C, reaction time = 5 hours, reactant to catalyst mass ratio = 30).

Catalyst	Conversion (%)	Selectivity (mol%)					
		Anisole	o-Cresol *	Methyl-anisoles	Xylenols	Phenol	Other
H-ZSM-5	0.4	6.6	17.3	12.4	25.6	38.1	0.0
H-Beta	0.3	13.3	25.1	5.2	25.6	30.8	0.0
H-Mordenite	0.5	0.0	14.4	17.6	25.2	42.8	0.0
H-USY	0.6	50.7	11.2	6.5	12.6	19.0	0.0
H-MCM-22 (UCT)	0.6	0.6	25.8	1.8	35.0	36.8	0.0
Silica-alumina	0.2	7.5	31.4	0.0	30.6	30.5	0.0

* No m-cresol was formed;

Table 6.17: Conversion and product selectivities obtained from alkylation of toluene with methanol over H-ZSM-5 and H-MCM-22 (UCT) (liquid phase standard reaction conditions: 200°C, methanol : toluene molar ratio = 1, reaction time = 5 hours, reactants to catalyst mass ratio = 39.4).

Zeolite	Toluene conversion (%)	Selectivity (mol%)				Methanol* conversion (%)
		Xylenes	Benzene	Ethyl-benzene	Trimethyl-benzenes	
H-ZSM-5	0.2	36.2	34.4	9.2	20.2	0.1
H-MCM-22 (UCT)	0.1	40.9	49.1	0.0	10.0	0.01

* Methanol conversion to alkylbenzenes calculated from side-chain balance.

Table 6.18: Xylene and cresol isomer distributions obtained from methylation of toluene and phenol, respectively (liquid phase standard reaction conditions: 200°C, methanol : toluene or phenol molar ratio = 1, reaction time = 5 hours, reactants to catalyst mass ratio = 39.4).

Zeolite	o-Xylene (%)	p-Xylene (%)	m-Xylene (%)	p/o-Xylene ratio
H-ZSM-5	39.4	24.0	36.6	0.61
H-MCM-22 (UCT)	33.5	29.6	36.9	0.88
Thermodynamic equilibrium*	21	24	55	1.1
	o-Cresol (%)	p-Cresol (%)	m-Cresol (%)	p/o-Cresol ratio
H-ZSM-5	72.6	27.4	0.0	0.38
H-MCM-22 (UCT)	45.5	54.5	0.0	1.20
Thermodynamic equilibrium**	37	16	47	ca. 0.43

* Thermodynamic equilibrium calculated from data from Stull *et al.* [1969];

** Preliminary data of Böhringer and Fletcher [2003] at 350°C. Note that the effect of reaction temperature on cresol isomer distribution is minor, cf. Section 2.2.2.6.

the benzene ring. The alkylation of toluene with methanol was carried out under the liquid phase standard reaction conditions (cf. Table 6.1).

Table 6.17 shows the results of the toluene alkylation over H-ZSM-5 and H-MCM-22 (UCT) in terms of toluene conversion and product selectivities. Toluene conversion was < 1% in both cases studied, whereas, phenol conversion was 9.7 and 5.7%, respectively under identical conditions (cf. Table 6.4). The major products formed from toluene methylation were xylenes, benzene and trimethylbenzenes. Methanol conversion by alkylation was significantly lower than toluene conversion (as calculated via side-chain balance).

In terms of the distribution of the xylene isomers (cf. Table 6.18), H-MCM-22 (UCT) produced a higher p- and lower o-selectivity than H-ZSM-5. The xylene isomer distribution differs substantially from the cresol isomer distribution obtained by phenol methylation in terms of a high m-isomer content and lower o-isomer content. However, H-MCM-22 (UCT) produced higher p/o-ratios than H-ZSM-5 with both the reaction systems under these reaction conditions.

6.8 Summary

The key results from the study of liquid phase alkylation of phenol with methanol are:

Reproducibility

- Experimental results were reproducible with minor scatter;

Material balances

- Material balances, based on the aromatic nuclei, were very good;

Influence of conversion on selectivity

- Product selectivities, measured at 200°C, were essentially independent of phenol conversion for all the catalysts i.e. reaction time and reactants to catalyst ratio only influenced conversion, not selectivity;

Comparison of the catalyst studied

- Catalysts studied exhibited very different activities with respect to phenol conversion, corresponding to the following order: H-ZSM-5 > H-MCM-22 (DE2) $\approx$ H-Beta $\approx$ H-Mordenite >> H-MCM-22 (UCT) >> H-USY >> amorphous silica-alumina. Activity differed by a factor of 7 between the zeolites. Amorphous silica-alumina showed comparably minor activity;

- Anisole, o-cresol and p-cresols were the major products formed at 200°C and conversions less than 10%;

- The major by-products at 200°C and conversions less than 10% were methylanisoles. No xylenols were obtained under these conditions;

- No m-cresol is formed over any of the catalysts at 200°C and conversions less than 10%;

- H-ZSM-5 and H-Mordenite produced the highest cresol selectivities;

- H-MCM-22 (UCT) produced the highest p/o-cresol ratio;

- Test reactions, 1,3,5-TIPB and n-hexane cracking, showed that over internally selectively sodium-exchanged zeolites (ZSM-5 and MCM-22 (UCT)), the total activity was much more affected than the activity of the external/mesoporous surface indicating that the sodium-exchange was essentially internal;

- Internally selectively sodium-exchanged H/Na-ZSM-5 and H/Na-MCM-22 (UCT) zeolites, in which the internal acidity of the crystals is essentially inertized, showed a lower activity and a lower p/o-cresol ratio than the non-modified, acid samples;

Effect of reaction parameters

- Effect of reaction temperature
  - Increasing reaction temperature increased phenol conversion, as expected;
  - Over H-ZSM-5 and H-Beta, increasing reaction temperature decreased the anisole selectivity and increased the cresols selectivity;
  - Over H-MCM-22 (UCT), increasing reaction temperature had no effect on the product selectivities;
  - The p/o-cresol ratio over the different zeolites hardly changed with increasing reaction temperature;
- Effect of methanol : phenol ratio
  - The effect of the methanol : phenol ratio on conversion was inconsistent with the four catalyst samples studied, namely H-ZSM-5, H-Beta, H-MCM-22 (UCT) and amorphous silica-alumina;
  - Increasing the methanol : phenol ratio, resulted in anisole preferentially forming and the cresol selectivity declining. Minor inconsistency was observed over H-ZSM-5 where the common trend appears at ratios < 1;
  - Increasing the methanol : phenol ratio over H-ZSM-5, H-Beta and amorphous silica-alumina, had a minor effect on the p/o-cresol ratio which was close to the thermodynamic equilibrium as determined by Böhringer and Fletcher [2003];
  - Increasing the methanol : phenol ratio increased the p/o-cresol ratio over H-MCM-22 (UCT) to almost double the equilibrium content in a p/o-mixture;
- Effect of the addition of water
  - Addition of an equimolar amount of water to the reactants decreased the conversion i.e. activity of the catalysts, significantly;
  - Addition of an equimolar amount of water has less and inconsistent influence on selectivities;

Conversion of major products of phenol methylation

- Anisole converted readily over the catalysts to methylanisoles, phenol and cresols;
- In presence of phenol in equimolar amounts, anisole does not react under the reaction conditions applied (200°C);
- Cresols do not readily react over the catalysts under the reaction conditions applied (200°C);

Alkylation of toluene with methanol compared to phenol alkylation with methanol

- The reactivity of toluene with methanol was poor compared to phenol;
- H-MCM-22 (UCT) produced a higher p/o-ratio than H-ZSM-5 with both reaction systems;
- Meta-isomer formation was significant, i.e. greater when the methyl substituent was present (toluene) than when the hydroxyl substituent was present (phenol).

Chapter 7

Gas phase alkylation of phenol with methanol

This chapter presents the results obtained in the gas phase alkylation of phenol with methanol over zeolites H-ZSM-5, H-MCM-22 (UCT), H-MCM-22 (DE1), H-MCM-22 (DE2), H-MCM-22 (DE3) and amorphous silica-alumina. It begins with the examination of the reproducibility of experiments and verification of material balances in the system used. This is followed by an investigation into the relationship between phenol conversion, product selectivities, cresol isomer distribution as well as deactivation with time-on-stream over all the catalysts. All the catalysts are then compared at the same reaction conditions. This section includes phenol conversion over internally selectively sodium-exchanged ZSM-5 and MCM-22 (UCT) as well as steamed H-MCM-22 (DE1). The effects of reaction temperature, methanol : phenol ratio, weight hourly space velocity and the reactants partial pressure are examined. The conversion of the major primary products, namely anisole, o-cresol and p-cresol, over H-MCM-22 (UCT) is examined, also the conversion of m-cresol and an anisole/phenol mixture. In all cases the comparison is done according to the conversion of the aromatic reactant, product selectivity, O-alkylation versus C-alkylation and cresol isomer distribution with special regard to the p/o-cresol ratio. Finally, the isomer distribution obtained in the methylation of toluene with methanol over H-ZSM-5 and H-MCM-22 (UCT) are compared with those obtained from phenol methylation. The chapter closes with a summary of all the key results. Reaction conditions and reaction data for the gas phase phenol methylation with methanol are given in Appendix E.

7.1 Gas phase standard reaction conditions

A standard reaction condition was defined and applied to most of the experiments in the gas phase and also taken as the base case for parameter variation studies. These gas phase standard reaction conditions are given in Table 7.1.

Table 7.1: Gas phase standard reaction conditions applied.

Reaction temperature	300°C
Total reaction pressure	1 bar
Reactants partial pressure	0.2 bar
Methanol : phenol molar ratio	1
$WHSV_{reactants}$	14 $g_{(phenol+methanol)}/(g_{catalyst} \cdot h)$
Carrier gas	Nitrogen

7.2 Experimental reproducibility and material balance

7.2.1 Experimental reproducibility

The reproducibility of experiments in the gas phase reaction system was carried out under the gas phase standard reaction conditions (Table 7.1) over H-MCM-22 (UCT). Results are given in Figure 7.1. The criteria used to evaluate reproducibility are:

- phenol conversion;
- selectivity to anisole;
- selectivity to cresols and the isomers distribution;
- selectivity to other products, namely xylenols and methylanisoles.

The system showed equivalent reproducibility characteristics for the methylation of phenol in the gas phase.

7.2.2 Material balance

Appendix A shows a typical GC trace obtained in the gas phase phenol methylation with methanol. Material balances are calculated on a carbon mole balance including methanol and light by-products. Carbon balances were found to fall between 95 and 100% in all the cases studied, cf., for instance, Figures 7.9, 7.11 and 7.13. A model calculation of a material balance is shown in Appendix D.

7.2.3 Considering catalyst deactivation

Since catalysts deactivated with time-on-stream, fresh catalyst was applied for each and every set of reaction conditions. Experiments continued until a quasi-steady state was reached or up to 10 hours, respectively. Results from catalyst comparison are given as a function of time-on-stream. Results from parameter variation compare averaged data obtained in the quasi-steady state.

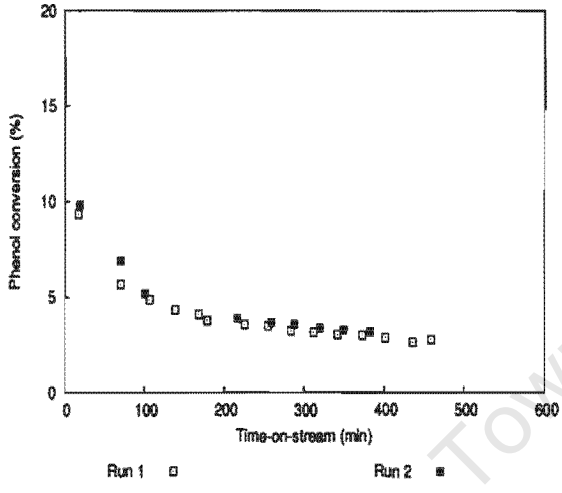

(a) Phenol conversion

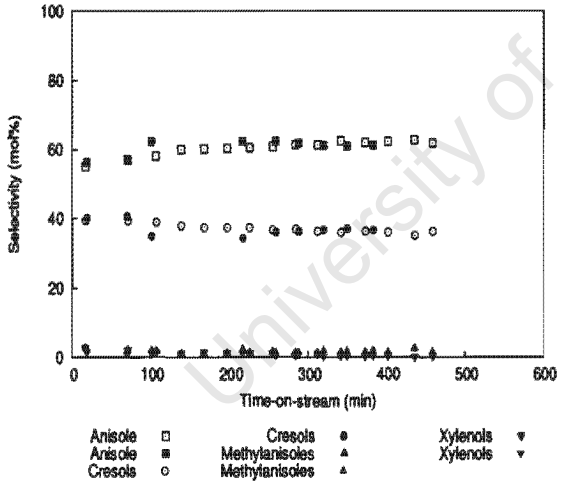

(b) Product selectivity

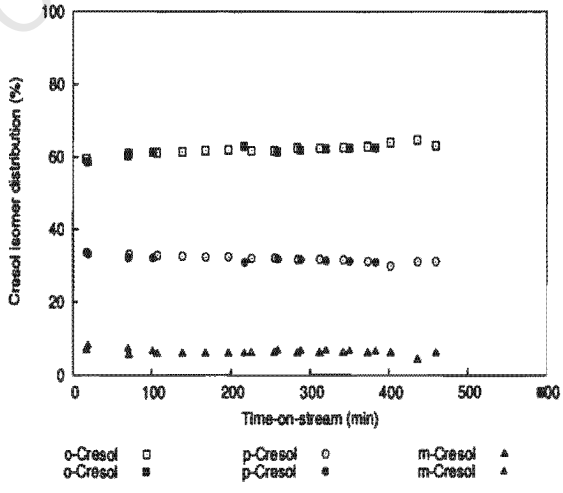

(c) Cresol isomer distribution

Figure 7.1: The reproducibility of results from the gas phase reaction system (catalyst H-MCM-22 (UCT), open symbols run 1; closed symbols run 2; gas phase standard reaction conditions: 300°C, total pressure = 1 bar, reactants partial pressure = 0.2 bar, methanol : phenol molar ratio = 1, WHSV = 14 h^{-1}).

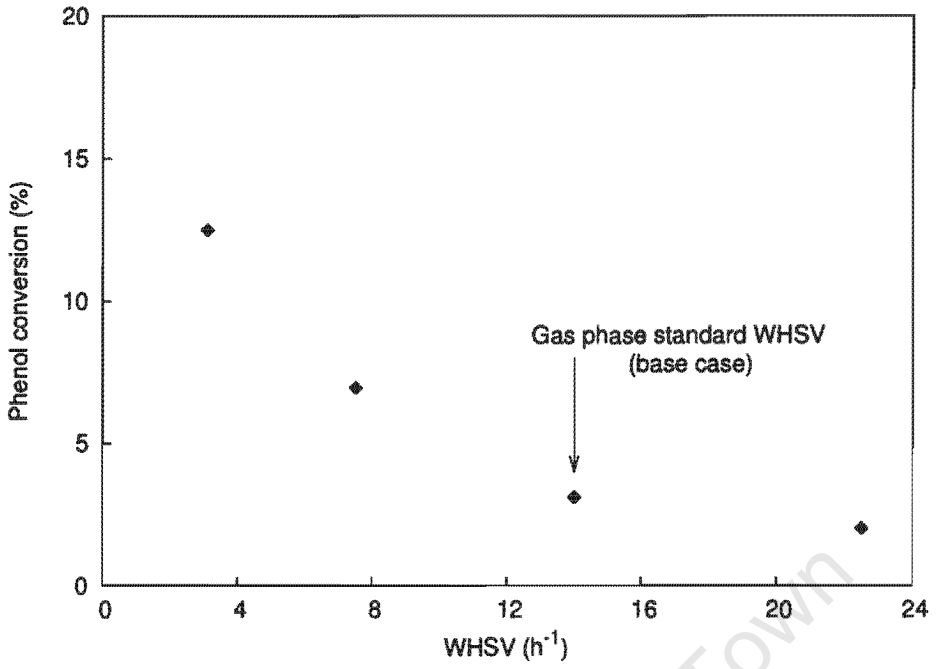

Figure 7.2: The effect of weight hourly space velocity on phenol conversion over H-MCM-22 (UCT). Data points represent quasi-steady state averages (gas phase standard reaction conditions: 300°C, total pressure = 1 bar, reactants partial pressure = 0.2 bar, methanol : phenol molar ratio = 1, varying weight hourly space velocity).

7.3 Relationship between phenol conversion, catalyst deactivation and product selectivity

As different catalysts were studied at different activities, the effect, which phenol conversion has on product selectivity, first needed to be evaluated in order to allow a valid comparison of the different catalysts. This is particularly important since catalysts should only be compared at constant conversions.

7.3.1 Relationship between phenol conversion and selectivity

Phenol conversion was varied via varying weight hourly space velocity (Figure 7.2) and comparisons were made at constant activity level of the catalysts, i.e. in quasi-steady state. Figure 7.3 shows the relationship of phenol conversion and product selectivity. As can be seen from Figure 7.3, phenol conversion did effect the product selectivities slightly. The selectivity to cresols decreased and the selectivity to anisole increased moderately as conversion was increased. The cresol isomer distribution changed as well. The percentage o-cresol declined moderately with increasing conversion, whereas both the percentages of p- and m-cresol increased correspondingly.

7.3.2 Relationship between catalyst deactivation and selectivity

Reactions were carried out under the gas phase standard reaction conditions (cf. Table 7.1). Figure 7.4 shows that phenol conversion declines with time-on-stream over all the catalysts investigated.

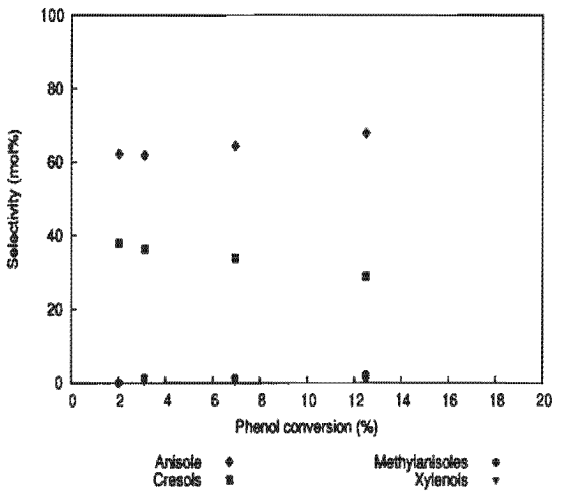

(a) Product selectivity

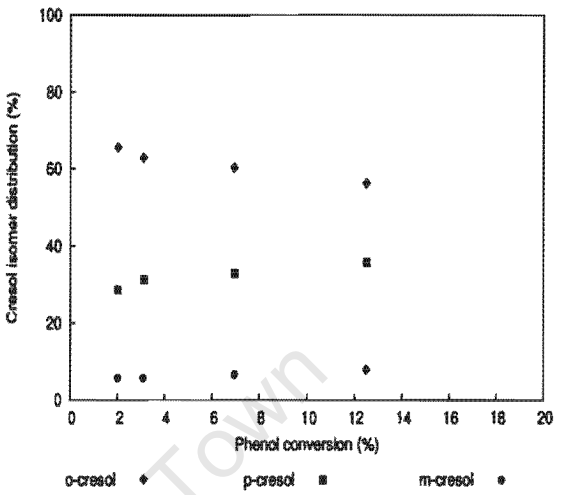

(b) Cresol isomer distribution

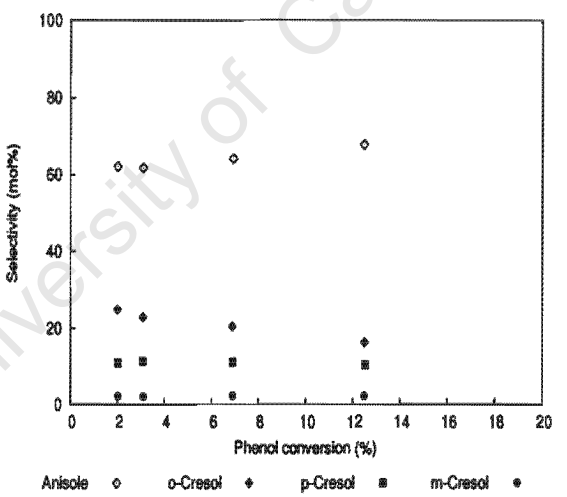

(c) Product selectivity

Figure 7.3: The relationship between phenol conversion, varied through varying weight hourly space velocity, and product selectivity as well as cresol isomer distribution over H-MCM-22 (UCT). Data points represent quasi-steady state averages (gas phase standard reaction conditions: 300°C, total pressure = 1 bar, reactants partial pressure = 0.2 bar, methanol : phenol molar ratio = 1).

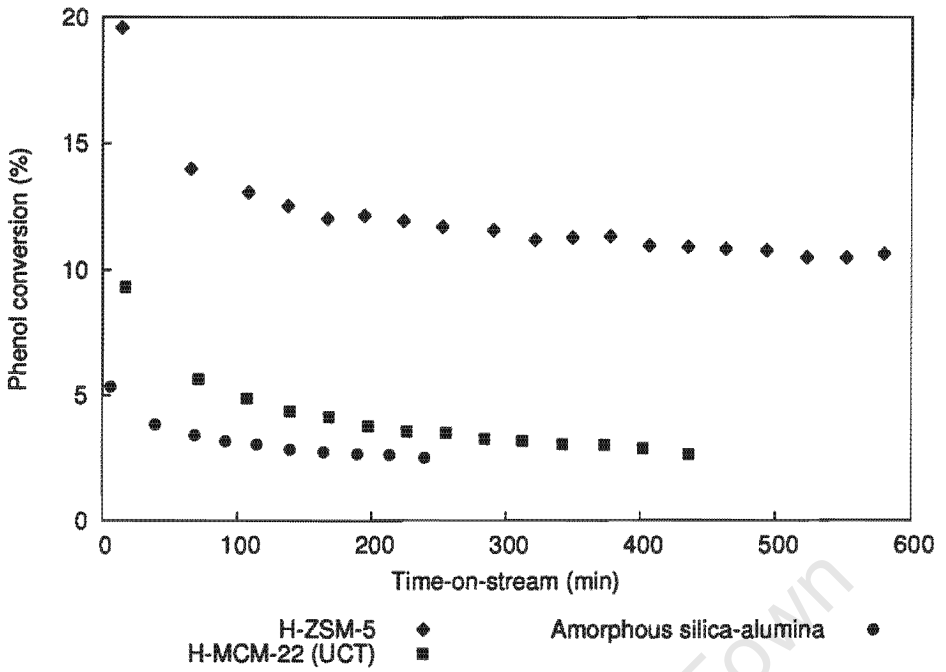

Figure 7.4: Phenol conversion versus time-on-stream obtained over H-ZSM-5, H-MCM-22 (UCT) and amorphous silica-alumina at gas phase standard reaction conditions (300°C, total pressure = 1 bar, reactants partial pressure = 0.2 bar, methanol : phenol molar ratio = 1, WHSV = 14 h^{-1}).

The relationship between catalyst deactivation and selectivities is shown in Figure 7.5 for the zeolites H-ZSM-5, H-MCM-22 (UCT) and amorphous silica-alumina. For H-ZSM-5 and H-MCM-22 (UCT), there was a noticeable change in product selectivities with deactivation-induced decline of phenol conversion (Figures 7.5 (a) and (b)). The selectivity to cresols decreased and the selectivity to anisole increased as deactivation proceeded, i.e. as the conversion decreased. Note the opposite trends of cresol and anisole selectivities with conversion, dependent on whether conversion was changed through deactivation/coking or was changed via varying space velocity (Figure 7.5 (b)) Product selectivities over silica-alumina were found to be hardly influenced by deactivation i.e. almost independent of phenol conversion at these reaction conditions and at the low conversions studied.

Figure 7.6 shows the relationship between deactivation and the cresol isomer distribution for the three catalysts. For H-ZSM-5 and H-MCM-22 (UCT) there was a slight but inconsistent influence of increasing catalyst deactivation, i.e. decreasing phenol conversion on the cresol isomer distribution. Over silica-alumina the cresol isomer distribution was found to be essentially uninfluenced by deactivation. There is no difference to space-velocity-induced changes to conversion in the cresol isomer distribution (Figure 7.6 (b)).

7.3.3 Effect of reaction parameters compared at different conversions

As seen in Section 7.3.1, conversion does influence the product selectivities. When studying the effect of catalyst deactivation (Section 7.3.2) as well as in the parameter variation section (Section 7.5), comparisons are made at different conversions. However, the effect which space velocity (Section 7.3.1) has on product selectivity is attributed to the change in conversion. Therefore, comparing

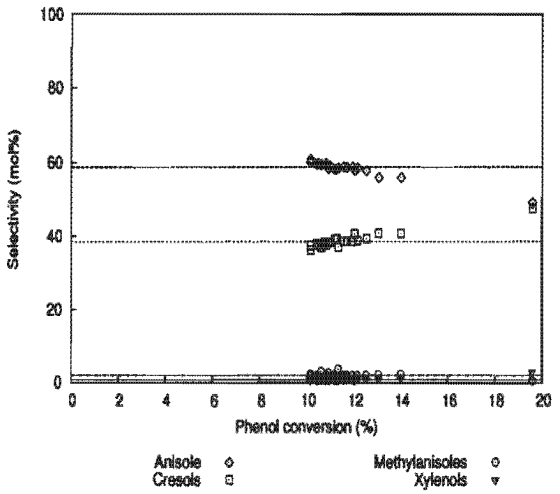

(a) H-ZSM-5

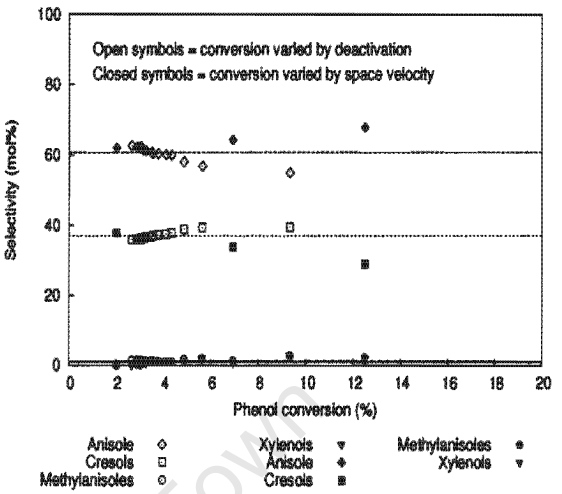

(b) H-MCM-22 (UCT)

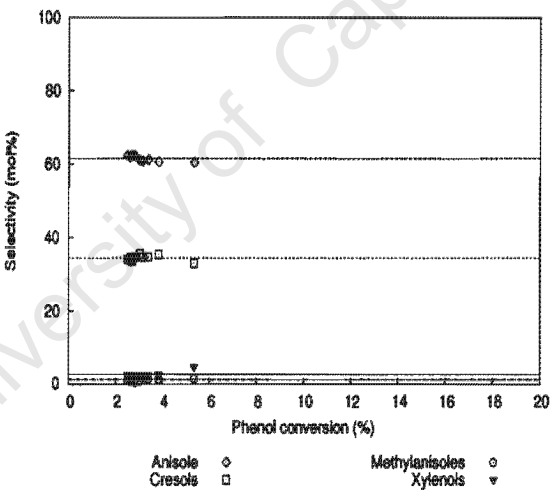

(c) Silica-alumina

Figure 7.5: Product selectivities versus phenol conversion at gas phase standard reaction conditions. Phenol conversion varied as a result of deactivation with time-on-stream (open symbols) or was varied by varying weight hourly space velocity with data points representing the average of quasi-steady state samples (closed symbols in figure (b)) (300°C, total pressure = 1 bar, reactants partial pressure = 0.2 bar, methanol : phenol molar ratio = 1, WHSV = 14 h^{-1} for deactivation studies). Horizontal lines indicate the average of data points (open symbols).

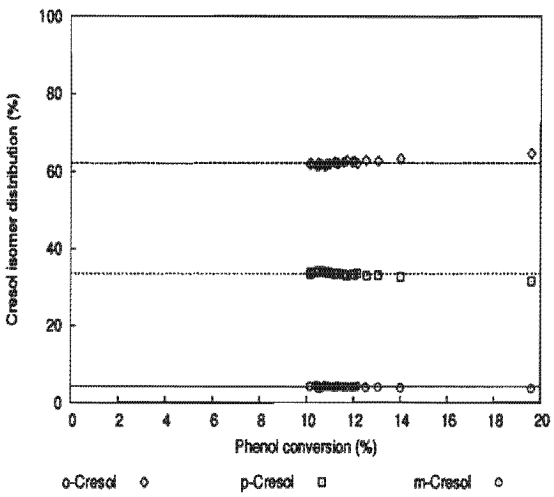

(a) H-ZSM-5

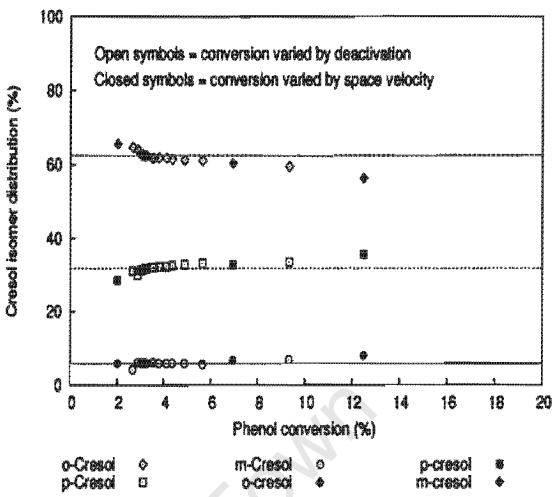

(b) H-MCM-22 (UCT)

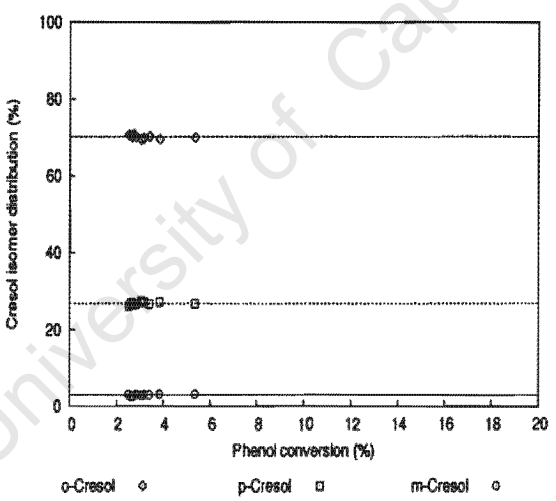

(c) Silica-alumina

Figure 7.6: Cresol isomer distribution versus phenol conversion at gas phase standard reaction conditions. Phenol conversion varied as a result of deactivation with time-on-stream (open symbols) or was varied by varying weight hourly space velocity with data points representing the average of quasi-steady state samples (closed symbols in figure (b)) (300°C, total pressure = 1 bar, reactants partial pressure = 0.2 bar, methanol : phenol molar ratio = 1, WHSV = 14 h^{-1}) for deactivation studies). Horizontal lines indicate the average of data points (open points).

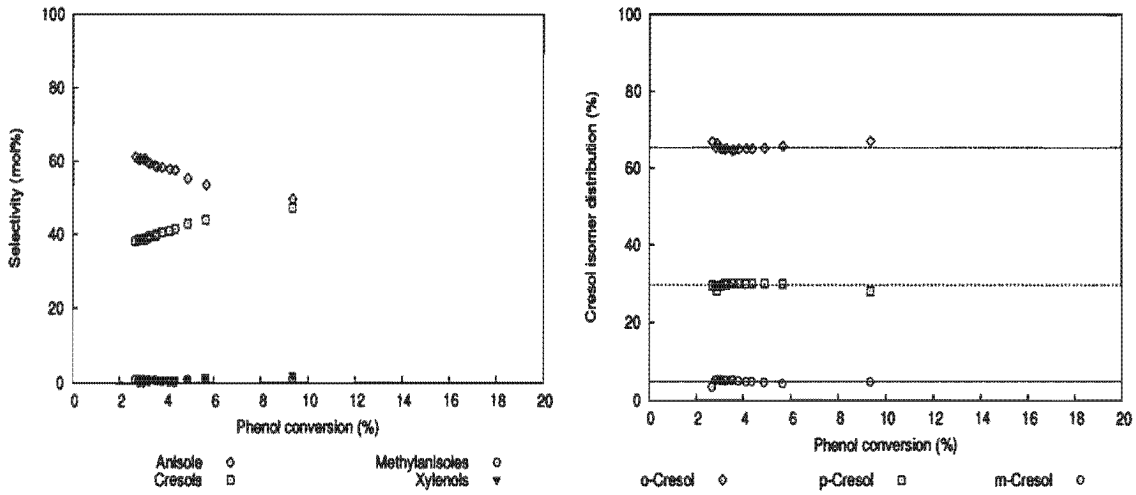

(a) Product selectivity

(b) Cresol isomer distribution

Figure 7.7: The true effect of deactivation on product selectivity and cresol isomer distribution over H-MCM-22 (UCT) derived from Figures 7.5 (b) and 7.6 (b) (gas phase standard reaction conditions: 300°C, total pressure = 1 bar, reactants partial pressure = 0.2 bar, methanol : phenol molar ratio = 1, WHSV = 14 h^{-1}). The horizontal lines indicate the average of data points.

the effect of deactivation and reaction parameter variation with that of space velocity allows the determination of any effect of the parameter on the product selectivity in the absence of the effect of conversion (cf. Figures 7.5 (b) and 7.6(b)). In the case where there is a clear effect of a reaction parameter on the product selectivity, the conversion effect is eliminated by subtracting the conversion, i.e. space velocity effect from the total effect thereby obtaining an at least semi-quantitative effect of the reaction parameter only. This is demonstrated in determining the true effect of deactivation on product selectivity and cresol isomer distribution (Figure 7.7). Figure 7.7 (a) clearly shows that anisole selectivity increased and cresol selectivity decreased as deactivation proceeded. Deactivation hardly effects the cresol isomer distribution (Figures 7.7 (b) and 7.8).

7.4 Comparison of different acid zeolite catalysts and amorphous silica-alumina

7.4.1 Reactions over different H-zeolites and amorphous silica-alumina

The activities and selectivities of zeolites H-ZSM-5, H-MCM-22 (UCT) and amorphous silica-alumina were compared at the gas phase standard reaction conditions (cf. Table 7.1). The catalysts were compared in terms of phenol conversion, product selectivities and cresol isomer distributions.

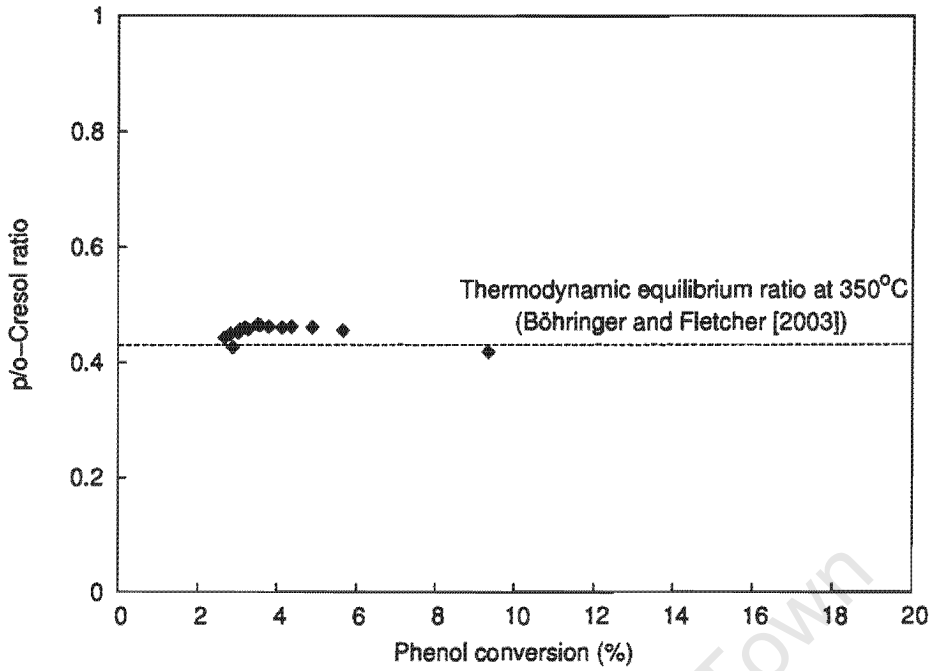

Figure 7.8: The true effect of deactivation on p/o-cresol ratio under gas phase standard reaction conditions (300°C, total pressure = 1 bar, reactants partial pressure = 0.2 bar, methanol : phenol molar ratio = 1, WHSV = 14 h^{-1}). The horizontal line represents thermodynamic equilibrium as obtained by Böhringer and Fletcher [2003] at 350°C.

7.4.1.1 H-ZSM-5

Figures 7.9 and 7.10 show the carbon mass balance, phenol conversion, product selectivity and cresol isomer distribution over zeolite H-ZSM-5 as a function of time-on-stream at the gas phase standard reaction conditions (cf. Table 7.1). The carbon balance is very close to 100%, which means that neither coke or high boiling components nor non-detectable carbon containing compounds were formed. The phenol conversion decreased with time-on-stream, levelling off at approximately 10% with a product distribution of mainly anisole (ca. 59 mol%) and cresols (ca. 38 mol%) and minor amounts of methylanisoles (ca. 2 mol%) and xylenols (ca. 1%) (Figure 7.10 (a)). The product selectivity profile hardly changed with time-on stream but a slight increase in anisole selectivity at the expense of cresol selectivity is obvious. In terms of cresol isomer distribution, an almost constant o-cresol : p-cresol : m-cresol ratio of 62 : 34 : 4 was obtained. This corresponds to an initial p/o-cresol ratio of 0.5 and a ratio of 0.55 in the quasi-steady state (Figure 7.15), which is above the thermodynamic equilibrium of ca. 0.43 as obtained by Böhringer and Fletcher [2003] at 350°C but close to the statistical ratio of 0.5. Note that some m-cresol was formed over H-ZSM-5 at 300°C (Figure 7.10 (b)).

7.4.1.2 H-MCM-22 (UCT)

Figures 7.11 and 7.12 show the carbon mass balance, phenol conversion, product selectivities and cresol isomer distribution produced over H-MCM-22 (UCT) as a function of time-on-stream under the gas phase standard reaction conditions (cf. Table 7.1). From Figure 7.11 it can be seen that the conversion decreases rapidly initially, steeper than with H-ZSM-5 (cf. Figure 7.9) and then starts

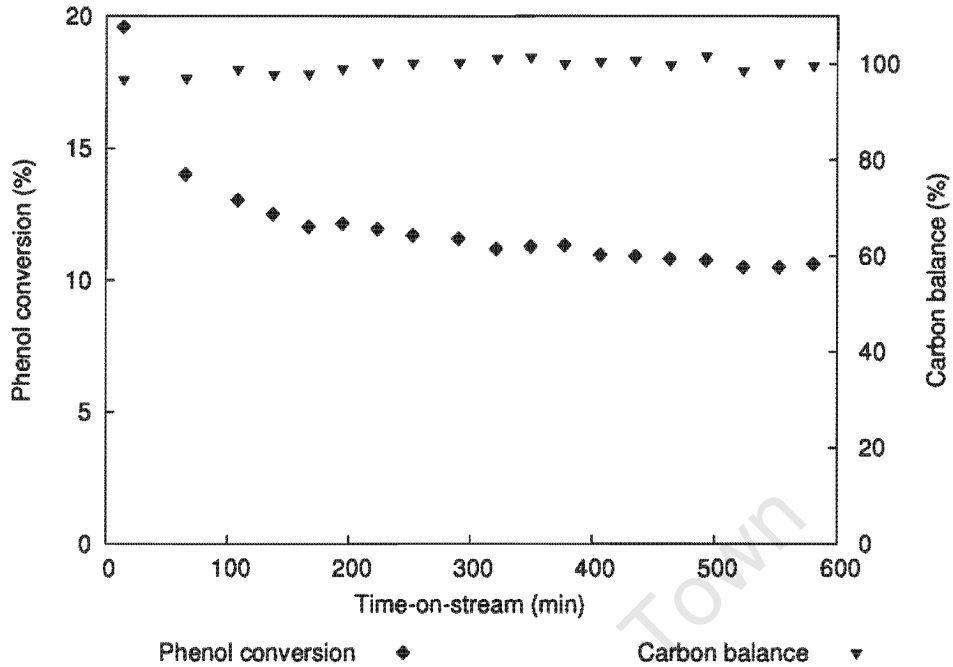

Figure 7.9: Phenol conversion and carbon balance obtained over H-ZSM-5 at gas phase standard reaction conditions (300°C, total pressure = 1 bar, reactants partial pressure = 0.2 bar, methanol : phenol molar ratio = 1, WHSV = 14 h^{-1}).

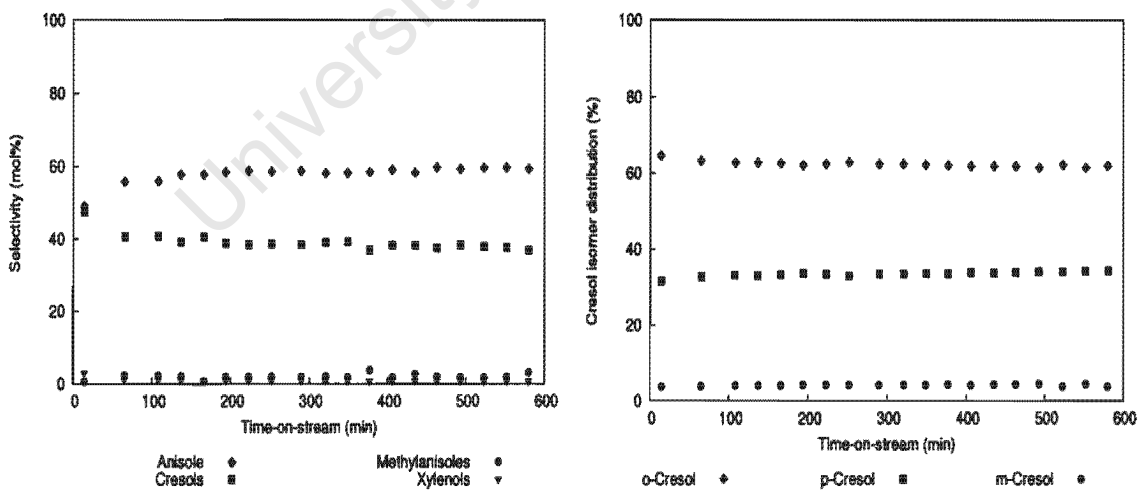

(a) Product selectivity

(b) Cresol isomer distribution

Figure 7.10: Product selectivity and cresol isomer distribution obtained over H-ZSM-5 at gas phase standard reaction conditions (300°C, total pressure = 1 bar, reactants partial pressure = 0.2 bar, methanol : phenol molar ratio = 1, WHSV = 14 h^{-1}).

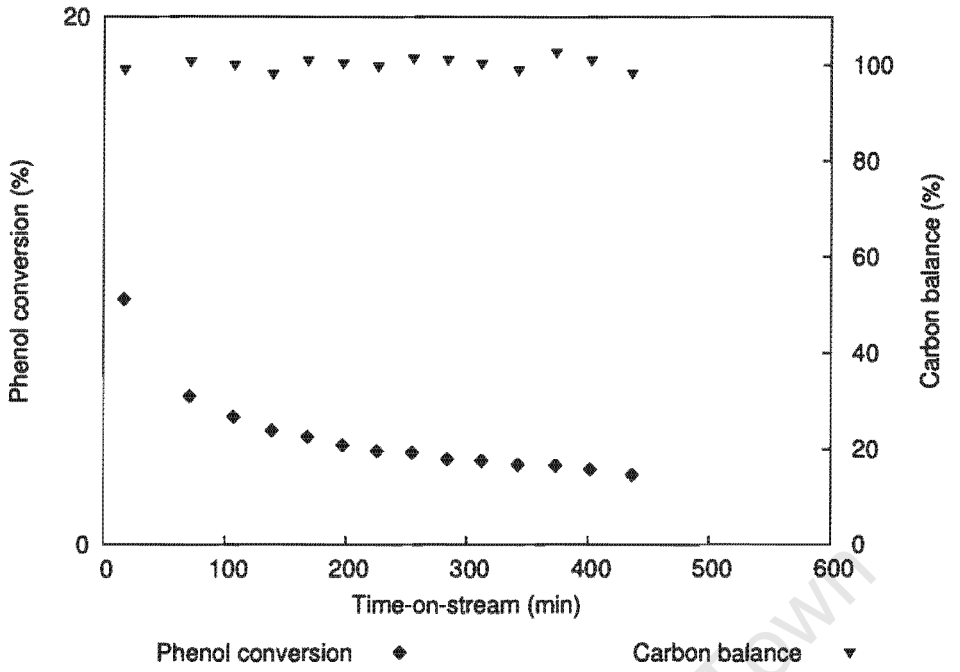

Figure 7.11: Phenol conversion and carbon balance obtained over H-MCM-22 (UCT) at gas phase standard reaction conditions (300°C, total pressure = 1 bar, reactants partial pressure = 0.2 bar, methanol : phenol molar ratio = 1, WHSV = 14 h^{-1}).

levelling out at a steady state value below 4 %. The initial activity is higher than that of H-ZSM-5 but the quasi-steady state activity is lower than with H-ZSM-5. For H-MCM-22 (UCT), anisole and cresols are the dominant products formed (Figure 7.12 (a)), with anisole having the highest selectivity (ca. 62 mol%). As with H-ZSM-5 the selectivity to anisole increases slightly with time-on-stream at the expense of cresol selectivity. The cresol isomer distribution (Figure 7.12 (b)) shows that o-cresol (ca. 63 mol%) is the dominant isomer formed. The p/o-cresol ratio in the quasi-steady state was 0.50, which is slightly lower than that obtained over H-ZSM-5 but still above equilibrium and corresponds to the statistical p/o-ratio. Some m-cresol (6% of the cresol fraction) was also produced over H-MCM-22 (UCT) under these reaction conditions (Figure 7.12 (b)). The cresol distribution is practically invariant.

7.4.1.3 Silica-alumina

Figures 7.13 and 7.14 show the carbon mass balance, phenol conversion, product selectivity and cresol isomer distribution produced over amorphous silica-alumina as a function of time-on-stream at the gas phase standard reaction conditions (cf. Table 7.1). Silica-alumina showed similar behaviour to H-MCM-22 (UCT) and H-ZSM-5 in terms of a decreasing phenol conversion with time-on-stream (Figure 7.13). However, the initial decrease appears less and correspondingly the product selectivity and cresol isomer distribution were found to be almost constant with time-on-stream. Phenol conversion was approximately 2.5% and the product selectivity was ca. 62 mol% anisole, ca. 34 mol% cresols, ca. 1 mol% methylanisoles and ca. 3 mol% xylenols. The cresol isomer distribution of o : p : m-cresol was 71 : 26 : 3 with a p/o-cresol ratio of approximately 0.37 (Figure 7.15). This p/o-cresol ratio is much lower than that obtained over zeolites H-ZSM-5 and H-MCM-22 (UCT) and even below the

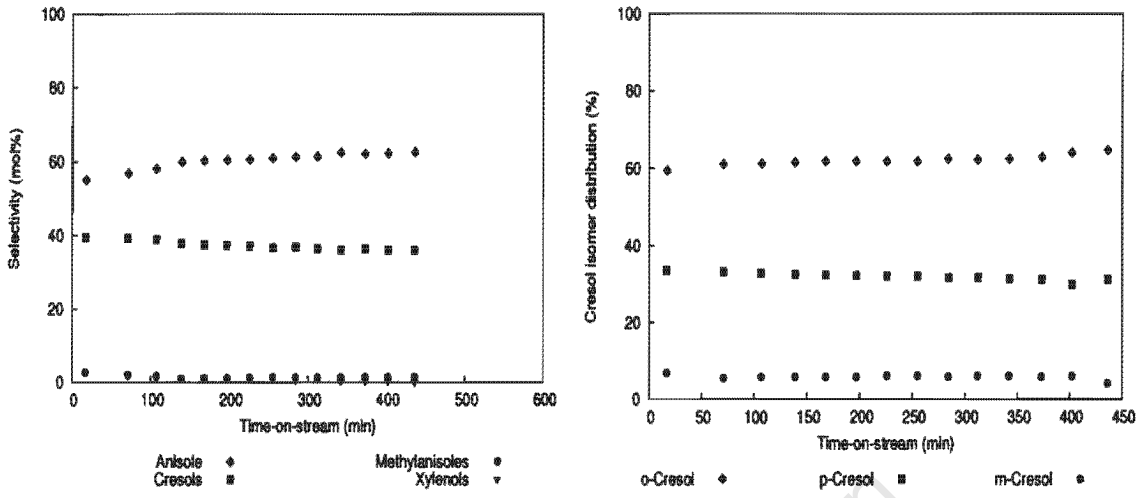

(a) Product selectivity

(b) Cresol isomer distribution

Figure 7.12: Product selectivity and cresol isomer distribution obtained over H-MCM-22 (UCT) at gas phase standard reaction conditions (300°C, total pressure = 1 bar, reactants partial pressure = 0.2 bar, methanol : phenol molar ratio = 1, WHSV = 14 h^{-1}).

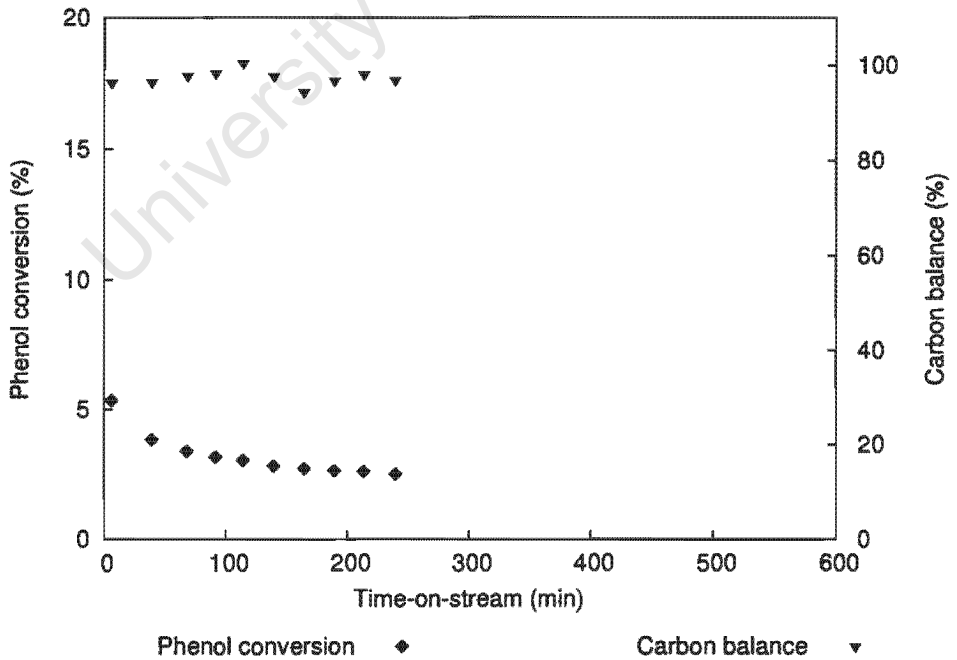

Figure 7.13: Phenol conversion and carbon balance obtained over silica-alumina at gas phase standard reaction conditions (300°C, total pressure = 1 bar, reactants partial pressure = 0.2 bar, methanol : phenol molar ratio = 1, WHSV = 14 h^{-1}).

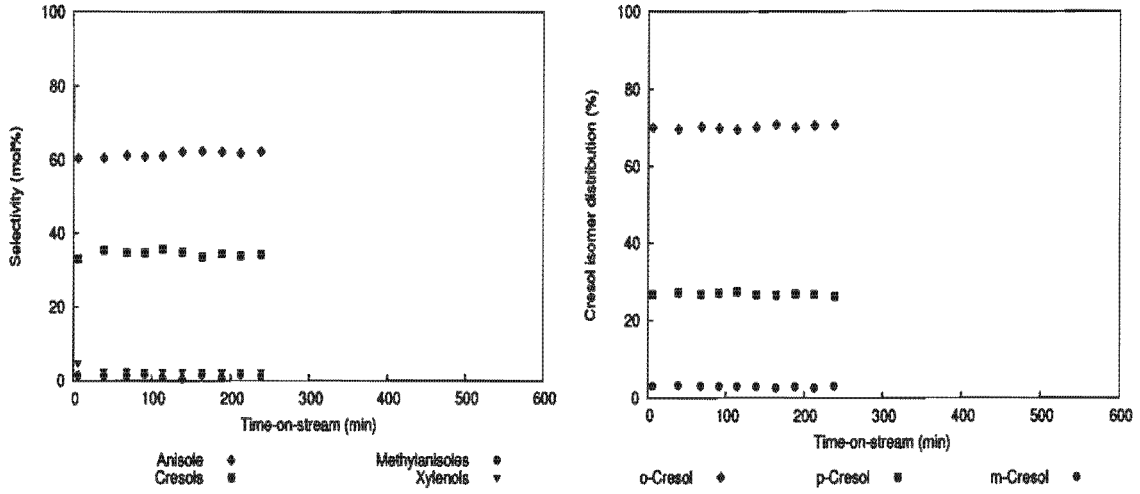

(a) Product selectivity

(b) Cresol isomer distribution

Figure 7.14: Product selectivity and cresol isomer distribution obtained over silica-alumina at gas phase standard reaction conditions (300°C, total pressure = 1 bar, reactants partial pressure = 0.2 bar, methanol : phenol molar ratio = 1, WHSV = 14 h^{-1}).

thermodynamic equilibrium of ca. 0.43 as obtained by Böhringer and Fletcher [2003] at 350°C.

7.4.1.4 Summary of results obtained from the different catalysts

Figure 7.4 shows that over H-ZSM-5, H-MCM-22 (UCT) and amorphous silica-alumina, phenol conversion decreased with time-on-stream. The quasi-steady state activity decreased from H-ZSM-5 > H-MCM-22 (UCT) > silica-alumina. Anisole was the preferred product, as obtained over these catalysts in the liquid phase (cf. Section 6.4.1). Figure 7.15 summarises the p/o-cresol ratios obtained over the different catalysts. H-ZSM-5 and H-MCM-22 have similar p/o-cresol ratio around 0.5 whereas silica-alumina has a lower p/o-cresol ratio of 0.37.

7.4.2 Comparison of the different H-MCM-22 samples

Samples H-MCM-22 (DE1), H-MCM-22 (DE2), H-MCM-22 (DE3) synthesised at the University of Delaware were compared with H-MCM-22 (UCT) in terms of phenol conversion, product selectivity, cresol isomer distribution and p/o-cresol ratio (at gas phase standard reaction conditions) as shown in Figures 7.16 to 7.19, respectively. The results of the physico-chemical characterization of all these catalysts have been described in Chapter 5. With phenol methylation, H-MCM-22 samples consistently show a more pronounced initial decline of activity than the other catalysts. H-MCM-22 (DE2) was the most active H-MCM-22 sample in terms of phenol conversion (Figure 7.16). It is interesting to note that H-MCM-22 (DE1) was the only catalyst of the series and in fact over all the catalysts studied in the gas phase to favour the formation of cresols over that of anisole (Figure 7.17 (a) compared to Figures 7.17 (b) - (d), 7.10 (a) and 7.14 (a)). In terms of cresol isomer distribution there were minor changes with time-on-stream over all the H-MCM-22 samples. At quasi-steady state

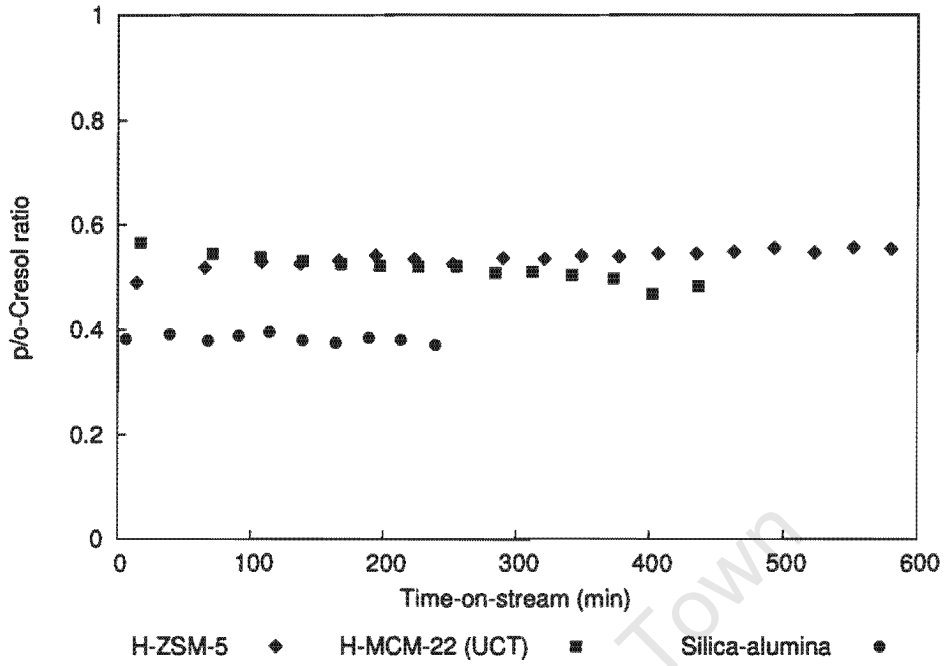

Figure 7.15: Comparison of the p/o-cresol ratio obtained over H-ZSM-5, H-MCM-22 (UCT) and silica-alumina at standard gas phase reaction conditions (300°C, total pressure = 1 bar, reactants partial pressure = 0.2 bar, methanol : phenol molar ratio = 1, WHSV = 14 h^{-1}).

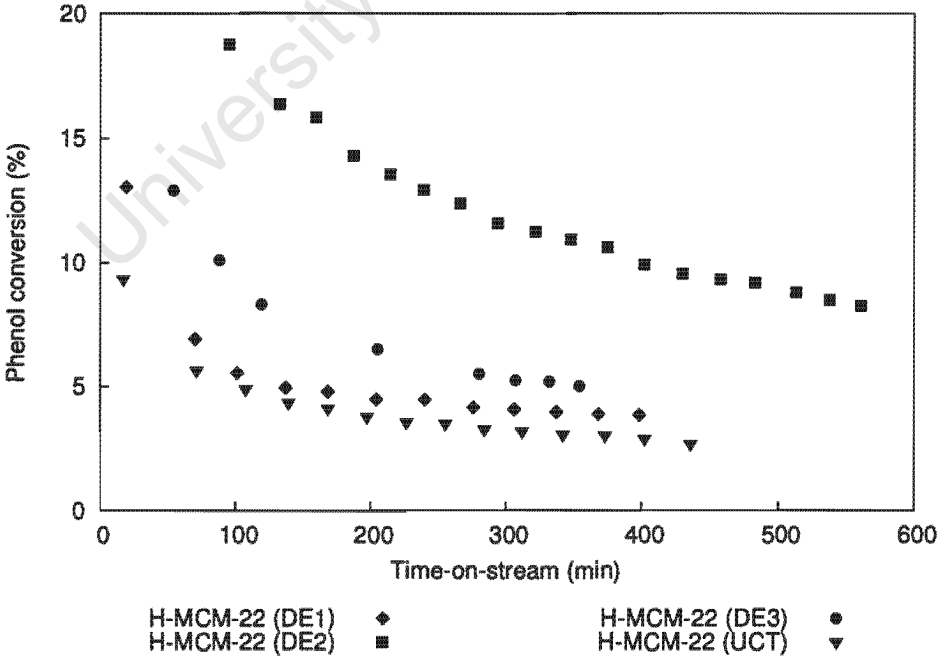

Figure 7.16: The effect of using different H-MCM-22 samples on phenol conversion at gas phase standard reaction conditions (300°C, total pressure = 1 bar, reactants partial pressure = 0.2 bar, methanol : phenol molar ratio = 1, WHSV = 14 h^{-1}).

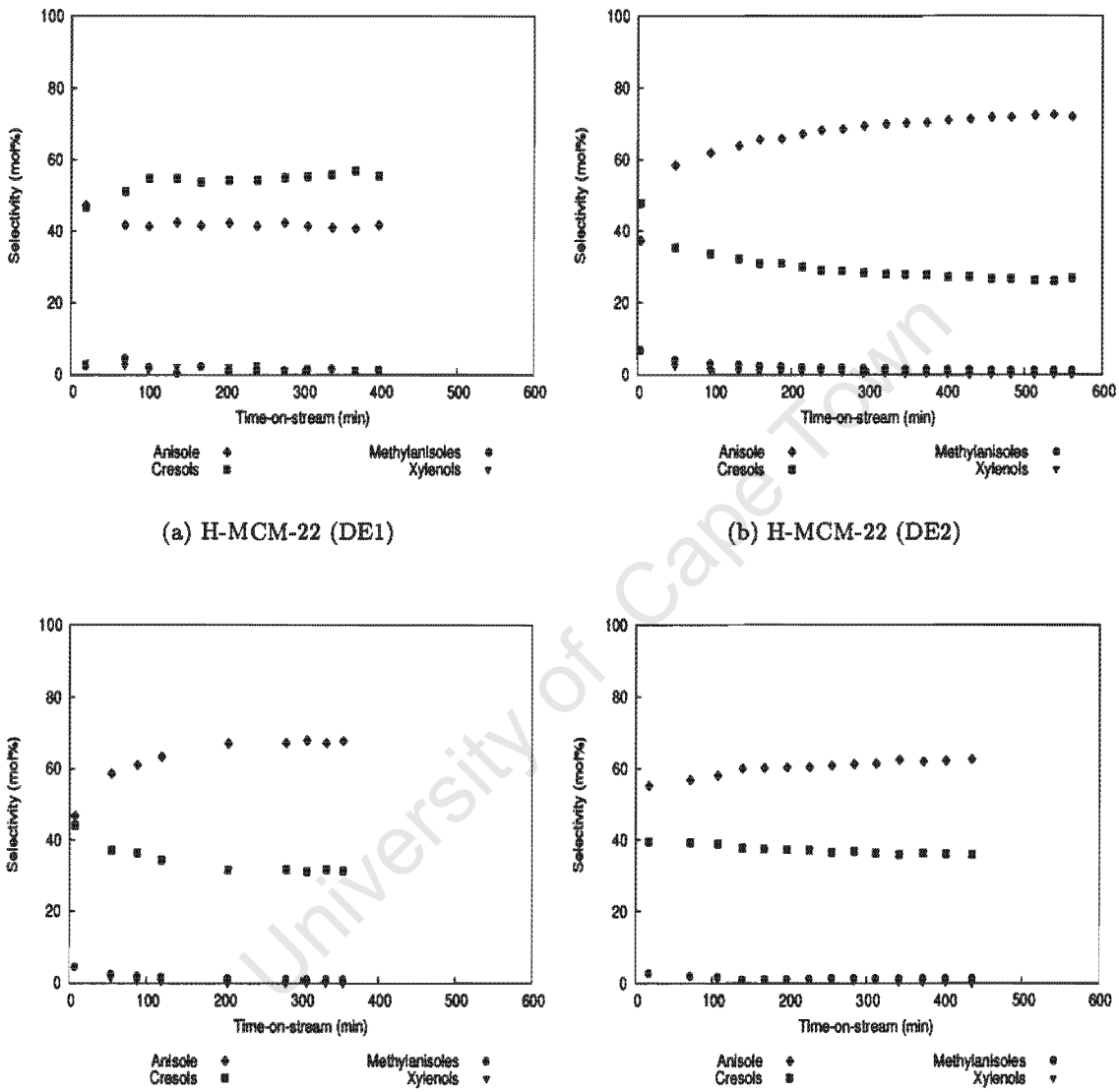

(a) H-MCM-22 (DE1)

(b) H-MCM-22 (DE2)

(c) H-MCM-22 (DE3)

(d) H-MCM-22 (UCT)

Figure 7.17: The effect of using different H-MCM-22 samples on product selectivity at gas phase standard reaction conditions (300°C, total pressure = 1 bar, reactants partial pressure = 0.2 bar, methanol : phenol molar ratio = 1, WHSV = 14 h^{-1}).

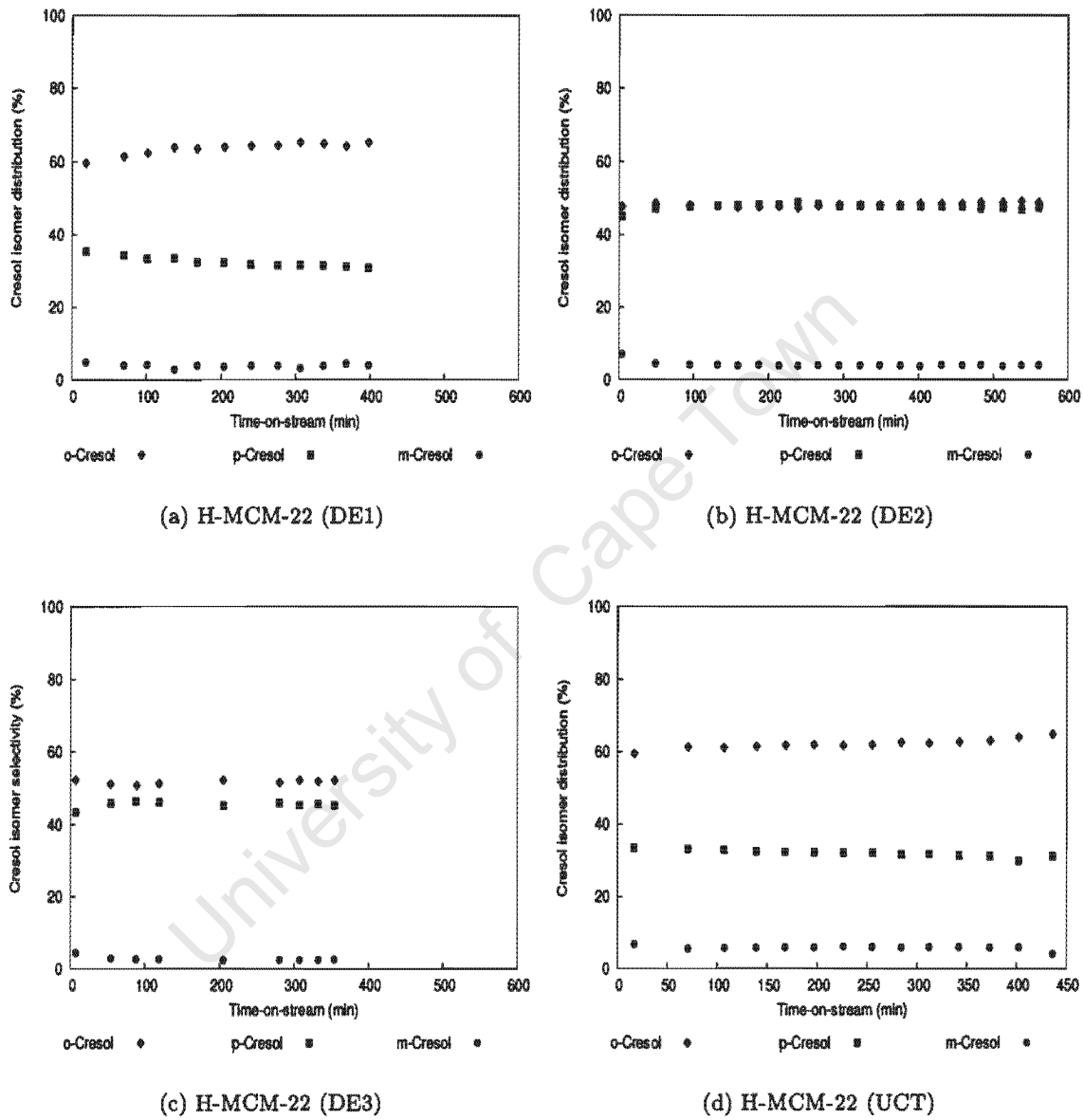

(a) H-MCM-22 (DE1)

(b) H-MCM-22 (DE2)

(c) H-MCM-22 (DE3)

(d) H-MCM-22 (UCT)

Figure 7.18: The effect of using different H-MCM-22 samples on cresol isomer distribution at gas phase standard reaction conditions (300°C, total pressure = 1 bar, reactants partial pressure = 0.2 bar, methanol : phenol molar ratio = 1, WHSV = 14 h^{-1}).

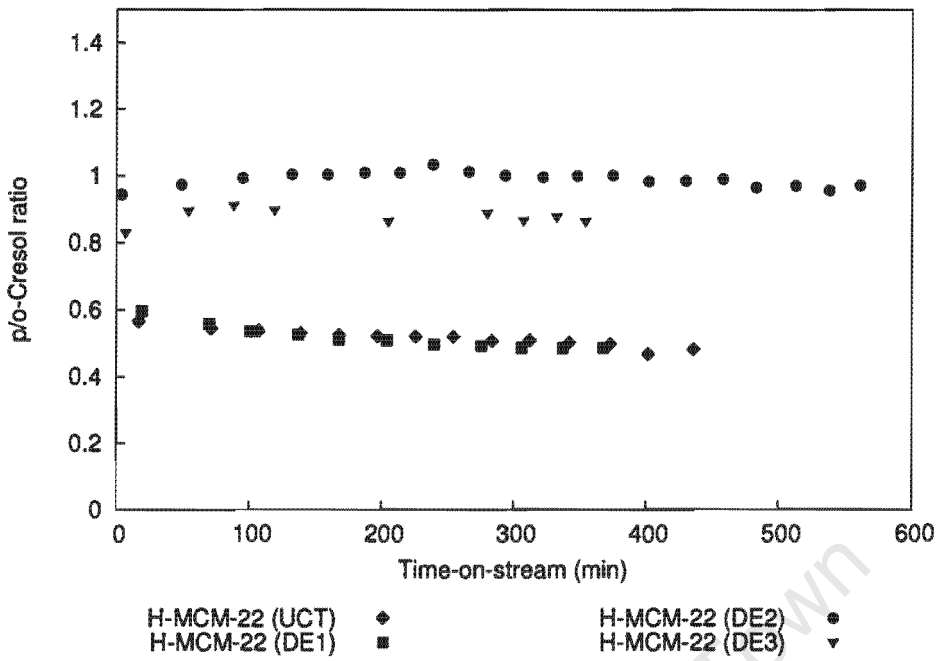

Figure 7.19: Comparison of the p/o-cresol ratios obtained over the different H-MCM-22 samples at gas phase standard reaction conditions (300°C, total pressure = 1 bar, reactants partial pressure = 0.2 bar, methanol : phenol molar ratio = 1, WHSV = 14 h^{-1}).

(Figure 7.18), H-MCM-22 (DE1) and H-MCM-22 (UCT) showed a lower p-selectivity (with p/o-cresol ratios around 0.5) than H-MCM-22 (DE2) and H-MCM-22 (DE3). H-MCM-22 (DE2) produced the highest p/o-cresol ratio of 0.97, closely followed by H-MCM-22 (DE3) with a p/o-cresol ratio of 0.85 (Figure 7.19).

7.4.3 Reactions over internally selectively sodium-exchanged ZSM-5 and MCM-22 (UCT)

Internal selectively sodium-exchange of ZSM-5 and MCM-22 (UCT) was carried out as described in Section 4.1.2. Section 6.4.2.1 describes the results of the test reactions, 1,3,5-TIPB cracking (to probe the activity of the external mesoporous surface of the zeolite crystals) and n-hexane cracking (to probe the total activity), used to kinetically characterize these catalysts. It was shown that over internally selectively sodium-exchanged zeolites (ZSM-5 and MCM-22 (UCT)), the total activity was much more affected than the activity of the external/mesoporous surface indicating that the poisoning was essentially internal.

7.4.3.1 Internally selectively sodium-exchanged H/Na-ZSM-5 compared to H-ZSM-5

Phenol conversion (Figure 7.20) over H-ZSM-5 and H/Na-ZSM-5 (12% and 3%, respectively, in the quasi-steady state) was 4 times lower over the internally selectively sodium-exchanged catalysts due to the poisoning of the internal acid sites. Another major difference in these two catalysts was obtained in the product selectivity (Figure 7.21). In the quasi-steady state the internally exchanged H/Na-ZSM-5 produced much less anisole than cresol (O/C-alkylation ratio = 0.41) which is directly the

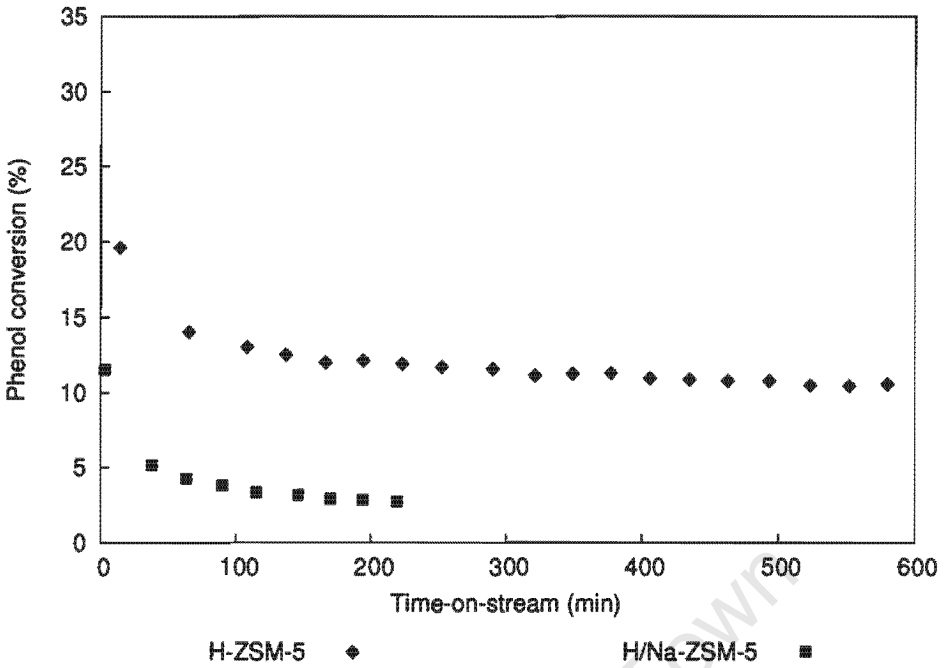

Figure 7.20: The effect of internally selectively sodium-exchange of H-ZSM-5 on phenol conversion at gas phase standard reaction conditions (300°C, total pressure = 1 bar, reactants partial pressure = 0.2 bar, methanol : phenol molar ratio = 1, WHSV = 14 h^{-1}).

opposite for H-ZSM-5 (O/C-alkylation ratio = 1.7). This major difference in selectivity is not due to different conversions but persists when catalyst are compared at equal conversion (i.e. between the fresh, selectively sodium-exchanged sample and the pure acid sample in quasi-steady state). The cresol isomer distribution hardly differed over the H/Na-ZSM-5 and H-ZSM-5 (Figure 7.22). In the quasi-steady state a p/o-cresol ratio of 0.50 was found for H/Na-ZSM-5 compared to 0.48 for the pure acid catalyst. Both the values are just slightly higher than the thermodynamic equilibrium ratio of ca. 0.43 as obtained by Böhringer and Fletcher [2003] but correspond with the statistical p/o-cresol ratio. Except in the very beginning of the experiments, there were minor changes of selectivities with time-on-stream.

7.4.3.2 Internally selectively sodium-exchanged H/Na-MCM-22 (UCT) compared to H-MCM-22 (UCT)

Phenol conversion (Figure 7.23) over H-MCM-22 (UCT) and internally selectively sodium-exchanged H/Na-MCM-22 (UCT) (13% and 5%, respectively, in the quasi-steady state) was decreased over the latter by a factor of almost 3. Contrary to what was observed in the case of ZSM-5, the product selectivities over H-MCM-22 (UCT) and H/Na-MCM-22 were similar (Figure 7.24). In the quasi-steady state, the O/C-alkylation ratio obtained over the internally exchanged and the pure acid catalyst was 1.7. At equal conversions (comparing the fresh, selectively sodium-exchanged sample and the pure acid sample in quasi-steady state) the O/C-alkylation ratio over the internally exchanged catalyst and the pure acid catalyst was almost as high. In the quasi-steady state the p/o-cresol ratio was 0.50 with both the selectively exchanged and the pure acid samples (Figure 7.25), again just slightly higher than the thermodynamic equilibrium of ca. 0.43 as obtained by Böhringer and

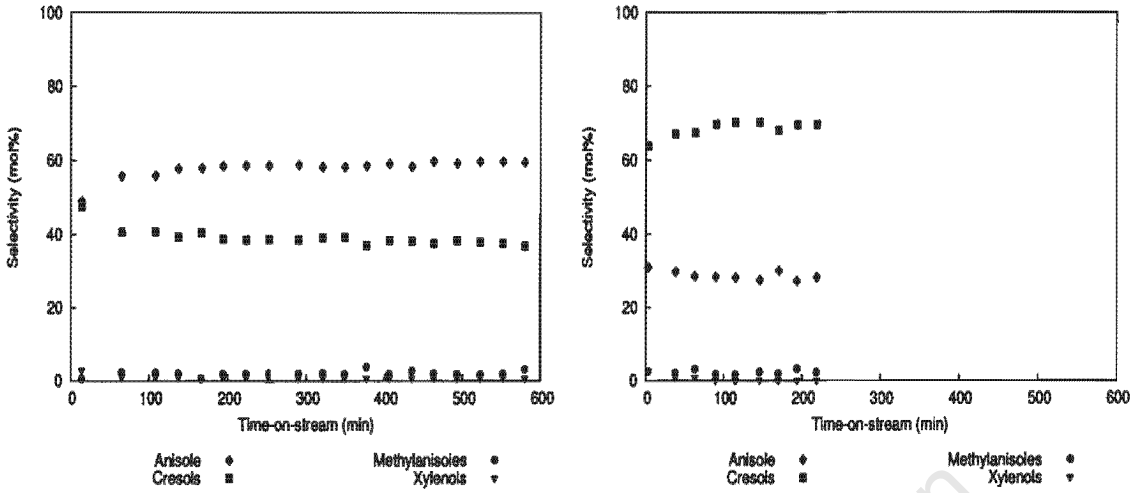

(a) H-ZSM-5 (b) H/Na-ZSM-5

Figure 7.21: The effect of internally selectively sodium-exchange of H-ZSM-5 on product selectivity at gas phase standard reaction conditions (300°C, total pressure = 1 bar, reactants partial pressure = 0.2 bar, methanol : phenol molar ratio = 1, WHSV = 14 h^{-1}).

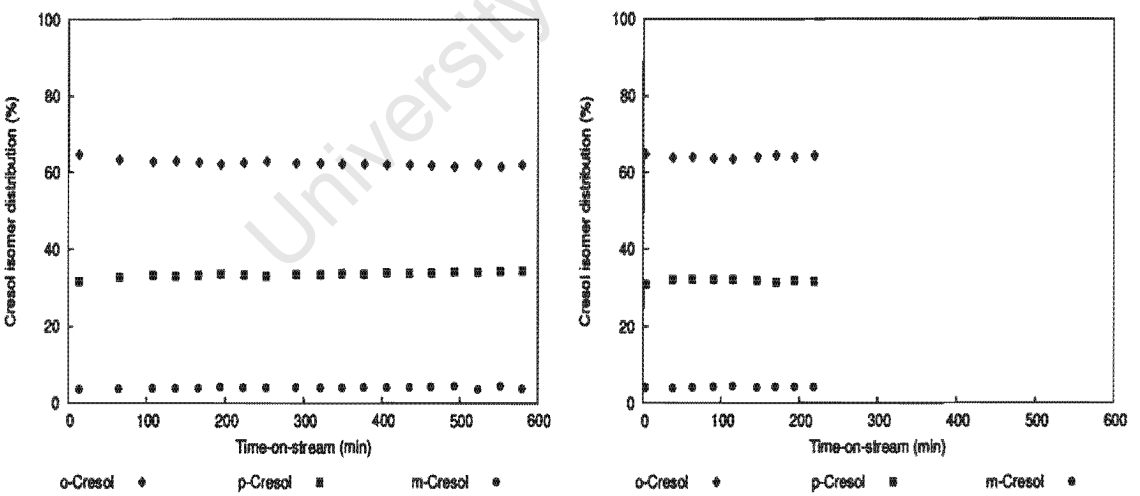

(a) H-ZSM-5 (b) H/Na-ZSM-5

Figure 7.22: The effect of internally selectively sodium-exchange of H-ZSM-5 on cresol isomer distribution at gas phase standard reaction conditions (300°C, total pressure = 1 bar, reactants partial pressure = 0.2 bar, methanol : phenol molar ratio = 1, WHSV = 14 h^{-1}).

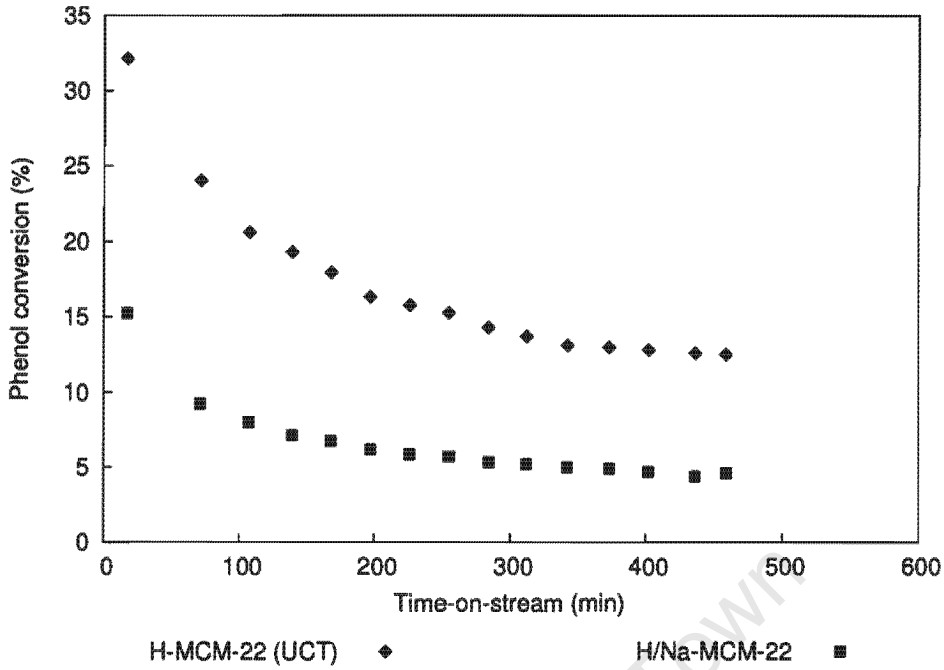

Figure 7.23: The effect of internally selectively sodium-exchange of H-MCM-22 (UCT) on phenol conversion at gas phase standard reaction conditions (300°C, total pressure = 1 bar, reactants partial pressure = 0.2 bar, methanol : phenol molar ratio = 1, WHSV = 14 h^{-1}).

Fletcher [2003] and corresponding with the statistical p/o-cresol ratio as in the case of H-ZSM-5 and H/Na-ZSM-5 (cf. Figure 7.22). There was minor changes of selectivities with time-on-stream, except at very low time-on-stream.

7.4.4 Steamed H-MCM-22 (DE1)

Sample H-MCM-22 (DE1) was steamed with a view to assessing the effect of extra-framework aluminium on the activity and product selectivity. The steaming conditions are described in Section 4.13 and Table 4.1. The phenol methylation reactions over both the steamed and unsteamed H-MCM-22 (DE1) were done at the gas phase standard reaction conditions (cf. Table 7.1). Figure 7.26 shows that the steaming enhanced the phenol conversion from 4% to 11%, compared after 300 min time-on-stream. Such an increase in phenol conversion with mild steaming is expected, cf. Section 2.1.4.1.2. In terms of product selectivity, a major difference was obtained. Steaming the catalysts promoted the formation of anisole relative to cresols (65 mol% vs 32 mol%) as shown in Figure 7.27. Steaming also changed the cresol isomer distribution by decreasing the percentage of the o-cresol fraction, increasing the percentage of the m-cresol fraction and slightly increasing the percentage of the p-cresol fraction (Figure 7.28). Steaming increased the p/o-cresol ratio slightly from 0.48 to 0.54.

The differences in selectivities due to steaming are not an effect of conversion, as comparing at equal conversion (fresh unsteamed catalyst versus quasi-steady state steamed catalyst) the differences persist, slightly reduced in the case of anisole/cresol selectivity.

Comparison with Section 7.3.1 and Figure 7.3 indicates that the observed differences obtained over the steamed and unsteamed samples essentially reflect the influence of conversion.

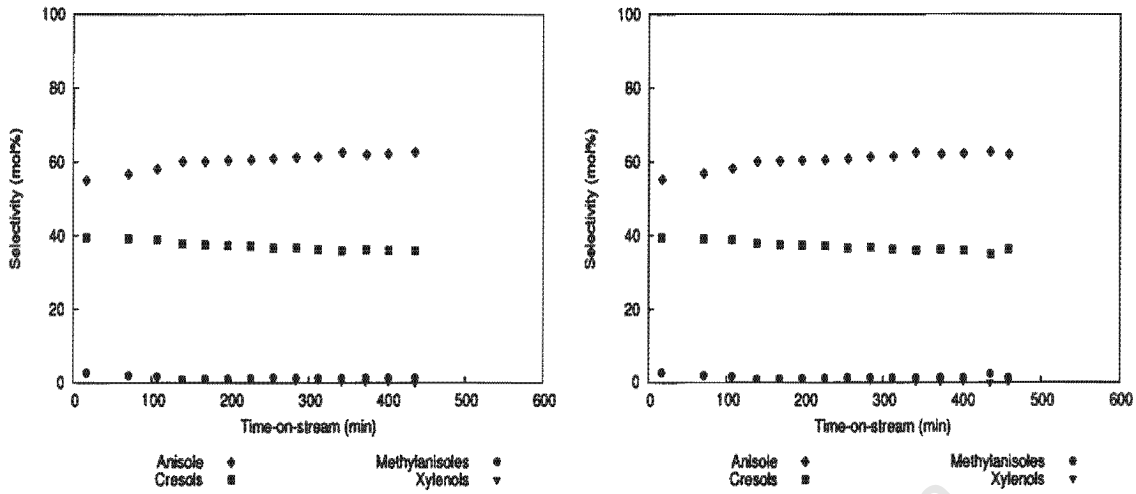

(a) H-MCM-22 (UCT)

(b) H/Na-MCM-22 (UCT)

Figure 7.24: The effect of internally selectively sodium-exchange of H-MCM-22 (UCT) on product selectivity at gas phase standard reaction conditions (300°C, total pressure = 1 bar, reactants partial pressure = 0.2 bar, methanol : phenol molar ratio = 1, WHSV = 14 h^{-1}).

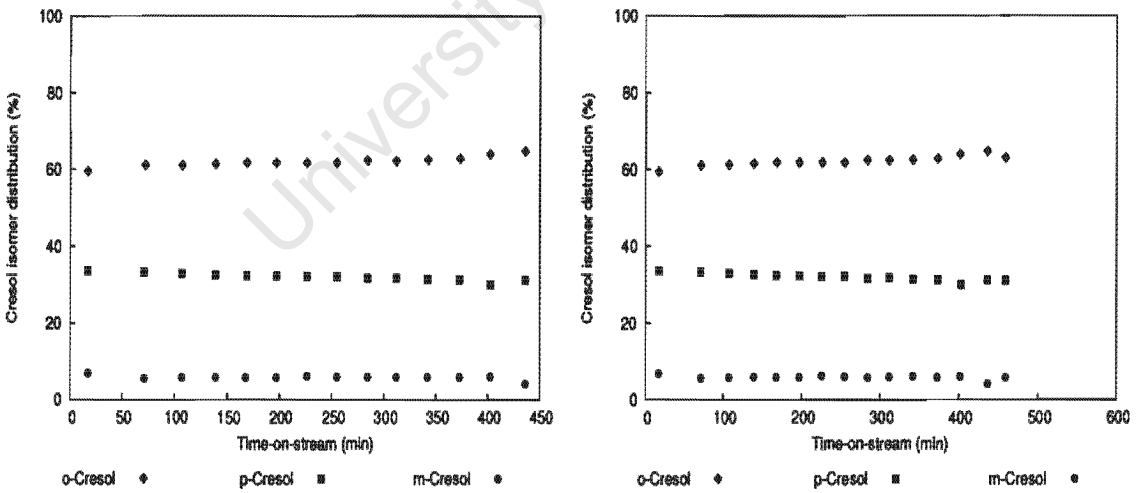

(a) H-MCM-22 (UCT)

(b) H/Na-MCM-22 (UCT)

Figure 7.25: The effect of internally selectively sodium-exchange of H-MCM-22 (UCT) on cresol isomer distribution at gas phase standard reaction conditions (300°C, total pressure = 1 bar, reactants partial pressure = 0.2 bar, methanol : phenol molar ratio = 1, WHSV = 14 h^{-1}).

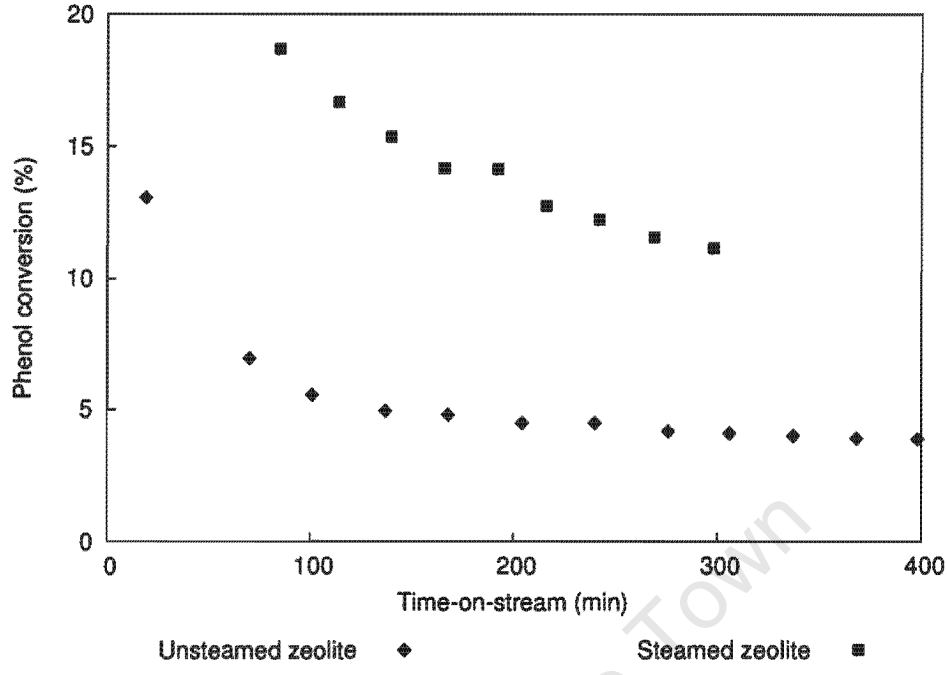

Figure 7.26: The effect of steaming H-MCM-22 (DE1) on phenol conversion at gas phase standard reaction conditions (300°C, total pressure = 1 bar, reactants partial pressure = 0.2 bar, methanol : phenol molar ratio = 1, WHSV = 14 h^{-1}). For steaming conditions cf. Section 4.13 and Table 4.1.

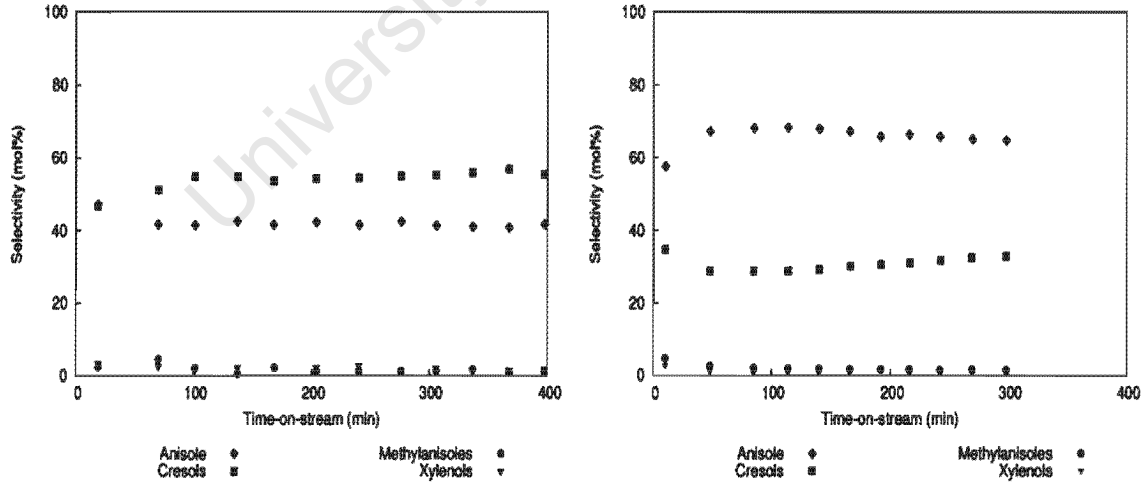

(a) Unsteamed zeolite

(b) Steamed zeolite

Figure 7.27: The effect of steaming H-MCM-22 (DE1) on product selectivity at gas phase standard reaction conditions (300°C, total pressure = 1 bar, reactants partial pressure = 0.2 bar, methanol : phenol molar ratio = 1, WHSV = 14 h^{-1}). For steaming conditions cf. Section 4.13 and Table 4.1.

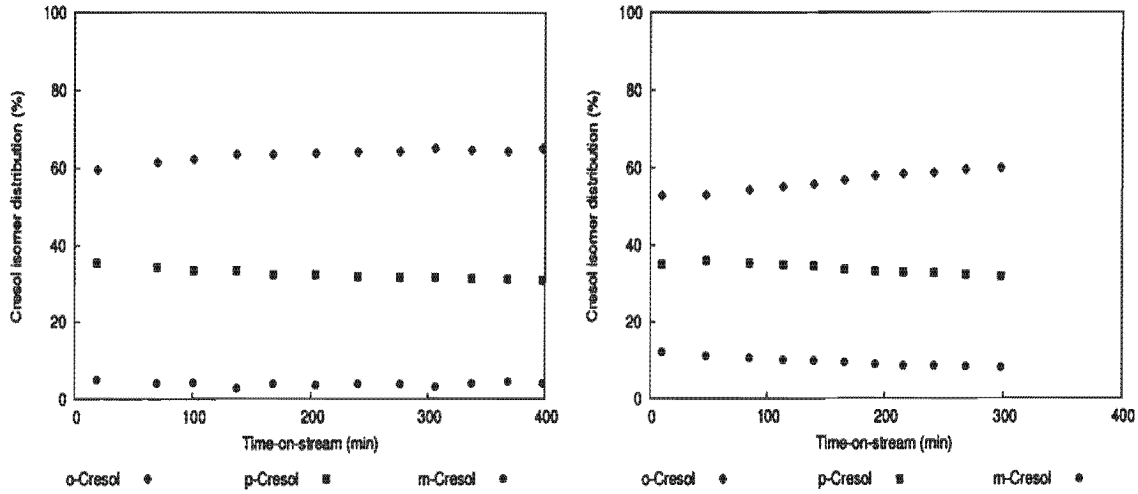

(a) Unsteamed zeolite

(b) Steamed zeolite

Figure 7.28: The effect of steaming H-MCM-22 (DE1) on the cresol isomer distribution at gas phase standard reaction conditions (300°C, total pressure = 1 bar, reactants partial pressure = 0.2 bar, methanol : phenol molar ratio = 1, WHSV = 14 h^{-1}). For steaming conditions cf. Section 4.13 and Table 4.1.

7.5 Effect of reaction parameters

The data points given in this section represent averaged quasi-steady state data.

7.5.1 Effect of reaction temperature

The effect of reaction temperature on the phenol methylation was studied between 200°C and 400°C over H-MCM-22 (UCT) under the gas phase standard reaction conditions (cf. Table 7.1). As expected, the phenol conversion increased exponentially with increasing temperature (Figure 7.29). The effect of reaction temperature on product selectivity showed a discontinuous profile (Figure 7.30). At 270°C, the anisole formation passed over a maximum of 63% and correspondingly the cresols formation passed through a minimum of 36%. Above ca. 360°C, C-alkylation was preferred. The selectivity to methylanisoles and xylenols increased with reaction temperature, however, on a low level (< 5%). The cresol isomer distribution (Figure 7.30 (b)) showed a shift towards thermodynamic equilibrium with increasing reaction temperature. The m-cresol selectivity increased with increasing reaction temperature and both the o- and p-cresol selectivities decreased, changing from an o : p : m ratio of 67 : 33 : 0 at 200°C to that of 60 : 24 : 16 at 400°C. The p/o-cresol ratio appears to be close to the statistical p/o-cresol ratio of 0.5 at low temperature and decreased slightly with increasing reaction temperature as shown in Figure 7.31, eventually reaching thermodynamic equilibrium.

Note that selectivities in the above are not compared at equal conversion. As conversion increases with reaction temperature and as conversion has an effect on product selectivity as shown in Section 7.3.1, the determination of the true temperature effect on product selectivity and cresol isomer distribution needs to be examined. A comparison of results obtained through varying space velocity

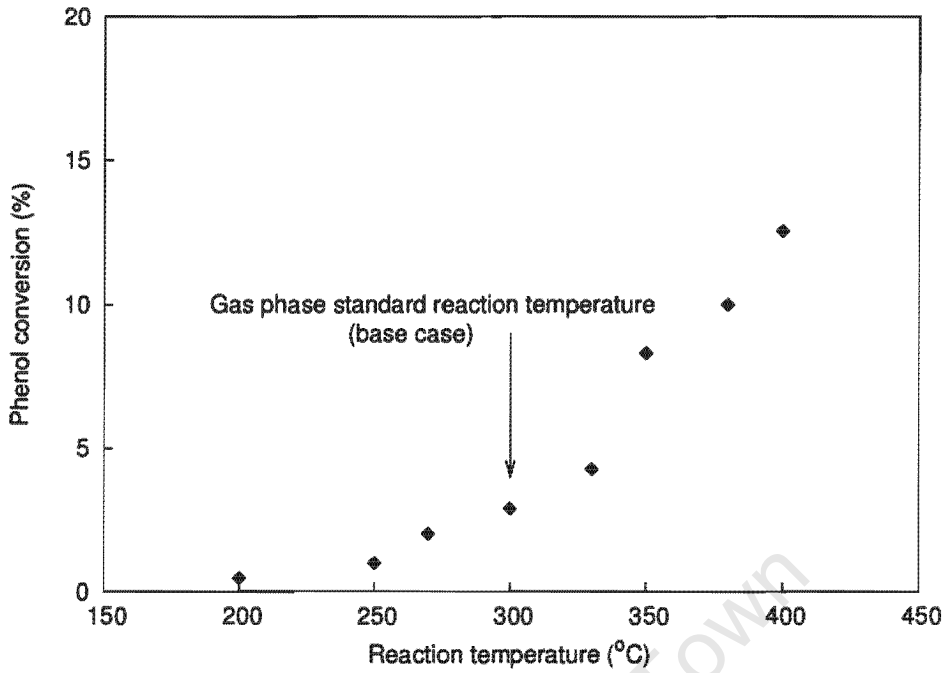

Figure 7.29: The effect of reaction temperature on the phenol conversion over H-MCM-22 (UCT) (gas phase standard reaction conditions: total pressure = 1 bar, reactants partial pressure = 0.2 bar, methanol : phenol molar ratio = 1, WHSV = 14 h^{-1}, varying reaction temperature).

and results obtained through varying reaction temperature as a function of conversion (Figure 7.32) shows that there is a deviation, i.e. a direct effect of reaction temperature on product selectivity and cresol isomer distribution in addition to the indirect effect by conversion. Separating the indirect effect of conversion from the direct effect of reaction temperature, as described in Section 7.3.3, shows, semi-quantitatively, however, the true effect of reaction temperature on product selectivity and cresol isomer distribution (Figure 7.33). In selectivities, there was still a reversal of the trends at 220°C (Figure 7.33 (a)) and a major change in product selectivity occurred at higher reaction temperatures where the increase in cresol selectivity with increasing reaction temperature was pronounced (Figure 7.33 (a)). In the cresol isomer distribution (Figure 7.33 (b)), the fraction of p-cresol appeared to decrease more steeply with increasing reaction temperature leading to a more pronounced decrease in the true p/o-cresol ratio with increasing reaction temperature (Figure 7.34), eventually resulting in p/o-cresol ratios (0.28 at 400°C) far lower than the equilibrium ratio or statistical ratio.

7.5.2 Effect of methanol : phenol ratio

The effect of the reactants methanol : phenol ratio on the product selectivity was studied using H-MCM-22 (UCT) at the gas phase standard reaction conditions (cf. Table 7.1) with constant weight hourly space velocity of total feed. The methanol : phenol molar ratios studied were between 0.3 and 6. The phenol conversion increased significantly with increasing methanol : phenol ratio (Figure 7.35). The product selectivity (Figure 7.36) showed an increase in anisole selectivity and a corresponding decrease in cresol selectivity with increasing methanol : phenol ratio. Up to a methanol : phenol molar ratio of 2 the o- and p-cresol fraction in cresols increased whereas the m-cresol fraction decreased. At

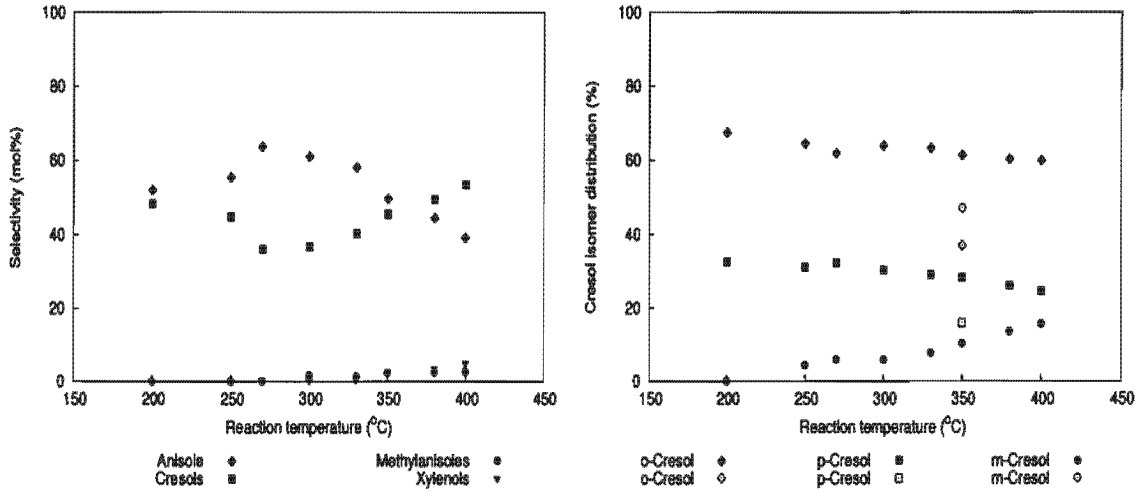

(a) Product selectivity

(b) Cresol isomer distribution

Figure 7.30: The effect of reaction temperature on product selectivity and cresol isomer distribution over H-MCM-22 (UCT) (open symbols represent thermodynamic equilibrium as obtained by Böhringer and Fletcher [2003]; gas phase standard reaction conditions: total pressure = 1 bar, reactants partial pressure = 0.2 bar, methanol : phenol molar ratio = 1, WHSV = 14 h^{-1}, varying reaction temperature).

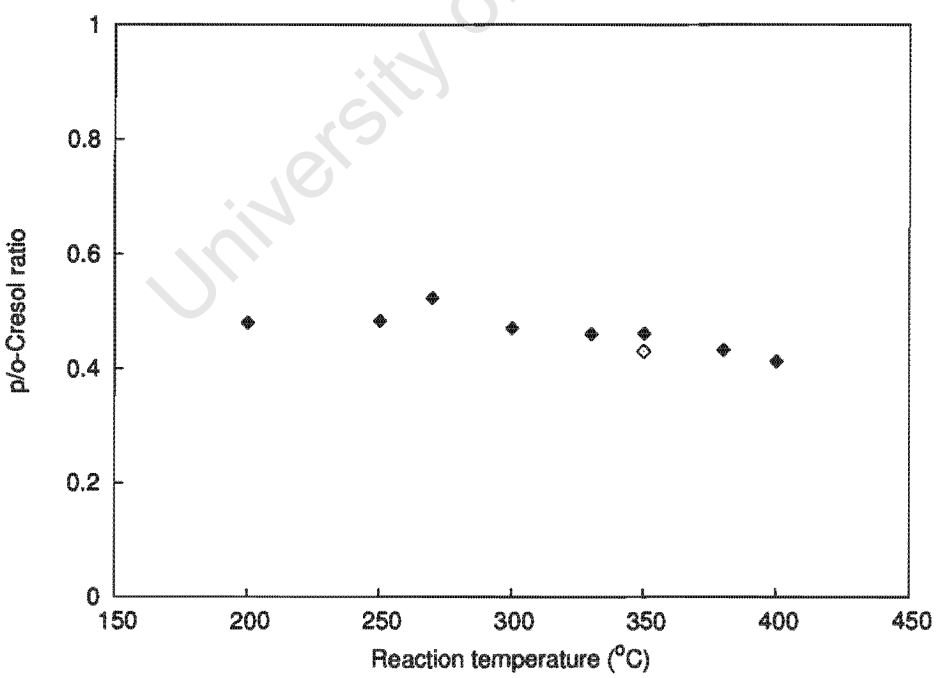

Figure 7.31: The effect of reaction temperature on the p/o-cresol ratio over H-MCM-22 (UCT) (open symbol represent thermodynamic equilibrium ratio as obtained by Böhringer and Fletcher [2003]; gas phase standard reaction conditions: total pressure = 1 bar, reactants partial pressure = 0.2 bar, methanol : phenol molar ratio = 1, WHSV = 14 h^{-1}, varying reaction temperature).

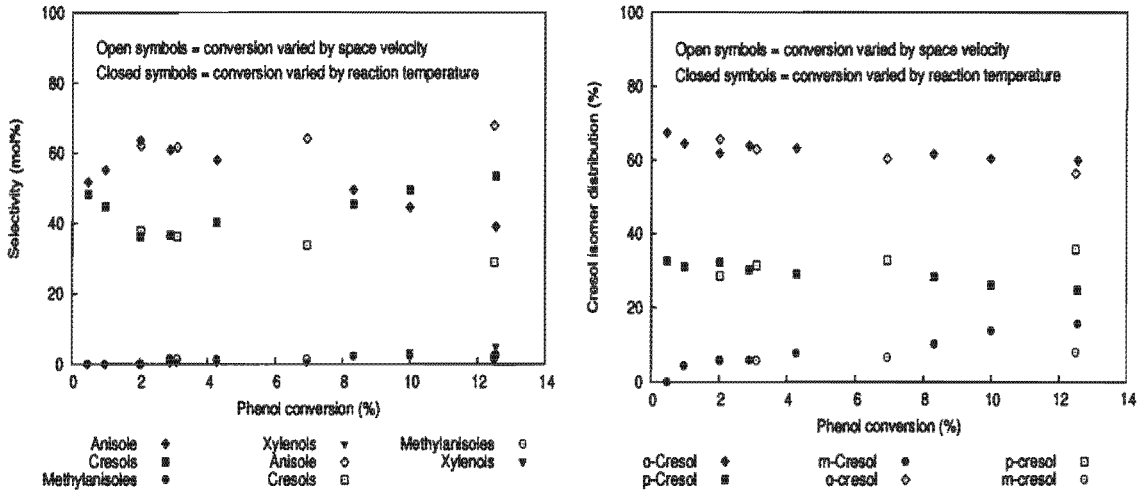

(a) Product selectivity

(b) Cresol isomer distribution

Figure 7.32: The effect of reaction temperature and conversion on product selectivity and cresol isomer distribution compared over H-MCM-22 (UCT). Phenol conversion varied as a result of reaction temperature (closed symbols) or was varied by varying weight hourly space velocity (open symbols). All data points represent the average of quasi-steady state samples (gas phase standard reaction conditions: total pressure = 1 bar, reactants partial pressure = 0.2 bar, methanol : phenol molar ratio = 1, WHSV = 14 h^{-1}, varying reaction temperature or varying weight hourly space velocity at 300°C, respectively).

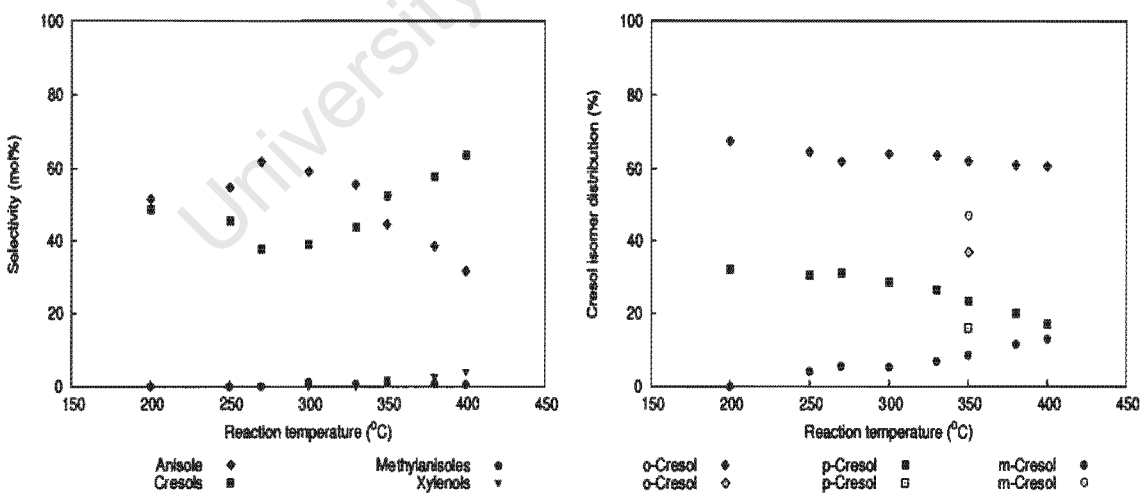

(a) Product selectivity

(b) Cresol isomer distribution

Figure 7.33: The true effect of reaction temperature on product selectivity and cresol isomer distribution over H-MCM-22 (UCT) (gas phase standard reaction conditions: total pressure = 1 bar, reactants partial pressure = 0.2 bar, methanol : phenol molar ratio = 1, WHSV = 14 h^{-1}, varying reaction temperature). Open symbols in Figure (b) indicate thermodynamic equilibrium as obtained by Böhringer and Fletcher [2003].

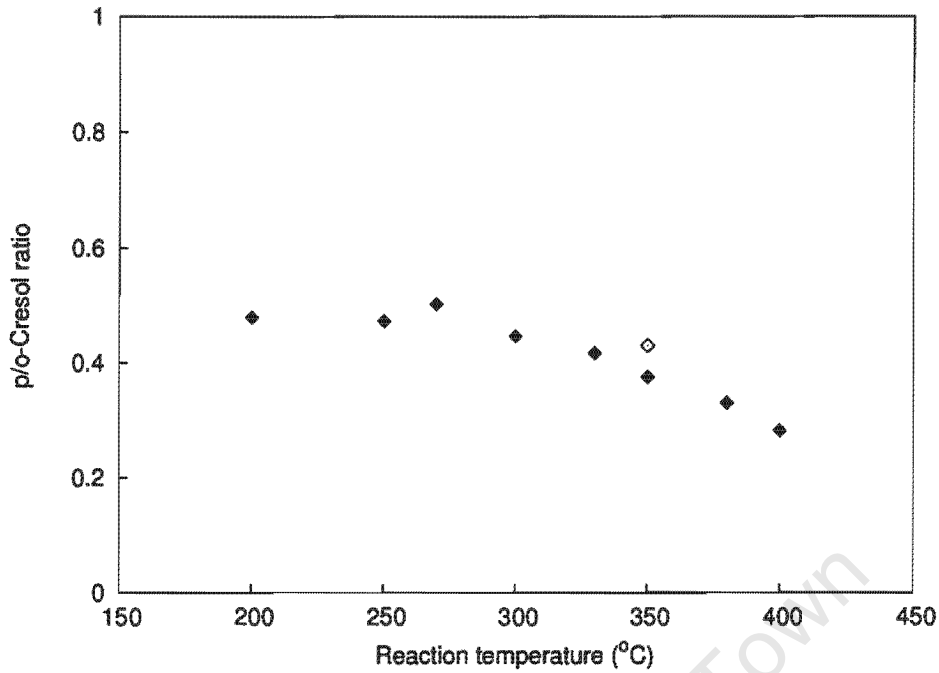

Figure 7.34: The true effect of reaction temperature on the p/o-cresol ratio over H-MCM-22 (UCT) (gas phase standard reaction conditions: total pressure = 1 bar, reactant partial pressure = 0.2 bar, methanol : phenol molar ratio = 1, WHSV = 14 h^{-1}, varying reaction temperature). Open symbol indicates thermodynamic equilibrium as obtained by Böhringer and Fletcher [2003].

higher methanol : phenol ratios this trend appeared reversed. According to Figure 7.37, the p/o-cresol ratio was above the thermodynamic equilibrium and close to the statistical ratio of 0.5 but appears slightly increased at the highest methanol : phenol ratio.

Note that selectivities are not compared at equal conversions. As phenol conversion increased with increasing methanol : phenol ratio, it is necessary to compare and, if necessary, separate the direct effect of methanol : phenol ratio on product selectivity and cresol isomer distribution from that of the indirect effect of conversion. Comparison with results obtained through varying weight hourly space velocity is shown in Figure 7.38. Figure 7.38 shows that in fact there is no direct effect of methanol : phenol ratio. There is only an effect on conversion which, indirectly, is resulting in the change in product selectivity and cresol isomer distribution observed.

7.5.3 Effect of weight hourly space velocity

The effect of weight hourly space velocity (WHSV) was studied between 3 and 23 h^{-1} under gas phase standard reaction conditions. The phenol conversion decreased from 13% to 2% with increasing weight hourly space velocity (Figure 7.39). The anisole selectivity decreased slightly and correspondingly the cresol selectivity increased with increasing weight hourly space velocity (Figure 7.40 (a)). With respect to the cresol isomer distribution, the o-cresol percentage increased whereas p-cresol and m-cresol percentage decreased with increasing weight hourly space velocity (Figure 7.40 (b)). Plotted as selectivities, p- and m-cresol showed no effect of space velocity but o-cresol selectivity increased simultaneously to the decrease in anisole selectivity (Figure 7.40 (c)). The p/o-cresol ratio decreased

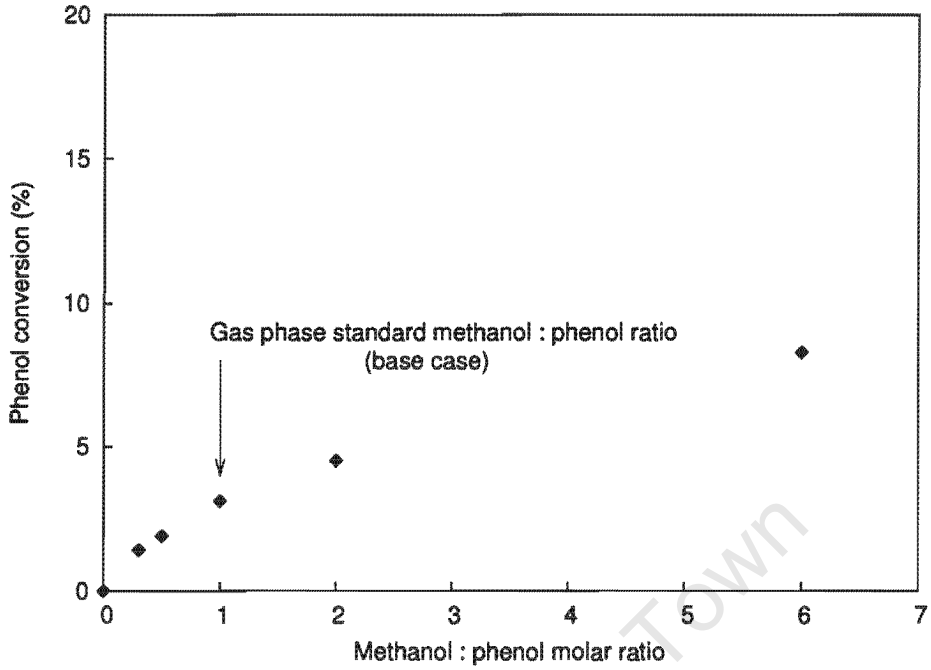

Figure 7.35: The effect of the methanol : phenol ratio on phenol conversion over H-MCM-22 (UCT) (gas phase standard reaction conditions: 300°C, total pressure = 1 bar, reactants partial pressure = 0.2 bar, $WHSV_{reactants}$ = 14 h^{-1}, varying methanol : phenol ratios).

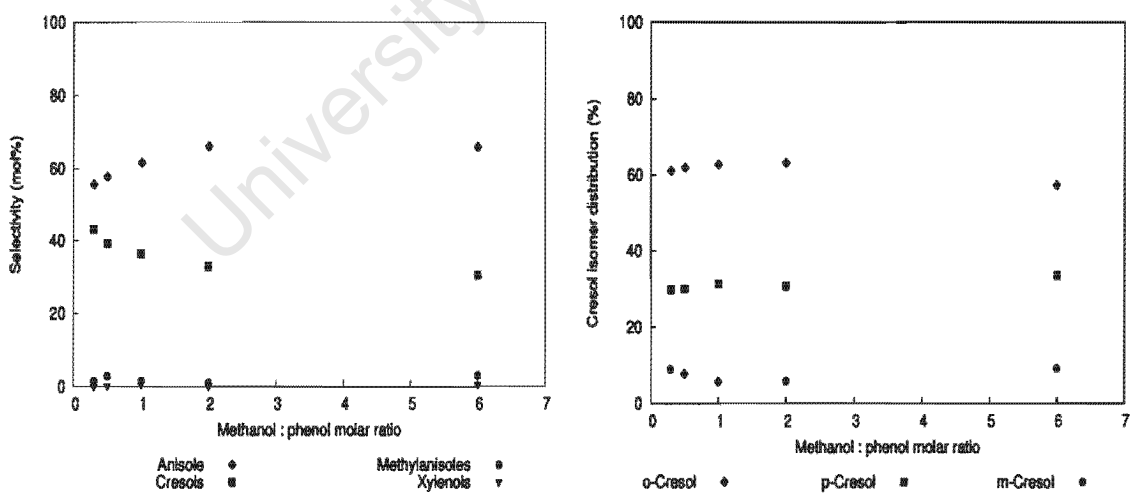

(a) Product selectivity

(b) Cresol isomer distribution

Figure 7.36: The effect of the methanol : phenol ratio on product selectivity and cresol isomer distribution over H-MCM-22 (UCT) (gas phase standard reaction conditions: 300°C, total pressure = 1 bar, reactants partial pressure = 0.2 bar, $WHSV_{reactants}$ = 14 h^{-1}, varying methanol : phenol ratios).

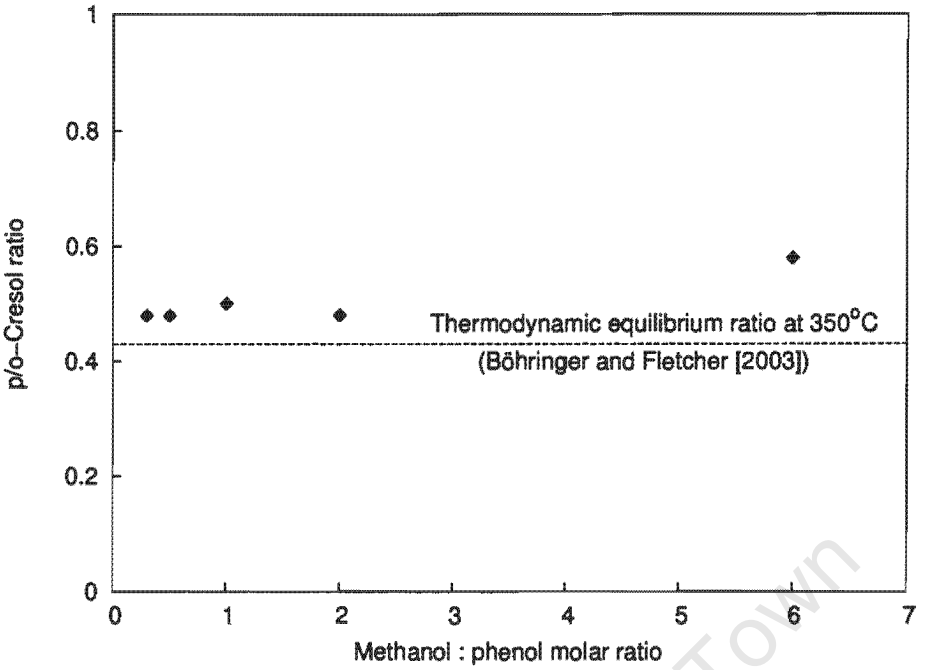

Figure 7.37: The effect of the methanol : phenol ratio on the p/o-cresol ratio over H-MCM-22 (UCT) (gas phase standard reaction conditions: 300°C, total pressure = 1 bar, reactants partial pressure = 0.2 bar, $WHSV_{reactants}$= 14 h^{-1}, varying methanol : phenol ratios).

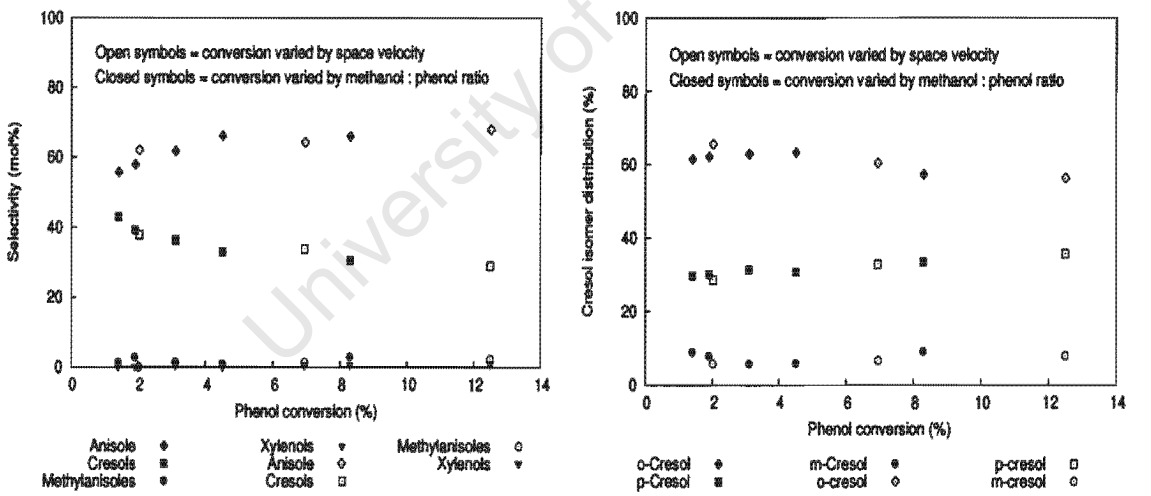

(a) Product selectivity

(b) Cresol isomer distribution

Figure 7.38: The effect of the methanol : phenol ratio and conversion on product selectivity and cresol isomer distribution over H-MCM-22 (UCT). Phenol conversion varied as a result of varying methanol : phenol ratio (closed symbols) or was varied by varying weight hourly space velocity (open symbols) with data points in both cases representing the average of quasi-steady state samples (gas phase standard reaction conditions: 300°C, total pressure = 1 bar, reactants partial pressure = 0.2 bar, $WHSV_{reactants}$ = 14 h^{-1} at varying methanol : phenol ratios or varying weight hourly space velocity at methanol : phenol molar ratio = 1).

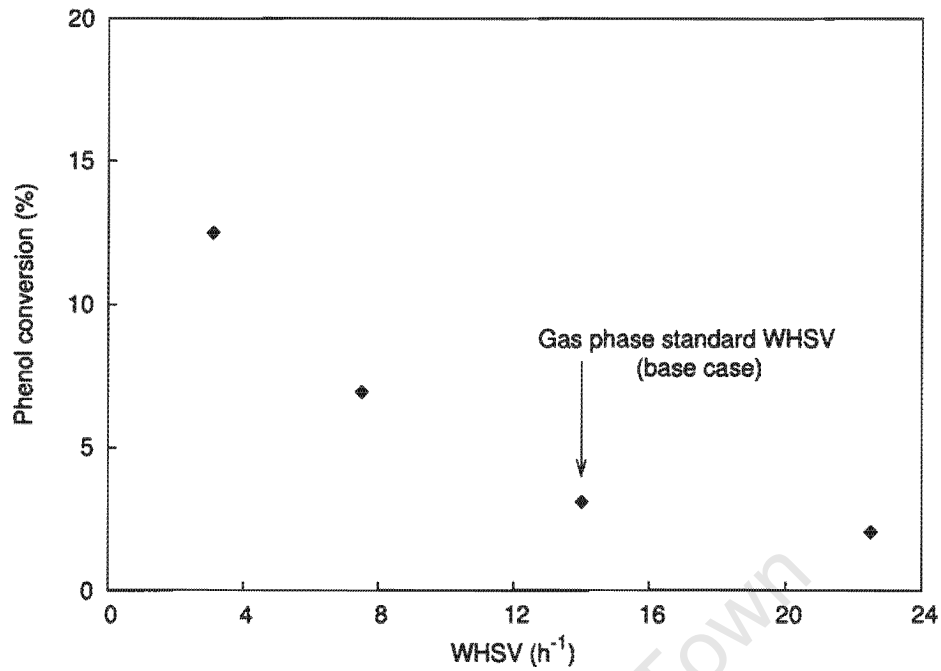

Figure 7.39: The effect of weight hourly space velocity on phenol conversion over H-MCM-22 (UCT) (gas phase standard reaction conditions: 300°C, total pressure = 1 bar, reactants partial pressure = 0.2 bar, methanol : phenol ratio = 1, varying weight hourly space velocity).

from 0.63 to 0.44 with increasing weight hourly space velocity (as shown in Figure 7.41). It appears, however, that the p/o-cresol ratio is not approaching the equilibrium ratio of ca. 0.43 as obtained by Böhringer and Fletcher [2003] but crosses the equilibrium line as the trend persists. In Figure 7.3 and Section 7.3.1, selectivity and cresol isomer distribution were presented as a function of conversion. Anisole selectivity increased moderately with conversion and in the cresol fraction, the percentage o-cresol decreased simultaneously.

7.5.4 Effect of reactants partial pressure

The reactants partial pressure was varied between 0.2 and 0.8 bar at gas phase standard reaction conditions (cf. Table 7.1) over H-MCM-22 (UCT). Initially, between 0.2 and 0.34 bar reactants partial pressure, the phenol conversion increased from 6% to 9% then levelled off (Figure 7.42).

The product selectivity was slightly affected over the range of reactants partial pressures studied (Figure 7.43 (a)) with anisole selectivity decreasing slightly and cresol selectivity correspondingly increasing with increasing reactant partial pressure. Slight trends seem to appear in the cresol isomer distribution (Figure 7.43 (b)) and in the p/o-cresol ratio (Figure 7.44), however, these trends are in the range of scatter.

As phenol conversion initially increased with increasing reactant partial pressure, it is necessary to compare and if necessary, to separate the direct effect of reactant partial pressure on product selectivity and cresol isomer distribution and the indirect effect of conversion, which is obtained by varying space velocity. Figure 7.45 shows that the results do not differ so that in fact there was no

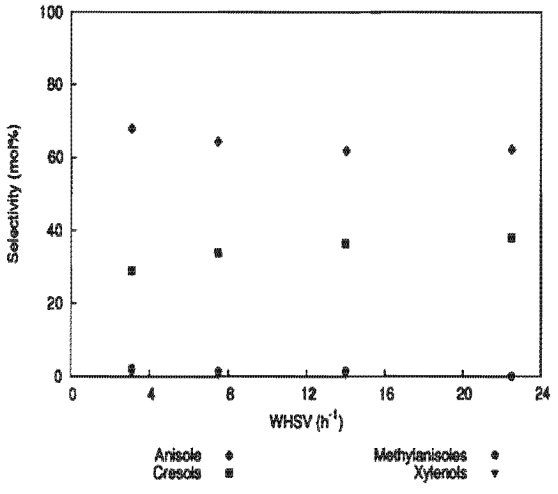

(a) Product selectivity

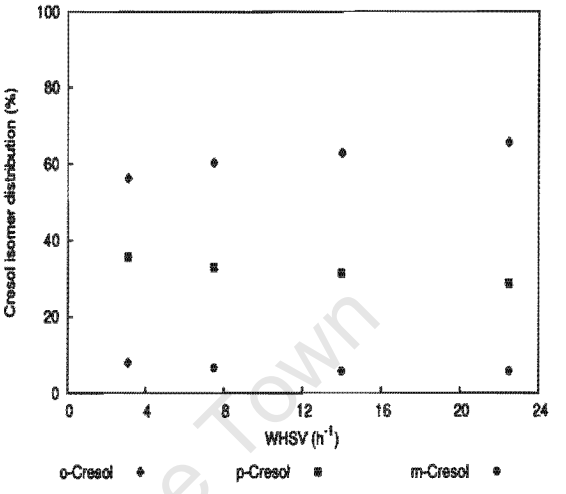

(b) Cresol isomer distribution

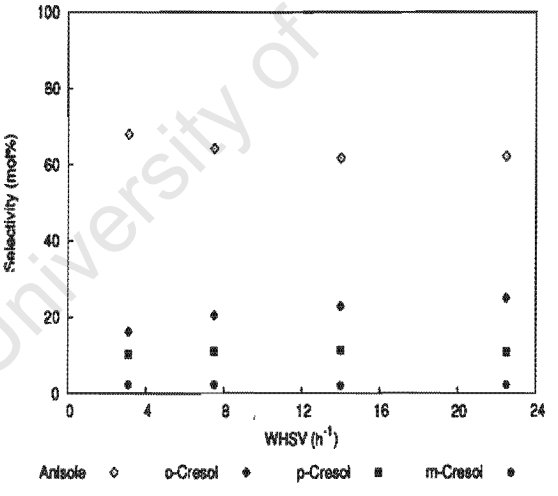

(c) Product selectivity

Figure 7.40: The effect of weight hourly space velocity on product selectivity and cresol isomer distribution over H-MCM-22 (UCT) (gas phase standard reaction conditions: 300°C, total pressure = 1 bar, reactants partial pressure = 0.2 bar, methanol : phenol ratio = 1, varying weight hourly space velocity).

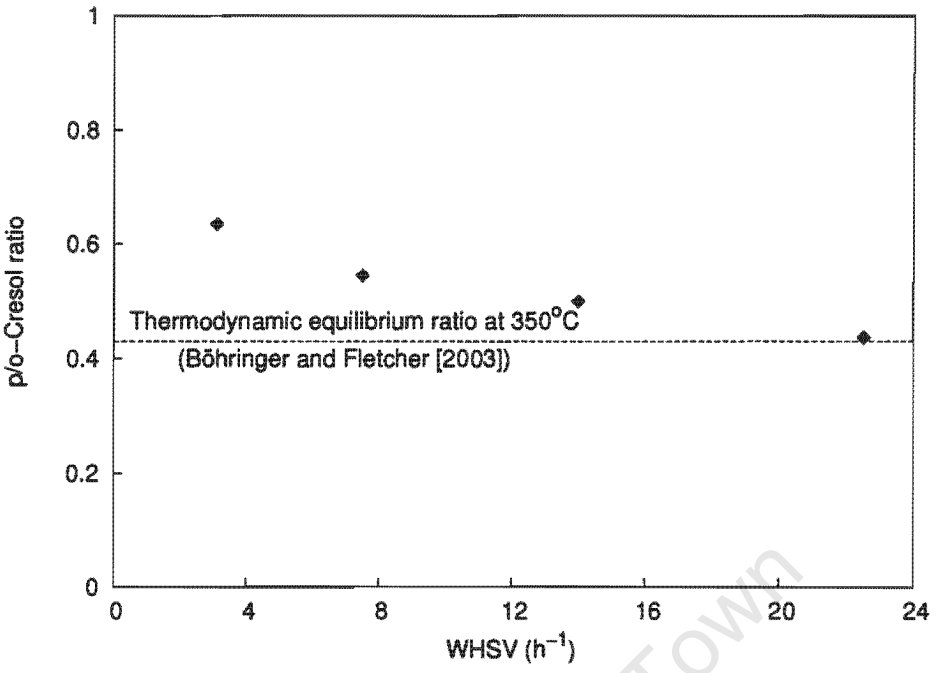

Figure 7.41: The effect of weight hourly space velocity on the p/o-cresol ratio obtained over H-MCM-22 (UCT). Horizontal line indicates thermodynamic equilibrium as obtained by Böhringer and Fletcher [2003] (gas phase standard reaction conditions: 300°C, total pressure = 1 bar, reactants partial pressure = 0.2 bar, methanol : phenol ratio = 1, varying weight hourly space velocity).

direct effect of reactant partial pressure but only an indirect effect of conversion on product selectivity and cresol isomer distribution.

7.6 Conversion of the major phenol methylation products over H-MCM-22 (UCT)

Conversion of pure anisole, o-cresol, p-cresol and m-cresol, respectively, over H-MCM-22 (UCT) under the gas phase standard reaction conditions (cf. Table 7.1, expect the methanol : phenol ratio is replace by either pure anisole or an anisole : phenol ratio = 1) was studied to determine the extent to which secondary reactions occurred at the reaction conditions used. The effect of the presence of phenol on anisole conversion was also studied.

Tables 7.2 and 7.3 show the results of these product conversions over H-MCM-22 (UCT). Anisole converted mainly to methylanisoles and co-product phenol as expected from transalkylation between two anisoles. If diluted with phenol, anisole conversion declined. As yields indicate, this is in particular due to a decline in the transalkylation products, which occurred to a much lower extend. Instead of phenol and methylanisoles, cresols are then the major products. In terms of cresol isomer distribution, o-cresol is the major isomer formed in both the pure anisole conversion and the conversion of the anisole/phenol mixture. Since the percentages of p-cresol differ significantly, the p/o-cresol ratio from anisole conversion is very low (0.16), whereas a much higher p/o-cresol ratio (0.53), which is somewhat above equilibrium or statistical ratio, results from converting the anisole/phenol mixture.

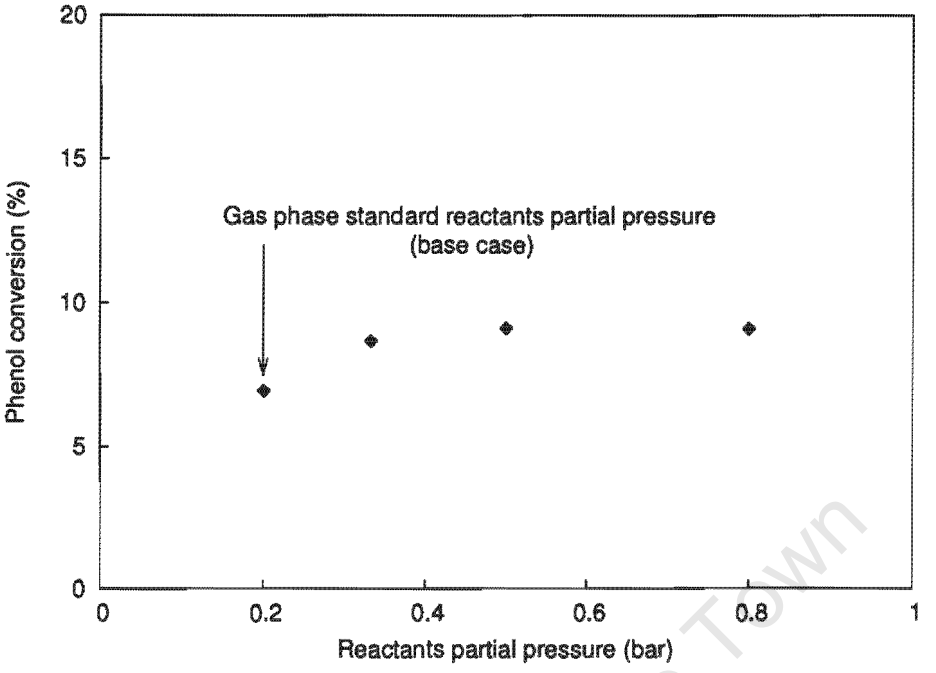

Figure 7.42: The effect of reactants partial pressure on phenol conversion over H-MCM-22 (UCT) (reaction conditions: 300°C, total pressure = 1 bar, methanol : phenol molar ratio = 1, WHSV = 7.5 h^{-1}, varying reactants partial pressure).

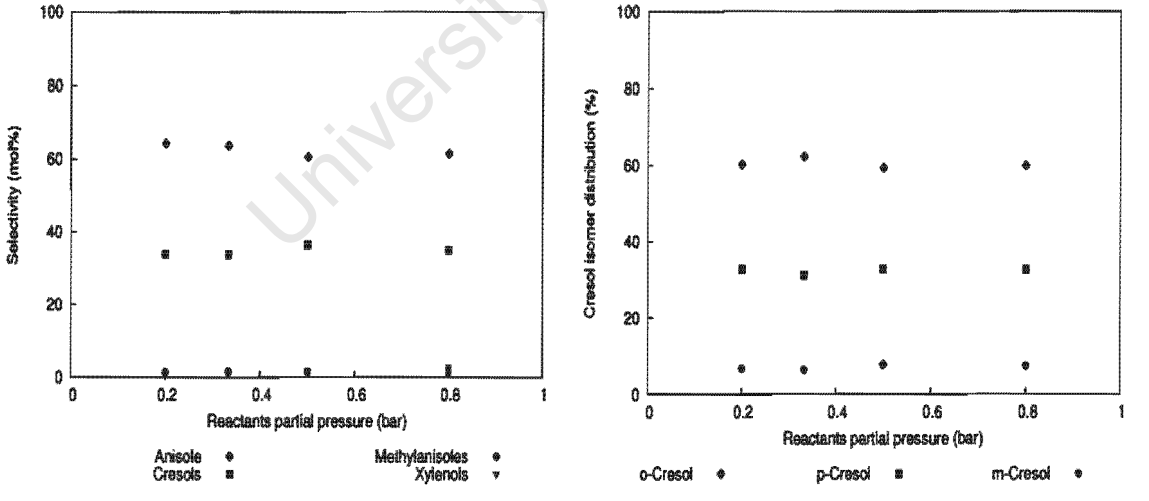

(a) Product selectivity

(b) Cresol isomer distribution

Figure 7.43: The effect of reactants partial pressure on product selectivity and cresol isomer distribution over H-MCM-22 (UCT) (reaction conditions: 300°C, total pressure = 1 bar, methanol : phenol molar ratio = 1, WHSV = 7.5 h^{-1}, varying reactants partial pressure).

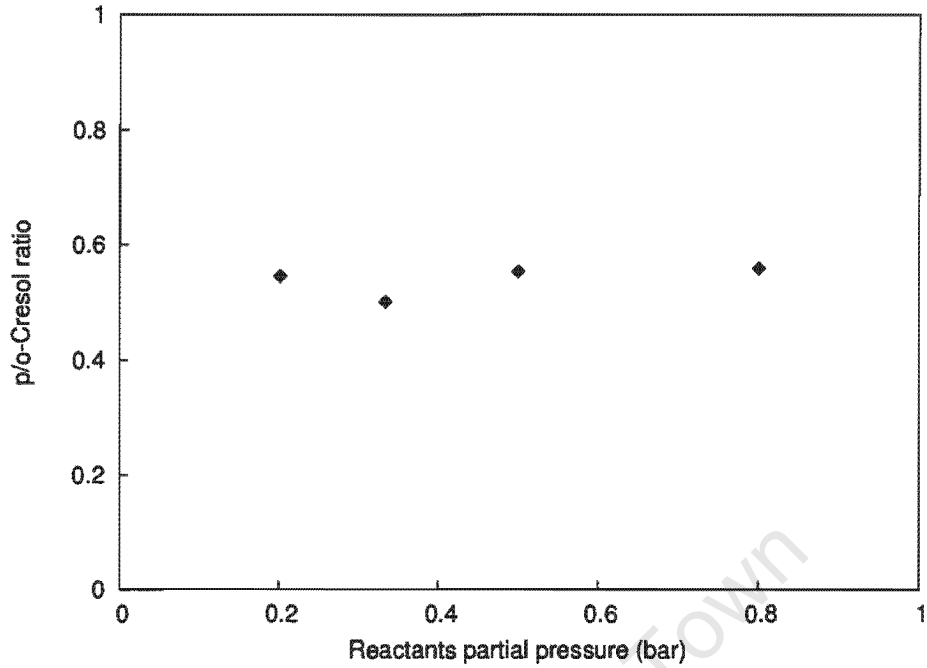

Figure 7.44: The effect of reactants partial pressure on the p/o-cresol ratio over H-MCM-22 (UCT) (reaction conditions: 300°C, total pressure = 1 bar, methanol : phenol molar ratio = 1, WHSV = 7.5 h^{-1}, varying reactants partial pressure).

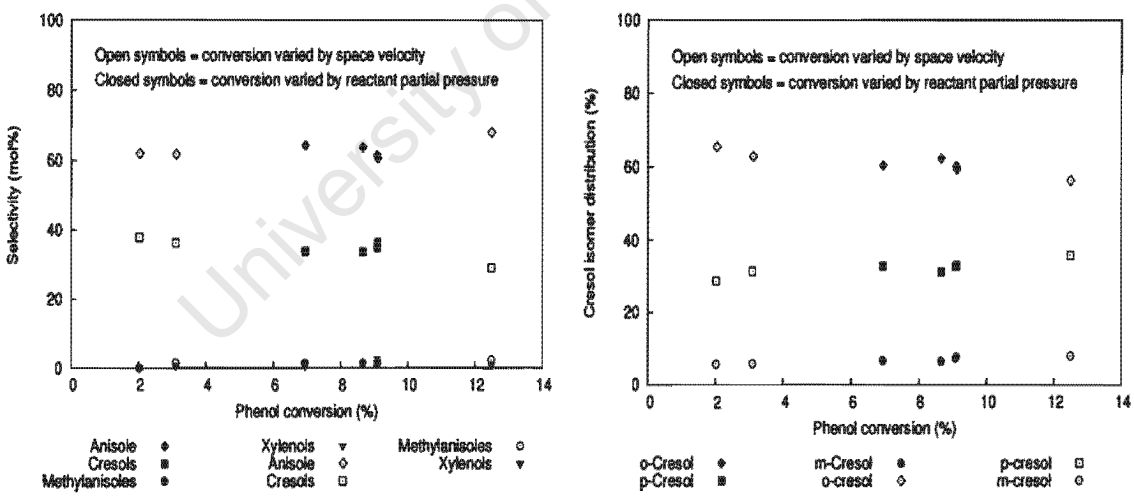

(a) Product selectivity

(b) Cresol isomer distribution

Figure 7.45: The effect of reactants partial pressure and conversion on product selectivity and cresol isomer distribution over H-MCM-22 (UCT). Phenol conversion varied as a result of varying reactants partial pressure (closed symbols) or was varied by varying weight hourly space velocity (open symbols) with data points in both cases representing the average of quasi-steady state samples (reaction conditions: 300°C, total pressure = 1 bar, methanol : phenol molar ratio = 1, WHSV = 7.5 h^{-1}, varying reactants partial pressure).

Table 7.2: Conversion, product selectivities and product yields from anisole and cresols conversion over H-MCM-22 (UCT) at gas phase standard reaction conditions (300°C, total pressure = 1 bar, reactants partial pressure = 0.2 bar, methanol : phenol molar ratio = 1, WHSV = 14 h^{-1}).

Reactants	Conversion (%)	Selectivity (mol%)				
		Anisole	Cresols	Methylanisoles	Xylenols	Phenol
Anisole	6.5	-	19.2	37.8	2.1	40.9
Anisole/phenol*	3.7**	-	68.8	12.7	1.5	17.1
o-Cresol	3.9	0.2	68.0	0.0	15.9	15.9
p-Cresol	7.3	0.7	88.2	0.0	5.7	5.4
m-Cresol	3.6	0.0	97.7	0.0	1.2	1.1

* Anisole/phenol 1:1 molar mixture;
** Anisole conversion.

Reactants	Yields (mol %)				
	Anisole	Cresols	Methylanisoles	Xylenols	Phenol
Anisole	-	1.2	2.5	0.1	2.7
Anisole/phenol*	-	2.5	0.5	0.1	0.6
o-Cresol	0.01	2.7	0.0	0.6	0.6
p-Cresol	0.1	6.4	0.0	0.4	0.4
m-Cresol	0.0	3.5	0.0	0.05	0.05

* Anisole/phenol 1:1 molar mixture.

The conversion of the pure cresol isomers over H-MCM-22 (UCT) results mainly in isomerization products and less in the transalkylation products (xylenols and phenol). With regard to transalkylation products, o-cresol shows the highest selectivity, whereas m-cresol is almost non-reactive. In the isomerization of o- and p-cresol, m-cresol is the major product. Isomerizing m-cresol mainly yields the p-isomer.

Table 7.3: Cresol distribution from the conversion of anisole and cresols over H-MCM-22 (UCT) at gas phase standard reaction conditions (300°C, total pressure = 1 bar, reactants partial pressure = 0.2 bar, methanol : phenol molar ratio = 1, WHSV = 14 h^{-1}).

Reactants	o-Cresol (%)	p-Cresol (%)	m-Cresol (%)	p/o-Cresol ratio
Anisole	69	11	20	0.16
Anisole/phenol*	53	28	19	0.53
o-Cresol	-	15	85	-
p-Cresol	9	-	91	-
m-Cresol	26	74	-	2.85

* Anisole/phenol 1:1 molar mixture.

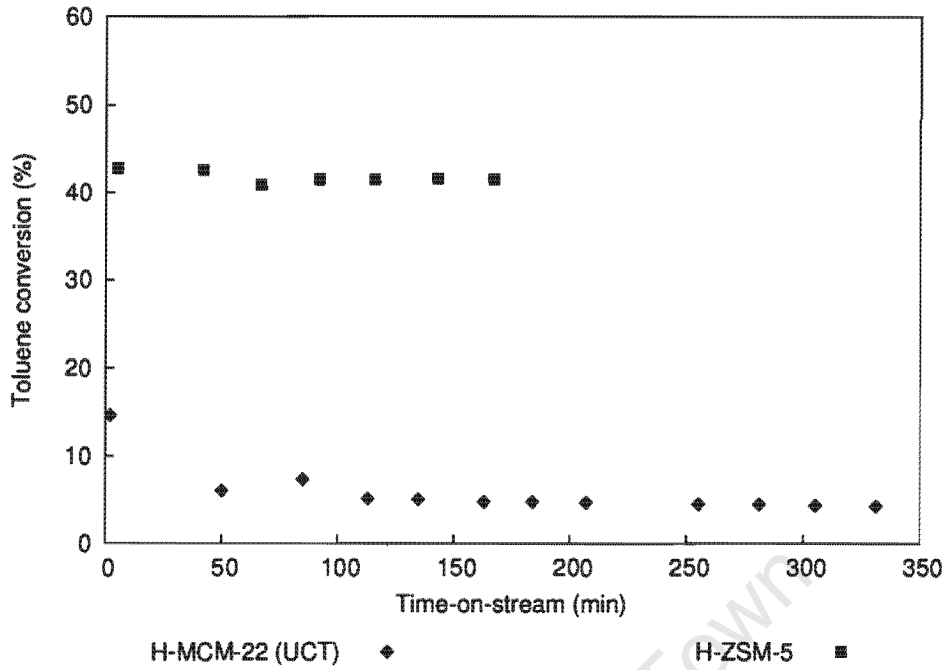

Figure 7.46: Toluene conversion for the toluene methylation reaction over H-ZSM-5 and H-MCM-22 (UCT) at gas phase standard reaction conditions (300°C, total pressure = 1 bar, reactants partial pressure = 0.2 bar, methanol : toluene molar ratio = 1, WHSV = 14 h^{-1}).

7.7 Alkylation of toluene with methanol over H-ZSM-5 and H-MCM-22 (UCT)

The alkylation of toluene with methanol was carried out as a test reaction intended to compare the effect of the hydroxyl group with the effect of a methyl group on a benzene ring on the methylation reaction. It was hypothesised that the methanol would interact significantly different with the $-OH$ group of the phenol and the $-CH_3$ group of the toluene. The toluene alkylation was carried out at gas phase standard reaction conditions (cf. Table 7.1, expect that the methanol : phenol ratio is replace by the methanol : toluene ratio).

Higher conversion was obtained in toluene methylation than in phenol methylation (Figure 7.46) as well as almost immediate stabilisation of catalyst activity (cf. Figures 7.9 and 7.11). The difference was more pronounced over H-ZSM-5 (four-fold) than H-MCM-22 (UCT), where it was less than double in the quasi-steady state. In terms of toluene methylation, H-ZSM-5 was approximately 10 times more active than H-MCM-22 (UCT) (Figure 7.46).

Over H-ZSM-5, xylenes and trimethylbenzenes were the major products formed from toluene alkylation with methanol (Figure 7.47 (a)). In terms of the xylene isomer distribution, o-xylene was slightly favoured over an equal percentage of p- and m-xylene (Figure 7.47 (b)). The equilibrium distribution of the xylene isomers at 300°C was o : p : m = 23 : 22 : 55 calculated from Stull's *et al.* [1969] data. So o- and p-xylene appear equilibrated, not so for m-xylene.

Over H-MCM-22 (UCT), xylenes and trimethylbenzenes were also the major products (Figure 7.48 (a)). But selectivity towards the latter was significantly lower. The cresol isomer distribution

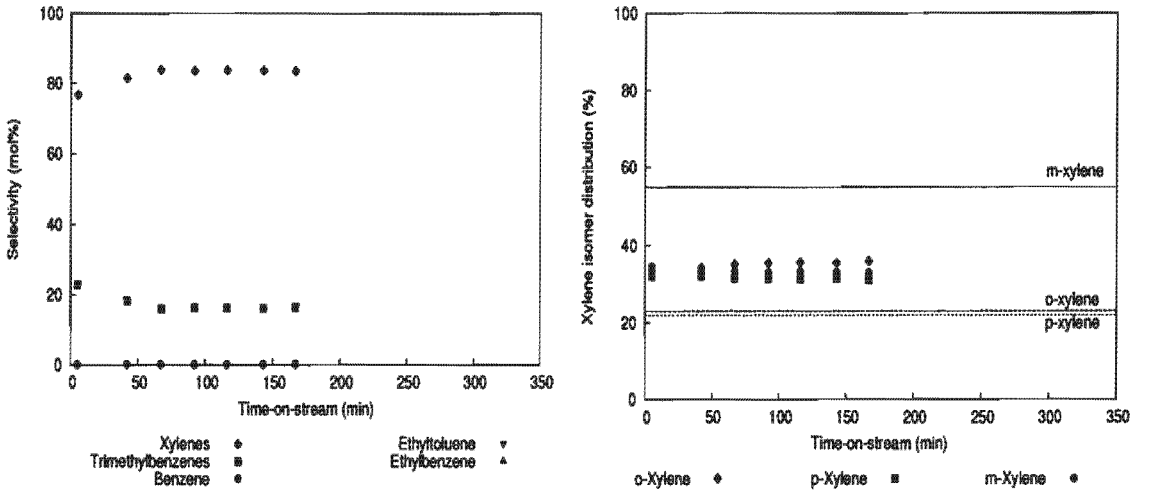

(a) Product selectivity

(b) Xylene isomer distibution

Figure 7.47: Product selectivity and xylene isomer distribution obtained from toluene methylation over H-ZSM-5 at gas phase standard reaction conditions (300°C, total pressure = 1 bar, reactants partial pressure = 0.2 bar, methanol : toluene molar ratio = 1, WHSV = 14 h^{-1}). Horizontal lines in figure (b) represent thermodynamic equilibrium as calculated using Stull's et al. [1969] data.

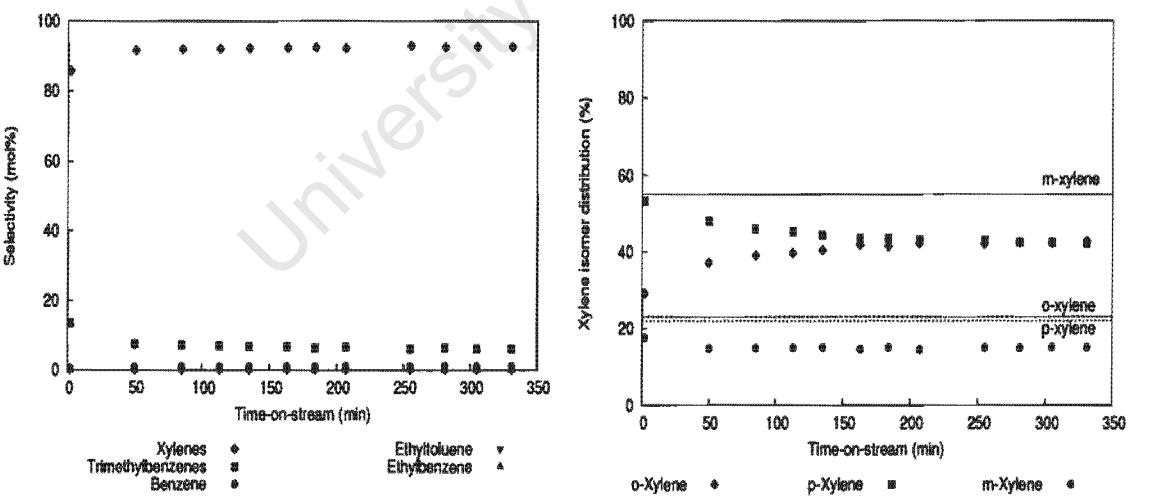

(a) Product selectivity

(b) Xylene isomer distribution

Figure 7.48: Product selectivity and xylene isomer distribution obtained from toluene methylation over H-MCM-22 (UCT) at gas phase standard reaction conditions (300°C, total pressure = 1 bar, reactants partial pressure = 0.2 bar, methanol : toluene molar ratio = 1, WHSV = 14 h^{-1}). Horizontal lines in figure (b) represent thermodynamic equilibrium as calculated using Stull's et al. [1969] data.

differed to that obtained over H-ZSM-5 in that a much lower percentage of m-xylene was found, whereas equal percentage of o- and p-xylene at steady state indicate equilibrium between these two isomers again (Figure 7.48 (b)).

Table 7.4 compares the product selectivities obtained from toluene alkylation and phenol alkylation over both H-ZSM-5 and H-MCM-22 (UCT) in the quasi-steady state and at similar conversions (as far as possible). As discussed above, conversion were higher for the aromatic hydrocarbon compared to phenol. Di-methylation is more prevalent with toluene than with phenol. The percentage of the m-isomer is much higher in the xylenes fraction from toluene methylation than in the cresols fraction from phenol methylation, in particular over H-ZSM-5. The p/o-ratio is around 0.5 in cresols but around 1 in the xylenes.

7.8 Summary

All results were obtained under the gas phase standard reaction conditions (300°C, total pressure = 1 bar, reactants partial pressure = 0.2 bar, methanol : phenol molar ratio = 1, WHSV = 14 h^{-1}) with just one parameter being changed in the parameter variation studies. In summary, the key results for the low pressure gas phase alkylation of phenol with methanol, carried out in a continuous plug flow reactor system, are:

Reproducibility

- Experimental results are reproducible with minor scatter;

Material balances

- Material balances based on carbon balances, including methanol and light by-products, came out even;

Influence of conversion on selectivity

- Phenol conversion, varied via setting different space velocities, moderately influenced selectivity.
- The selectivity to cresols decreased and the selectivity to anisole increased as conversion increased;
- The cresol isomer distribution showed a moderate decrease in o-cresol and a corresponding increase in both p- and m-cresol;

Influence of deactivation on selectivity

- Besides the indirect effect of declining conversion there was a direct effect, which deactivation had on selectivity;
- This direct effect was found to be opposite to the indirect effect, i.e. deactivation resulted in anisole selectivity to increase and cresol selectivity to decrease;
- There was no effect of deactivation on the cresol isomer distribution;

Table 7.4: Comparison of toluene alkylation with phenol alkylation over H-ZSM-5 and H-MCM-22 (UCT) under gas phase standard reaction conditions (300°C, total pressure = 1 bar, reactants partial pressure = 0.2 bar, methanol : phenol or methanol : toluene molar ratio = 1, WHSV = 14 h^{-1}).

H-ZSM-5	Toluene alkylation steady state average	H-ZSM-5	Phenol alkylation steady state average	Phenol alkylation Initial sample
Toluene conversion (%)	41.4	Phenol conversion (%)	10.2	19.6
Product selectivities (mol%)		Product selectivities (mol%)		
Ethylbenzene	0.1	Anisole	59.6	49.0
Xylenes	83.4	Cresols	37.6	47.4
Trimethylbenzenes	16.3	Xylenols	0.7	2.9
Other	0.2	Other	2.1	0.7
Xylene isomer distribution (%)		Cresol isomer distribution (%)		
o-	35.6	o-	61.8	64.7
p-	31.4	p-	34.0	31.6
m-	33.0	m-	4.2	3.7
p/o-Xylene ratio	0.88	p/o-Cresol ratio	0.55	0.49

H-MCM-22 (UCT)	Toluene alkylation steady state average	H-MCM-22 (UCT)	Phenol alkylation steady state average	Phenol alkylation 140 hours sample*
Toluene conversion (%)	4.3	Phenol conversion (%)	3.8	4.3
Product selectivities (mol%)		Product selectivities (mol%)		
Ethylbenzene	0.0	Anisole	61.9	60.1
Xylenes	92.8	Cresols	36.3	37.9
Trimethylbenzenes	6.0	Xylenols	0.5	1.1
Other	1.2	Other	1.3	0.9
Xylene isomer distribution (%)		Cresol isomer distribution (%)		
o-	42.7	o-	62.9	61.5
p-	42.2	p-	31.3	32.6
m-	15.1	m-	5.8	5.9
p/o-Xylene ratio	0.99	p/o-Cresol ratio	0.50	0.53
Thermodynamic equilibrium p/o-xylene ratio	0.96**	Thermodynamic equilibrium p/o-cresol ratio	ca. 0.43***	

* Time-on-stream;

** Thermodynamic equilibrium calculated using Stull *et al.* [1969] data at 300°C;

*** Thermodynamic equilibrium as found by Böhringer and Fletcher [2003] at 350°C.

Comparison of catalysts studied

- The catalysts activities in the quasi-steady state decreased in the following order: H-ZSM-5 > H-MCM-22 (DE2) >> H-MCM-22 (DE3) > H-MCM-22 (DE1) > H-MCM-22 (UCT) > amorphous silica-alumina;
- H-MCM-22 samples, consistently, showed a more pronounced initial decline of activity than the other catalysts;
- Anisole, o-cresol and p-cresol were the major products;
- m-Cresol and higher methylated compounds (methylanisoles and xylenols) were obtained in trace amounts;
- O-alkylation was favoured over C-alkylation, at 300°C, over all the catalysts studied except for H-MCM-22 (DE1);
- p/o-Cresol ratios were between 0.37 (amorphous silica-alumina) and 0.97 over H-MCM-22 (DE2);
- The percentage of the m-isomer in the cresol fraction was low over all the catalysts studied (< 5%);

Effect of secondary modification of zeolite catalysts

- Internally selectively sodium-exchanged H-ZSM-5 and H-MCM-22 (UCT)
  - Catalyst activity decreased substantially over the internally selectively sodium-exchanged zeolites H/Na-ZSM-5 and H/Na-MCM-22 (UCT);
  - The only relevant effect on selectivity was obtained over H/Na-ZSM-5, where the O/C-alkylation of 0.41 was obtained compared to 1.7 over the pure acid zeolite;
- Steaming H-MCM-22 (DE1)
  - Steaming resulted in an enhanced activity by approximately 3 times;
  - Steaming resulted in a reversal in the O/C-alkylation ratio;
  - Steaming hardly effected the cresol isomer distribution;
  - Essentially, the results from steaming reflect the influence of conversion;

Effect of reaction parameters, studied with H-MCM-22 (UCT)

- Reaction temperature
  - Phenol conversion increased exponentially with increasing reaction temperature;
  - Reaction temperature does directly affect the product selectivity and cresol isomer distribution;

  - The O/C-alkylation ratio passed through a maximum at ca. 270°C;
  - Above 360°C, C-alkylation was favoured over O-alkylation;
  - The highest p/o-cresol ratios of 0.5 were obtained at the lowest reaction temperatures studied, namely 200 - 270°C;
  - Above 270°C, p/o-cresol ratios declined to quite low values (0.28 at 400°C);

- Methanol : phenol ratio

  - Phenol conversion increased significantly with increasing methanol : phenol ratio;
  - There was no direct effect of methanol : phenol ratio on product selectivity and cresol isomer distribution;
  - Observed changes in selectivity were in fact an indirect effect of changing conversion;

- Space velocity

  - Phenol conversion decreased with increasing space velocity;
  - Space velocity moderately effected product selectivity;
  - Increasing space velocity increased the cresols selectivity, decreased the anisole selectivity;
  - Increasing space velocity decreased the p/o-cresol ratio;

- Reactants partial pressure

  - Phenol conversion increased sharply between 0.2 and 0.34 bar reactant partial pressure and then levelled out;
  - Reactant partial pressure did not directly effect the product selectivity nor the cresol isomer distribution in the range studied;
  - The effect of reactant partial pressure on product selectivity and cresol isomer distribution was in fact an indirect result of changing conversion;

Conversion of the major products of phenol methylation over H-MCM-22 (UCT)

- Conversion of pure anisole resulted mainly in the formation of methylanisoles and phenol by transalkylation. Of the cresol fraction formed, the majority was o-cresol;

- Dilution of anisole with phenol resulted in reduced anisole conversion, substantially reduced formation of transalkylation products and mainly in the formation of cresols, preferentially o-cresol;

- Conversion of pure cresols resulted mainly in the isomerization to the other cresols. m-Cresol was the favoured isomer from o- and p-cresol, p-cresol was the favoured isomer from m-cresol;

Alkylation of toluene with methanol over H-ZSM-5 and H-MCM-22 (UCT)

- Both catalysts were more active for toluene methylation than phenol methylation;
- In the toluene methylation, mainly xylenes and trimethylbenzenes were formed;
- Di-methylation was more pronounced with the toluene than with the phenol;
- H-ZSM-5 produced almost equal amounts of the three different xylene isomers, whereas over H-MCM-22 (UCT) the m-isomer was suppressed;
- Over both catalysts, the p- and o-xylene appear to be in equilibrium.

Response of phenol conversion, O/C-alkylation ratio and p/o-cresol ratio on the variation of reaction parameters and catalyst

- Phenol conversion
  - Phenol conversion decreased with time-on-stream but settled on a quasi-steady state level after 3 - 4 hours;
  - Highest quasi-steady state phenol conversion obtained over H-ZSM-5 and steamed H-MCM-22 (DE1);
  - Sodium-exchanging the internal acid sites, reduced phenol conversion substantially;
  - Phenol conversion increased with decreasing space velocity, increasing reaction temperature, increasing methanol : phenol ratio and increasing reactants partial pressure;
- O/C-alkylation ratio
  - O/C-alkylation ratio increased moderately with increasing conversion;
  - Highest quasi-steady state O/C-alkylation ratio of 2.7 was observed over H-MCM-22 (DE2) and lowest ratios of 0.8 and 0.4 were observed over H-MCM-22 (DE1) and internally selectively sodium-exchanged H/Na-ZSM-5 respectively, which were the only samples with an O/C-alkylation ratio < 1;
  - O/C-alkylation ratio increased with increasing methanol : phenol ratio, increasing reactants partial pressure (initially) and steaming. All these effects, however, are of indirect nature, only reflecting the effect of increasing conversion;
  - O/C-alkylation ratio decreased with increasing temperature above 270°C and increasing weight hourly space velocity;
  - Reaction temperature is the only reaction parameter which produced a direct effect on product selectivity and cresol isomer distribution;
- p/o-Cresol ratio
  - p/o-Cresol ratio increased moderately with increasing conversion;

- Highest quasi-steady state p/o-cresol ratio of 0.97 was observed over H-MCM-22 (DE2) and lowest ratio of 0.37 and 0.47 were observed over amorphous silica alumina and H-MCM-22 (DE1), respectively;
- Internally selectively sodium-exchange of the internal acid sites had no effect on the p/o-cresol ratio;
- p/o-Cresol ratios over the acid zeolites were around 0.5 or higher;
- p/o-Cresol ratio over amorphous silica-alumina was lower than those obtained over zeolites at approximately 0.38;
- p/o-Cresol ratio increased slightly with decreasing space velocity, increasing reactants partial pressure, increasing methanol : phenol ratio and steaming. All these effects, however, are of indirect nature, only reflecting the effect of increasing conversion;
- p/o-Cresol ratio decreased with increasing reaction temperature in particular above 270°C;
- Reaction temperature is the only reaction parameter which produced a direct effect on p/o-cresol ratio.

Chapter 8

Discussion

This chapter discusses the results obtained in the thesis in the study of the phenol alkylation with methanol over the different, mainly zeolites, catalysts. It begins with a discussion on whether the reaction is thermodynamically or kinetically controlled under the reaction conditions used in this study (cf. Chapter 4). This is followed by a discussion of the effect of phenol conversion on product selectivity since in the absence or presence of an effect different catalysts can or cannot be compared at different conversions. The reaction mechanism is then evaluated by considering the conversion of the major product species (anisole, o-cresol and p-cresol) and the effect of reaction conditions, namely reaction temperature, methanol : phenol ratio, space velocity, reactant partial pressure and influence of water. This is followed by a comparison of the product selectivities obtained over the different catalysts. The effect of the different reaction phases or reaction pressure on the product selectivity is then discussed and also the question of possible competitive adsorption between phenol and methanol. The chapter ends with the comparison of toluene methylation and phenol methylation in order to probe briefly the extent to which the hydroxyl group on phenol has a different structure directing influence than the methyl group on toluene.

8.1 Thermodynamic equilibria versus kinetics

Anisole was found to be the preferred product formed over all the catalysts, both in the liquid phase and gas phase. From a consideration of thermodynamic equilibria, however, it is predicted that cresols and not anisole will almost exclusively be formed at the temperatures and pressures investigated in this study (cf. Sections 2.2.2.4 and 2.2.2.5). Also, no m-cresol was formed over any of the catalysts studied at low temperature (200 - 250°C) in the liquid phase (cf. Table 6.5) and a small amount of m-cresol was formed at elevated temperatures (300 - 400°C) in the gas phase (less than 5% of the cresol fraction, cf. Figures 7.10, 7.12 and 7.14) even though m-cresol is thermodynamically the most stable cresol isomer (cf. Section 2.2.2.6).

Since the hydroxyl group on the benzene ring is known kinetically to be strongly ortho- and para-directing (cf. Section 2.2.1.3), these product distributions clearly indicate that under the reaction conditions used in this study, the phenol methylation reaction is kinetically and not thermodynamically controlled.

It was observed that the p/o-cresol ratios obtained over some of the catalysts in the liquid and gas

phases are close to the thermodynamic equilibrium ratio (0.43 reported by Böhringer and Fletcher [2003] at 350°C (cf. Figure 2.33)). However, this does not infer thermodynamic equilibria between the two isomers as the p/o-cresol ratio is also close to the statistical ratio, viz 0.5 which is the statistical ratio expected due to the possibility of methylating the two ortho positions on the phenol compared to only the one para position which exists).

8.2 Product selectivity as a function of phenol conversion

8.2.1 The direct influence of conversion

In the low temperature, high pressure liquid phase studies (200°C, batchwise), the phenol conversions for all the catalysts were held less than 16%, i.e. the reaction was operated differentially. Phenol conversion was varied by a factor of 10, approximately, by varying reaction time and the reactants : catalyst mass ratio. For all the catalysts studied the product selectivity and cresol isomer distribution was found to be essentially independent of phenol conversion (as shown in Figures 6.1 and 6.2). This indicates that no secondary reactions occur under the given reaction conditions and thus allows the comparison of the product selectivities obtained over the catalysts at different phenol conversions.

In the high temperature, low pressure gas phase studies the effect of changing phenol conversion on product selectivity was studied by varying the space velocity as shown in Figures 7.2 and 7.3. Comparison in the quasi-steady state region shows that the phenol conversion, varied by changing space velocity, influenced the product selectivity significantly. However, this influence was restricted to increasing the anisole selectivity and correspondingly decreasing the o-cresol selectivity with increasing phenol conversion. All other selectivities remained unchanged. This is apparent when considering the effect of conversion on anisole and cresol isomers (Figure 7.3 (c)). The possible reason for this very specific product change is discussed in Section 8.3.4.

8.2.2 The influence of deactivation

At the low reaction temperatures used in the liquid phase experiments (200°C), the phenol conversion was varied by both reaction time and reactants : catalyst mass ratio which produced similar results (cf. Figure 6.1 and 6.2). This indicates that no noticeable deactivation occurred in the liquid phase under the reaction conditions studied.

At higher reaction temperatures, such as those used in the gas phase studies (300 - 400°C), the catalysts deactivated rapidly over the first two hours-on-stream and then reached a quasi-steady state with respect to phenol conversion (cf. Figures 7.4, 7.16, 7.23 and 7.26). Surprisingly, this was accompanied by little or no change (the former essentially being in the very beginning of the experiments) in product selectivity with time-on-stream (cf. Figures 7.10, 7.12, 7.14, 7.17 - 7.19, 7.24, 7.25, 7.27 and 7.28) and corresponding with changing of conversion (cf. Figures 7.5 and 7.6).

There are two opposite effects that influence the product selectivity with time-on-stream at elevated temperatures in the gas phase, namely the deactivation by coke deposition and the corresponding change in the phenol conversion. The effect of the latter is discussed in Section 8.2.1.

So why does time-on-stream behaviour i.e. the significant decline of conversion due to deactivation, have only a minor effect on selectivity despite the major change in conversion? The true effect of

deactivation on product selectivity has been derived in Section 7.3.2. Figure 7.7 shows that anisole selectivity increases and at the same time cresol selectivity decreases with decreasing phenol conversion due to deactivation. This could be due to increasing coke formation which increases the diffusional resistances in the zeolite pores or at the pore openings on the zeolite cystallite's surface, respectively, thereby increasing the preference for the slimmest molecule viz. anisole.

Therefore, the true effect of deactivation and the effect of the corresponding increasing conversion at elevated temperature in the gas phase counteract against each other resulting in an overall none or little effect on product selectivity with time-on-stream, the only reasonably relevant effect being anisole selectivity and - in the opposite direction - cresols selectivity.

In the liquid phase, however, the results discussed in Section 8.2.1 stating that the selectivities are independent of phenol conversion, give the true effect of conversion and is not countered by deactivation as was found in the gas phase.

8.3 Reaction mechanism

In the alkylation of phenol with methanol the products observed in this study were anisole, o-, p- and m-cresol, methylanisoles and xylenols. The proposed overall mechanism for the alkylation of phenol with methanol was derived from the results obtained by investigating the phenol methylation reaction, product selectivities, product conversions (namely anisole and cresols), the effect of reaction temperature, the effect of methanol : phenol ratio, the effect of reactants partial pressure, the effect of weight hourly space velocity and the influence of water.

8.3.1 Conversion of product species

The conversion of each of the major reaction products (namely, anisole, o-cresol and p-cresol) over the different catalysts was studied to aid in the understanding of the reaction pathway. These reactions were carried out in the liquid and gas phase and the results were presented in Tables 6.11 to 6.16, 7.2 and 7.3.

8.3.1.1 Anisole conversion

Anisole converted over the different catalysts to form methylanisoles, cresols, xylenols and phenol with methylanisoles and phenol as the major products. Methylanisoles are formed from a bimolecular interaction between two anisole molecules (Figure 8.1) and phenol is a by-product of this reaction. o-Cresol can be formed via a monomolecular methyl shift from anisole (cf. Figure 2.38) or from dealkylation of methylanisole (cf. Figure 2.49). p-Cresol can be formed from o-cresol via two successive 1,2-methyl shift reactions (cf. Figure 2.31) or from the dealkylation of methylanisole (cf. Figure 2.49). m-Cresol can be formed from o- or p-cresol via a single 1,2-methyl shift reaction (cf. Figure 2.31). p-Cresol and m-cresol were formed in the gas phase anisole conversions over H-MCM-22 (UCT) thus indicating the existence of the above mentioned reactions. In the liquid phase no m-cresol was found in the product over any of the catalysts studied and therefore it can be deduced that p-cresol must be formed by a route other than the 1,2-methyl shift isomerization reactions of o-cresol. Jacobs *et al.*

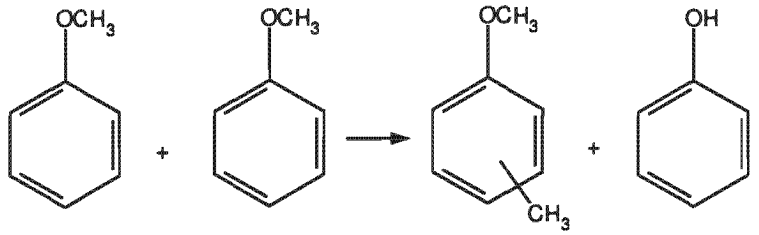

Figure 8.1: Bimolecular formation of methylanisoles from anisole.

[1988] also observed that at low temperature of 180°C, p-cresol was not formed from o-cresol via the 1,2-methyl shift reactions.

Anisole was also reacted in the presence of phenol to determine the influence of phenol on the product selectivities. Cresols were the major product formed from the anisole/phenol mixture. An anisole molecule reacting with a phenol molecule forms cresol and another phenol as shown in Figure 8.2. As the formation of methylanisoles from two anisole molecules also results in the formation of a phenol molecule (Figure 8.1), this phenol could in fact react with another anisole to form cresol, thereby resulting in an autocatalytically reacting system.

The presence of phenol with anisole resulted in the anisole conversion decreasing from 21% (anisole feed) to 1% (anisole/phenol feed) over H-MCM-22 (UCT) in the liquid phase. This decrease can not be explained in terms of dilution of the anisole with phenol. It indicates instead that the anisole is inhibited from reacting further by the presence of phenol. In the gas phase, the decrease in the conversion (from 6.5% (anisole feed) to 3.6% (anisole/phenol feed)) over H-MCM-22 (UCT) can be explained by the dilution of anisole with phenol which predicts that the conversion will decrease by a factor of 2. The measured anisole conversion in fact decreased by factor of 1.8. Therefore, in the gas phase, the presence of the phenol does not inhibit the anisole from reacting further.

In the gas phase, the cresols yield from the reaction of the anisole/phenol mixture over H-MCM-22 (UCT) was 2.5%. If the co-product phenol formed (shown in Figure 8.2) is included the yield of both the cresol and phenol was 5.0 %. If it is assumed that the reactivity of the anisole and phenol pair is the same as the anisole and anisole pair, the yield of cresols and phenol would be expected to be 2.4% (yield of cresols from reaction of anisole was 1.2%, cf. Table 7.2). But it is in fact double the expected yield which reflects the higher reactivity of phenol towards ring alkylation. This is consistent with the findings of Marczewski *et al.* [1989] that the alkylation of phenol by anisole was twice as fast as the alkylation of anisole by anisole over H-USY. This is a result of the hydroxyl group (phenol) being a much more effective activator of the benzene ring for electrophilic substitution than a methoxy group (anisole) [Sykes, 1986b; Morrison and Boyd, 1987].

The p/o-cresol ratio increased in the presence of phenol from 0.16 (anisole feed) to 0.53 (anisole/phenol feed) over H-MCM-22 (UCT) in the gas phase indicating that the reaction of anisole with phenol preferentially forms p-cresol. The increase in p/o-cresol may be due to a decrease in the intramolecular rearrangement of anisole to o-cresol in the presence of phenol in favour of the bimolecular alkylation of phenol with anisole, which as stated above is a faster reaction than the self-alkylation of anisole.

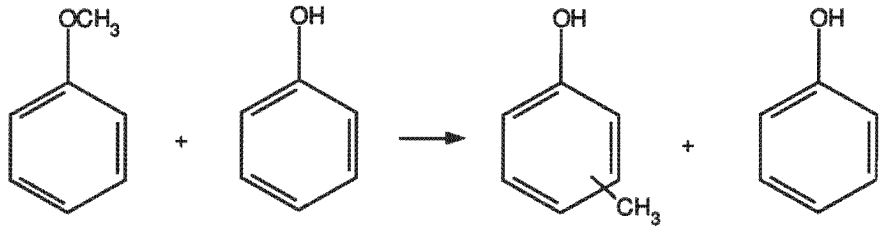

Figure 8.2: Cresol formation from anisole and phenol.

8.3.1.2 Cresol conversions

Cresol isomerization can occur via 1,2-methyl shift or via transalkylation reactions (cf. Section 2.2.4.3 and Figures 2.31 and 2.45) or by subsequent disproportionation reactions to first yield xylenols and phenol and then the different cresol isomers (cf. Section 2.2.6.2 and Figure 2.55). The isomerization of o-cresol and p-cresol yields the thermodynamically favoured isomer m-cresol as expected via 1,2-methyl shift in the gas phase.

In the liquid phase experiments, however, no m-cresol was found over any of the catalyst studied. This indicates that the cresol isomerization reaction via a 1,2-methyl shift does not occur. Also in the liquid phase, the conversion of the o-cresol and p-cresol are very low (less than 1%) indicating that conversion of the cresol isomers to the other isomer via isomerization and to xylenols via disproportionation essentially does not occur at the low reaction temperature used in the study (200°C).

In the gas phase over H-MCM-22 (UCT), the cresols conversions are between 4% and 7% with relatively high m-cresol selectivities indicating that these reactions do occur. The isomerization to disproportionation ratio was found to be 2.2 for reaction of o-cresol, 7.7 for the reaction of p-cresol and 40.7 for the reaction of m-cresol (isomerization to disproportionation ratio as defined by Imbert *et al.* [1997a]). Thus, for the reaction of m-cresol, the major reaction is the isomerization via a 1,2-methyl shift whereas for o-cresol and p-cresol reactions, isomerization to m-cresol via a 1,2-methyl shift was also the major reaction but the disproportionation does also occur.

In the reaction of cresols in the gas phase, anisole formed less than 0.7 mol% of the product distribution and as already stated, the cresols did not react further in the liquid phase. This shows that the anisole is not formed from cresols in either phase and therefore that anisole is formed only as a primary product.

8.3.2 Effect of reaction temperature

The effect of reaction temperature on the product selectivities (cf. Figure 7.30 (a)) can be divided into low temperature and high temperature effects. At the low temperature (200 - 270°C) as used in the liquid phase experiments, increasing the temperature influences the apparent reaction rate constants (cf. Section 8.6). At the higher temperatures (300 - 400°C) as used in the gas phase experiments, the approach to thermodynamic equilibrium influences the product selectivity resulting in an increase in the cresol selectivity and an increase in the amount of m-cresol in the cresol fraction.

In both phases the O/C-alkylation decreased with increasing reaction temperature and this is consistent with findings of Pierantozzi and Nordquist [1986]; Parton *et al.* [1989a]; Santacesaria *et al.* [1990b]; Bautista *et al.* [1993]; Landau *et al.* [1997] and Balasubramanian *et al.* [2000]. Balasubra-

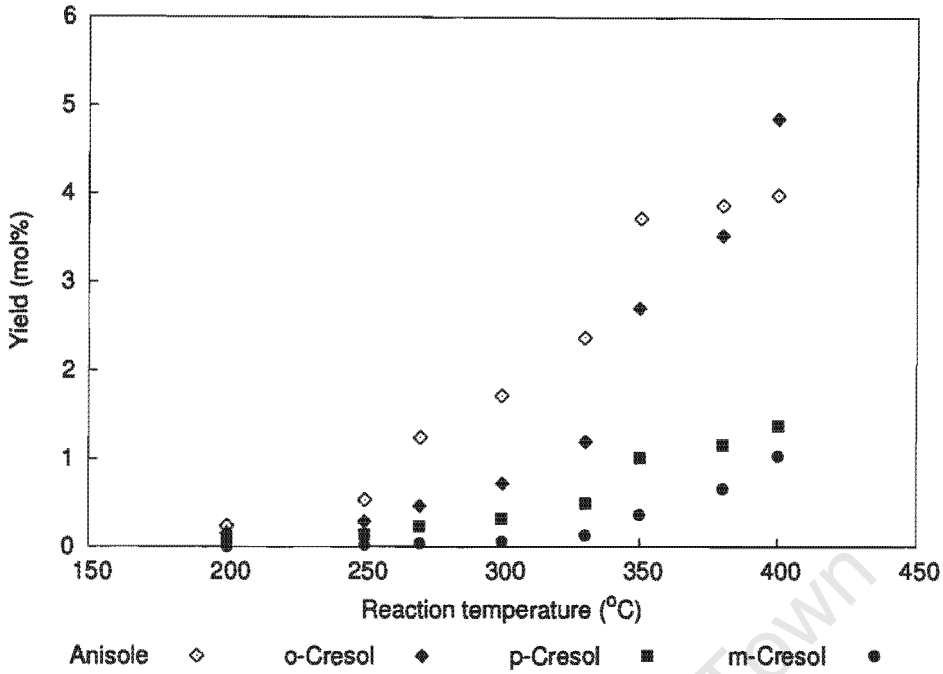

Figure 8.3: Yields of anisole, o-cresol, p-cresol and m-cresol from the gas phase phenol methylation reaction as a function of reaction temperature.

manian *et al.* [2000] and Santacesaria *et al.* [1990b] disagree on the reason for the decrease in anisole selectivity with increasing reaction temperature. Balasubramanian *et al.* [2000] stated that it may be due to the conversion of anisole to o-cresol whereas Santacesaria *et al.* [1990b] stated it was due to the higher activation energy required for C-alkylation which would increase the C-alkylation selectivity with increasing reaction temperature.

Figure 8.3 shows the yields of anisole, o-cresol, p-cresol and m-cresol for the gas phase phenol methylation reaction as a function of reaction temperature. The sudden change at 350°C is unexpected because there was no change in experimental system, procedure or catalyst. As can be seen in Figure 8.3, at the higher temperatures (above 350°C) the yield of anisole only increased slightly whereas the yield of o-cresol increased sharply. This indicates that increasing the reaction temperature increased the internal rearrangement of anisole to o-cresol which is in agreement with Balasubramanian *et al.* [2000].

The reaction temperature has the largest influence on the primary reactions (cf. Figures 6.7 and 7.30(a)), namely O-alkylation and C-alkylation to anisole and cresols, respectively. The apparent activation energies for O-alkylation and C-alkylation were determined via the Arrhenius equation (Equation 8.1).

$$\ln(k) = \ln A - \frac{E}{R}\left(\frac{1}{T}\right) \tag{8.1}$$

where:

- k is the reaction rate constant (see below);
- A is the pre-exponential factor or frequency factor;

- E is the activation energy (J/mol);
- R is the gas constant (8.314 J/mol·K);
- T is the temperature (K).

At differential conversions in a plug flow reactor the mass balance yields the following expression:

$$\frac{W}{F_{A0}} \cdot (-r_A) = X_A \tag{8.2}$$

where:

- W is the weight of catalyst;
- F_{A0} is the entering molar flowrate of species A;
- $(-r_A)$ is the rate of consumption of species A;
- X_A is the conversion of species A.

Thus if the space velocity, F_{A0}/W (moles feed/time.weight of catalyst) is kept constant, as was the case in the present study, it can be assumed that the rate $(-r_A)$ is proportional to the conversion (X_A). Moreover, since $(-r_A) = f(k, C_A)$ it can be assumed that if the exit concentration of the reactants are approximately constant, since $C_A = C_{A0}(1 - X_A)$, then $(-r_A)$ is proportional to the rate constant (k). To distinguish between O-alkylation and the C-alkylation, the rate constant were then taken as proportional to the anisole yield or cresol yield, respectively.

Figures 8.4 and 8.5 show typical Arrhenius plots obtained and the apparent activation energies thus obtained for the different catalysts are summarized in Table 8.1. The large difference in the apparent activation energies between O-alkylation and C-alkylation as found by Santacesaria *et al.* [1990b] over γ-alumina (67 kJ/mol and 134 kJ/mol, respectively, cf. Section 2.2.3.2) was not obtained over the different zeolites studied in this present work. Santacesaria *et al.* [1990a] obtained apparent activation energies over H-ZSM-5, with overall apparent activation energies between 50 and 70 kJ/mol and between 29 and 41 kJ/mol for anisole formation. Similar apparent activation energies were obtained over H-ZSM-5 and the different H-MCM-22 samples (cf. Table 8.1). It is noted that the activation energy required for C-alkylation was higher than that required for O-alkylation over the zeolites studied (except over H-MCM-22 (UCT) in the liquid phase where they were equal). Note that the apparent activation energies were not obtained over zeolite H-Beta in the liquid phase due to very high conversions obtained over H-Beta indicating that it was not in the differential conversion regime.

The low apparent activation energies (less than 50 kJ/mol) obtained over H-ZSM-5 and H-MCM-22 (liquid and gas phase), implies that the reactions are controlled by either diffusion or adsorption. That is, at low temperature high adsorption leads to high surface coverage which favours a maximum reaction rate whereas at higher temperatures, low adsorption leads to lower surface coverage and a decrease in the reaction rate. Santacesaria *et al.* [1990a] also attributed the low activation energies over H-ZSM-5 to intracrystalline diffusion which affected the reaction rates.

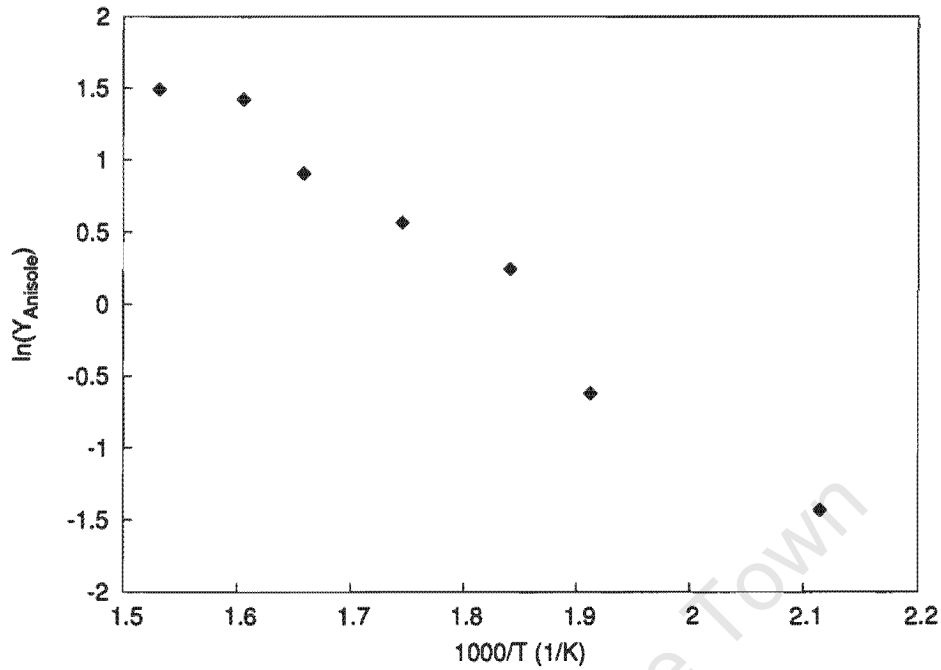

Figure 8.4: Determination of activation energy for O-alkylation over H-MCM-22 (UCT) in the *gas phase.*

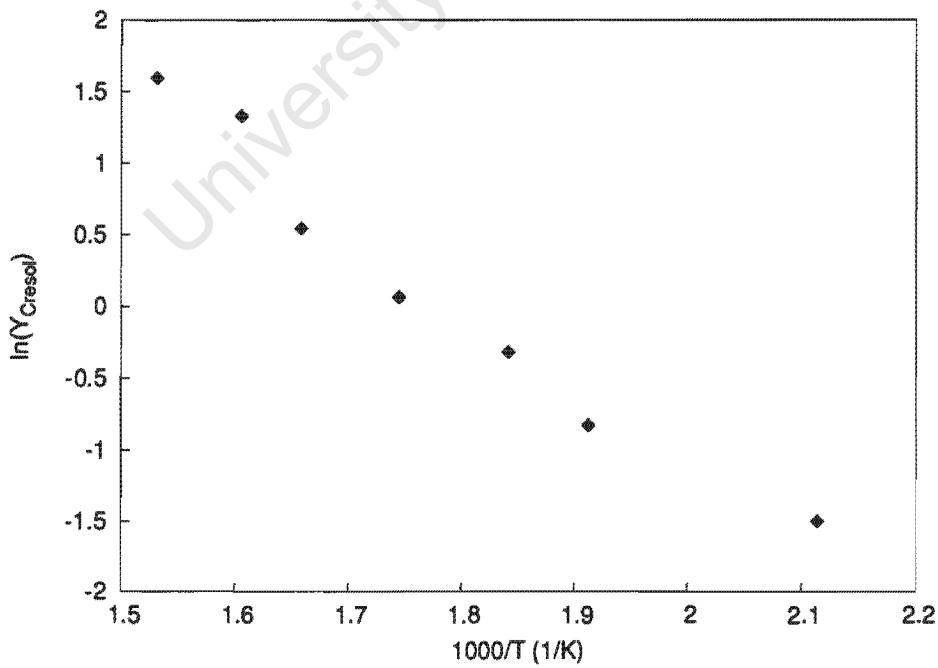

Figure 8.5: Determination of activation energy for C-alkylation over H-MCM-22 (UCT) in the *gas phase.*

Table 8.1: Apparent activation energies over different catalysts.

Catalyst	Reaction phase	Apparent activation energy (kJ/mol)		
		Overall	O-alkylation	C-alkylation
H-ZSM-5	Liquid	38	32	48
H-MCM-22 (UCT)	Liquid	39	39	39
H-MCM-22 (UCT)	Gas	45	42	47

8.3.3 Effect of methanol : phenol ratio

The effect of the methanol : phenol ratio on product selectivity was shown in Figure 6.10 - 6.13 and 7.35 - 7.38. In both phases, as the methanol : phenol feed ratio increased the anisole selectivity increased and the cresol selectivity decreased. Conversely, as the phenol concentration in the feed increased so the selectivity to cresols increased and anisole selectivity decreased. This indicates that cresols are formed from the reaction of anisole and phenol, which is also reflected in results obtained in the reactions of anisole and the anisole/phenol mixture.

In the gas phase (Figure 7.38), changes in the methanol : phenol ratio did not directly affect the product selectivity or the cresol isomer distribution. Instead the methanol : phenol ratio only affected the product selectivity via changing the phenol conversion. As the methanol : phenol ratio has no direct effect of the product selectivity and anisole and cresols are formed by parallel reactions, this indicates that the methylation of phenol to either product must have the same reaction orders in the rate expression with respect to phenol and methanol.

8.3.4 Effect of space velocity

The effect of weight hourly space velocity on the product distribution was studied in the gas phase and was shown in Figures 7.39 to 7.41. Anisole selectivity decreased with increasing space velocity whereas cresol selectivity increased. At low residence time, i.e. high weight hourly space velocity, both anisole and cresol are formed. This indicates that both anisole and cresol are primary products.

In terms of the p/o-cresol ratio, Figure 7.41 shows that the p/o-cresol ratio did not level off at the equilibrium but crossed the equilibrium line at high space velocity and low conversion. The primary p/o-cresol ratio, obtained by extrapolating to zero residence time as shown in Figure 8.6, is 0.38. This implies that the p/o-cresol ratio is not influenced by the approach to equilibrium through secondary reactions and that the proximity to the equilibrium value, i.e 0.43, and statistical ratio, i.e 0.5, is coincidental.

As the residence time is increased (Figure 7.40 (b)), i.e. decreasing weight hourly space velocity, o-cresol selectivity decreased whereas p-cresol and m-cresol selectivities increased. However, studying the cresol selectivity in comparison to anisole selectivity (as shown in Figure 7.40 (c)), shows that the selectivity to p-cresol and m-cresol remain essentially constant with varying weight hourly space velocity whereas with decreasing space velocity the selectivity to o-cresol decreased with a corresponding increase in anisole selectivity. The only explanation for this observation, according to the reaction mechanism, is that at the low space velocity, i.e. high residence times, the internal rearrangement of

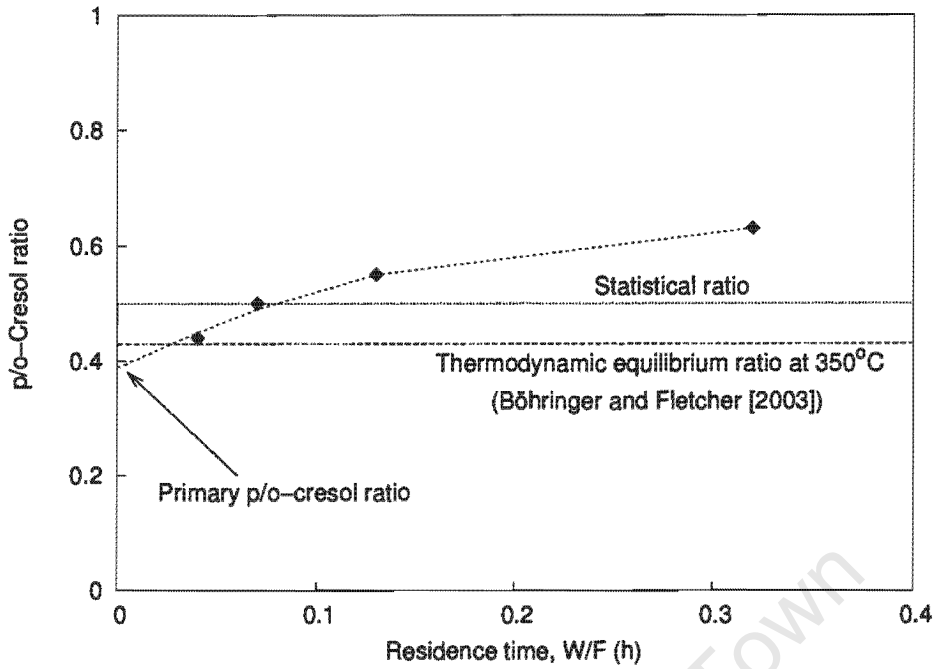

Figure 8.6: Determination of the primary p/o-cresol ratio at 300°C from phenol alkylation with methanol.

anisole to o-cresol reaction is reduced. This is not expected as increasing the residence times should result in an increase in the secondary reactions. The reason for the internal rearrangement of anisole to o-cresol decreasing at low space velocities is not understood. The formation of by-product water by phenol methylation is not thought to inhibit the anisole rearrangement as most of the water is formed rather quickly from the methanol to dimethyl ether reaction. Thus the amount formed by the phenol methylation does not add significantly to the water already present in the reaction mixture and so it is unlikely to inhibit the conversion of anisole to o-cresol. A possibility is that the cresols are inhibiting the rearrangement of anisole to o-cresol as cresols preferentially adsorb on the acid sites because they are less acidic than anisole [Sykes, 1986a].

8.3.5 Effect of reactants partial pressure

The effect of reactants partial pressure on the product distribution was studied in the gas phase and was shown in Figures 7.42 to 7.45. As Figure 7.45 indicates the reactants' partial pressure does not directly affect the product selectivity or cresol isomer distribution at low total pressure but only indirectly affects the selectivities through changes in phenol conversion. This indicates that all the reactions are of the same reaction order as proposed in Section 8.3.3. This is consistent with the findings of Santacesaria *et al.* [1990a] at low conversions.

8.3.6 Water

The effect of water on the phenol conversion, product selectivities and cresol isomer distribution was studied in the liquid phase and the results were shown in Section 6.5.5, Tables 6.9 and 6.10. Water is formed from the conversion of the methanol to dimethyl ether (cf. Section 2.2.2.1) and

in the formation of anisole and cresols. The formation of dimethyl ether is rapid and so it can be approximated that the reactant mixture also includes water. Therefore, the role of water on the phenol conversion, product selectivities and cresol isomer distribution needs to be considered although water formed via a surface reaction and water present in the reactant mixture often behave differently.

From Figure 2.25, the thermodynamic equilibrium conversion of methanol to dimethyl ether is ca. 90% leading to a phenol : water molar ratio of 1 : 0.45. Increasing the water concentration to a phenol : water molar ratio of 1 : 1.25, resulted in a decrease in the phenol conversion. The effect of the water on the product selectivities and cresol isomer distribution was inconsistent and minor. The decrease in the phenol conversion may be due to the dilution effect. If the reaction rate was assumed to be first order in both methanol and phenol, the expected decrease in activity is 50% and if the reaction rate is assumed to zero order in phenol and first order in methanol then the expected decrease in activity would be 30%. The activity, as indicated by phenol conversion, actually decreased by 69% for H-ZSM-5, 65% for H-Beta and 81% for H-MCM-22. This indicates that the dilution effect could be influencing the phenol conversion but it does not account for the total loss in the activity.

The activity could be influenced, in addition to the dilution effect, by the competitive adsorption of the water on the acid sites thereby reducing the number of available acid sites for the phenol methylation reaction which would in turn decrease the overall phenol conversion.

8.3.7 Summary of the overall reaction mechanism

For the gas phase alkylation of phenol with methanol the proposed overall reaction mechanism is shown in Figure 8.7. The proposed mechanism is as follows:

- Two parallel reactions occur, namely O-alkylation and C-alkylation;
- Both anisole and cresol are primary products;
- Cresols are also formed in a secondary step by either:
  - monomolecular methyl shift of the anisole → o-cresol
  - bimolecular reaction between anisole and phenol → o-cresol and p-cresol;
- Cresols do not react to form anisole;
- o-Cresol and p-cresol are primary products from the phenol methylation reaction and secondary products from the conversion of anisole;
- m-Cresol is formed from isomerization of the other cresol isomers;
- Methylanisole was formed from anisole transalkylation;
- Xylenols are formed from the methylation of the cresols. This was not proved by reacting cresols with methanol but assumed as methanol is in the reaction mixture and xylenols are not formed from methylanisoles.

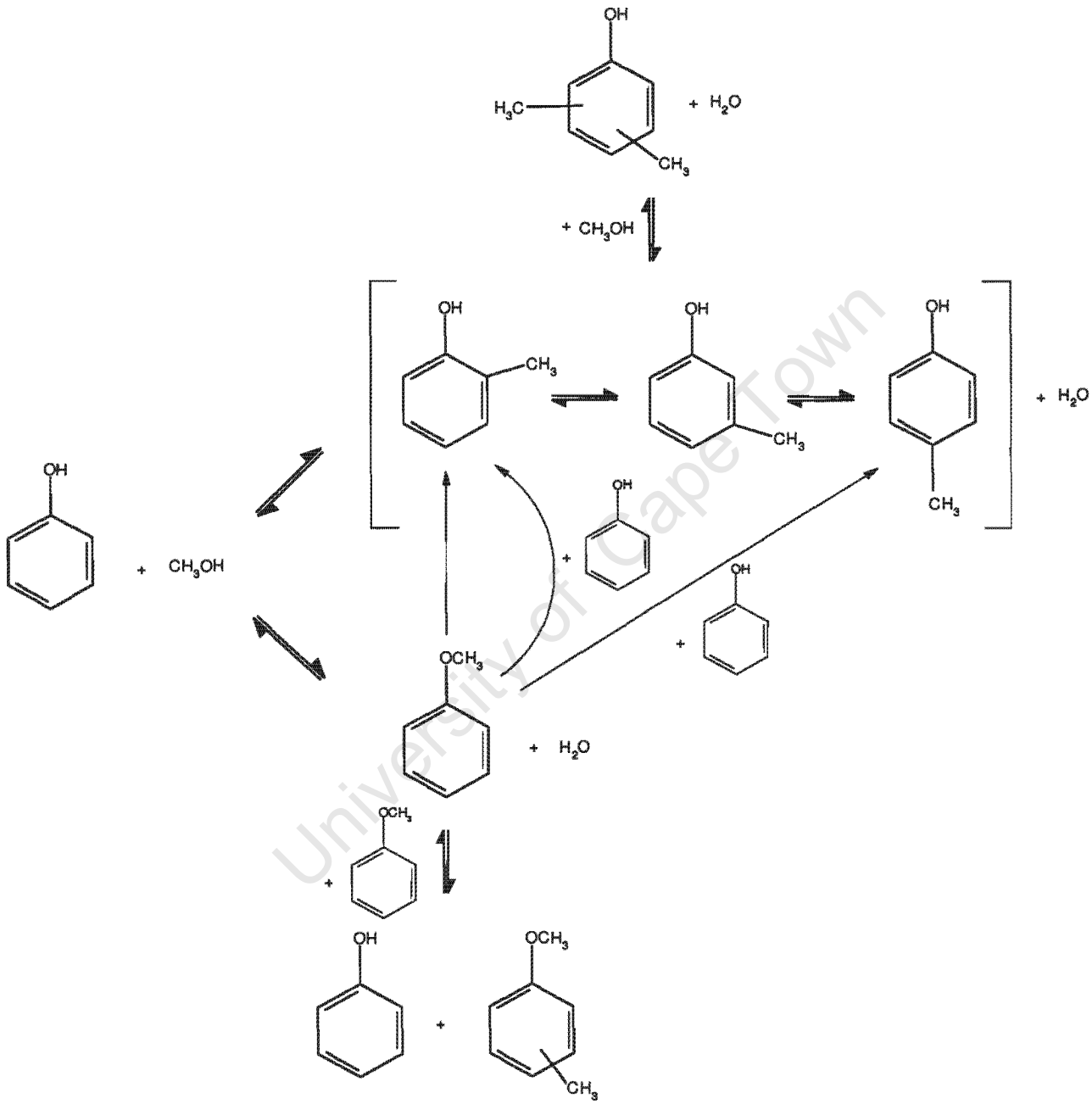

Figure 8.7: The proposed overall reaction mechanism for the alkylation of phenol with methanol over zeolites in the *gas phase*.

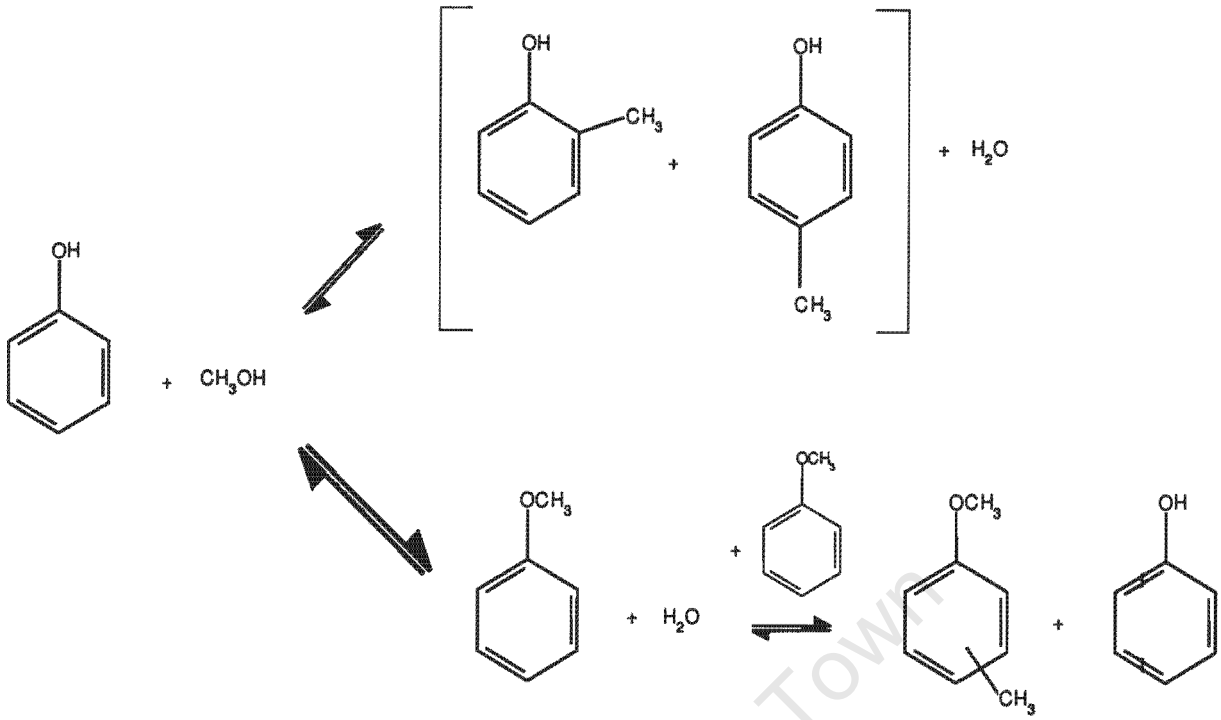

Figure 8.8: Proposed mechanism for the alkylation of phenol with methanol in the *liquid phase*.

For the liquid phase, the proposed overall mechanism for the alkylation of phenol with methanol is shown in Figure 8.8. The proposed mechanism is as follows:

- Two parallel reactions occur, namely O-alkylation and C-alkylation;
- Anisole and cresols are primary products;
- Main reaction is the O-alkylation to anisole;
- The conversion of anisole to cresols in the presence of phenol essentially does not occur;
- Cresols are only formed from the alkylation of phenol with methanol;
- Cresols do not react further to form either other cresol isomer, xylenols or anisole;
- No m-cresol was formed;
- Methylanisole was formed form anisole transalkylation.

8.4 Comparison of the different catalysts

Zeolite H-MCM-22 was studied in the alkylation of phenol with methanol because of its unique channel structure which consists of supercages, which are defined by 12 membered rings but has openings defined by 10 membered rings, and a independent 10 membered ring channel (cf. Section 2.1.1.5). In

Table 8.2: Phenol alkylation with methanol over the different catalysts studied in this thesis.

Catalyst	Liquid phase*			Gas phase**		
	Phenol conversion (mol%)	O/C-alkylation ratio	p/o-Cresol ratio	Phenol conversion (mol%)	O/C-alkylation ratio	p/o-Cresol ratio
H-ZSM-5	9.7	3.6	0.38	10.2	1.7	0.55
H-Beta	8.3	11.1	0.47	-	-	-
H-Mordenite	8.0	5.0	0.48	-	-	-
H-USY	1.4	11.1	0.60	-	-	-
H-MCM-22 (UCT)	5.7	16.7	1.20	3.8	1.7	0.50
H-MCM-22 (DE1)	-	-	-	3.9	0.8	0.47
H-MCM-22 (DE2)	8.6	25.0	1.02	8.5	2.7	0.97
H-MCM-22 (DE3)	-	-	-	5.2	2.2	0.87
Silica-alumina	0.5	14.3	0.45	2.5	1.8	0.37

* Liquid phase standard conditions: 200°C, starting pressure = 16 bar, reaction time = 5 hours, methanol : phenol molar ratio = 1, reactants : catalyst mass ratio = 39.4;

** Gas phase standard conditions: 300°C, total pressure = 1 bar, feed partial pressure = 0.2 bar, methanol : phenol molar ratio = 1, WHSV = 14 h^{-1}.

order to characterize the role of the 10 membered ring and the 12 membered ring structures, H-ZSM-5 was used as an example of a 10 membered ring zeolite and H-Beta, H-Mordenite and H-USY were studied as typical 12 membered ring zeolites although they have different structures. Amorphous silica-alumina was then studied as a non-shape selective catalyst.

Table 8.2 summarises the phenol conversion, O/C-alkylation ratio and the p/o-cresol ratio for all the catalysts studied in this thesis. The most striking aspect of Table 8.2 is the high p/o-cresol ratios obtained over the H-MCM-22 samples in the liquid phase.

This section begins by discussing the characteristics of the catalysts to determine their effect on the phenol conversion, product selectivities and cresol isomer distribution. Then the phenol conversion over the different catalysts is discussed. Finally, the high p/o-cresol ratios over the H-MCM-22 samples are considered.

8.4.1 The effect of catalyst parameters on phenol conversion, product selectivities and cresol isomer distribution

As the different catalysts studied have different zeolite characteristics (cf. Chapter 5), such as bulk Si/Al ratio, BET surface area, microporous and mesoporous area, microporous and mesoporous volume and acid site strength, the effect of these parameters need to be considered to determine their effect on phenol conversion, product selectivity and cresol isomer distribution. The following characteristics of the catalysts were found to have no obvious effect on the phenol conversion, product selectivity and cresol isomer distribution:

- BET surface area;
- Microporous area;
- Mesoporous area;

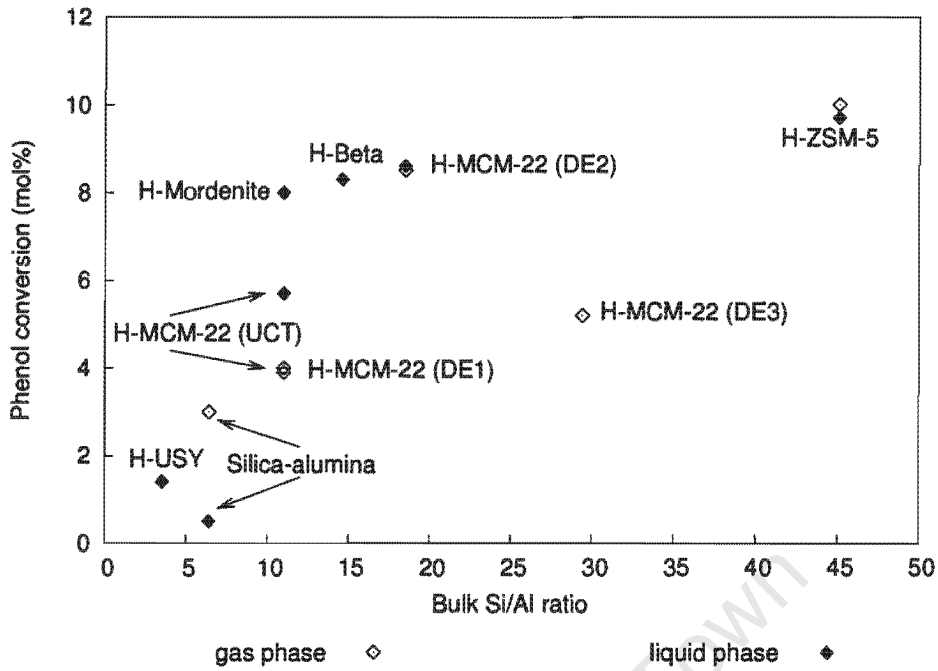

Figure 8.9: The effect of bulk bulk Si/Al ratio on the phenol conversion.

- Microporous volume;
- Mesoporous volume.

The bulk Si/Al ratio and acid strength of the acid site, as determined by the maximum temperature of the major desorption peak in the NH_3-TPD, were found to influence the phenol conversion, product selectivity and cresol isomer distribution.

8.4.1.1 The effect of bulk Si/Al ratio over the different catalysts

The bulk Si/Al ratio of the different catalysts affected the phenol conversion. As the bulk Si/Al ratio increased there was a general trend that the phenol conversion increased in both the gas and liquid phase as shown in Figure 8.9. However, there was no clear relationship between the bulk Si/Al ratio and the O/C-alkylation ratio or the p/o-cresol ratio. Therefore, the high p/o-cresol ratios obtained in the H-MCM-22 samples cannot be explained in terms of their bulk Si/Al ratio.

8.4.1.2 The effect of acid site strength over the different H-MCM-22 samples

The strength of acid sites can be determined by ammonia temperature programmed desorption (NH_3-TPD) (cf. Section 4.1.4.5). The maximum temperature of the major desorption peak (T_{max}) obtained from the NH_3-TPD is an indication of the strength of the acid sites (cf. Section 5.5 and Table 5.4). Figures 8.10 and 8.11 show the dependence of phenol conversion and product selectivity on maximum temperature over the different H-MCM-22 samples, respectively. Generally, there is a clear trend that the phenol conversion increased with increasing maximum temperature (T_{max}) and this was the case for both phases.

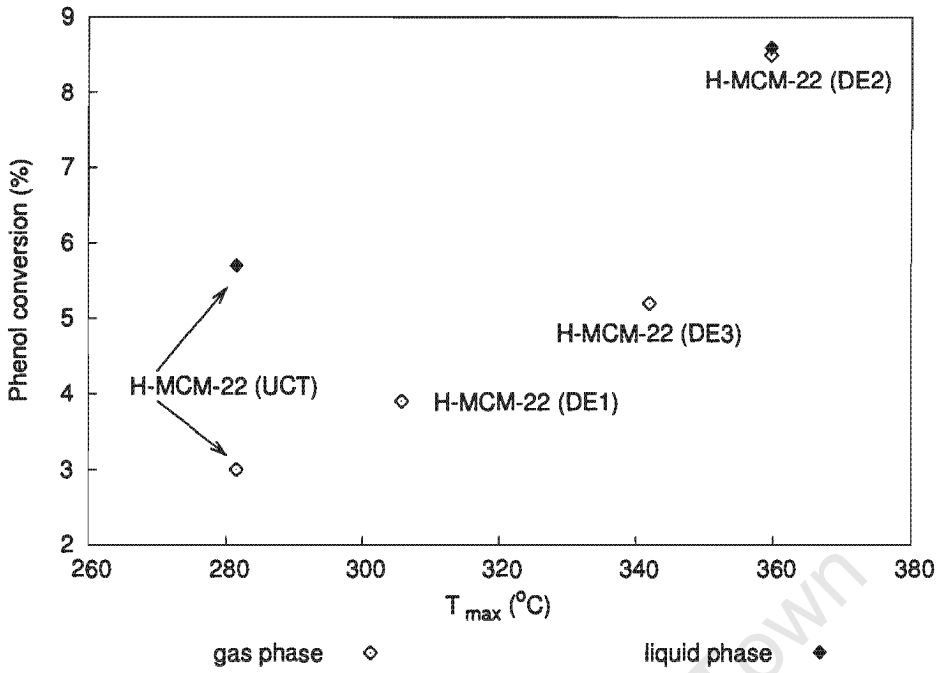

Figure 8.10: The effect of maximum temperature (T_{max}) on the phenol conversion of the different H-MCM-22 samples.

Over the different H-MCM-22 samples, the O/C-alkylation ratio showed an increasing trend with increasing acid site strength (T_{max}) in the liquid phase while in the gas phase the O/C-alkylation ratio appears not to depend on the acid site strength (Figure 8.11 (a)). This is inconsistent with the findings of Garcia *et al.* [1996] and Pierantozzi and Nordquist [1986] (cf. Section 2.2.3.3). They found that the O/C-alkylation ratio decreased with increasing acid strength and this was attributed to cresol formation requiring higher acid strength than anisole formation. Pierantozzi and Nordquist [1986] studied a wide range of different acid catalysts with different type and strength of acid sites ranging from $BaSO_4$ to zeolite H-ZSM-5. Garcia *et al.* [1996] made these conclusions from the initial results (after 15 minutes-on-stream) whereas after the initial results no difference was found between the sample of different acid site strengths. Marczewski *et al.* [1988] disagreed with Garcia *et al.* [1996] and Pierantozzi and Nordquist [1986] by stating that the product selectivity is independent of the strength of the acid sites. The large increase in the liquid phase O/C-alkylation ratio with increasing T_{max} may be a result of the high sensitivity of the ratio to small changes in cresol selectivity. When comparing all the catalysts studied (as shown in Figure 8.12 (a)) there seemed to be no relationship between O/C-alkylation ratio and T_{max}.

In terms of the p/o-cresol ratio, in the gas phase the p/o-cresol ratio showed an increasing trend with increasing acid strength whereas for the liquid phase the p/o-cresol ratio hardly changed for H-MCM-22 (Figure 8.11 (b)). In the liquid phase there are only two data points and so it is hardly possible to draw a conclusion on the relationship between acid site strength and p/o-cresol ratio. In the gas phase, the presence of stronger acid sites seemed to favour an increase in p-cresol selectivity, however, considering all the catalysts studied in this thesis, there was no clear evidence of a relationship between p/o-cresol ratios found in these samples and acid strength (Figure 8.12 (b)).

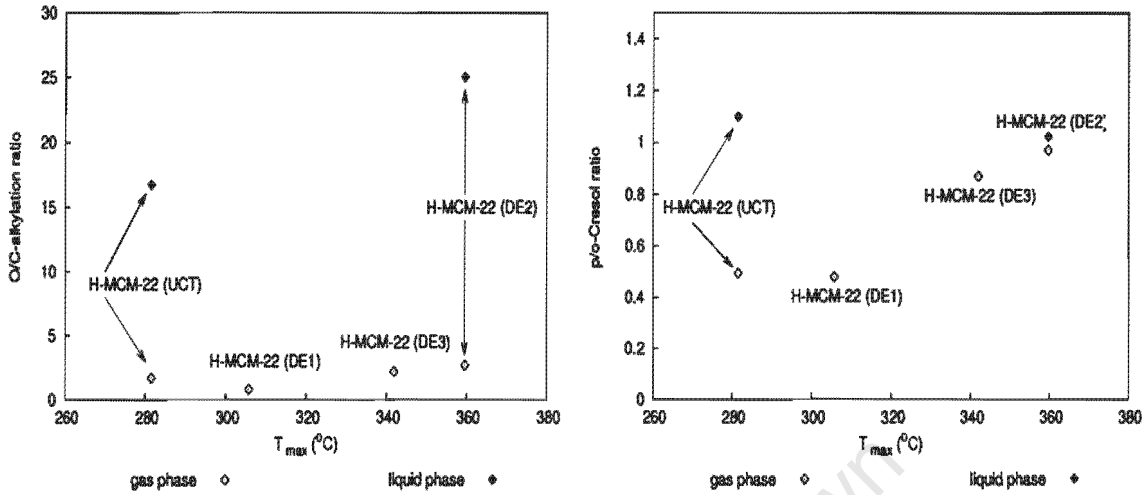

(a) O/C-alkylation ratio (b) p/o-cresol ratio

Figure 8.11: The effect of maximum temperature (T_{max}) on the O/C-alkylation ratio and the p/o-cresol ratio of the different H-MCM-22 samples.

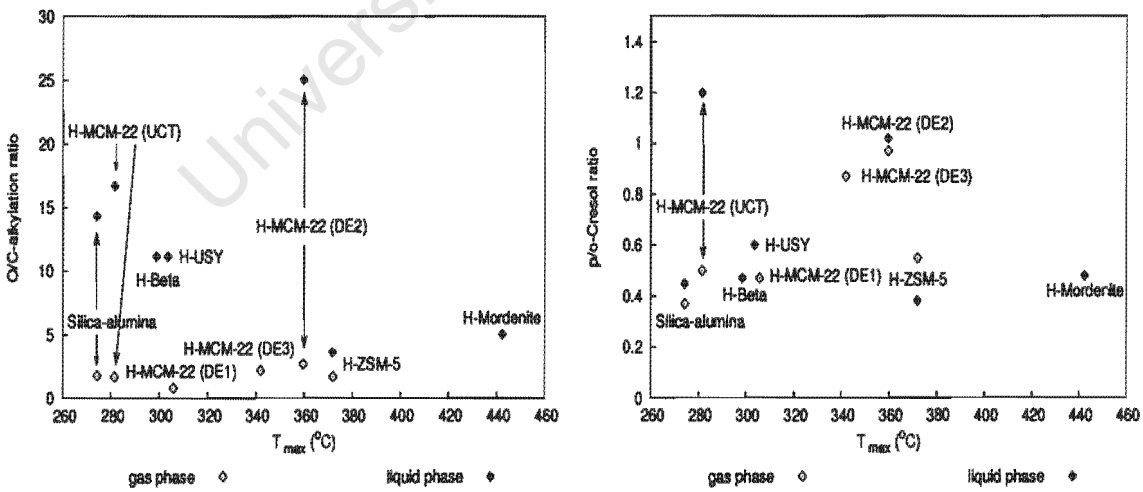

(a) O/C-alkylation ratio (b) p/o-cresol ratio

Figure 8.12: The effect of maximum temperature (T_{max}) on O/C-alkylation ratio and the p/o-cresol ratio over the different catalysts.

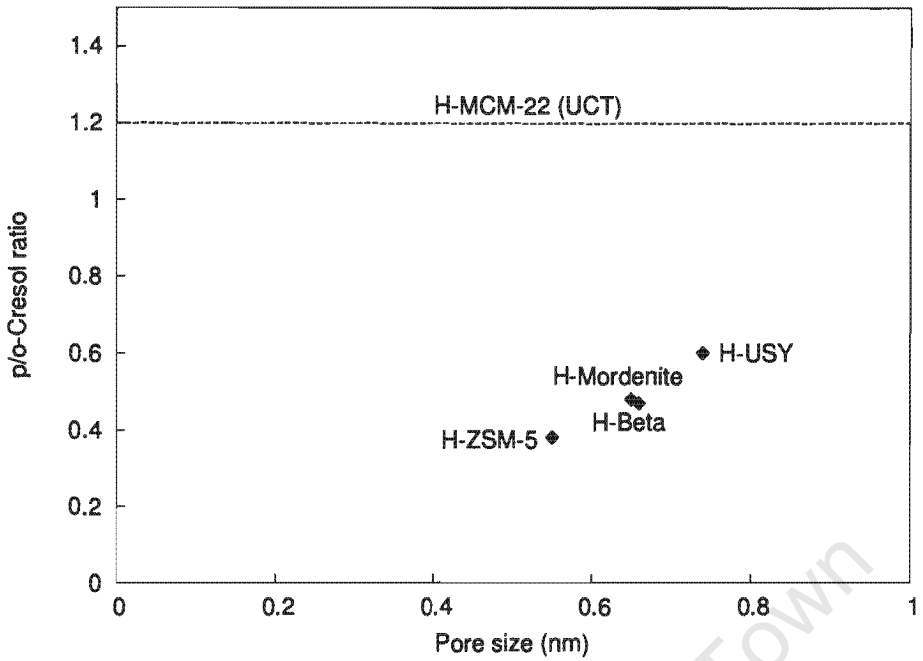

Figure 8.13: The effect of pore size on the p/o-cresol ratio over different catalysts in the *liquid phase*.

8.4.1.3 The effect of pore size

Zeolite MCM-22 was studied because of its channel system which is defined by both 10 and 12 membered ring channels. The liquid phase p/o-cresol ratio obtained over H-MCM-22 (UCT) was then compared with that of H-ZSM-5, H-Beta, H-Mordenite and H-USY as shown in Figure 8.13. In the liquid phase, it is clearly seen that zeolite H-MCM-22 (UCT) does not behave as a typical 10 membered ring or a 12 membered ring zeolite. In the gas phase, however, Table 8.2 shows that H-MCM-22 (UCT) behaves similar to that of H-ZSM-5 with respect to O/C-alkylation ratio and p/o-cresol ratio. Therefore, the reaction phase affects the p/o-cresol ratio in H-MCM-22 (UCT) quite significantly and this is further investigated in Section 8.5.

8.4.2 Phenol conversion

In terms of phenol conversion, H-ZSM-5 was the most active catalyst studied. The lower deactivation rate of phenol conversion in the case of H-ZSM-5 was probably due to it being less susceptible to coking during the initial reaction period as shown in Figure 7.5. Zeolite ZSM-5 has a three dimensional channel system with channel intersections in the order of 9 Å allowing the products to diffuse out quickly thereby minimizing coke formation.

The low phenol conversion over H-USY may be due to coke formation by promoting the formation of polyaromatics or polyalkylated species inside the zeolite pores or supercages. Guisnet *et al.* [1991] investigated the coke formation in the phenol alkylation reaction over H-USY. They found that the deactivation of H-USY occurred by limitation or blockage of the access of the reactant to the active acid sites. Guisnet *et al.* [1991] classified the coke compounds into four families, namely polymethylanisoles, methoxy (or hydroxy) methyldiphenylmethanes, methyldibenzofurans and benzylmethyldibenzofurans. They found that polymethylanisoles first blocked the pores and were later

Table 8.3: Boiling points of alkylation products.

Compounds	Boiling points (°C)
Anisole	155
Methylanisoles	170 - 176
Dimethylanisoles	182 - 201
Cresols	191 - 203
Xylenols	203 - 227
Trimethylphenols	ca. 222

transformed into methoxy (or hydroxy) methyldiphenylmethanes and methyldibenzofurans. After long reaction times, methoxy (or hydroxy) methyldiphenylmethanes and methyldibenzofurans were turned into benzylmethyldibenzofurans. The blocking of the pores by the dimethylanisoles is due to their strong adsorption in the zeolite pores and therefore the diffusion of these compounds is slower than the alkylation reaction. Therefore, the deactivation of the H-USY is considered to be due to the formation of compounds that limit or block the diffusion of the reactants to the acid sites or that of the products from the sites to the outer surface. As a result of the low phenol conversion, H-USY was not investigated in the gas phase. Zeolite MCM-22 has a structure which consists of two independent channel systems. One of these channel systems consists of supercages which, like the supercages in USY, could experience a coke formation phenomena similar to that described above for USY.

Silica-alumina also showed a very low phenol conversion activity (< 1% in the liquid phase and 2.6% in the gas phase). This may also be due to the alkylation products forming compounds that are less volatile at these reaction temperatures, shown in Table 8.3, than the alkylation products themselves which then in turn block the active acid sites.

In comparing their liquid and gas phase phenol conversion activities, H-ZSM-5 and H-MCM-22 (DE2) had similar conversions in both phases. Silica-alumina showed a higher phenol conversion in the gas phase whereas H-MCM-22 (UCT) gave a lower phenol conversion in the gas phase compared to the liquid phase. The latter was not expected as the gas phase reactions were carried out at a higher temperature (300°C) than the liquid phase (200°C).

8.4.3 Comparison between zeolites and amorphous silica-alumina

In the liquid phase, in terms of the p/o-cresol ratio, silica-alumina (0.45) behaves similarly to zeolite H-Beta (0.47) and H-Mordenite (0.48), i.e. to the large pore zeolites (cf. Table 8.2). The p/o-cresol ratios obtained over these zeolites corresponded with the statistical p/o-cresol ratio of 0.5. Only the H-MCM-22 samples indicated any shape selectivity in terms of both the high O/C-alkylation ratio (16.7) and p/o-cresol ratio (1.20) as both anisole and p-cresol are the slimmest molecules in the product spectrum. H-ZSM-5 had a comparatively low O/C-alkylation ratio (3.6) and p/o-cresol ratio (0.38) compared to the other zeolites and silica-alumina. Venuto *et al.* [1966]; Jacobs *et al.* [1988] and Parton *et al.* [1989a] hypothesised that the low O/C-alkylation ratio and p/o-cresol ratio over H-ZSM-5 is due to the intermolecular rearrangement of anisole to o-cresol in the zeolite pores or channel intersections which would suppress the transalkylation reactions for the formation of o-cresol and p-cresol. In the conversion of anisole over the zeolites, H-ZSM-5 produced the most o-cresol of

all the zeolites studied which supports the above argument, viz. of anisole undergoing intermolecular rearrangement to o-cresol.

In the gas phase, the O/C-alkylation ratio obtained over silica-alumina is similar to those obtained over the zeolites, namely 1.8 versus 1.7 (cf. Table 8.2). However, the p/o-cresol ratio (0.37) was lower than that found over the zeolites (ca. 0.5, corresponding to the statistical p/o-cresol ratio). Silica-alumina contains both Brønsted and Lewis acid sites as well as Lewis basic sites. The Brønsted acid sites are selectively poisoned by coking [Santacesaria *et al.*, 1990b] which results in the Lewis acid and basic sites influencing the product formation. Santacesaria *et al.* [1990b] showed that the Lewis acid and basic pair were highly o-selective. This would result in the silica-alumina having a lower p/o-cresol ratio than that found in the zeolites.

8.4.4 p/o-Cresol ratios over the various H-MCM-22 samples compared to the other catalysts

The H-MCM-22 samples show the highest p/o-cresol ratio in both the gas and liquid phase alkylation of phenol with methanol (cf. Table 8.2). An explanation for the high p/o-cresol ratio over the different H-MCM-22 samples compared to the other catalysts can be found by studying the effect of phenol conversion on the O/C-alkylation and p/o-cresol ratio, the interrelationship between the rate of reaction and diffusion resistances as characterized by a modified Thiele Modulus, the internally selectively sodium-exchange of MCM-22 (UCT) and ZSM-5 and the steaming of H-MCM-22 (DE1).

8.4.4.1 Relationship between O/C-alkylation ratio, p/o-cresol ratio and phenol conversion

The different catalysts were compared at slightly different phenol conversions and therefore the effect of phenol conversion on the O/C-alkylation ratio and p/o-cresol ratio needs to be determined. Figure 8.14 shows that there is no relationship between phenol conversion and these ratios in the liquid phase. However, Figure 8.15 shows that there is a trend of increasing O/C-alkylation ratio as p/o-cresol ratio increases in the liquid phase. Similar relationships were obtained for the gas phase. The reason for this relationship between O/C-alkylation ratio and p/o-cresol ratio is not conversion as there is no effect of conversion on these ratios (Figure 8.14). However, anisole and p-cresol are both the slimmest product molecules and a reason for the relationship could be shape selective effects which would increase the selectivity to both these molecules.

8.4.4.2 Thiele Modulus

The Thiele Modulus is a dimensionless expression which relates the reaction rate to the diffusional rate. The Thiele Modulus allows for the effect of catalyst particle size on the p/o-cresol ratio for the different catalysts to be determined. The Thiele Modulus for a first order reaction is given in Equation 8.3.

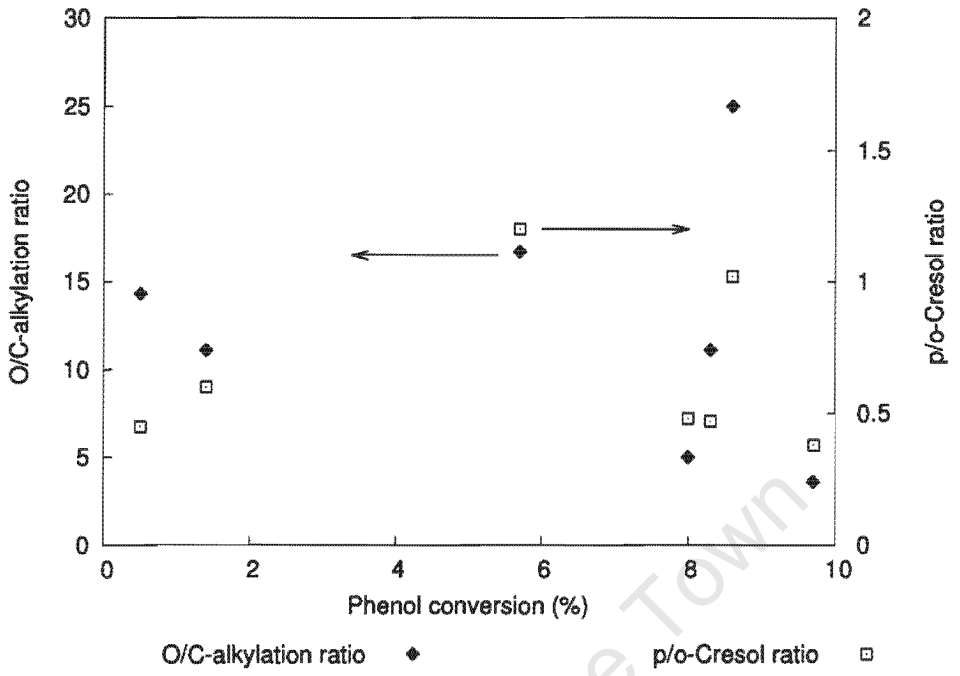

Figure 8.14: The relationship between O/C-alkylation ratio and p/o-cresol ratio with phenol conversion in the *liquid phase*.

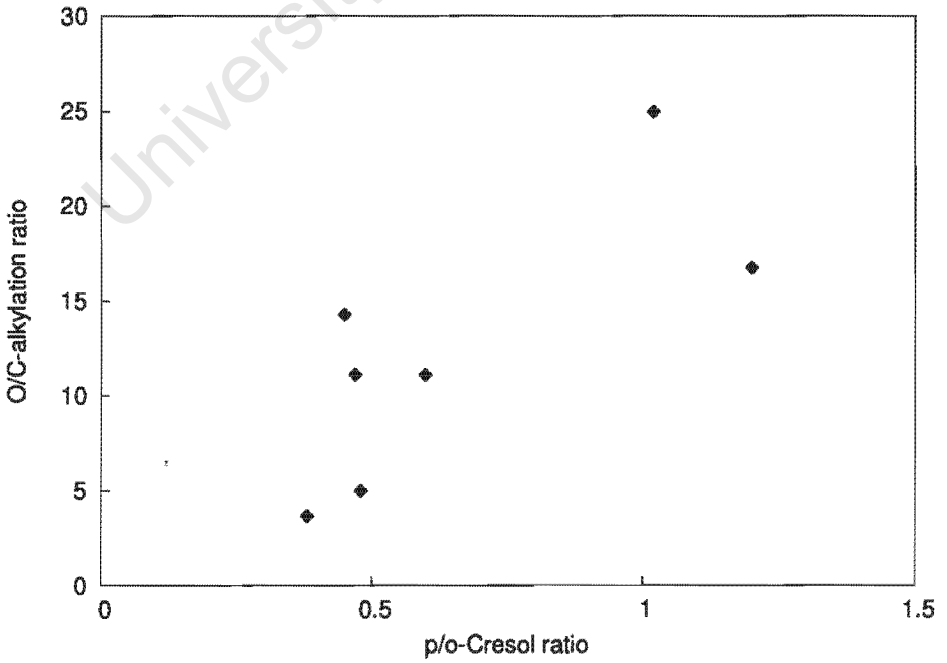

Figure 8.15: The relationship between O/C-alkylation ratio and p/o-cresol ratio in the *liquid phase*.

$$\begin{aligned} \phi &= \sqrt{\frac{kr_p^2}{D_e}} && \text{flat plate} \\ \phi &= \frac{1}{2}\sqrt{\frac{kr_p^2}{D_e}} && \text{cylinder} \\ \phi &= \frac{1}{3}\sqrt{\frac{kr_p^2}{D_e}} && \text{spherical} \end{aligned} \tag{8.3}$$

where:

- ϕ is the Thiele Modulus;
- k is the reaction rate constant;
- r_p is the radius of the catalyst particle;
- D_e is the effective diffusional constant.

If the reaction rate has second order kinetics a factor C_{sc}, which corresponds to the concentration on the surface of the catalyst, is present in the square root as shown in Equation 8.4.

$$\begin{aligned} \phi &= \sqrt{\frac{kC_{sc}r_p^2}{D_e}} && \text{flat plate} \\ \phi &= \frac{1}{2}\sqrt{\frac{kC_{sc}r_p^2}{D_e}} && \text{cylinder} \\ \phi &= \frac{1}{3}\sqrt{\frac{kC_{sc}r_p^2}{D_e}} && \text{spherical} \end{aligned} \tag{8.4}$$

As discussed in Section 8.3.2, the reaction rate constant (k) can be taken to be proportional to the phenol conversion in the phenol methylation reaction. If it is assumed that reaction rate depends on the number of aluminium atoms present, then we can assume that the reaction rate constant (k) is also proportional to the aluminium on the microporous BET surface area of the zeolite, assuming the aluminium is evenly distributed between the micropores and mesopores. By substitution in the Thiele Modulus and assuming a constant C_{sc}, we get Equations 8.5 and 8.6, respectively:

$$\phi_I \propto \text{factor} \times \sqrt{\frac{X \times r_p^2}{D_e}} \tag{8.5}$$

$$\phi_{II} \propto \text{factor} \times \sqrt{\frac{Al \times \frac{A_{micropores}}{A_{mesopores}} \times r_p^2}{D_e}} \tag{8.6}$$

where:

- ϕ_I and ϕ_{II} are the modified Thiele Modulus values for each case;
- factor = 1, 1/2 or 1/3 depending on the crystal shape as shown in Equation 8.4;
- X is the phenol conversion;

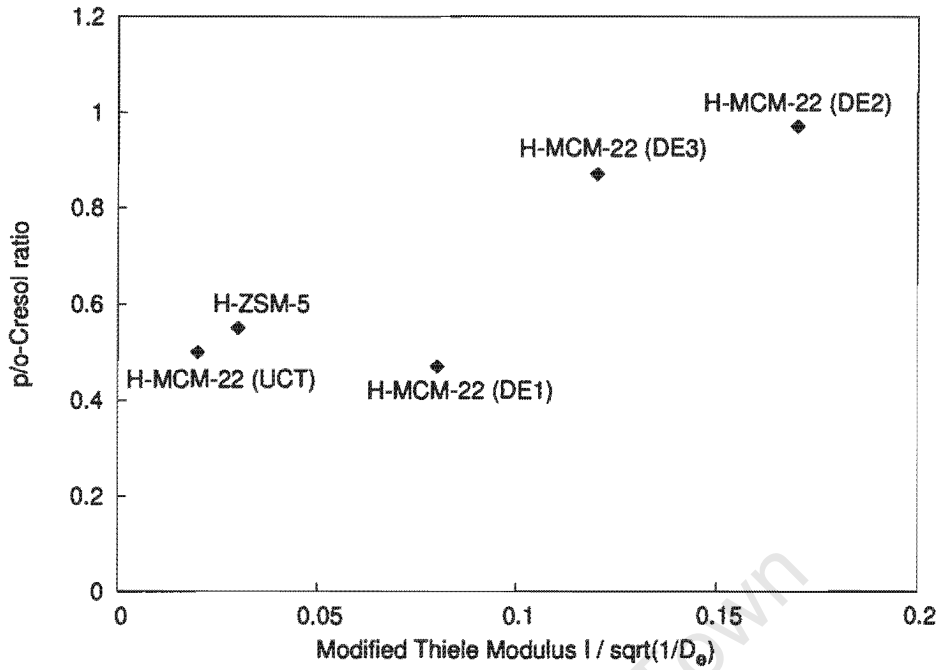

Figure 8.16: p/o-Cresol ratio in the gas phase as a function of the Modified Thiele Modulus I.

- Al is the total aluminium content of the catalyst;
- $A_{micropores}$ is the BET microporous area of the catalyst (cf. Table 5.2);
- $A_{mesopores}$ is the BET mesoporous area of the catalyst (cf. Table 5.2).

Figures 8.16 and 8.17 show the gas phase relationship between the p/o-cresol ratios and the modified Thiele Modulus I and II, respectively. The Thiele Modulus for H-ZSM-5, H-Beta and H-USY was based on spherical crystal shape while H-MCM-22 was approximated as a cylinder and H-Mordenite as a flat plate which is based on the zeolites pore system dimensionality. It can be seen from these two figures that, in both cases, in the gas phase the p/o-cresol ratios generally increased as the modified Thiele Modulus increased. This implies that increasing the crystal size of the zeolite, as shown for H-MCM-22, increases the p/o-cresol ratio. By increasing the crystal size, the diffusional pathway is increased and this increases the selectivity to the slimmest of the two molecules, namely p-cresol.

8.4.4.3 Internally selectively sodium-exchanged ZSM-5 and MCM-22 (UCT)

Tables 8.4 and 8.5 summarises the effect of internally selectively sodium-exchange for ZSM-5 and MCM-22, respectively, where H/Na-zeolite represents the activity of the internally sodium-exchanged zeolite crystals and H-form of the zeolite represents both the activity on the internal surface and the external surface. The results show an increase in o-cresol and p-cresol yield when comparing the H-form of the zeolite to the sodium-exchanged sample. However, the increase in the yield of p-cresol is greater than the increase in the yield of o-cresol. This indicates there is shape selective internal mass transfer control, which favours the p-isomer, amongst the cresols formed internally. The

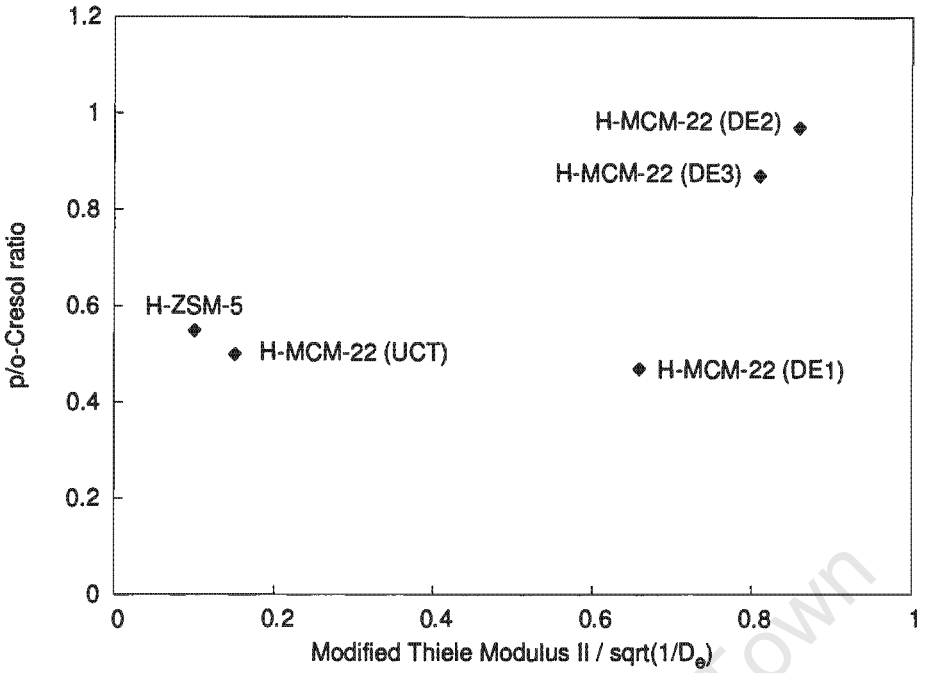

Figure 8.17: p/o-Cresol ratio in the gas phase as a function of the Modified Thiele Modulus II.

effect is much more pronounced over MCM-22 (UCT) than ZSM-5 as seen by the relative increase in $Y_{p-cresol}/Y_{o-cresol}$.

There is a large difference in increase activity between the ZSM-5 (from 1.2 to 9.7%) and MCM-22 (UCT) (from 2.3 to 5.7%) samples, when comparing the selectively sodium-exchanged and the H-form of the zeolite. Calculation of the volume to surface area ratios of these two catalysts are given in Table 8.6. As can be seen in Table 8.6, for the ZSM-5 sample this value is twice that of the MCM-22 (UCT) sample. This could explain the higher increase in activity (phenol conversion) with ZSM-5 when the active sites in the internal pore system is included.

8.4.4.4 Steaming of H-MCM-22 (DE1)

The results of steaming H-MCM-22 (DE1) were given in Figures 7.26 to 7.28. Table 8.7 summarises the results in terms of O/C-alkylation ratio and p/o-cresol ratio.

The phenol conversion increased from 3.9 % to 11.1 % on mild steaming of the zeolite H-MCM-22 (DE1). Mild steaming of a zeolite removes aluminium from the framework and produces extra-framework aluminium as discussed in Section 2.1.4.1. This process is stepwise with the removal of the aluminium proceeding bond by bond. This aluminium which is partially bonded to the framework is regarded as highly active. This may therefore account for the increase in the phenol conversion.

Mild steaming also results in an increase in the O/C-alkylation ratio (from 0.8 to 2.0) due to the higher formation of anisole. This may be due to two reasons. Firstly, the aluminium partially bonded to the framework exhibits Lewis acidity which, as described in Section 2.2.3.2, favours the formation of anisole. Secondly, the extra-framework $[Al_xO_y]$ species obstruct the narrow pores, thus increasing the diffusional resistance in the pores and thereby favouring the formation of the more

Table 8.4: Internally selectively sodium-exchange over ZSM-5 in the *liquid phase*.

	Sodium-exchanged H/Na-ZSM-5*	H-ZSM-5*	H/(H/Na) **	(H-H/Na)/(H/Na) ***
Phenol conversion (%)	1.2	9.7		
Yield of cresols (%)	0.23	2.08		
Yield of o-cresol ($Y_{o-cresol}$, %)	0.18	1.50		
Yield of p-cresol ($Y_{p-cresol}$, %)	0.05	0.57		
Increase $Y_{o-cresol}$****			8.5	7.4
Increase $Y_{p-cresol}$****			11.2	10.4
Relative increase in $Y_{p-cresol}/Y_{o-cresol}$ (%)			132	141

* Data derived from Tables 6.8 and 6.9;
** H/(H/Na) represents the ratio between the pure acid zeolite and the sodium-exchanged zeolite;
*** (H-H/Na) represents the contribution of the internal acid sites;
**** Increase in yield refers to increase in the yield when investigating the H-zeolite relative to the sodium-exchanged zeolite.

Table 8.5: Internally selectively sodium-exchange over MCM-22 (UCT) in the *liquid phase*.

	Sodium-exchanged H/Na-MCM-22*	H-MCM-22*	H/(H/Na) **	(H-H/Na)/(H/Na) ***
Phenol conversion (%)	2.3	5.7		
Yield of cresols (%)	0.13	0.31		
Yield of o-cresol (%)	0.08	0.14		
Yield of p-cresol (%)	0.05	0.17		
Increase $Y_{o-cresol}$			1.8	0.8
Increase $Y_{p-cresol}$			3.4	2.4
Relative increase in $Y_{p-cresol}/Y_{o-cresol}$ (%)			189	300

* Data derived from Tables 6.8 and 6.9;
** H/(H/Na) represents the ratio between the pure acid zeolite and the sodium-exchanged zeolite;
*** (H-H/Na) represents the contribution of the internal acid sites;
**** Increase in yield refers to increase in the yield when investigating the H-zeolite relative to the sodium-exchanged zeolite.

Table 8.6: Volume to surface area ratios for ZSM-5 and MCM-22 (UCT).

	ZSM-5	MCM-22 (UCT)
Crystal morphology	Spherical	Platelet
Volume	$4/3\pi r^3$	$\pi r^2 d$
Surface area	$4\pi r^2$	$2\pi r^2 + 2\pi rd$
Radius (μm)*	0.15	0.1
Thickness (μm)*	-	0.1
Volume (μm^3)	0.014	0.003
Surface area (μm^2)	0.282	0.126
Volume/surface area (μm)	0.050	0.024

* Data from Table 5.1.

Table 8.7: The effect of steaming H-MCM-22 (DE1) on O/C-alkylation ratio and p/o-cresol ratio.

	H-MCM-22 (DE1)*	Steamed H-MCM-22 (DE1)*
Phenol conversion (%)	3.9	11.1
O/C-alkylation ratio	0.8	2.0
p/o-Cresol ratio	0.47	0.53

* Data derived from Figures 7.26 to 7.28.

linear molecule, anisole.

The increased diffusional resistance in the pores due to the obstruction of the extra-framework aluminium may also explain the increase in the p/o-cresol ratio (from 0.47 to 0.53).

8.4.4.5 Summary

In summary, it has been proposed that product shape selectivity, which results in the increase of p-cresols in the H-MCM-22 samples, is a result of increasing the crystal size of the MCM-22 samples (namely, the MCM-22 (DE1) and MCM-22 (DE2) samples compared to the MCM-22 (UCT) sample), internally selectively sodium-exchanging the internal active sites of ZSM-5 and MCM-22 (UCT) and steaming H-MCM-22 (DE1).

8.5 Comparison of liquid phase and gas phase alkylation of phenol with methanol

8.5.1 Pressure effect on the p/o-cresol ratio over H-MCM-22 (UCT)

The essential difference between results obtained in the gas phase and liquid phase experiments was considered to be a result of a pressure effect. Figures 8.18 and 8.19 show the p/o-cresol ratio observed over H-MCM-22 (UCT) in both gas phase and liquid phase at different reaction temperatures and different pressures, respectively. Figures 8.18 and 8.19 show that a significant difference was obtained over H-MCM-22 (UCT) in the liquid phase compared to the gas phase.

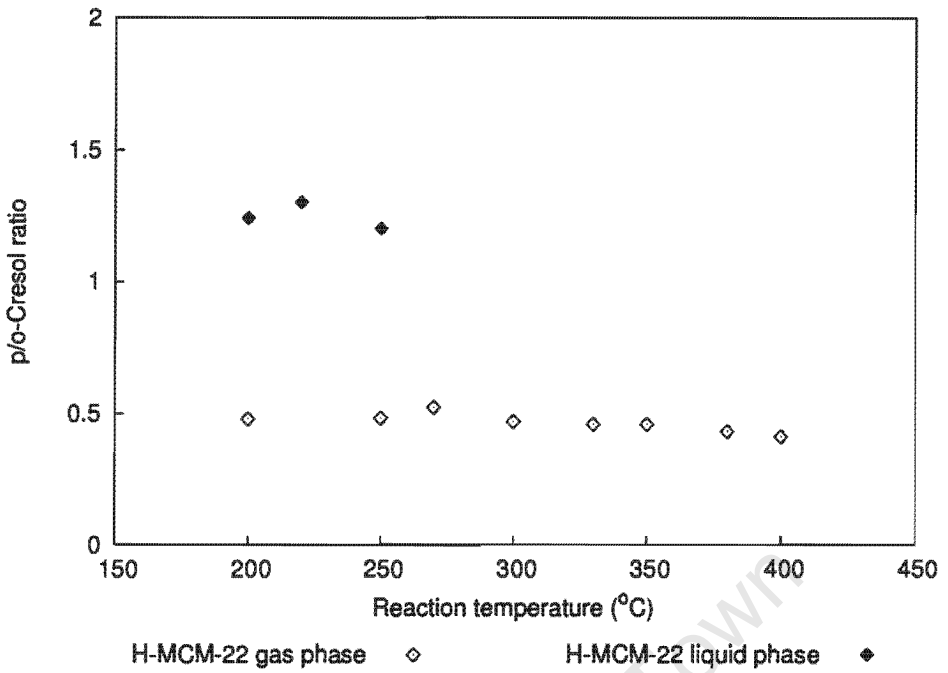

Figure 8.18: p/o-Cresol ratios observed over H-MCM-22 (UCT) in the gas and liquid phases as a function of reaction temperature.

As shown in Figure 8.20, H-MCM-22 (UCT) was found to show no enhanced shape selectivity in the gas phase when compared to the other zeolites, namely H-ZSM-5 and silica-alumina. As shown in Section 8.4.4.2, MCM-22 (UCT) has a similar value of the modified Thiele Modulus as H-ZSM-5, therefore resulting in similar p/o-cresol ratios in the gas phase. Thus in the gas phase over H-MCM-22 (UCT), no enhanced product shape selectivity was evident, whereas increasing the pressure (liquid phase) resulted in the p/o-cresol increasing quite substantially. A possible explanation could be a result of the effective increase in the diffusional resistance inside the zeolite pores with increasing pressure. Marczewski *et al.* [1996] found that the phenol is strongly adsorbed in the zeolites at low temperatures of 200°C. Therefore, at the low temperatures, the zeolite's pores are highly occupied by phenol molecules. Increasing the pressure will increase the occupancy of the pores and thereby effectively increase the diffusional resistance inside the pores. Product shape selectivity will therefore increase with increasing pressure thereby resulting in an increase in the p/o-cresol ratio over H-MCM-22 (UCT).

Zeolite H-ZSM-5, however, showed no enhanced para-selectivity with increasing pressure compared to zeolite H-MCM-22 (UCT). This may be due to the channel structure of these two zeolites. MCM-22 can allow bimolecular reaction to occur resulting in the formation of the slimmest isomer (p-cresol) in the supercages whereas the 10 membered ring channels of ZSM-5 would promote the intramolecular rearrangement of anisole to o-cresol. This is confirmed by the reaction of anisole over these zeolites in the liquid phase where H-ZSM-5 had a very low p/o-cresol ratio (0.25) compared to that over H-MCM-22 (1.1).

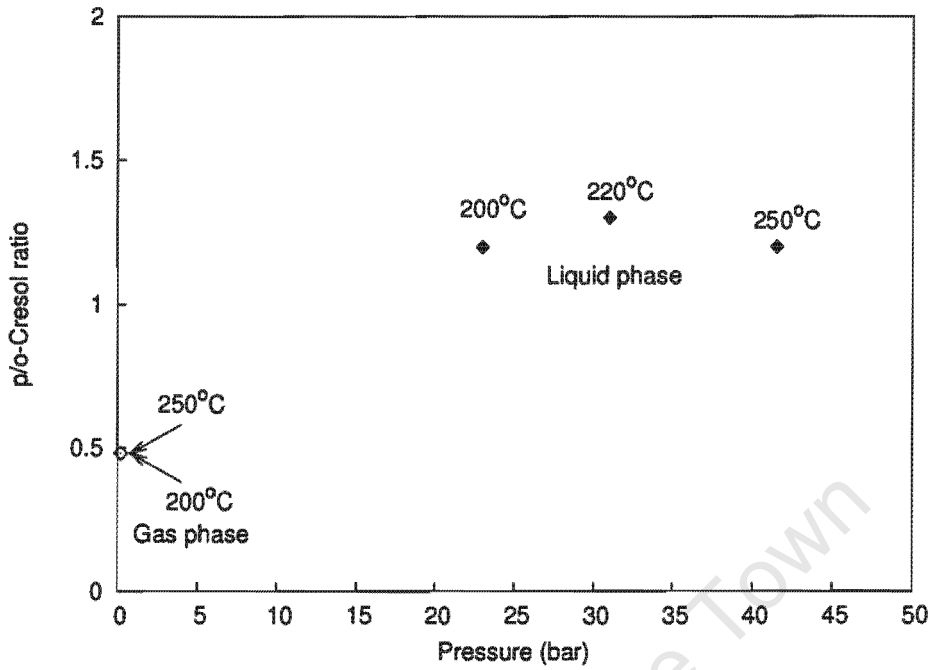

Figure 8.19: p/o-Cresol ratio as a function of reactant partial pressure (in the gas phase) and autogeneous pressure (in the liquid phase) over H-MCM-22 (UCT).

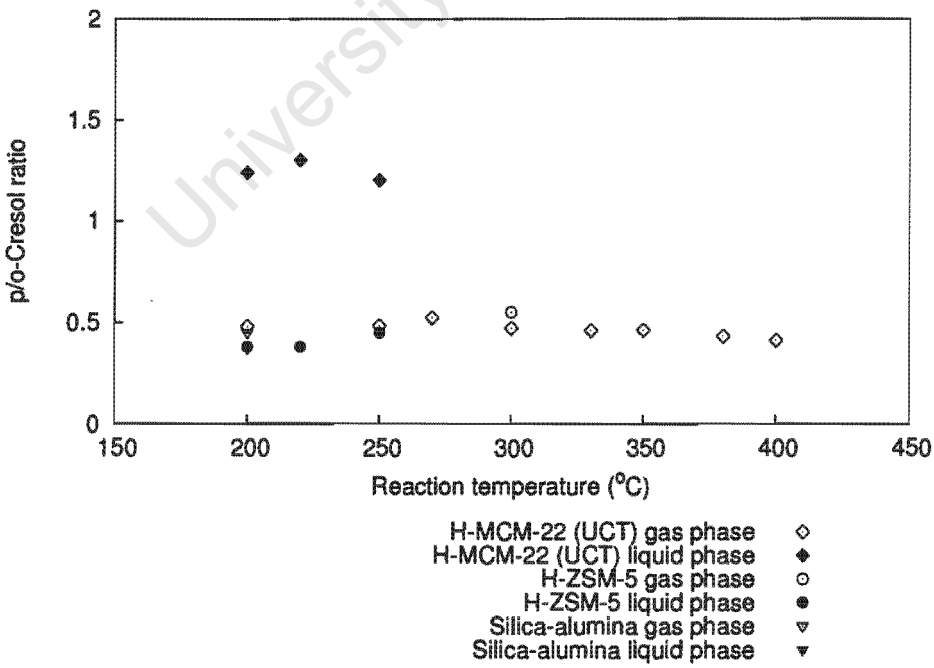

Figure 8.20: p/o-Cresol ratios observed over H-ZSM-5, H-MCM-22 (UCT) and silica-alumina in the gas and liquid phases as a function of reaction temperature.

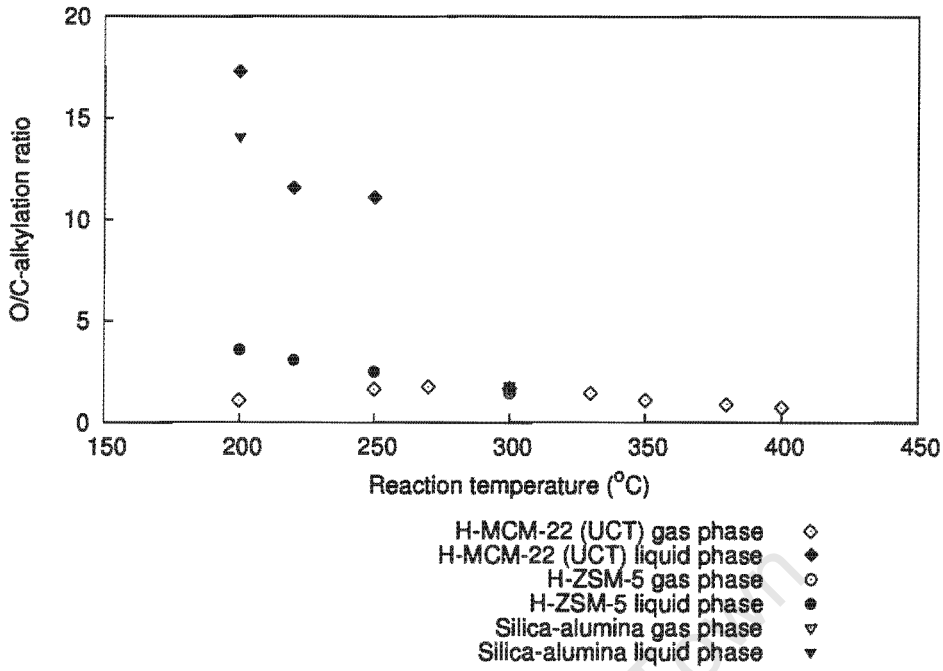

Figure 8.21: O/C-alkylation ratio observed over H-ZSM-5, H-MCM-22 (UCT) and silica-alumina in the gas and liquid phases as a function of reaction temperature.

8.5.2 Comparison of the O/C-alkylation ratio in the liquid and gas phase

Figure 8.21 shows the O/C-alkylation ratio as a function of reaction temperature in both the liquid and gas phase. Comparing for example the gas and liquid phase results over H-MCM-22 (UCT) at 250°C, it is seen that in the gas phase a lower O/C-alkylation ratio (0.61) is observed compared to the liquid phase (11.1). This means that the difference in the different phases is not due to the different temperatures used in the phases (200°C versus 300°C). The O/C-alkylation ratio was found to be related to the p/o-cresol ratio (Figure 8.14), and Figures 8.20 and 8.21 shows the same trend. The higher O/C-alkylation ratio in the liquid phase over H-MCM-22 (UCT) can be explained using to the same reasoning as the high p/o-cresol ratio (cf. Section 8.6.1). That is, increasing the pressure (from gas phase to liquid phase), results in an effective increase in the diffusional resistance inside the zeolite pores thereby increasing the selectivity of the slimmest molecule, namely anisole.

The low O/C-alkylation ratio obtained over H-ZSM-5 may also be the result of intramolecular rearrangement of anisole to o-cresol which as mentioned in the section above was thought to be the possible reason for the low p/o-cresol ratio.

Amorphous silica-alumina showed a high O/C-alkylation ratio in the liquid phase even though silica-alumina is a non-shape selective catalyst (cf. Figure 8.21). Santacesaria *et al.* [1990b] also obtained a high O/C-alkylation ratio over silica-alumina although Santacesaria *et al.* [1990b] do not state at what pressure phenol methylation over silica-alumina was studied. The phenol conversion over the silica-alumina in the liquid phase was very low (0.5%). At these low conversions and reaction temperature, the cresol formed remains on the catalyst surface whereas anisole due to its lower boiling point may leave the surface of silica-alumina giving an appearance of a high O-alkylated product.

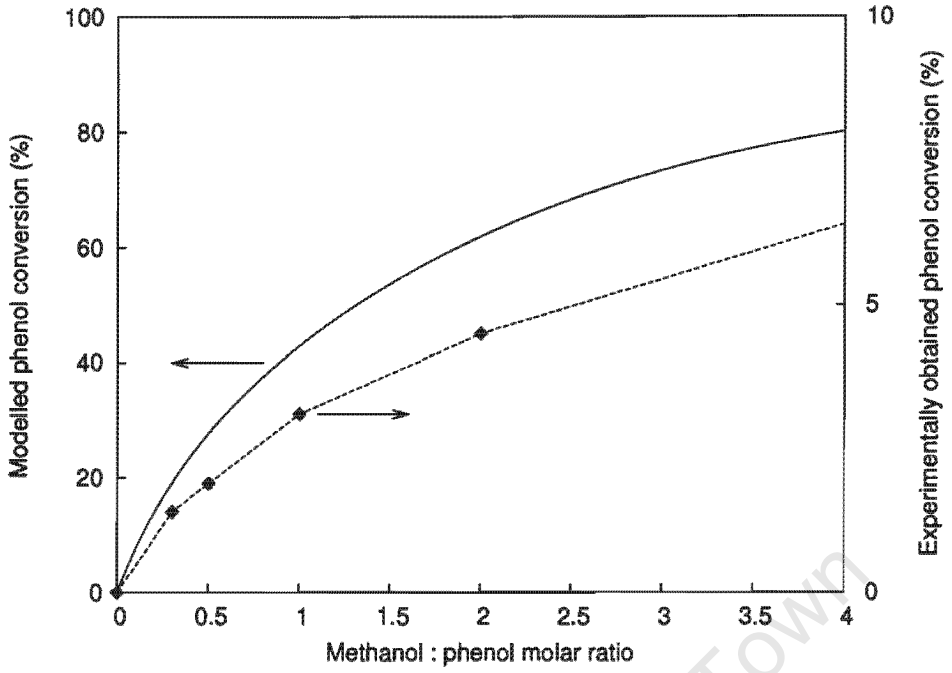

Figure 8.22: Modelling of the conversion of phenol versus the feed methanol : phenol ratio as an irreversible second order reaction.

8.6 Competitive adsorption between methanol and phenol

In the literature there is no consensus about whether there is competitive adsorption between the alkylating agent (methanol) and the aromatic compound (phenol) (cf. Section 2.2.3.4). As discussed in Section 2.2.1.1, phenol is 1 000 000 times more acidic than methanol [Sykes, 1986b]. Therefore, from the chemistry of phenol and methanol, methanol is the preferred adsorbed species given that the adsorption site is an active Brønsted acid site.

The change in phenol conversion with increasing methanol : phenol ratio was modelled as an overall irreversible second order reaction (Figure 8.22). The model predicted that phenol conversion increased sharply at the low methanol : phenol ratio and then started to level off. This trend was observed in the gas and liquid phase alkylation of phenol with methanol over H-MCM-22 (Figures 6.10 and 7.35). However, in the liquid phase, H-ZSM-5 and H-Beta showed very different trends between phenol conversion and methanol : phenol ratio (Figure 6.10) and do not fit the above mentioned model.

The phenol conversion with increasing methanol : phenol ratio was also modelled by irreversible second order kinetics with adsorption assuming Langmuir adsorption. If the preferred adsorbed species is methanol then the predicted output of the model is shown in Figure 8.23. If the preferred adsorbed species is phenol then the predicted model shows that the phenol conversion increases with increasing methanol : phenol ratio. Over H-ZSM-5 and H-Beta, Figure 6.10 showed that the phenol conversion increased rapidly, reached a maximum and then decreased slowly with feed methanol : phenol ratio. This is precisely what is predicted by the second order kinetics with methanol adsorption. Details of the models are given in Appendix G.

There is arguably a reasonably good correlation between the predicted and experimental values

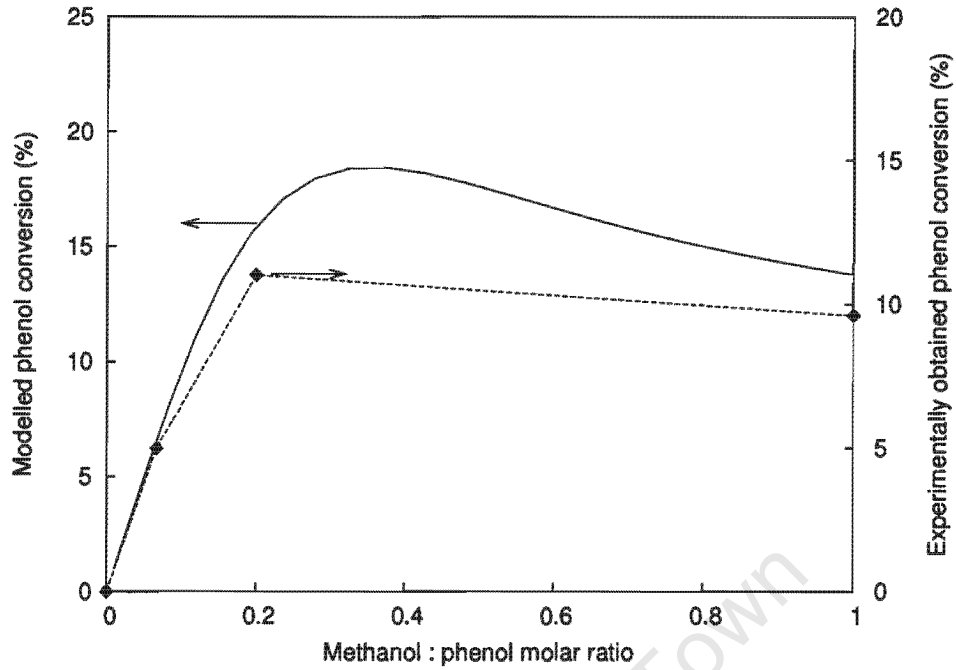

Figure 8.23: Modelling of the conversion of phenol versus the feed methanol : phenol ratio as a second order reaction with Langmuir adsorption of methanol.

obtained in both phases. This indicates that it is reasonable to assume a rate expression of the form:

$$r = k\, P_{methanol}\, P_{phenol}$$

No further kinetic analysis was carried out in this present work except for the estimation of the activation energies (cf. Section 8.3.2).

8.7 Toluene alkylation versus phenol alkylation with methanol

Toluene alkylation was compared with phenol alkylation with methanol in order to investigate the extent to which the hydroxyl group in phenol has a different influence to the methyl group on the benzene ring in the case of toluene. The results are shown in Sections 6.7 and 7.6 for the liquid phase and gas phase, respectively.

In the liquid phase, toluene methylation reaction over H-ZSM-5 resulted in disproportionation through transalkylation accounted for almost half of the product whereas over H-MCM-22 transalkylation accounted for more than 80% of the products. The comparison of phenol alkylation and toluene alkylation in the liquid phase therefore does not show any useful information.

In the gas phase, the product formed is over 99% from toluene methylation hereby allowing the comparison of toluene alkylation and phenol alkylation in the gas phase. Table 8.8 shows the comparison for H-ZSM-5 and H-MCM-22 for toluene alkylation and phenol alkylation with methanol. In phenol alkylation with methanol, alkylation can occur at the oxygen and at the benzene ring. Over H-ZSM-5 and H-MCM-22, in phenol alkylation, alkylation at the oxygen is preferred (anisole/cresol ratio

Table 8.8: Comparison of toluene alkylation with phenol alkylation over H-ZSM-5 and H-MCM-22 (UCT).

	H-ZSM-5	H-MCM-22 (UCT)
Ethylbenzene/xylene ratio	0.001	0.0
Anisole/cresol ratio	1.7	1.7
p/o-xylene ratio	0.88	0.99
p/o-cresol ratio	0.55	0.50

= 1.7) whereas in toluene alkylation there is exclusively alkylation on the ring (ethylbenzene/xylene ratio = 0.001). Therefore, the hydroxyl group on the phenol promotes the O-alkylation.

Over both H-ZSM-5 and H-MCM-22 (UCT), the p/o-xylene ratio is higher than the p/o-cresol ratio. Xylenes have a larger kinetic molecular diameter than cresols [Imbert *et al.*, 1997a], therefore the shape selective formation of p-isomer will be higher in toluene alkylation than in phenol alkylation.

Chapter 9

Conclusions

This chapter summarises the finding of the results obtained in the liquid and gas phase alkylation of phenol with methanol over H-ZSM-5, H-Beta, H-Mordenite, H-USY, H-MCM-22 and silica-alumina and ends with some recommendations on further investigations into phenol methylation over zeolites.

9.1 Thermodynamics versus kinetics

Alkylation of phenol with methanol, over the reaction conditions studied and over all the different catalysts used in this thesis, was found to be kinetically and not thermodynamically controlled. Therefore, it was possible to obtain products containing little or no m-cresol. This is important due to the high costs of separating the para and meta isomers of cresol.

9.2 Product selectivity as a function of phenol conversion

In the liquid phase, product selectivity and cresol isomer distribution was found to be independent of phenol conversion. This meant that the studies of the different catalysts and the reaction parameters investigated could be carried out and comparisons made of the various results.

In the gas phase, however, phenol conversion, as varied by space velocity, did affect the product selectivity and this may be due to the intramolecular rearrangement of anisole to o-cresol. Therefore, when comparing different catalysts and reaction parameters it was necessary to first establish if the parameter or the changing phenol conversion resulted in the change in product selectivity.

Deactivation was found to have an opposite effect on product selectivity when compared to changing phenol conversion via space velocity. This was attributed to coke formation increasing the diffusional resistance within the zeolite pores thereby increasing the preference for the slimmest molecule, namely anisole.

9.3 Reaction mechanism

In the alkylation of phenol with methanol the products were anisole, o- and p-cresols, methylanisoles and xylenols. The overall mechanism for the alkylation of phenol with methanol was derived from the

results obtained by investigating: phenol methylation reactions, product selectivities, product conversions (namely anisole and the isomers of cresol), effect of reaction temperature, effect of methanol : phenol ratio, effect of reactants partial pressure, effect of weight hourly space velocity and effect of water. The following proposed mechanism was derived for the liquid and gas phase:

- In the liquid phase, viz. high pressure and low temperatures, only the primary parallel reactions occur i.e. the alkylation of phenol with methanol to produce anisole, o-cresols and p-cresol. Anisole was the major product formed in the liquid phase over all the different catalysts and reaction conditions studied in this thesis.
- In the gas phase, viz. low pressures and high temperatures, secondary reactions occur as well as the primary parallel reactions. The secondary reactions are the intramolecular rearrangement of anisole to o-cresol, alkylation of phenol with anisole to form o-cresol and p-cresol, the conversion of cresols to xylenols, the self-alkylation of anisole to yield methylanisoles and phenol as well as the isomerization of o-cresol and p-cresol to m-cresol.

The following additional pointers were also found while investigating the above mentioned parameters:

- Alkylation of phenol with anisole occurred twice as fast as alkylation of anisole with anisole;
- Higher p/o-cresol ratio was obtained from the alkylation of phenol with anisole than from the alkylation of anisole with anisole;
- Anisole is only formed as a primary product;
- The intramolecular rearrangement of anisole to o-cresol increased with increasing reaction temperature;
- Essentially no difference was found between the apparent activation energies of O-alkylation and C-alkylation (45 kJ/mol for C-alkylation compared to 42 kJ/mol for O-alkylation over H-MCM-22 (UCT) in the gas phase);
- The overall apparent activation energies obtained were low (less than 50 kJ/mol) which implies that the reactions were controlled by diffusion or adsorption;
- In the gas phase, the reactions of phenol and methanol to either anisole or cresols must have the same reaction order with respect to phenol and methanol;
- The primary p/o-cresol ratio obtained in the gas phase was 0.38;
- The internal rearrangement of anisole to o-cresol decreased at low space velocities.

9.4 Comparison of the different catalysts

9.4.1 Effect of catalyst parameters on phenol conversion, product selectivity and cresol isomer distribution

The differences in the zeolite characterization could not explain the different O/C-alkylation ratios and the p/o-cresol ratios obtained over the zeolites and especially not the high p/o-cresol ratios obtained

over the H-MCM-22 samples. The phenol conversion was found to be affected by the bulk Si/Al ratio and the acid site strength. These two parameters are dependent on each other as increasing the bulk Si/Al ratio will increase the acid site strength.

Comparing H-MCM-22 to the other zeolites in terms of pore dimensions indicated different trends for liquid and gas phase. In the liquid phase MCM-22 did not correlate with either the 10 or 12 membered ring zeolites in terms of p/o-cresol ratio. In the gas phase, however, MCM-22 was found to be similar to H-ZSM-5 in term of p/o-cresol ratio. This indicates that the reaction phase plays an important role in the high p/o-cresol ratio over H-MCM-22.

9.4.2 Comparison of the zeolites with amorphous silica-alumina

Product selectivities observed over amorphous silica-alumina represents the non-shape selective product spectrum. Over amorphous silica-alumina it was observed that the activity in terms of phenol conversion was very low (less than 3%) for the phenol methylation reaction in both phases. In the liquid phase, similar p/o-cresol ratios were obtained over silica-alumina and the 12 membered ring zeolites, namely H-Beta and H-Mordenite. Zeolite ZSM-5, however, produced a much lower O/C-alkylation ratio and p/o-cresol ratio than silica-alumina. This is not generally expected as ZSM-5 has shown a high shape selectivity in other reactions, such as toluene alkylation. It was proposed by Venuto *et al.* [1966]; Jacobs *et al.* [1988] and Parton *et al.* [1989a] that the low O/C-alkylation ratio and p/o-cresol ratio is due to the intramolecular rearrangement of anisole to o-cresol as the bimolecular reactions would be suppressed in the ZSM-5 channels.

In the gas phase, the silica-alumina produced a much lower p/o-cresol ratio compared to the zeolites. This could be due to silica-alumina containing Lewis acid and basic sites besides Brønsted acid sites. The Lewis acid and basic pair are ortho-selective as found by Santacesaria *et al.* [1990b], therefore resulting in a lower p/o-cresol ratio over silica-alumina compared to that of the zeolites.

9.4.3 Comparison of the different types of zeolites

9.4.3.1 Activity

H-ZSM-5 was the most active zeolite, in terms of phenol conversion, for the phenol methylation reaction of all the zeolites studied. This could be a result of ZSM-5 being less susceptible to coke formation due to its three-dimensional channel system and large channel intersections. H-USY has the lowest phenol conversion probably due to coke formation which limits or blocks access of the reactant to the active sites.

9.4.3.2 p/o-Cresol ratio

The MCM-22 samples showed the highest p/o-cresol ratios of all the zeolites studied in both reaction phases. In the gas phase the p/o-cresol ratio was found to be quite stable with time-on-stream.

Internally sodium-exchanged MCM-22 and ZSM-5 showed that there is shape-selective internal mass transfer control, which favours the formation of the p-cresol and this effect was more pronounced over MCM-22 than over ZSM-5. This results in a much higher p/o-cresol ratio for MCM-22 (UCT) than for ZSM-5.

The different MCM-22 samples with different particle sizes were compared via a modified Thiele Modulus to take into account the different crystal morphology. The Thiele Modulus was modified by assuming that the rate constant was proportional to the phenol conversion and the amount of aluminium in the micropores. As was seen the p/o-cresol ratio increased with increasing values of the modified Thiele Modulus. That is, increasing the diffusional pathway in MCM-22 resulted in an increase in the slimmest of the cresol isomers, namely p-cresol.

9.4.3.3 O/C-alkylation ratio

A direct relationship between the O/C-alkylation ratio and the p/o-cresol ratio was observed. This relationship was not related to the phenol conversion but due to shape selectivity as anisole and p-cresol, both which are the slimmest molecules.

Steaming MCM-22 (DE1) resulted in an increase in the O/C-alkylation ratio (from 0.8 to 2.0) and a mild increase in p/o-cresol ratio from 0.48 to 0.53. Steaming also enhanced the activity of the zeolite by almost three-fold. The increase in the O/C-alkylation ratio was attributed to either the increase in Lewis acidity or due to the extra-framework aluminium blocking the pores and thereby increasing the diffusional resistance in the pores promoting the formation of the slimmest molecules, namely anisole and p-cresol.

9.5 Comparison between gas and liquid phase

The major difference between the gas and liquid phases was the pressure. In the gas phase the reactants partial pressure was 0.2 bar whereas in the liquid phase the autogeneous pressure ranged between 18 and 25 bar. Comparing the p/o-cresol ratio at the same temperature but with different pressures showed an increase of 2.5 times with increasing pressure. This was attributed to the increase in occupancy of molecules inside the pores which would effectively increase the diffusional resistance inside the pore. This would result in an increase in the production of the slimmest molecule, namely p-cresol. This could also account for the increase in the O/C-alkylation ratio as anisole is also one of the slimmest molecules.

9.6 Competitive adsorption between phenol and methanol

Over H-MCM-22 (UCT), in both phases, the relationship between phenol conversion and the methanol : phenol ratio could be modelled using irreversible second order kinetics. Over ZSM-5 and H-Beta in the liquid phase, however, the relationship between phenol conversion and the methanol : phenol ratio could be modelled using irreversible second order kinetics with Langmuir adsorption of methanol.

9.7 Toluene methylation versus phenol methylation

Toluene alkylation was compared to phenol alkylation with methanol in order to investigate the influence of the hydroxyl group in phenol compared to the methyl group in toluene over H-ZSM-5 and H-MCM-22 (UCT). Studying toluene alkylation in the liquid phase did not yield useful information

as disproportionation was the major reaction influencing the product spectrum whereas in the gas phase the products formed are due to toluene methylation.

In the gas phase , the large difference between toluene methylation and phenol methylation is that in toluene methylation, alkylation only occurred on the ring whereas with phenol methylation the preferred site for alkylation is the oxygen.

The p/o-xylene ratios were higher than the p/o-cresol ratios over both catalysts. This was attributed to the larger kinetic diameters of the xylenes compared to that of the cresols.

9.8 Recommendations for further investigation into phenol methylation over zeolites

In view of the above conclusions the following recommendations are given for further investigations into the phenol methylation over zeolites:

- Relative adsorption strengths (ΔH_{abs}) of phenol and the alkylating agent methanol on different catalyst surfaces is required to add more information on the competitive adsorption between these two molecules;
- Diffusional studies are required for the cresol isomers over the different catalysts in order to provide more information on the diffusional constraints of these molecules;
- Further investigations into MCM-22 are required. MCM-22 has two independent pore systems and therefore information on which pore system results in the high p/o-cresol ratio may give further information on other zeolites which could increase the p/o-cresol ratio. Investigating the phenol methylation reaction over ITQ-2 might also give more information on the reactions occurring in the different pore systems of MCM-22 as well as on surface "nests";
- Investigating larger crystal sizes is an important area for further studies for the different zeolites to improve the p/o-cresol ratio;
- Detailed kinetic investigations are required for a more comprehensive understanding of this reaction in zeolites;
- Anisole is always the major product when comparing anisole and cresols selectivity. Further investigations into ways of suppressing this reaction would be a great value in increasing the yield of p-cresol.

References

Augustine R.L., *Heterogeneous catalysis for the synthetic chemist*, chapter 10, 198, Dekker, New York (1995).

Baerlocher C., Meier W.M. and Olson D.H., *Altas of zeolite framework types*, Elsvier Science, Amsterdam, 5th edition (2001).

Balasubramanian V.V., Pandurangan A., Palanichamy M. and Murugesan V., "Methylation of phenol over ion-exchanged β-zeolites", *Indian Journal of Chemical Technology*, **7(4)**: 149–154 (2000).

Balsama S., Beltrame P., Beltrame P.L., Carniti P., Forni L. and Zuretti G., "Alkylation of phenol with methanol over zeolites", *Applied Catalysis*, **13**: 161–170 (1984).

Barrer R.M., *Hydrothermal chemistry of zeolites*, chapter 1, 1–42, Academic Press, London (1982a).

Barrer R.M., *Hydrothermal chemistry of zeolites*, chapter 2, 43–104, Academic Press, London (1982b).

Barrer R.M., "Synthesis of zeolites", in "Zeolites. Synthesis, structure, technology and application", edited by B. Držaj, S. Hočevar and S. Pejovnik, volume 24 of *Studies in Surface Science and Catalysis*, 1–26, Elsevier Science B.V., Amsterdam (1985).

Bautista F.M., Campelo J.M., Garcia A., Luna D., Marinas J.M., Romero A., Navio J.A. and Macias M., "Anion treatment (F^- or SO_4^{2-}) of $AlPO_4$-Al_2O_3 (25wt% Al_2O_3) catalyst. IV. Catalytic performance in the alkylation of phenol with methanol", *Applied Catalysis A: General*, **99**: 161–173 (1993).

Bautista F.M., Campelo J.M., Garcia A., Luna D., Marinas J.M., Romero A.A. and Urbano M.R., "$AlPO_4$-Al_2O_3 catalysts with low alumina content. VII. Anisole conversion in the presence of methanol", *Reaction Kinetics and Catalysts Letters*, **56(2)**: 349–362 (1995).

Böhringer W. and Fletcher J.C.Q., "Prelimary laboratory data (unpublished)", (2003), Catalysis Research Unit, Department of Chemical Engineering, University of Cape Town.

Beck J.S. and Haag W.O., "Alkylation of aromatics", in "Handbook of Heterogeneous Catalysis", edited by G. Ertl, H. Knozinger and J. Weitkamp, volume 5, 2123–2136, VCH, Weinheim (1997).

Beltrame P., Beltrame P.L., Carniti P., Castelli A. and Forni L., "Alkylation of phenol with anisole over zeolites or γ-alumina", *Applied Catalysis*, **29**: 327–334 (1987).

Blauwhoff P.M.M., Gosselink J.W., Kieffer E.P., Sie S.T. and Stork W.H.J., "Zeolites as catalysts in industrial processes", in "Catalysis and zeolites. Fundamentals and applications", edited by J. Weitkamp and L. Puppe, 437–538, Springer, Berlin (1999).

Breck D.W., *Zeolite molecular sieves: Structure, chemistry and use*, chapter 2. Structure of zeolites, 29–185, John Wiley and Sons, New York (1974a).

Breck D.W., *Zeolite molecular sieves: Structure, chemistry and use*, chapter 4. The synthetic zeolites, 245–378, John Wiley and Sons, New York (1974b).

Brunner E., "Characterization of solid acids by spectroscopy", *Catalysis Today*, **38**: 361–376 (1997).

Chakrabarty D.K., Subramanian S., Mitra A. and Satyanarayana C.V.V., "Para-selective butylation of phenol over silicoaluminophosphate molecular sieve SAPO-11 catalyst", *Applied Catalysis A: General*, **159**: 229–240 (1997).

Chang C.D., "Hydrocarbons from methanol", *Catalysis Reviews - Science and Engineering*, **25(1)**: 1–118 (1983).

Chang N.S., Chen C.C., Chu S.J., Chen P.Y. and Chuang T.K., "Acidity effect of ZSM-5 zeolites on phenol methylation reaction", in "Zeolites as catalysts, sorbents and detergent builders", edited by H.G. Karge and J. Weitkamp, volume 46 of *Studies in Surface Science and Catalysis*, 223–230, Elsevier Science B.V. (1989).

Chantal P.D., Kaliaguine S. and Grandmaison J.L., "Reactions of phenolic compounds over HZSM-5", *Applied Catalysis*, **18**: 133–145 (1985).

Chen N.Y., Garwood W.E. and Dwyer F.D., *Shape selective catalysis in industrial applications*, chapter 4, 62–144, Marcel Dekker, New York, 2nd edition (1996).

Chester A.W., Fung A.S., Kresge C.T. and Roth W.J., "Modified MCM-56, its preparation and use", *US Patent 5,779,882* (1998).

Choi W.C., Kim J.S., Lee T.H. and Woo S.I., "Balancing acidity and basicity for highly selective and stable modified MgO catalysts in the alkylation of phenol with methanol", *Catalysis Today*, **63**: 229–236 (2000).

Coker E.N., Hees P.S., Sotak C.H., Dixon A.G., Thompson R.W. and Sacco, Jr A., "Zeolite synthesis in unstirred batch reactors. I. Nuclear magnetic resonance imaging of non-uniform pre-mixing", *Microporous Materials*, **3(6)**: 623–636 (1995).

Corma A., "Sorption, diffusion and catalytic properties of zeolites containing 10- and 12-member ring pores in the same structure", *Microporous and Mesoporous Materials*, **21**: 487–495 (1998).

Corma A., Corell C. and Pérez-Pariente J., "Synthesis and characterization of the MCM-22 zeolite", *Zeolites*, **15**: 2–8 (1995).

Corma A., Martinez A., Arroyo P.A., Monteiro J.L.F. and Sousa-Aguiar E.F., "Isobutane/2-butene alkylation on zeolite beta: Influence of post-synthesis treatments", *Applied Catalysis A: General*, **142(1)**: 139–150 (1996).

Corma A., Martinez-Soria V. and Schnoeveld E., "Alkylation of benzene with short-chain olefins over MCM-22 zeolite: Catalytic behaviour and kinetic mechanism", *Journal of Catalysis*, **192**: 163–173 (2000).

Csicsery S.M., "Shape-selective catalysis in zeolites", *Zeolites*, **4(3)**: 202–213 (1984).

Daubert T.E. and Danner R.P. (eds.), *Physical and thermodynamic properties of the pure chemicals. Data compilation*, Hemisphere Pub. Corp., New York (1989).

De Vos D.E., Ernst S., Perego C., O'Connor C.T. and Stöcker M., "Standard reaction of the International Zeolite Association for activity characterization: Ethylbenzene disproportionation over LaNaY", *Microporous and Mesoporous Materials*, **56(2)**: 185–192 (2002).

Debras G., Gourgue A., Nagy J.B. and De Clippelair G., "Physiochemical characterization of pentasil type materials. IV. Thermal and steam stability, dealumination and aluminum exchange", *Zeolites*, **6**: 241–248 (1986).

Derouane E.G., "New aspects of molecular shape-selectivity: Catalysis by zeolite ZSM-5", in "Catalysis by zeolites", edited by B. Imelik, C. Naccache, Y. Ben Taarit, J.C. Vedrine, G. Coudurier and H. Praliaud, volume 5 of *Studies in Surface Science and Catalysis*, 5–18, Elsevier Science B.V., Amsterdam (1980).

Engel D.J., Malloy T.P. and Shoffner J.P., "Isomerization of cresols", *US Patent 4,503,269* (1985).

Ernst S., "Synthesis of more recent aluminosilcates with a potential in catalysis and adsorption", in "Synthesis", edited by H.G. Karge and J. Weitkamp, volume 1 of *Molecular Sieves*, 65–96, Springer-Verlag, Berlin (1998).

Feast S. and Lercher J.A., "Synthesis of intermediates and fine chemicals using molecular sieve catalysts", in "Recent advances and new horizons in zeolite science and technology", edited by H. Chon, S.I. Woo and S.E. Park, volume 102 of *Studies in Surface Science and Catalysis*, 363–412, Elsevier Science B.V. (1996).

Feijen E.J.P., Martens J.A. and Jacobs P.A., "Hydrothermal zeolite synthesis", in "Handbook of heterogeneous catalysis", edited by G. Ertl, H. Knözinger and J. Weitkamp, volume 1, 311–324, Wiley-VCH, Weinheim (1997).

Fernandes L.D., Monteiro J.L.F., Sousa-Aguiar E.F., Martinez A. and Corma A., "Ethylbenzene hydroisomerization over bifunctional zeolite based catalysts: The influence of framework and extraframework composition and zeolite structure", *Journal of Catalysis*, **177**: 363–377 (1998).

Fiege H. and Bayer AG, *Ulmann's encyclopedia of industrial chemistry*, electonic release Cresols and xylenols, Wiley-VCH, Weinheim, 6th edition (2001).

Flanigen E.M., "Zeolites and molecular sieves. An historical perspective", in "Introduction to zeolite science and practice", edited by H. van Bekkum, E.M. Flanigen and J.C. Jansen, volume 58 of *Studies in Surface Science and Catalysis*, 13–34, Elsevier Science B.V. (1991).

Garcia L., Giannetto G., Goldwasser M.R., Guisnet M. and Magnoux P., "Phenol alkylation with methanol: effect of sodium content and ammonia selective poisoning of an HY zeolite", *Catalysis Letters*, **37**: 121–123 (1996).

Güray I., Warzywoda J., Bac N. and Sacco Jr. A., "Synthesis of zeolite MCM-22 under rotating and static conditions", *Microporous and Mesoporous Materials*, **31**: 241–251 (1999).

Gibson J.P., Edwards G.C., Peters A.W., Rajagopalan K., Wormsbecher R.F., Roberie T.G. and Shatlock M.P., "Penta-co-ordinated aluminium in zeolites and aluminosilicates", *Journal of Chemical Society. Chemical Communications*, 91–92 (1987).

Gläser R., Li R., Hunger M., Ernst S. and Weitkamp J., "Zeolite HNU-87: synthesis, characterization and catalytic properties in the shape-selective conversion of methylnaphthalenes", *Catalysis Letters*, **50**: 141–148 (1998).

Green J.H.S., "Normal frequencies, thermodynamic properties and equilibrium of the cresols", *Chemistry and Industry*, 1575–1576 (1962).

Guisnet M., Neves I., Ribeiro F.R., Canaff C., Magnoux P. and Perot G., "Coking, aging and regeneration of zeolites. XII - Composition of coke formation on USHY during phenol alkylation with methanol - mode of formation", in "Catalyst deactivation", edited by C.H. Bartholomew and J.B. Butt, volume 68 of *Studies in Surface Science and Catalysis*, 735–743, Elsevier Science B.V., Amsterdam (1991).

Guth J.L. and Kessler H., "Synthesis of aluminosilicate zeolites and related silica-based materials", in "Catalysis and zeolites. Fundamentals and applications", edited by J. Weitkamp and L. Puppe, chapter 1, 1–52, Springer, Berlin (1999).

Haag W.O. and Lago R.M., "Isomerization of paraffin hydrocarbons using zeolites with high steam-enhanced acidity", *US Patent 4,374,296* (1983).

Haggin J., "Structure of zeolite Beta determined", *Chemical and Engineering News*, **66**: 23–27 (20 June 1988).

Halász I., Horváth J., Mándy T., Schmidt L. and Tasnádi E., "Hydrothermal behaviour of zeolites in FCC catalysts", in "Zeolites: Synthesis, structure and technology and application", edited by B. Držaj, S. Hočevar and S. Pejovnik, volume 24 of *Studies in Surface Science and Catalysis*, 393–399, Elsevier Science, Amsterdam (1985).

Hart H. and Schuetz R.D., *Organic chemistry. A short course*, chapter 6. Alcohols and phenols, 118–143, Houghton Mifflin, Boston, 4th edition (1972a).

Hart H. and Schuetz R.D., *Organic chemistry. A short course*, chapter 7. Ethers, 144–157, Houghton Mifflin, Boston, 4th edition (1972b).

Haung F.Y., Yang S.M. and Chen L.Y., "Methylation reaction of phenol using HZSM-5 as catalyst", *Huaxue*, **44(1)**: 6–12 (1986), as cited in Parton *et al.* [1989a].

Higgins J.B., LaPierre R.B., Schlenker J.L., Rohrman A.C., Wood J.D., Kerr G.T. and Rohrbaugh W.J., "The framework topology of zeolite Beta", *Zeolites*, **8**: 446–452 (1988).

Hong Y., Gruver V. and Fripiat J.J., "Role of Lewis activity in the isomerization of n-pentane and o-xylene on dealuminated H-Mordenites", *Journal of Catalysis*, **150**: 421–429 (1994).

Hunger M., Ernst S. and Weitkamp J., "Multinuclear solid-state n.m.r. investigation of zeolite MCM -22", *Zeolites*, **15**: 188–192 (1995).

Imbert F.E., Gnep N. and Guisnet M., "Cresol isomerization on HZSM-5", *Journal of Catalysis*, **172**: 307–313 (1997a).

Imbert F.E., Gnep N.S., Ayrault P. and Guisnet M., "Effects of commercial HFAU structural parameters over m-cresol transformation", *Applied Catalysis A: General*, **215(2)**: 225–234 (2001).

Imbert F.E., Gnep S. and Guisnet M., "Transformation of meta- and ortho-cresol over HY", *Catalysis Letters*, **49**: 121–128 (1997b).

Imbert F.E., Guisnet M. and Gnep S., "Comparison of cresol transformation on USHY and HZSM-5", *Journal of Catalysis*, **195**: 279–286 (2000).

IZA, "Database of zeolite structures", *www.iza-structure.org/databases* (2002a).

IZA, "IZA synthesis commission", *www.iza-synthesis.org* (2002b).

Jacobs J.M., Parton R.F., Boden A.M. and Jacobs P.A., "Self-alkylation of anisole over acid medium-pore zeolites", in "Heterogeneous Catalysis and Fine Chemicals", edited by M. Guisnet, J. Barrault, C. Bouchoule, D. Duprez, C. Montassier and G. Pérot, volume 41 of *Studies in Surface Science and Catalysis*, 221–230, Elsevier Science B.V. (1988).

Jansen J.C. and Wilson S.T., "The preparation of oxide molecular sieves", in "Introduction to zeolite science and practice", edited by H. van Bekkum, E.M. Flanigen, P.A. Jacobs and J.C. Jansen, volume 137 of *Studies in surface science and catalysis*, 175–227, Elsevier Science, Amsterdam, 2nd edition (2001).

Jongkind H., Datema K.P., Nabuurs S., Seive A. and Stork W.H.J., "Synthesis and characterisation of zeolites using saturated cyclic amines as structure-directing agents", *Microporous Materials*, **10**: 149–161 (1997).

Juttu G.G. and Lobo R.F., "Characterization and catalytic properties of MCM-56 and MCM-22 zeolites", *Microporous and Mesoporous Materials*, **40**: 9–23 (2000).

Karge H.G., Hunger M. and Beyer H.K., "Characterization of zeolites - Infrared and nuclear magnetic resonance spectroscopy and X-ray diffraction", in "Catalysis and zeolites. Fundamentals and applications", edited by J. Weitkamp and L. Puppe, 198–326, Springer, Berlin (1999).

Kennedy G.J., Lawton S.L., Fung A.S., Rubin M.K. and Steuernagel S., "Multinuclear MAS NMR studies of zeolites MCM-22 and MCM-49", *Catalysis Today*, **49**: 385–399 (1999).

Kuehl G.H. and Timken H.K.C., "Acid sites in zeolite Beta: effects of ammonium exchange and steaming", *Microporous and Mesoporous Materials*, **35-36**: 521–532 (2000).

Laan J.A.M. and Ward J.P., "Selective mono ortho-alkylation of phenol with an aluminium catalyst", *Chemistry and Industry*, **January**: 34–35 (1987).

Lago R.M., Haag W.O., Mikovsky R.J., Olson D.H., Hellring S.D., Schmitt K.D. and Kerr G.T., "The nature of catalytic sites in HZSM-5 - Activity enhancement", in "New Developments in zeolite science and technology", edited by Y. Murakami, A. Iijima and J.W. Ward, volume 28 of *Studies in Surface Science and Catalysis*, 677–684, Elsevier Science B.V., Amsterdam (1986).

Landau M.V., Kogan S.B., Tavor D., Herskowitz M. and Koresh J.E., "Selectivity in heterogeneous catalytic processes", *Catalysis Today*, **36**: 497–510 (1997).

Lawton S.L., Leonowicz M.E., Partridge R.D., Chu P. and Rubin M.K., "Twelve-ring pockets on the external surface of MCM-22 crystals", *Microporous and Mesoporous Materials*, **23**: 109–117 (1998).

Löwenstein W., "The distribution of aluminum in the tetrahedra of silicates and aluminates?", *The American Mineralogist*, **39**: 92–96 (1954).

Lee S.C., Lee S.W., Kim K.S., Lee T.J., Kim D.H. and Kim J.C., "O-alkylation of phenol derivatives over basic zeolites", *Catalysis Today*, **44**: 253–258 (1998).

Leonowicz M.E., Lawton J.A., Lawton S.L. and Rubin M.K., "MCM-22: A molecular sieve with two independent multidimensional channel systems", *Science*, **264**: 1910–1913 (1994).

Mabaso E.I., *Catalytic conversion of ethylbenzene over acid zeolites*, Master's thesis, University of Cape Town, South Africa (2000).

Maesen T. and Marcus B., "The zeolite scene - An overview", in "Introduction to zeolite science and practice", edited by H. van Bekkum, E.M. Flanigen, P.A. Jacobs and J.C. Jansen, volume 137 of *Studies in Surface Science and Catalysis*, 1–9, Elsevier Science B.V., Amsterdam, 2nd edition (2001).

Marczewski M., Bodibo J.P., Perot G. and Guisnet M., "Alkylation of aromatics Part I. Reaction network of the alkylation of phenol by methanol on USHY zeolite", *Journal of Molecular Catalysis*, **50**: 211–218 (1989).

Marczewski M., Perot G. and Guisnet M., "Alkylation of aromatics II. Alkylation of phenol with methanol on various zeolites", in "Heterogeneous Catalysis and Fine Chemicals", edited by M. Guiset, J. Barrault, C. Bouchoule, D. Duprez, C. Montassier and G. Perot, volume 41 of *Studies in Surface Science and Catalysis*, 273–282, Elsevier Science B.V. (1988).

Marczewski M., Perot G. and Guisnet M., "Alkylation of aromatics. Kinetics of phenol alkylation with methanol", *Reaction Kinetics and Catalysis Letters*, **57(1)**: 21–27 (1996).

Martens J.A., Souverijns W., van Rhijn W. and Jacobs P.A., "Acidity and basicity in zeolites", in "Handbook of Hetergeneous Catalysis", edited by G. Ertl, H. Knözinger and J. Weitkamp, volume 1, 324–365, Wiley-VCH, Weinheim (1997).

Maxwell I.E. and Stork W.H.J., "Hydrocarbon processing with zeolites", in "Introduction to Zeolite Science", edited by H. van Bekkum, E.M. Flanigen, P.A. Jacobs and J.C. Jansen, volume 137 of *Studies in Surface Science and Catalysis*, 747–819, Elsevier Science B.V., Amsterdam, 2nd edition (2001).

McCusker L.B. and Baerlocher C., "Zeolite structures", in "Introduction to zeolite science and pratice", edited by H. van Bekkum, E.M. Flanigen, P.A. Jacobs and J.C. Jansen, volume 137 of *Studies in Surface Science and Catalysis*, 37–67, Elsevier Science B.V., Amsterdam, 2nd edition (2001).

Möller K.P., Böhringer W., Schnitzler A.E., van Steen E. and O'Connor C.T., "The use of a jet loop reactor to study the effect of crystal size and co-feeding of olefins and water on the conversion of methanol over HZSM-5", *Microporous and Mesoporous Materials*, **29(1-2)**: 127–144 (1999).

Meier M.W. and Olson D.H., *Atlas of zeolite structure types*, Butterworth-Heinemann, Boston, 4th edition (1996).

Meier W.M., Kokotailo G.T., Lawton S.L. and Olson D.H., "Structure of synthetic zeolite ZSM-5", *Nature*, **272**: 437–438 (1978).

Mikovsky R.J. and Marshall J.F., "Random aluminum-ion siting in the Faujasite lattice", *Journal of Catalysis*, **44**: 170–173 (1976).

Morrison R.T. and Boyd R.N., *Organic Chemistry*, chapter 14. Electrophilic aromatic substitution, 499–529, Allyn and Bacon, Boston, 5th edition (1987).

Moscou L., "The zeolite scene", in "Introduction to zeolite science and practice", edited by H. van Bekkum, E.M. Flanigen and J.C. Jansen, volume 58 of *Studies in Surface Science and Catalysis*, 1–12, Elsevier Science B.V. (1991).

Naber J.E., de Jong K.P., Stork W.H.J., Kuipers H.P.C.E. and Post M.F.M., "Industrial applications of zeolite catalysis", in "Zeolites and related microporous materials: State of the art 1994", edited by J. Weitkamp, H.G. Karge, H. Pfeifer and W. Hölderich, volume 84 of *Studies in Surface Science and Catalysis*, 2197–2219, Elsevier Science B.V., Amsterdam (1994).

Nagy J.B., Bodart P., Hannus I. and Kiricsi I., *Synthesis, characterization and use of zeolitic microporous materials*, chapter 6, 119–131, DecaGen, Hungary (1998a).

Nagy J.B., Bodart P., Hannus I. and Kiricsi I., *Synthesis, characterization and use of zeolitic microporous materials*, chapter 8, 148–192, DecaGen, Hungary (1998b).

Nagy J.B., Bodart P., Hannus I. and Kiricsi I., *Synthesis, characterization and use of zeolitic microporous materials*, chapter 4, 59–92, DecaGen, Hungary (1998c).

Nagy J.B., Bodart P., Hannus I. and Kiricsi I., *Synthesis, characterization and use of zeolitic microporous materials*, chapter 7, 132–147, DecaGen, Hungary (1998d).

Namba S., Yashima T., Itaba Y. and Hara N., "Selective formation of p-cresol by alkylation of phenol with methanol over Y type zeolite", in "Catalysis by zeolites", edited by B. Imelik, C. Naccache, Y. Ben Taarit, J.C. Vedrine, G. Coudurier and H. Praliaud, volume 5 of *Studies in Surface Science and Catalysis*, 105–111, Elsevier Science B.V. (1980).

Narayanan S., Sultana A., Le Q.T. and Aurox A., "A comparative and multitechnical approach to the acid character of templated and non-templated ZSM-5 zeolites", *Applied Catalysis A: General*, **168(2)**: 373–384 (1998).

Nayak V.S. and Choudhary V.R., "Effect of hydrothermal treatments on acid strength distribution and catalytic properties of HZSM-5", *Applied Catalysis*, **10**: 137–145 (1984).

Newsam J.M., Treacy M.M.J., Koetsier W.T. and De Gruyter C.B., "Structural characterization of zeolite beta", *Proceedings of the Royal Society London*, **A 420**: 375–405 (1988).

Ntshabele J., *Acid catalysed alkylation of diphenyl ether with methanol*, Master's thesis, University of Cape Town (in preparation).

O'Connor C.T. and Haag W.O., "Personal communication", (1996).

O'Donovan A.W., *The effect of hydrothermal and acid dealumination on the structural, acidic and catalytic properties of mordenite*, Ph.D. thesis, University of Cape Town (1995).

Parton R.F., Jacobs J.M., Huybrechts D.R. and Jacobs P.A., "Shape-selective catalysis in zeolites with organic substrates containing oxygen", in "Zeolites as catalysts, sorbents and detergent builders", edited by H.G. Karge and J. Weitkamp, volume 46 of *Studies in Surface Science and Catalysis*, 163–192, Elsevier Science B.V. (1989a).

Parton R.F., Jacobs J.M., van Ooteghem H. and Jacobs P.A., "Comparison of the alkylation of anisole and phenol with methanol on pentasil and ultrastable zeolites", in "Zeolites as catalysts, sorbents and detergent builders", edited by H.G. Karge and J. Weitkamp, volume 46 of *Studies in Surface Science and Catalysis*, 211–221, Elsevier Science B.V. (1989b).

Pierantozzi R. and Nordquist A.F., "Selective O-alkylation of phenol with methanol", *Applied Catalysis*, **21**: 263–271 (1986).

Ravishankar R., Bhattacharya D., Jacob N.E. and Sivasanker S., "Characterization and catalytic properties of zeolite MCM-22", *Microporous Materials*, **4**: 83–93 (1995).

Röger H.P., Krämer M., Möller K.P. and O'Connor C.T., "Effects of in-situ chemical vapour deposition using tetraethyoxysilane on the catalytic and sorption properties of ZSM-5", *Microporous and Mesoporous Materials*, **21**: 607–614 (1998).

Renaud M., Chantal P.D. and Kaliaguine S., "Anisole production by alkylation of phenol over ZSM-5", *The Canadian Journal of Chemical Engineering*, **64**: 787–791 (1986).

Rubin M.K. and Chu P., "Composition of synthetic porous crystalline material, its synthesis and use", *US Patent 4,954,325* (1990).

Sano T., Wakabayashi S., Oumi Y. and Uozumi T., "Synthesis of large mordenite crystals in the presence of aliphatic alcohol", *Microporous and Mesoporous Materials*, **46(1)**: 67–74 (2001).

Santacesaria E., Di Serio M., Ciambelli P., Gelosa D. and Carrà S., "Catalytic alkylation of phenol with methanol: Factors influencing activities and selectivities II. Effect of intracrystalline diffusion and shape selectivity on H-ZSM-5 zeolite", *Applied Catalysis*, **64**: 101–117 (1990a).

Santacesaria E., Grasso D., Gelosa D. and Carrà S., "Catalytic alkylation of phenol with methanol: Factors influencing activities and selectivities. I. Effect of different acid sites evaluated by studying the behaviour of the catalysts: γ-alumina, Nafion-H, silica-alumina and phosphoric acid", *Applied Catalysis*, **64**: 83–99 (1990b).

Shao C., Kim H.Y., Li X., Park S.J. and Lee D.R., "Synthesis of high-silica content mordenite with different SiO_2/Al_2O_3 ratios by using benzene-1,2-diol as additives", *Materials Letters*, **56(1-2)**: 24–29 (2002).

Stach H. and Jänchen J., "Relationship between acid-strength and framework aluminum content in dealuminated mordenites", *Zeolites*, **12**: 152–154 (1992).

Stach H., Jänchen J. and Lohse U., "Relationship between acid strength and framework aluminium content in dealuminated faujasites", *Catalysis Letters*, **13**: 389–393 (1992).

Steck W., Lermer H., Schwarzmann M. and Dockner T., "Preparation of mixtures of isomeric cresols with a molar ratio of para- to meta-cresol of at least 0.6:1 to 10:1", *US Patent 5,015,785* (1990).

Stull D.R., Westrum Jr. E.F. and Sinke G.C., *The chemical thermodynamics of organic compounds*, chapter 10. Chemical thermodynamics of compounds of carbon, hydrogen and oxygen, 368–456, Wiley, New York (1969).

Sykes P., *A guidebook to mechanism in organic chemistry*, chapter 3. The strengths of acids and bases, 53–76, Longman Scientific and Techanical, Essex, 6th edition (1986a).

Sykes P., *A guidebook to mechanism in organic chemistry*, chapter 6. Electrophilic and nucleophilic substitution in aromatic systems, 130–177, Longman Scientific and Techanical, Essex, 6th edition (1986b).

Szostak R., *Handbook of molecular sieves*, van Nostrand, Reinhold, New York (1992).

Szostak R., "Secondary synthesis methods", in "Introduction to zeolite science and practice", edited by H. van Bekkum, E.M. Flanigen, P.A. Jacobs and J.C. Jansen, volume 137 of *Studies in Surface Science and Catalysis*, 261–297, Elsevier Science B.V., Amsterdam, 2nd edition (2001).

Tanabe K., "Catalysis by solid bases and related subjects", in "Catalysis by acids and bases", edited by B. Imelik, C. Naccache, G. Coudurier, Y. Ben Taarit and J.C. Vedrine, volume 20 of *Studies in Surface Science and Catalysis*, 1–14, Elsevier Science B.V. (1985).

Tanabe K. and Nishizaki T., "The selectivity of oxide catalysts for the alkylation of phenols with methanol", in "Proceedings of the 6th International Congress on Catalysis", edited by G. Bond, P.B. Wells and F.C. Tompkins, 863–871, The Chemical Society, England (1977).

Treacy M.M.J. and Newsam J.M., "Two new three-dimensional twelve-ring zeolite frameworks of which zeolite beta is a disordered intergrowth", *Nature*, **332**: 249–251 (1988).

Venuto P.B., "Organic catalysis over zeolites: A perspective on reaction paths within micropores", *Microporous Materials*, **2**: 297–411 (1994).

Venuto P.B., Hamilton L.A., Landis P.S. and Wise J.J., "Organic reactions catalyzed by crystalline aluminosilicates. I Alkylation reactions", *Journal of Catalysis*, **5**: 81–98 (1966).

von Ballmoss R. and Higgins J.B., "Collection of simulated x-ray powder patterns for zeolites", *Zeolites*, **10(5)**: 397S–514S (1990).

Wang Q.L., Giannetto G. and Guisnet M., "Dealumination of zeolites. III. Effect of extra-framework aluminium species on the activity, selectivity and stability of Y zeolites in n-heptane cracking", *Journal of Catalysis*, **130**: 471–482 (1991).

Weast R.C. (ed.), *CRC handbook of chemistry and physics*, chapter C, C45–C553, CRC Press, Florida, 1st student edition (1991).

Weissermel K. and Arpe H.J., *Industrial organic chemistry*, 347–361, Wiley-VCH, Weinheim, 3rd edition (1997).

Weisz P.B., "Molecular shape selective catalysis", *Pure and Applied Chemistry*, **52**: 2091–2103 (1980).

Weitkamp J. and Ernst S., "Catalytic test reactions for probing the pore width of large and super-large pore molecular sieves", *Catalysis Today*, **19**: 107–150 (1994).

Weitkamp J., Ernst S. and Puppe L., "Shape-selective catalysis in zeolites", in "Catalysis and zeolites. Fundamentals and applications", edited by J. Weitkamp and L. Puppe, 327–376, Springer, Berlin (1999).

Williams B.A., Miller J.T., Snurr R.Q. and Kung H.H., "An explanation of the differences in catalytic hydrocarbon cracking activity between steam and chemically dealuminated Y zeolites", *Microporous and Mesoporous Materials*, **35-36**: 61–74 (2000).

Xu J., Yan A.Z. and Xu Q.H., "Alklyation of phenol with methanol on H-beta zeolite", *Reaction Kinetics Catalysis Letters*, **62(1)**: 71–74 (1997).

Zaiku X., Qingling C., Bo C. and Chengfang Z., "Influence of alkalinity on particle size distribution and crystalline structure in synthesis of zeolite beta", *Crystal Engineering*, **4(4)**: 359–372 (2001).

Appendices

Appendix A

Typical GC spectra obtained for the alkylation of phenol with methanol

Shown in Figure A.1 is a gas chromatograph for the liquid phase taken from the liquid phase phenol methylation with methanol. The liquid phase was analysed using a HP 5890A gas chromatograph with a RH-1 column with the GC conditions given in Table A.1.

Figure A.2 shows the gas chromatograph for the gas phase phenol methylation with methanol. The gaseous products were analysed with on-line sampling using a Varian 3400 GC with a CP-cresol column. GC set-up and conditions are given in Table A.2.

Table A.1: The GC set-up and conditions for the analysis of the liquid phase products.

Gas chromatography	HP 5890A
Column	RH-1
Length and inner diameter	60 m, 0.25 mm
Stationary phase	100% Dimethylpolysiloxane
Film thickness	0.25μm
Carrier gas	Hydrogen
Column head pressure	1.1 bar
Injector	Split injector
Injector temperature	250°C
Split	1 : 100
Detector	Flame ionisation detector
Detector temperature	325°C
Temperature program	5 min isothermal at 50°C, heat at 10°C/min to 250°C, hold for 5 min at 250°C.

Table A.2: The GC set-up and conditions for the analysis of the gas phase products.

Gas chromatography	Varian 3100
Column	CP cresol fused silica WCOT
Length and inner diameter	50 m, 0.25 mm
Film thickness	0.2μm
Make-up gas	Nitrogen
Carrier gas	Hydrogen
Column head pressure	4 bar
Injector	Split injector
Injector temperature	200°C
Split	1 : 80
Detector	Flame ionisation detector
Detector temperature	200°C
Temperature program	50°C for 3 min, heat to 120°C at 15°C/min, hold at 120°C for 40 min.

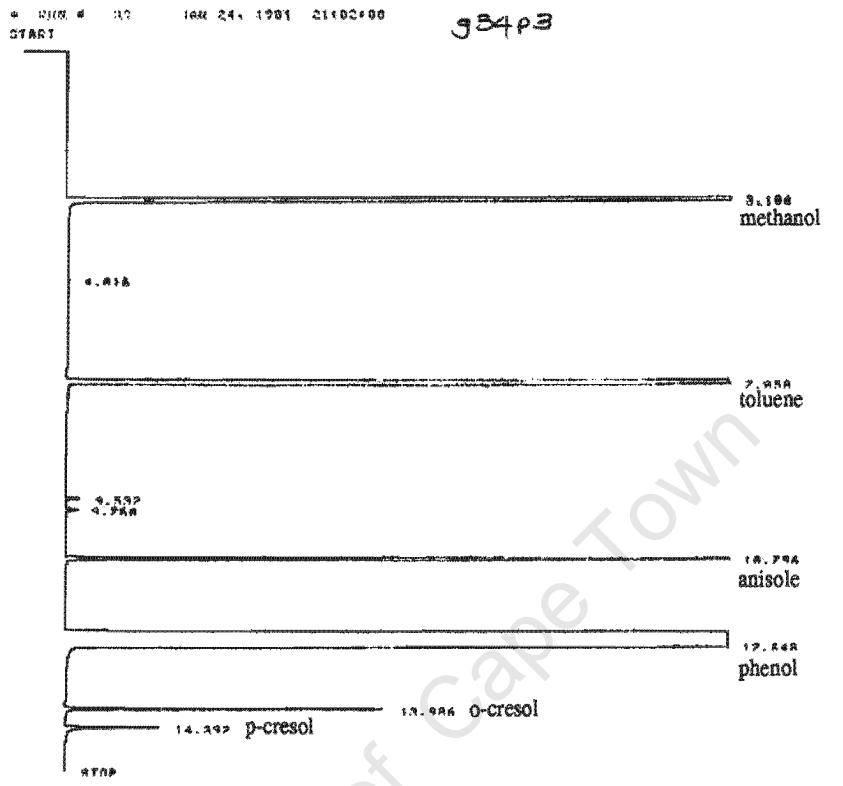

RUN# 39 JAN 24, 1991

SIGNAL FILE: M:\SIGNAL.RAW
AREA%

RT	AREA	TYPE	WIDTH	AREA%
3.186	585838	PV	.018	5.37914
3.138	672787	VB	.026	6.18538
4.016	247	PB	.032	.00227
7.856	1322297	PB	.047	12.47484
9.532	1237	BB	.029	.01137
9.768	1607	PB	.045	.01478
10.786	142146	PB	.032	1.30698
12.648	7514528	PB	.105	69.09341
13.986	26742	PB	.029	.24588
14.392	9356	PB	.034	.08603

TOTAL AREA=1.0874E+07
MUL FACTOR=1.0000E+00

Figure A.1: Gas chromatograph of the liquid phase taken from the autoclave of the liquid phase alkylation of phenol with methanol.

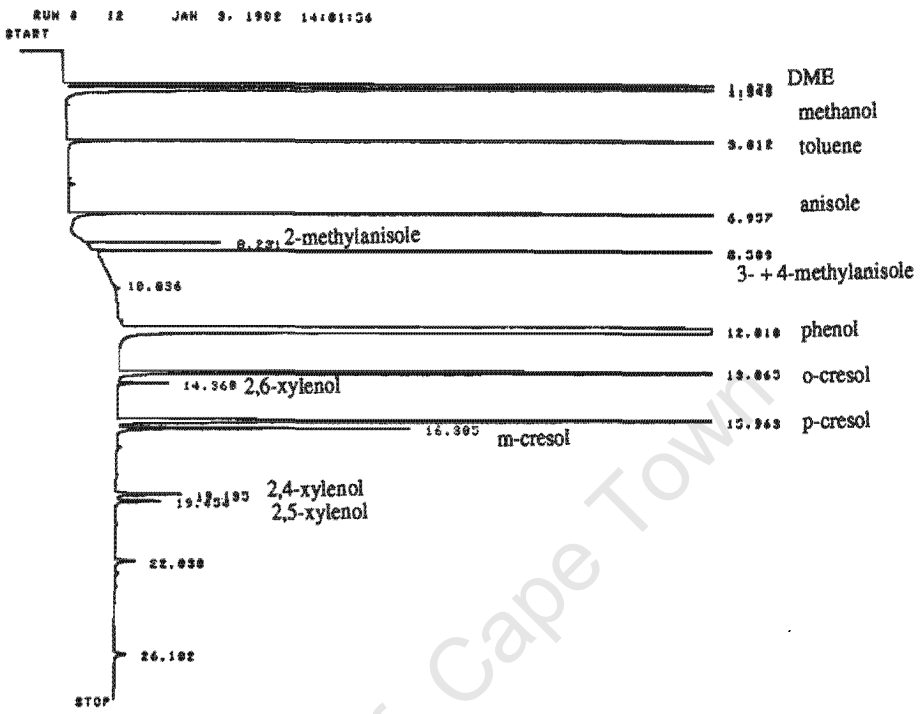

RUN# 12 JAN 3, 1992 14:01:34

AREA%

RT	AREA	TYPE	WIDTH	AREA%
1.378	43338	PB	.019	3.91828
1.549	62327	BB	.067	5.63047
3.812	50963	PB	.023	4.60543
4.957	176284	PB	.024	15.93853
8.231	2406	BB	.024	.21743
8.389	10256	PB	.021	.92708
10.836	1218	PV	1.186	.10935
12.018	600611	PB	.031	54.27634
13.863	81673	PB	.001	7.38867
14.368	2023	PV	.033	.44388
15.963	50130	PP	.183	4.53198
16.385	14839	PB	.069	1.34279
19.133	4247	BB	.008	.38398
19.434	2938	BP	.089	.26659
22.038	1872	VV	.116	.16917
26.182	1183	BP	.141	.10789

TOTAL AREA-1106388
VOL FACTOR-1.0000E+00

Figure A.2: Gas chromatograph of the gas phase alkylation of phenol with methanol.

Appendix B

Material balance for the liquid phase alkylation of phenol with methanol

Firstly, the autoclave was weighed before and after a run to make sure that there were no major leaks during the run. A overall mass balance was done by:

$$\text{Mass balance (\%)} = \frac{\text{weight of autoclave after run}}{\text{weight of autoclave before run}} \times 100$$

Typical values for the weight of the autoclave before and after a run are 3.015kg and 3.010kg, respectively. This gives an overall mass balance around 99.8%. The difference in weight was attributed to the loss of methanol and dimethyl ether in the gas phase which did not condense upon cooling of the autoclave to room temperature as confirmed by analysis of the gas in the autoclave after an experiment.

Material balances on a ring mole basis was also done. This is because a material balance over the lighter components (methanol, dimethyl ether and water), which did not completely condense upon cooling, could not be done.

Material balances were calculated on a ring mole basis with an exact amount of internal standard added to a known sample mass. Toluene was used as an internal standard as it was not produced in the phenol methylation reaction. A small sample volume (typically 3 ml) was removed from the autoclave and centrifuged to remove the catalyst particles. The sample was then weighed and a known mass of toluene was added to the sample. The sample was then analysed in a GC to obtain the mass % of the ring compounds in the sample.

The mass percentage of the ring compound in the sample was calculated from:

$$\text{mass \% of compound i} = \frac{A_i RF_i}{\Sigma(A_i RF_i)}$$

where:

- i is only the ring compounds (namely, phenol, anisole, cresols, methylanisoles and xylenols);
- A_i is the area on the GC peak of compound i;

- RF_i is the mass response factor of compound i.

The mass of the autoclave with the liquid after the reaction less the actual autoclave mass and the mass of the catalyst added gives the mass of the liquid in the autoclave. This mass of liquid after reaction contains methanol, dimethyl ether and water. The total mass of ring compounds in the sample analysed was then determined by:

$$\text{Mass of ring compounds in sample + toluene (g)} = \frac{\text{mass of internal standard}}{\text{ring mass\% of the internal standard}}$$

$$\text{Mass of ring compounds in sample (g)} = (\text{mass of ring compounds in sample + toluene}) - \text{mass of toluene}$$

Therefore the total mass of ring compounds is therefore:

$$\text{Total mass of ring compounds (g)} = \frac{\text{mass of ring compounds in sample}}{\text{sample mass}} \times \text{mass of liquid in autoclave}$$

Then the mass of ring compounds in the autoclave can be calculated by:

$$\text{Mass of ring compound i in autoclave (g)} = \frac{\text{mass \% of compound i} \times \text{total mass of ring compounds}}{(100 - \text{ring mass\% of internal standard in sample})}$$

The total moles of the ring compounds can then be calculated by:

$$\text{Moles of ring compound i in autoclave (moles)} = \frac{\text{mass ring compound i in autoclave}}{\text{molecular weight of ring compound i}}$$

The ring mole balance can then be calculated as follows:

$$\text{Ring mole balance (\%)} = \frac{\sum n_{\text{ring compounds}}}{n_{\text{feed phenol}}} \times 100$$

where:

- $n_{\text{ring components}}$ is the number of mole of the ring products;
- $n_{\text{feed phenol}}$ is the number of mole of phenol in the feed.

Phenol conversion, product selectivities and yields are calculated as follows:

$$\text{Phenol conversion (\%)} = \frac{\text{total moles of alkylated phenols formed}}{(\text{moles of alkylated phenols product + moles unconverted phenol})} \times 100$$

$$\text{Selectivity of product i (mol\%)} = \frac{\text{moles of product i formed}}{\text{total moles of alkylated phenols formed}} \times 100$$

$$\text{Yield of product i (\%)} = \frac{\text{mole of product i formed}}{(\text{moles of alkylated phenols products + moles unconverted phenol})} \times 100$$

Table B.1: Response factors used in the calculation of product selectivities.

Compounds	Response Factor (mass %)
Methanol	4.38
Dimethyl ether	3.15
Toluene	1
Phenol	1.28
Anisole	1.33
Cresols	1.26
Methylanisoles	1.31
Xylenols	1.23

Calculated response factors were used in the determination of product selectivities and are shown in Table B.1.

A model calculation for determination of ring mole balance, phenol conversion, product selectivities and cresol isomer distribution is shown in Table B.2.

Mass of toluene = 0.0189 g

Mass of product sample = 1.5396 g

Total mass of wet product from autoclave after reaction = 197.11 g

Mass of phenol in reactants = 147.1 g

Total mass of ring compounds from the autoclave = 145.38 g

Table B.2: Model calculation of ring mole balance, phenol conversion, product selectivities and yield for liquid phase phenol alkylation with methanol.

Compound	Reponse factor (RF)	GC Area	Area ×RF	Molecular weight	Mass %	Mass actual (g)	Mole	Selectivity (mol%)	Yield (%)
Toluene	1	27354	27354	92	1.64	-	-	-	-
Phenol	1.28	1092996	1399035	94	83.73	123.76	1.317	-	-
Anisole	1.33	173107	230232.3	108	13.78	20.37	0.189	94.2	12.1
o-Cresol	1.26	4098	5163.5	108	0.31	0.46	0.004	2.1	0.3
p-Cresol	1.26	5112	6441.1	108	0.39	0.57	0.005	2.6	0.3
m-Cresol	1.26	0	0	108	0.0	0.0	0.0	0.0	0.0
2-Methylanisole	1.31	2004	2625.2	122	0.15	0.23	0.002	1.1	0.1
3+4-Methylanisole	1.31	0	0	122	0.0	0.0	0.0	0.0	0.0
2,3-Xylenol	1.23	0	0	122	0.0	0.0	0.0	0.0	0.0
2,4-Xylenol	1.23	0	0	122	0.0	0.0	0.0	0.0	0.0
2,5-Xylenol	1.23	0	0	122	0.0	0.0	0.0	0.0	0.0
Xylenol	1.23	0	0	122	0.0	0.0	0.0	0.0	0.0
Xylenol	1.23	0	0	122	0.0	0.0	0.0	0.0	0.0
Xylenol	1.23	0	0	122	0.0	0.0	0.0	0.0	0.0
Other	1.2	0	0	130	0.0	0.0	0.0	0.0	0.0
Ring mole balance (%)	97.1								
Phenol conversion (%)	12.8								

Appendix C

Reaction conditions and data obtained from liquid phase phenol methylation with methanol

Table C.1: Reaction conditions and results obtained from liquid phase phenol methylation with methanol over H-ZSM-5.

Run number	Reactants	Temperature (°C)	Reactant to catalyst mass ratio	Final pressure (bar)	Methanol to phenol molar ratio	Reaction time (hours)
LP1	Methanol/phenol	200	250	48	5	9
LP4	Methanol/phenol	200	250	48	5	5
LP5	Methanol/phenol	200	250	48	5	5
LP6	Methanol/phenol	200	200	24	1	12
LP34	Methanol/phenol	200	39.4	33	5	5
LP35	Methanol/phenol	200	39.4	23	1	5
LP65	Methanol/phenol	220	39.4	29	1	5
LP66	Methanol/phenol	250	39.4	40	1	5
LP67	Methanol/phenol	200	39.4	8	0.2	5
LP68	Methanol/phenol	200	39.4	5	0.07	5
LP72	Methanol/phenol	200	39.4	22	1	5
LP84	Methanol/phenol/water	200	39.4	26	1	5

Run number	Phenol conversion (%)	Selectivity (mol%)				Cresol distribution (%)		
		Anisole	Cresols	Methylanisoles	Xylenols	o-	p-	m-
LP1	0.2	79.5	20.5	0.0	0.0	73.6	26.4	0.0
LP4	0.5	80.7	19.3	0.0	0.0	73.4	26.6	0.0
LP5	0.6	80.2	19.8	0.0	0.0	71.3	28.7	0.0
LP6	4.7	78.5	21.5	0.0	0.0	72.6	27.4	0.0
LP34	0.2	94.9	5.1	0.0	0.0	100	0.0	0.0
LP35	9.7	77.7	21.4	0.9	0.0	72.6	27.4	0.0
LP65	16.9	73.9	23.9	1.9	0.3	70.0	28.6	1.4
LP66	24.6	67.9	27.3	4.1	0.7	67.6	30.6	1.8
LP67	11.6	80.4	18.2	1.4	0.0	71.6	28.4	0.0
LP68	8.0	82.6	17.3	0.1	0.0	68.0	32.0	0.0
LP72	9.6	79.7	19.7	0.6	0.0	72.6	27.4	0.0
LP84	3.0	75.9	23.6	0.5	0.0	63.5	36.5	0.0

Table C.2: Reaction conditions and results obtained from liquid phase phenol methylation with methanol over H-Beta.

Run number	Reactants	Temperature (°C)	Reactant to catalyst mass ratio	Final pressure (bar)	Methanol to phenol molar ratio	Reaction time (hours)
LP9	Methanol/phenol	200	100	52	5	4
LP10	Methanol/phenol	200	59	27	1	8
LP11	Methanol/phenol	200	79	24	1	5
LP12	Methanol/phenol	200	39.4	24	1	5
LP14	Methanol/phenol	200	20	24	1	5
LP15	Methanol/phenol	200	39.4	22	1	5
LP22	Methanol/phenol	220	39.4	28	1	5
LP25	Methanol/phenol	200	39.4	8	0.2	5
LP29	Methanol/phenol	200	39.4	5	0.07	5
LP33	Methanol/phenol	200	39.4	53	5	5
LP37	Methanol/phenol	200	39.4	23	1	72
LP39	Methanol/phenol	250	39.4	39	1	5
LP61	Methanol/phenol	200	39.4	23	1	1
LP64	Methanol/phenol	180	39.4	18	1	5
LP83	Methano/phenol/water	200	39.4	24	1	5

Run number	Phenol conversion (%)	Selectivity (mol%)				Cresol distribution (%)		
		Anisole	Cresols	Methylanisoles	Xylenols	o-	p-	m-
LP9	1.2	93.5	6.5	0.0	0.0	69.1	30.9	0.0
LP10	6.9	91.9	7.7	0.4	0.0	70.3	29.7	0.0
LP11	4.9	91.4	7.9	0.7	0.0	72.9	27.1	0.0
LP12	8.2	91.6	7.9	0.5	0.0	69.7	30.3	0.0
LP13	9.1	92.3	7.7	0.0	0.0	69.7	30.3	0.0
LP14	13.4	91.0	8.1	0.9	0.0	68.5	31.5	0.0
LP15	8.3	91.2	8.3	0.5	0.0	67.9	32.1	0.0
LP22	28.8	89.9	8.8	1.3	0.0	68.4	31.6	0.0
LP25	13.8	81.2	16.8	1.8	0.2	68.1	31.9	0.0
LP29	6.2	69.6	29.2	1.2	0.0	67.2	32.8	0.0
LP33	4.6	97.5	2.5	0.0	0.0	100.0	0.0	0.0
LP37	34.5	87.5	9.1	3.2	0.2	69.2	30.8	0.0
LP39	44.4	68.8	20.3	8.9	0.9	63.4	34.0	2.6
LP61	2.8	91.6	8.4	0.0	0.0	66.6	33.4	0.0
LP64	2.4	93.0	7.0	0.0	0.0	68.8	31.2	0.0
LP71	9.3	92.0	8.0	0.0	0.0	67.9	32.1	0.0
LP83	2.9	94.9	5.1	0.0	0.0	74.7	25.3	0.0

Table C.3: Reaction conditions and results obtained from liquid phase phenol methylation with methanol over H-Mordenite.

Run number	Reactants	Temperature (°C)	Reactant to catalyst mass ratio	Final pressure (bar)	Methanol to phenol molar ratio	Reaction time (hours)
LP18	Methanol/phenol	200	39.4	21	1	5
LP19	Methanol/phenol	200	39.4	23	1	5
LP75	Methanol/phenol	200	39.4	24	1	5

Run number	Phenol conversion (%)	Selectivity (mol%)				Cresol distribution (%)		
		Anisole	Cresols	Methylanisoles	Xylenols	o-	p-	m-
LP18	0.1	87.3	12.7	0.0	0.0	71.0	29.0	0.0
LP19	1.0	85.0	15.0	0.0	0.0	69.2	30.8	0.0
LP75	8.0	82.8	16.2	1.0	0.0	67.6	32.4	0.0

Table C.4: Reaction conditions and results obtained from liquid phase phenol methylation with methanol over H-USY.

Run number	Reactants	Temperature (°C)	Reactant to catalyst mass ratio	Final pressure (bar)	Methanol to phenol molar ratio	Reaction time (hours)
LP7	Methanol/phenol	200	197	17	1	6
LP8	Methanol/phenol	200	79	20	1	11
LP20	Methanol/phenol	200	20	20	1	12

Run number	Phenol conversion (%)	Selectivity (mol%)				Cresol distribution (%)		
		Anisole	Cresols	Methylanisoles	Xylenols	o-	p-	m-
LP7	0.6	91.7	8.3	0.0	0.0	71.1	28.9	0.0
LP8	1.4	91.9	8.1	0.0	0.0	62.6	37.4	0.0
LP20	1.8	92.6	7.4	0.0	0.0	69.2	30.8	0.0

Table C.5: Reaction conditions and results obtained from liquid phase phenol methylation with methanol over H-MCM-22 (UCT).

Run number	Reactants	Temperature (°C)	Reactant to catalyst mass ratio	Final pressure (bar)	Methanol to phenol molar ratio	Reaction time (hours)
LP23	Methanol/phenol	200	39.4	23	1	6
LP38	Methanol/phenol	200	39.4	23	1	5
LP69	Methanol/phenol	200	39.4	24	1	12
LP70	Methanol/phenol	200	39.4	22	1	5
LP76	Methanol/phenol	200	39.4	24	1	6
LP77	Methanol/phenol	200	39.4	54	5	5
LP78	Methanol/phenol	200	39.4	6	0.07	5
LP79	Methanol/phenol	200	39.4	8	0.2	5
LP80	Methanol/phenol	220	39.4	31	1	5
LP81	Methanol/phenol	250	39.4	42	1	5
LP85	Methanol/phenol/water	200	39.4	22	1	5

Run number	Phenol conversion (%)	Selectivity (mol%)				Cresol distribution (%)		
		Anisole	Cresols	Methylanisoles	Xylenols	o-	p-	m-
LP23	12.9	91.3	7.3	1.4	0.0	42.4	57.6	0.0
LP38	5.7	93.6	5.4	1.0	0.0	45.5	54.5	0.0
LP69	13.2	94.2	4.7	1.1	0.0	44.4	55.6	0.0
LP70	2.3	93.5	6.5	0.0	0.0	43.2	56.8	0.0
LP76	6.3	90.9	7.7	1.4	0.0	43.7	56.3	0.0
LP77	6.8	98.4	1.4	0.2	0.0	43.0	57.0	0.0
LP78	0.4	77.6	22.4	0.0	0.0	52.9	47.1	0.0
LP79	1.2	82.3	17.4	0.3	0.0	56.6	43.4	0.0
LP80	9.6	92.7	6.0	1.3	0.0	41.5	56.2	2.3
LP81	16.3	90.4	7.8	1.5	0.3	43.9	53.4	2.7
LP85	1.1	90.0	5.6	4.4	0.0	37.6	62.4	0.0

Table C.6: Reaction conditions and results obtained from liquid phase phenol methylation with methanol over H-MCM-22 (DE2).

Run number	Reactants	Temperature (°C)	Reactant to catalyst mass ratio	Final pressure (bar)	Methanol to phenol molar ratio	Reaction time (hours)
LP89	Methanol/phenol	200	39.4	25	1	5

Run number	Phenol conversion (%)	Selectivity (mol%)				Cresol distribution (%)		
		Anisole	Cresols	Methylanisoles	Xylenols	o-	p-	m-
LP89	8.6	95.2	3.8	1.0	0.0	49.4	50.6	0.0

Table C.7: Reaction conditions and results obtained from liquid phase phenol methylation with methanol over internally selectively sodium-exchanged ZSM-5.

Run number	Reactants	Temperature (°C)	Reactant to catalyst mass ratio	Final pressure (bar)	Methanol to phenol molar ratio	Reaction time (hours)
LP87	Methanol/phenol	200	39.4	22	1	5

Run number	Phenol conversion (%)	Selectivity (mol%)				Cresol distribution (%)		
		Anisole	Cresols	Methylanisoles	Xylenols	o-	p-	m-
LP87	1.2	81.0	19.0	0.0	0.0	77.5	22.5	0.0

Table C.8: Reaction conditions and results obtained from liquid phase phenol methylation with methanol over internally selectively sodium-exchanged MCM-22 (UCT).

Run number	Reactants	Temperature (°C)	Reactant to catalyst mass ratio	Final pressure (bar)	Methanol to phenol molar ratio	Reaction time (hours)
LP88	Methanol/phenol	200	39.4	21	1	5

Run number	Phenol conversion (%)	Selectivity (mol%)				Cresol distribution (%)		
		Anisole	Cresols	Methylanisoles	Xylenols	o-	p-	m-
LP8P	2.3	93.8	5.7	0.5	0.0	59.8	40.2	0.0

Table C.9: Reaction conditions and results obtained from liquid phase phenol methylation with methanol over amorphous silica-alumina.

Run number	Reactants	Temperature (°C)	Reactant to catalyst mass ratio	Final pressure (bar)	Methanol to phenol molar ratio	Reaction time (hours)
LP24	Methanol/phenol	200	39.4	18	1	5
LP30	Methanol/phenol	200	39.4	6	0.2	5
LP31	Methanol/phenol	200	39.2	5	0.07	5
LP32	Methanol/phenol	200	39.4	34	5	5
LP36	Methanol/phenol	200	39.4	15	1	24

Run number	Phenol conversion (%)	Selectivity (mol%)				Cresol distribution (%)		
		Anisole	Cresols	Methylanisoles	Xylenols	o-	p-	m-
LP24	0.5	93.4	6.6	0.0	0.0	69.2	30.8	0.0
LP30	0.9	88.4	11.6	0.0	0.0	70.4	29.6	0.0
LP31	1.0	84.8	15.2	0.0	0.0	68.0	32.0	0.0
LP32	0.2	94.9	5.1	0.0	0.0	70.2	29.8	0.0
LP36	1.0	93.3	6.7	0.0	0.0	71.3	28.7	0.0

Table C.10: Reaction conditions and results obtained from the conversion of pure anisole and an anisole/phenol mixture over different catalysts.

Run number	Catalyst	Reactants	Temperature (°C)	Reactant to catalyst mass ratio	Final pressure (bar)	Reaction time (hours)
LP41	H-ZSM-5	Anisole	200	30	3	5
LP42	H-Beta	Anisole	200	30	2	5
LP44	H-Mordenite	Anisole	200	30	2	5
LP43	H-USY	Anisole	200	30	1.5	5
LP50	H-MCM-22 (UCT)	Anisole	200	30	2	5
LP49	Silica-alumina	Anisole	200	30	1.5	5
LP82	H-MCM-22 (UCT)	Anisole/phenol	200	30	5	5

Run number	Conversion (%)	Selectivity (mol %)				
		Cresols	Methylanisole	Xylenols	Phenol	Other
LP41	3.2	5.2	46.5	0.9	47.4	0.0
LP42	17.3	12.6	42.8	0.9	43.7	0.0
LP44	54.7	20.8	27.5	2.8	42.7	6.2
LP43	12.2	6.2	44.9	2.0	46.9	0.0
LP50	21.0	13.0	38.5	1.1	44.8	2.6
LP49	3.4	16.3	39.4	2.5	41.8	0.0
LP82	1.0	39.5	30.0	0.0	30.5	0.0

Run number	o-Cresol (%)	p-Cresol (%)	m-Cresol (%)
LP41	80.2	19.8	0.0
LP42	53.4	46.6	0.0
LP44	70.3	29.7	0.0
LP43	75.3	24.7	0.0
LP50	47.3	52.7	0.0
LP49	7.9	92.1	0.0
LP82	61.6	38.4	0.0

Table C.11: Reaction conditions and results obtained from o-cresol conversion over different catalysts.

Run number	Catalyst	Reactants	Temperature (°C)	Reactant to catalyst mass ratio	Reaction time (hours)
LP56	H-ZSM-5	o-Cresol	200	30	5
LP55	H-Beta	o-Cresol	200	30	5
LP58	H-Mordenite	o-Cresol	200	30	5
LP57	H-USY	o-Cresol	200	30	5
LP54	H-MCM-22 (UCT)	o-Cresol	200	30	5
LP53	Silica-alumina	o-Cresol	200	30	5

Run number	Conversion (%)	Selectivity (mol %)					
		Anisole	p-Cresol	Methyl-anisoles	Xylenols	Phenol	Other
LP56	0.4	4.6	0.0	0.0	47.7	47.7	0.0
LP55	0.5	0.0	0.7	0.0	36.2	54.1	9.0
LP58	0.6	0.0	10.2	0.0	44.9	44.9	0.0
LP57	0.3	0.0	0.6	0.0	49.7	49.7	0.0
LP54	0.9	0.0	22.6	0.0	33.1	40.6	3.7
LP53	0.4	0.0	0.0	0.0	43.5	52.6	3.9

Table C.12: Reaction conditions and results obtained from p-cresol conversion over different catalysts.

Run number	Catalyst	Reactants	Temperature (°C)	Reactant to catalyst mass ratio	Reaction time (hours)
LP45	H-ZSM-5	p-Cresol	200	30	5
LP46	H-Beta	p-Cresol	200	30	5
LP48	H-Mordenite	p-Cresol	200	30	5
LP47	H-USY	p-Cresol	200	30	5
LP52	H-MCM-22 (UCT)	p-Cresol	200	30	5
LP51	Silica-alumina	p-Cresol	200	30	5

Run number	Conversion (%)	Selectivity (mol%)					
		Anisole	o-Cresol	Methyl-anisoles	Xylenols	Phenol	Other
LP45	0.4	6.6	17.3	12.4	25.6	38.1	0.0
LP46	0.3	13.3	25.1	5.2	25.6	30.8	0.0
LP48	0.5	0.0	14.4	17.6	25.2	42.8	0.0
LP47	0.6	50.7	11.2	6.5	12.6	19.0	0.0
LP52	0.6	0.6	25.8	1.8	35.0	36.8	0.0
LP51	0.2	7.5	31.4	0.0	30.6	30.5	0.0

Table C.13: Reaction conditions and results obtained from alkylation of toluene with methanol over H-ZSM-5 and H-MCM-22 (UCT).

Run number	Catalyst	Reactants	Temperature (°C)	Reactant to catalyst mass ratio	Methanol to phenol molar ratio	Reaction time (hours)
LP92	H-ZSM-5	Methanol/toluene	200	30	1	5
LP90	H-MCM-22 (UCT)	Methanol/toluene	200	30	1	5

Run number	Toluene conversion (%)	Selectivity (mol%)			
		Xylenes	Benzene	Ethylbenzene	Trimethylbenzenes
LP92	0.2	36.2	34.4	9.2	20.2
LP90	0.1	40.9	49.1	0.0	10.0

Run number	o-Xylene (%)	p-Xylene (%)	m-Xylene (%)
LP92	39.4	24.0	36.6
LP90	33.5	29.6	36.9

Appendix D

Material balance for the gas phase alkylation of phenol with methanol

Toluene was used as an internal standard to calculate a mass balance as toluene was not a product in the phenol methylation reaction. Toluene was not observed as a product in the phenol methylation reaction. The internal standard was added via a saturator to the gaseous products after the reactor and before the GC as described in Section 4.3.1.

Calculation of the mass balance:

$$\text{Mass balance (\%)} = \frac{\Sigma(\text{mass of products})}{\text{mass flow of feed}} \times 100$$

The mass of the products are calculated as follows:

$$\Sigma(\text{mass of product i}) = \Sigma(\frac{\text{mass of internal standard}}{\text{mass \% of internal stand}}) \times (\text{mass \% of compound i})$$

The mass percentage was calculated from:

$$\text{mass \% of compound i} = \frac{A_i RF_i}{\Sigma(A_i RF_i)}$$

where:

- A_i is the area on the GC peak of compound i
- RF_i is the mass response factor of compound i.

A carbon balance was then performed by comparing the flow of carbon in the feed to the reactor to the carbon in the product stream. That is,

$$\text{Carbon balance (\%)} = \frac{\sum(n_i \times \text{carbon number})_i}{(n_{\text{methanol}} \times 1 + n_{\text{phenol}} \times 6)} \times 100$$

where:

- n_i is the moles of product i
- $n_{methanol}$ is the moles of methanol
- n_{phenol} is the moles of phenol.

Phenol conversion was calculated as follows:

$$\text{Phenol conversion (\%)} = \frac{\text{total moles of alkylated phenols formed}}{(\text{moles of alkylated phenols product} + \text{moles unconverted phenol})} \times 100$$

Product selectivities and yield were calculated as follows:

$$\text{Selectivity of product i (mol\%)} = \frac{\text{moles of product i formed}}{\text{total moles of alkylated phenols formed}} \times 100$$

$$\text{Yield of product i (\%)} = \frac{\text{mole of product i formed}}{(\text{moles of alkylated phenols products} + \text{moles unconverted phenol})} \times 100$$

Calculated response factors were used in the determination of product selectivities and are shown in Table B.1. A sample calculation is shown in Table D.1. The flowrate of toluene added via the saturator was 0.385 g/h, resulting in the total mass flowrate of the stream to be 12.71 g/h.

Table D.1: A model calculation of carbon balance, phenol conversion, product selectivities and cresol isomer distribution.

Compound	Response factors (RF)	Area	Area×RF	Molecular weight	Mass fraction	Mass (g/h)	Mole (mol/h)	Mol%	Carbon (mol/h)	Selectivity (mol%)	Yield (%)
Toluene	1	50965	50965	92	0.0303	0.385	0.0042	2.2711			
Methanol	4.38	62527	273868.3	32	0.1629	2.070	0.0647	35.0863	0.0647		
Dimethyl ether	3.15	43358	136577.7	46	0.0812	1.032	0.0224	12.1722	0.0449		
Phenol	1.28	600611	768782.1	94	0.4573	5.811	0.0617	33.4899	0.3705		
Anisole	1.33	176284	234457.7	108	0.1395	1.772	0.0164	8.8999	0.1149	52.41	18.17
o-cresol	1.26	81673	102908	108	0.0612	0.778	0.0072	3.9064	0.0504	23.00	7.98
p-cresol	1.26	50150	63189	108	0.0376	0.478	0.0044	2.3986	0.0310	14.13	4.90
m-cresol	1.26	14859	18722.3	108	0.0111	0.142	0.0013	0.7107	0.0092	4.19	1.45
2-Methylanisole	1.31	2406	3151.9	122	0.0019	0.024	0.0002	0.1059	0.0016	0.62	0.22
3+4-Methylanisole	1.31	10258	13438	122	0.0080	0.102	0.0008	0.4516	0.0067	2.66	0.92
2,3-xylenol	1.23	0	0	122	0	0	0	0	0	0	0.00
2,4-xylenol	1.23	4247	5223.8	122	0.0031	0.039	0.003	0.1755	0.0026	1.03	0.36
2,5-xylenol	1.23	2950	3628.5	122	0.0022	0.027	0.0002	0.1219	0.0018	0.72	0.25
2,6-xylenol	1.23	2025	2490.8	122	0.0015	0.019	0.0002	0.0837	0.0012	0.49	0.17
3,4-xylenol	1.23	1185	1457.6	122	0.0009	0.011	0.0001	0.0490	0.0007	0.29	0.10
3,5-xylenol	1.23	1872	2302.6	122	0.0014	0.017	0.0001	0.0774	0.0011	0.46	0.16
Other	1.20	0	0	130	0	0	0	0	0	0	0
Carbon balance (%)	98.7										
Phenol conversion (%)	34.7										

Appendix E

Data from the gas phase phenol methylation with methanol

Table E.1: Reaction conditions for gas phase phenol methylation with methanol.

Run number	Catalyst	Reactants	Reaction temperature (°C)	Total Pressure (bar)	Reactants partial pressure (bar)	Methanol to to phenol ratio	WHSV (h^{-1})
GP1	H-ZSM-5	Methanol/phenol	300	1	0.2	1	14
GP2	H-MCM-22 (UCT)	Methanol/phenol	300	1	0.2	1	14
GP3	Silica-alumina	Methanol/phenol	300	1	0.2	1	14
GP4	H-MCM-22 (DE1)	Methanol/phenol	300	1	0.2	1	14
GP5	H-MCM-22 (DE2)	Methanol/phenol	300	1	0.2	1	14
GP6	H-MCM-22 (DE3)	Methanol/phenol	300	1	0.2	1	14
GP7	Steamed H-MCM-22 (DE1)	Methanol/phenol	300	1	0.2	1	14
GP8	H/Na-ZSM-5	Methanol/phenol	300	1	0.2	1	14
GP9	H/Na-MCM-22	Methanol/phenol	300	1	0.2	1	14
GP10	H-MCM-22 (UCT)	Methanol/phenol	200	1	0.2	1	14
GP11	H-MCM-22 (UCT)	Methanol/phenol	250	1	0.2	1	14
GP12	H-MCM-22 (UCT)	Methanol/phenol	330	1	0.2	1	14
GP13	H-MCM-22 (UCT)	Methanol/phenol	350	1	0.2	1	14
GP14	H-MCM-22 (UCT)	Methanol/phenol	380	1	0.2	1	14
GP15	H-MCM-22 (UCT)	Methanol/phenol	400	1	0.2	1	14
GP16	H-MCM-22 (UCT)	Methanol/phenol	270	1	0.2	1	14
GP17	H-MCM-22 (UCT)	Methanol/phenol	300	1	0.2	0.3	14
GP18	H-MCM-22 (UCT)	Methanol/phenol	300	1	0.2	0.5	14
GP19	H-MCM-22 (UCT)	Methanol/phenol	300	1	0.2	2	14
GP20	H-MCM-22 (UCT)	Methanol/phenol	300	1	0.2	6	14
GP21	H-MCM-22 (UCT)	Methanol/phenol	300	1	0.2	1	7.5
GP22	H-MCM-22 (UCT)	Methanol/phenol	300	1	0.2	1	22.5
GP23	H-MCM-22 (UCT)	Methanol/phenol	300	1	0.2	1	3.1
GP24	H-MCM-22 (UCT)	Methanol/phenol	300	1	0.3	1	6
GP25	H-MCM-22 (UCT)	Methanol/phenol	300	1	0.5	1	6
GP26	H-MCM-22 (UCT)	Methanol/phenol	300	1	0.8	1	6

Table E.2: Results obtained from GP1.

Time-on-stream (min)	Carbon balance (%)	Phenol conversion (%)	Selectivity (mol%)				Cresol distribution (%)		
			Anisole	Cresols	Methylanisoles	Xylenols	o-	p-	m-
14	96.7	19.6	49.0	47.4	0.6	3.0	64.7	31.6	3.7
65	97.0	14.0	55.8	40.7	2.3	1.2	63.3	32.8	3.9
108	98.9	13.0	56.0	40.8	2.2	1.0	62.8	33.2	4.0
137	97.8	12.5	57.7	39.3	2.0	1.0	62.9	33.1	4.0
166	98.0	12.0	57.8	40.6	0.6	1.0	62.6	33.3	4.1
194	99.0	12.1	58.5	38.7	1.9	0.9	62.1	33.6	4.3
223	99.7	11.9	58.7	38.5	1.9	0.9	62.5	33.4	4.1
252	99.8	11.7	58.6	38.6	2.0	0.8	62.9	33.0	4.1
290	99.7	11.6	58.7	38.6	1.9	0.8	62.4	33.4	4.2
321	98.8	11.2	58.1	39.1	2.0	0.8	62.4	33.4	4.2
349	98.6	11.3	58.2	39.3	1.7	0.8	62.2	33.7	4.1
377	99.9	11.3	58.5	37.0	3.7	0.8	62.1	33.6	4.3
406	99.6	11.0	59.1	38.4	1.8	0.7	61.9	33.8	4.3
435	99.2	10.9	58.3	38.2	2.8	0.7	62.0	33.8	4.2
463	99.7	10.8	59.7	37.5	2.0	0.8	61.8	33.9	4.3
493	98.4	10.8	59.2	38.3	1.8	0.7	61.4	34.1	4.5
523	98.7	10.5	59.6	38.0	1.7	0.7	62.2	34.1	3.7
552	99.9	10.5	59.7	37.6	1.9	0.8	61.4	34.2	4.4
580	99.6	10.6	59.4	36.8	3.1	0.7	61.9	34.3	3.8

Table E.3: Results obtained from GP2.

Time-on-stream (min)	Carbon balance (%)	Phenol conversion (%)	Selectivity (mol%)				Cresol distribution (%)		
			Anisole	Cresols	Methylanisoles	Xylenols	o-	p-	m-
17	99.2	9.3	55.1	39.5	2.7	2.7	59.5	33.6	6.9
71	99.1	5.6	56.8	39.3	1.9	2.0	61.1	33.3	5.6
107	99.8	4.9	58.1	38.9	1.7	1.3	61.3	32.9	5.8
139	98.3	4.4	60.0	37.9	0.9	1.2	61.5	32.6	5.9
168	98.8	4.1	60.2	37.5	1.0	1.3	61.7	32.4	5.9
197	99.5	3.8	60.4	37.4	1.1	1.1	61.9	32.3	5.8
226	99.9	3.6	60.5	37.2	1.2	1.1	61.8	32.1	6.1
255	98.4	3.5	60.9	36.7	1.4	1.0	61.7	32.2	6.1
284	98.8	3.3	61.2	36.8	1.3	0.7	62.4	31.7	5.9
312	99.5	3.2	61.4	36.3	1.2	1.1	62.3	31.7	6.0
342	99.1	3.0	62.5	36.0	1.3	0.2	62.5	31.5	6.0
373	97.2	3.0	62.0	36.3	1.4	0.3	62.8	31.3	5.9
402	98.9	2.9	62.3	36.0	1.4	0.3	64.0	30.0	6.0
436	98.5	2.7	62.6	36.0	1.4	0.0	64.7	31.2	4.1

Table E.4: Results obtained from GP3.

Time-on-stream (min)	Carbon balance (%)	Phenol conversion (%)	Selectivity (mol%)				Cresol distribution (%)		
			Anisole	Cresols	Methylanisoles	Xylenols	o-	p-	m-
6	96.4	5.4	60.4	33.1	1.6	4.9	70.0	26.8	3.2
39	96.5	3.8	60.6	35.4	1.4	2.6	69.5	27.2	3.3
68	97.9	3.4	61.2	34.8	1.4	2.6	70.3	26.7	3.0
91	98.5	3.2	60.8	34.7	1.8	2.7	69.8	27.1	3.1
114	99.6	3.0	61.0	35.6	0.8	2.6	69.5	27.5	3.0
139	97.9	2.8	62.3	34.8	0.5	2.4	70.2	26.7	3.1
164	94.4	2.7	62.3	33.6	1.6	2.5	70.8	26.5	2.7
189	96.8	2.8	62.2	34.5	0.8	2.5	70.2	26.9	2.9
213	98.2	2.6	61.9	33.9	1.7	2.5	70.6	26.9	2.5
239	96.9	2.5	62.4	34.1	1.1	2.4	70.7	26.2	3.1

Table E.5: Results obtained from GP4.

Time-on-stream (min)	Carbon balance (%)	Phenol conversion (%)	Selectivity (mol%)				Cresol distribution (%)		
			Anisole	Cresols	Methylanisoles	Xylenols	o-	p-	m-
19	96.1	13.1	47.3	46.7	2.6	3.4	59.6	35.5	4.9
70	94.0	6.9	41.7	51.1	4.6	2.6	61.6	34.3	4.1
101	94.7	5.6	41.4	54.8	2.1	1.7	62.3	33.4	4.3
137	98.3	4.9	42.4	54.8	0.5	2.3	63.6	33.6	2.8
168	99.9	4.8	41.6	53.7	2.4	2.3	63.5	32.5	4.0
204	99.9	4.5	42.2	54.2	1.2	2.4	63.8	32.5	3.7
240	93.7	4.5	41.5	54.4	1.3	2.8	64.2	31.9	3.9
276	97.7	4.2	42.3	55.0	1.2	1.5	64.3	31.7	4.0
306	95.8	4.1	41.4	55.2	1.4	2.0	65.1	31.7	3.2
337	96.4	4.0	40.9	55.9	1.7	1.5	64.6	31.4	4.0
368	96.9	3.9	40.8	56.8	0.9	1.5	64.2	31.2	4.6
398	98.0	3.9	41.7	55.4	1.1	1.8	65.0	30.9	4.1

Table E.6: Results obtained from GP5.

Time-on-stream (min)	Carbon balance (%)	Phenol conversion (%)	Selectivity (mol%)				Cresol distribution (%)		
			Anisole	Cresols	Methylanisoles	Xylenols	o-	p-	m-
4	98.4	40.9	38.6	47.8	6.8	6.7	47.8	45.1	7.1
49	99.7	23.5	58.3	35.3	4.0	2.4	48.4	47.1	4.5
95	99.0	18.8	61.9	33.7	3.1	1.3	48.1	47.7	4.2
132	99.7	16.4	63.9	32.2	2.8	1.1	47.9	48.0	4.1
159	95.6	15.8	65.6	31.0	2.5	0.9	47.8	48.1	4.1
187	98.7	14.3	65.8	31.0	2.3	0.9	47.7	48.2	4.1
214	98.6	13.6	67.1	30.0	2.1	0.8	47.8	48.2	4.0
239	99.9	12.9	68.2	29.0	2.0	0.8	47.2	48.9	3.9
266	96.7	12.4	68.5	28.9	1.9	0.7	47.7	48.2	4.1
294	99.6	11.6	69.4	28.5	1.8	0.3	48.0	48.0	4.0
322	99.3	11.2	69.8	28.0	1.7	0.5	48.0	47.9	4.1
348	98.1	10.9	70.2	27.9	1.6	0.3	48.0	47.9	4.1
375	94.7	10.6	70.3	27.8	1.6	0.3	48.0	48.0	4.0
402	98.1	9.9	70.9	27.3	1.5	0.3	48.5	47.7	3.8
430	98.2	9.5	71.2	27.2	1.5	0.1	48.4	47.6	4.0
458	99.9	9.3	71.9	26.8	1.3	0.0	48.2	47.8	4.0
483	95.4	9.2	71.9	26.8	1.3	0.0	48.9	47.2	3.9
513	99.7	8.8	72.4	26.3	1.3	0.0	48.8	47.4	3.8
538	98.5	9.5	72.5	26.2	1.3	0.0	49.1	46.9	4.0
561	98.1	8.2	71.9	26.9	1.2	0.0	48.7	47.3	4.0

Table E.7: Results obtained from GP6.

Time-on-stream (min)	Carbon balance (%)	Phenol conversion (%)	Selectivity (mol%)				Cresol distribution (%)		
			Anisole	Cresols	Methylanisoles	Xylenols	o-	p-	m-
7	98.7	25.4	46.8	44.1	4.6	4.5	52.2	43.4	4.4
54	99.2	13.0	58.7	37.3	2.5	1.5	51.2	45.9	2.9
88	97.7	10.1	61.0	36.3	2.1	0.6	50.8	46.4	2.8
119	94.3	8.3	63.4	34.4	1.7	0.5	51.2	46.1	2.7
205	92.6	6.5	67.0	31.7	1.3	0.0	52.3	45.2	2.5
280	97.6	5.5	67.2	31.7	1.1	0.0	51.6	45.9	2.5
307	95.7	5.2	67.8	31.2	1.0	0.0	52.2	45.4	2.4
332	99.1	5.2	67.3	31.7	1.0	0.0	51.8	45.6	2.6
354	99.9	5.0	67.7	31.3	1.0	0.0	52.1	45.2	2.7

Table E.8: Quasi-steady state data for the investigation of steamed, internally selectively sodium-exchanged zeolites, reaction temperature, methanol : phenol ratio, reactants partial pressure, weight hourly space velocity.

Run number	Phenol conversion (%)	Selectivity (mol%)				Cresol distribution (%)		
		Anisole	Cresols	Methylanisoles	Xylenols	o-	p-	m-
GP7	11.6	65.2	32.4	1.6	0.8	59.4	32.2	8.4
GP8	2.9	28.3	69.3	2.4	0.0	64.2	31.6	4.2
GP9	4.7	62.3	35.9	1.6	0.2	63.4	31.0	5.6
GP10	0.5	51.8	48.2	0.0	0.0	67.4	32.6	0.0
GP11	1.0	55.3	44.7	0.0	0.0	64.5	31.1	4.4
GP12	4.3	58.0	40.3	1.3	0.4	63.2	29.1	7.7
GP13	8.3	49.6	45.5	2.3	2.6	61.4	28.3	10.3
GP14	10.0	44.6	49.5	2.5	3.4	60.2	26.1	13.7
GP15	12.8	39.1	53.3	2.6	5.0	59.7	24.6	15.7
GP16	2.0	63.6	36.1	0.0	0.3	61.8	32.3	5.9
GP17	1.4	55.6	43.0	1.4	0.0	61.3	29.7	9.0
GP18	1.9	57.8	39.2	2.9	0.1	62.1	30.1	7.8
GP19	4.5	66.1	32.9	1.0	0.0	63.3	30.8	5.9
GP20	8.3	66.0	30.5	3.0	0.5	57.3	33.5	9.2
GP21	6.9	64.2	33.8	1.4	0.6	60.4	32.9	6.7
GP22	2.0	62.1	37.9	0.0	0.0	65.6	28.6	5.8
GP23	12.5	67.9	29.0	2.2	0.9	56.3	35.7	8.0
GP24	8.7	63.6	33.7	1.5	1.2	62.3	31.2	6.5
GP25	9.1	60.5	36.4	1.5	1.6	59.4	32.8	7.8
GP26	9.1	61.4	34.9	1.4	2.3	59.9	32.7	7.4

Table E.9: Results obtained from product conversion over H-MCM-22 (UCT) .

Reactants	Conversion (%)	Selectivity (mol%)				
		Anisole	Cresols	Methylanisoles	Xylenols	Phenol
Anisole	7	-	19.2	37.8	2.1	40.9
Anisole/phenol*	4**	-	68.7	12.7	1.5	17.1
o-Cresol	4	0.2	68.0	0.0	15.9	15.9
p-Cresol	7	0.7	88.2	0.0	5.7	5.4
m-Cresol	4	0.0	97.7	0.0	1.2	1.1

* Anisole/ phenol molar mixture of 1 : 1;
** Anisole conversion.

Reactants	o-Cresol (%)	p-Cresol (%)	m-Cresol (%)	p/o-Cresol ratio
Anisole	69	11	20	0.16
Anisole/phenol	53	28	19	0.53
o-Cresol	-	15	85	-
p-Cresol	9	-	91	-
m-Cresol	26	74	-	2.85

Table E.10: Toluene alkylation with methanol over H-ZSM-5 and H-MCM-22 (UCT).

	H-ZSM-5	H-MCM-22 (UCT)
Toluene conversion	41.4	4.3
Product selectivities (mol%)		
Ethylbenzene	0.1	0.0
Xylene	83.4	92.8
Trimethylbensenes	16.3	6.0
Other	0.2	1.2
Xylene isomer distribution (%)		
o-	35.6	42.7
p-	31.4	42.2
m-	33.0	15.1

Appendix F

Ammonia temperature-programmed desorption curves for all the different catalysts

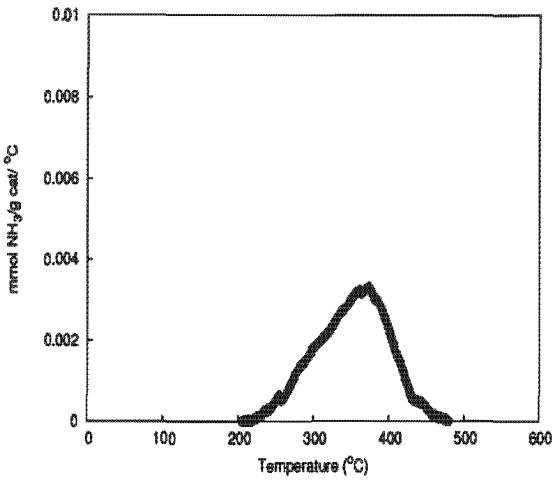

(a) H-ZSM-5

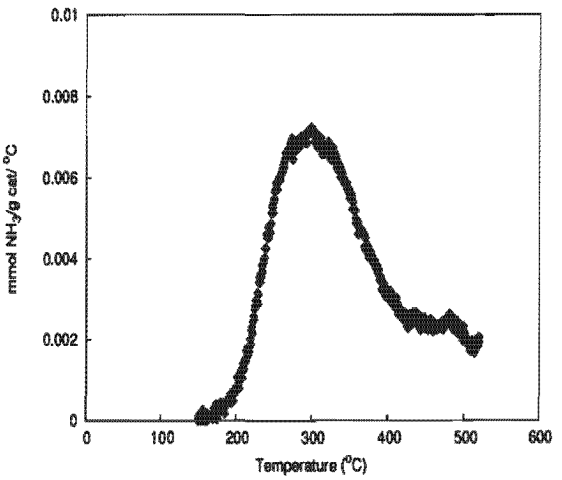

(b) H-Beta

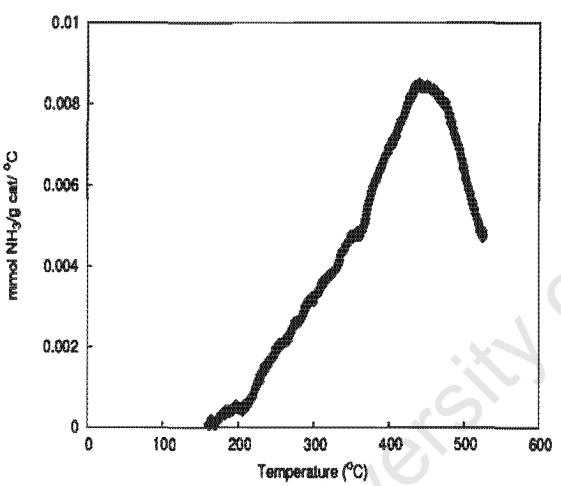

(c) H-Mordenite

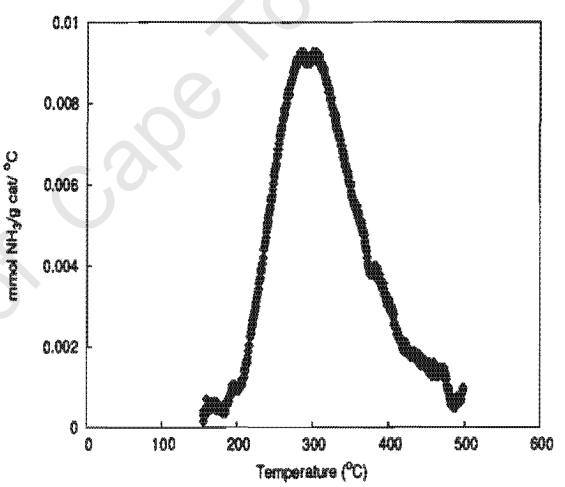

(d) H-USY

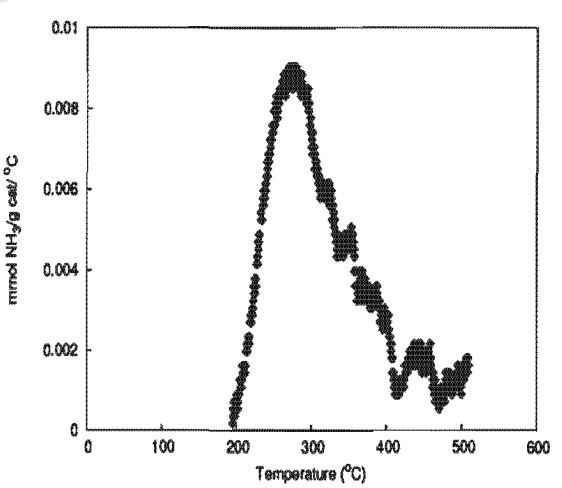

(e) Amorphous silica-alumina

Figure F.1: Temperature program desorption curve for zeolites H-ZSM-5, H-Beta, H-Mordenite, H-USY and amorphous silica-alumina.

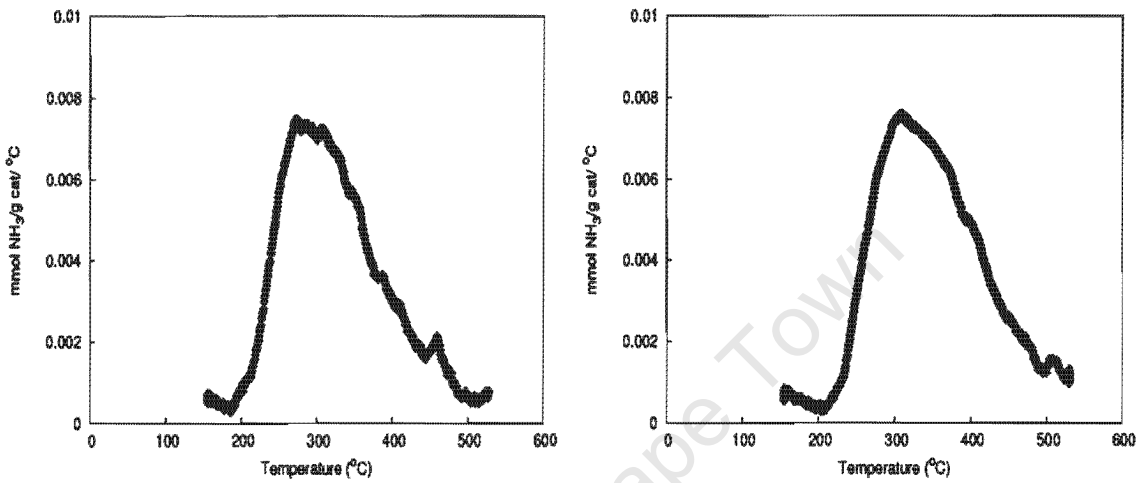

(a) H-MCM-22 (UCT)

(b) H-MCM-22 (DE1)

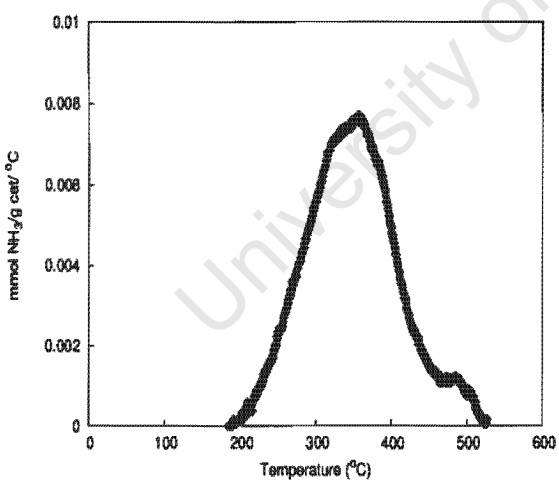

(c) H-H-MCM-22 (DE2)

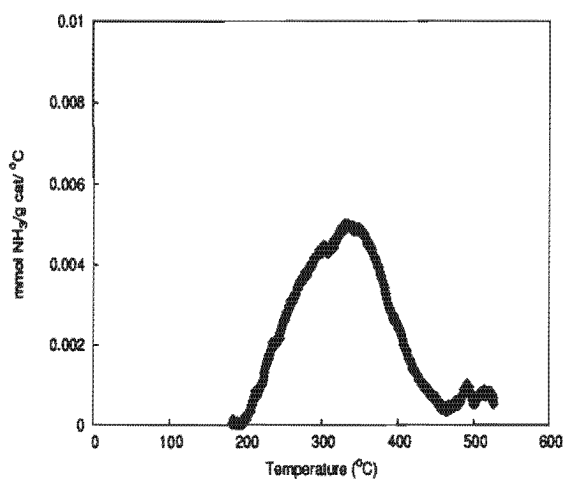

(d) H-MCM-22 (DE3)

Figure F.2: Temperature program desorption curve for the different zeolite H-MCM-22 samples.

Appendix G

Modelling of the batch methanol : phenol ratio data

Assuming irreversible second order with Langmuir adsorption:

$$K_A.C_A.C_s - C_{AS} = 0$$

$$K_B.C_B.C_s - C_{Bs} = 0$$

$$C_{SO} - C_S - C_{AS} - C_{BS} = 0$$

where:

- K_A is the equilibrium constant for species A;
- C_A is the concentration of species A;
- C_s is the concentration of vacant sites;
- C_{AS} is the concentration of species A on the catalyst surface;
- K_B is the equilibrium constant for species B;
- C_B is the concentration of species B;
- C_{BS} is the concentration of species B on the catalyst surface;
- C_{SO} is the initial concentration of vacant sites.

Find (C_{AS}, C_{BS},C_S) $\rightarrow$

$$\begin{bmatrix} C_{SO}.K_A.\frac{C_A}{(K_A.C_A+1+K_B.C_B)} \\ K_B.C_B.\frac{C_{SO}}{(K_A.C_A+1+K_B.C_B)} \\ \frac{C_{SO}}{(K_A.C_A+1+K_B.C_B)} \end{bmatrix}$$

Rate equation on the surface then become:

$$R_A = k_1.C_{AS}.C_{BS}$$

where

- R_A is rate of the formation of species A;
- k_1 is the rate constant.

Substituting from above yields:

$$R_A(C_A,\ C_B,\ k_1,\ K_A,\ K_B,\ C_{SO}) = \left[C_{SO}.K_A\frac{C_A}{(K_AC_A + 1 + K_B.C_B)}\right].\left[K_B.C_B.\frac{C_{SO}}{(K_A.C_A + 1 + K_B.C_B)}\right]$$

$$R_A(C_A,\ C_B,\ k_1,\ K_A,\ K_B,\ C_{SO}) = \frac{k_1.C_{SO}^2.K_A.K_B.C_A.C_B}{(K_A.C_A + 1 + K_B.C_B)^2}$$

Let A = methanol and B = phenol. For a reaction mixture of methanol : phenol ratio of 1:

$$X_B = \frac{C_{B0} - C_B}{C_{B0}}$$

$$C_B = C_{B0}.(1 - X_B)$$

$$C_A = C_{A0} - X_B.C_{B0} = C_{B0}.\left[\frac{C_{A0}}{C_{B0}} - X_B\right]$$

where:

- X_B is the conversion of species B;
- C_{B0} is the initial concentration of species B;
- C_{A0} is the initial concentration of species A.

Let ratio $= C_{A0}/C_{B0}$, then

$$C_A = C_{B0}.[\text{ratio} - X_B]$$

then the rate equation becomes:

$$R_A(C_{A0},\ C_{B0},\ \text{ratio},\ k_1,\ K_A,\ K_B,\ C_{SO}) = \frac{k_1.C_{SO}^2.K_A.K_B.(1 - X_A).(\text{ratio} - X_B)}{(K_A.C_{B0}.(\text{ratio} - X_B) + 1 + K_B.C_{B0}.(1 - X_B))^2} \quad \text{(G.1)}$$

Batch reactor design equations:

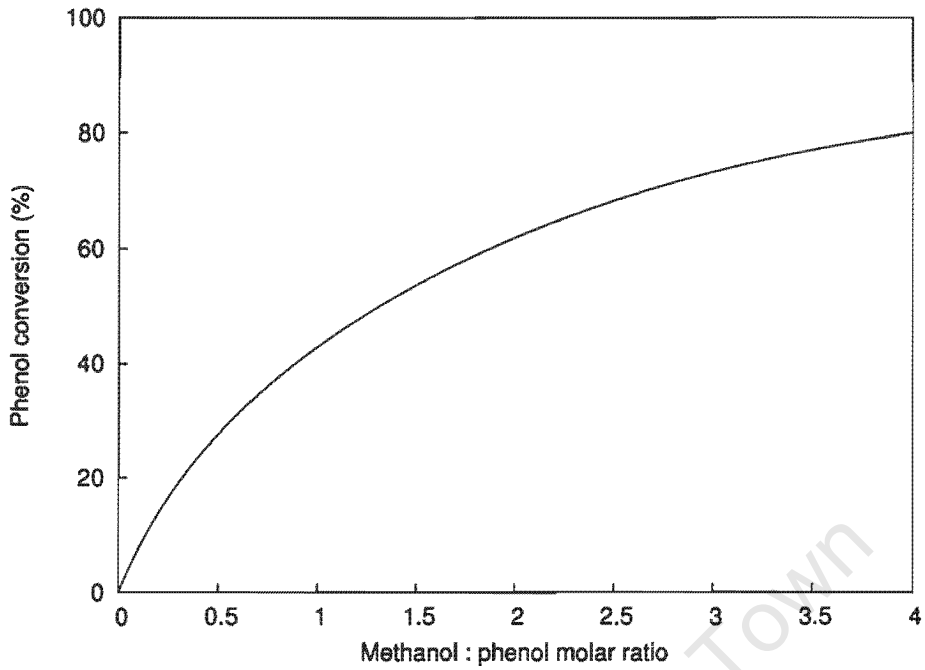

Figure G.1: Modelling of the conversion of phenol versus the methanol : phenol ratio as an irreversible second order reaction.

$$\frac{d}{dt}C_B = -R_A$$

$$\frac{d}{dt}X_B = \frac{R_A}{C_{B0}}$$

Assuming Langmuir model constants of:
$C_{S0} = 1$, $K_B = 0.05$, $K_A = 10$, $k_1 = 20$, ratio $= 10$, N $= 10$ and tf=1

$$C_{B0} = \frac{1}{\text{ratio} + 1}$$

$$C_{A0} = \text{ratio}.C_{B0}$$

The solution assuming second order irreversible kinetics is shown in Figure G.1. The solution to second order irreversible with Langmuir adsorption of methanol (Equation G.1) is given in Figure G.2.

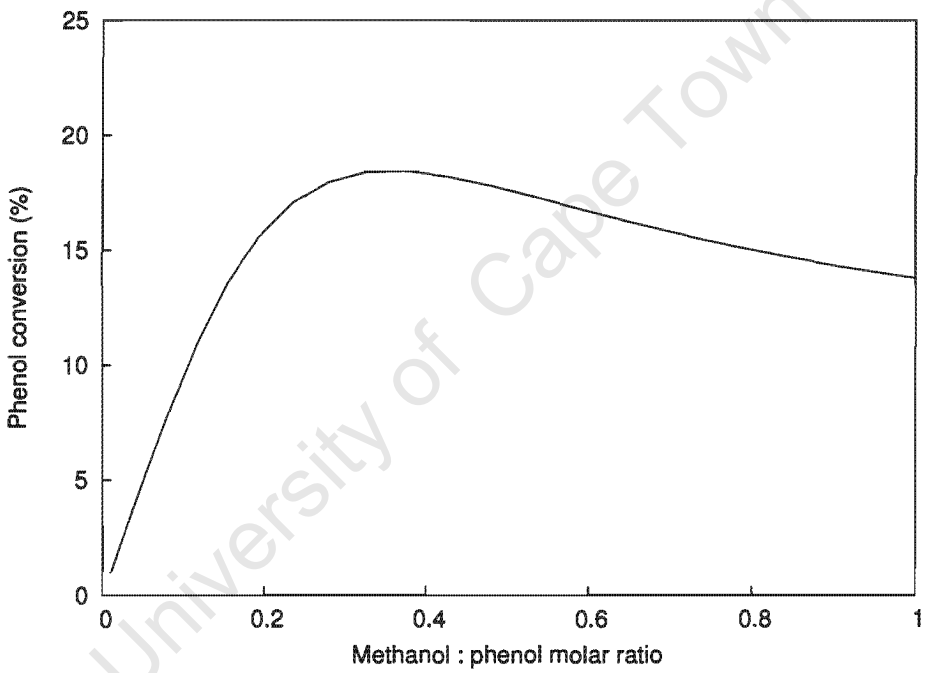

Figure G.2: Modelling of the conversion of phenol versus the methanol : phenol ratio as a second order irreversible reaction kinetics with Langmuir adsorption of methanol.